Nencki Institute of Experimental Biology

of Polish Academy of Sciences

Effects of Western diet in the development and progression of Non-alcoholic fatty liver disease

Inês Simões

Supervisors:

Mariusz Roman Wieckowski, PhD

Paulo Jorge Oliveira, PhD

Dissertation presented to obtain the Doctoral Degree in the discipline of Biological Sciences, specialization in Biochemistry

Warsaw, 2021

This doctoral thesis is part of a project that has received funding from the European Union's Horizon 2020 research and innovation programme under the Marie Sklodowska-Curie grant agreement No. 722619.

Aos meus pais que com todo o seu amor e apoio me permitiram sonhar e voar até à concretização deste sonho. Sem eles nada disto teria sido possível.

“Life is not easy for any of us.

But what of that?

We must have perseverance

and above all confidence in ourselves.

We must believe

that we are gifted for something

and that this thing must be attained.”

Marie Skłodowska-Curie

Table of contents

(This section has been divided into three complementary chapters dedicated to the three main objectives discussed in the present thesis.)

ACKNOWLEDGEMENTS

At the end of May 2017, I left my family, friends and country to pursue one dream: to get a PhD degree in the range of the most prestigious research fellowship programme, the Marie Skłodowska-Curie Actions created by the European Union. After four years, I am finishing one of the most important chapters of my life. I have been through a lot of work, challenges and emotions, and I couldn't finish this journey without expressing my gratitude to whom I met and helped me during all this amazing time.

First of all, I need to acknowledge to the European Union's Horizon 2020 research and innovation programme and to the FOIE GRAS project (Grant Agreement No. 722619) for the funding that allow the development of my PhD research work.

To the Nencki Institute of Experimental Biology and to the Nencki's PhD program studies for accepting me in the range of this project.

To Prof. Mariusz Wieckowski, to whom I need to express all the gratitude for choosing me and allowing me to develop my PhD in his group. Specially, I need to thank for all the support and for the environment created in order to feel his lab as my second home. In fact, I felt it. Thanks for all conversations, teachings and the opportunities created to become me as a scientist. Thanks for involving me in so many projects and all the experiences that allowed to spread our work around the world. Thanks for all the cakes specially the ones lovely prepared by Agnieszka.

Ao Prof. Paulo por me ter aceite no seu laboratório durante uma parte da minha tese. Este período contribuiu para o meu contínuo crescimento pessoal e profissional. Agradeço o excelente ambiente que encontrei, todo o suporte e ensinamentos que me foram dados. Agradeço também toda a disponibilidade e input dados durante a supervisão dos vários trabalhos incluídos nesta tese.

À Prof. Fernanda Borges e a todo o grupo de Química Medicinal da Universidade do Porto, em particular ao Doutor Pedro Soares pela supervisão da minha estadia no grupo e pela síntese química do composto usado no estudo animal presente nesta tese.

To Prof. John Jones that at the very end of this thesis, accepted me in his lab. Quero também expressar um enorme agradecimento ao Ludgero Tavares pelo tempo e por todos os ensinamentos. Mais ainda, por toda a confiança junto do 600.

To Prof. Hans Zischka for all the scientific contribution along these four years.

To all remaining members of FOIE GRAS consortium for the continuous advice and constructive discussions. I am honoured to be included in this programme.

To Justyna Janikiewicz, Prof. Agnieszka Dobrzyn and Prof. Michał Dabrowski for all the teachings and help along the four years of this work.

To the Department of Pathology at The Children's Memorial Health Institute, specially to Agnieszka Karkucinska-Wieckowska for the teachings, help and continuous support. It was an honour to collaborate with you.

To all my lab colleagues from Nencki, specially to Paulina, Magda, Monika and Agata for being not just my lab colleagues but friends always available to help me, to party or simply, to make long conversations. Thanks for creating such an amazing environment at work. I will keep our memories in a very special place of my heart. And now, I owe you the same hospitality that you prepared for me, so please visit me :P

À Yaiza que apareceu no momento certo. Só posso agradecer todos os ensinamentos, motivação e por me mostrar que não há impossíveis. Obrigada por todo o apoio e por me mostrar o caminho a seguir mesmo que fisicamente longe. Sem ti e as nossas conversas em português não teria sido a mesma coisa. Muchas gracias por todo mi amiga. Esta tesis también es tuya.

A todos os meus colegas do MitoXT com quem tive o prazer de privar aquando meu secondment no laboratório. Um agradecimento aos bravos que fizeram parte do estudo animal: ao Zé, ao Ricardo, à Susana, à Adriana e ao Rui. A todos quero agradecer pelos ensinamentos, simpatia e boa disposição.
Um especial agradecimento à Susana por toda a disponibilidade e sugestões. Ao Zé que foi mais que um mentor e ao Ricardo pelo companheirismo e discussão de ideias. Obrigada. O mérito desta tese a vocês se deve também.

To my ESR colleagues. This journey was unique because of this amazing group of people. We will always remember that together we are stronger, no matter what. Wish you the best and looking forward to see you again.

Aos meus pais que sempre estiveram lá e me apoiaram quando decidi largar tudo e perseguir mais um sonho longe deles e de todos. Esta tese não é minha, é nossa! Sou-vos eternamente grata!

Ao meu irmão que continua a ser um amigo de todas as horas, mesmo que a quatro horas de distância. Obrigada por seres o filho que ficou também a substituir a irmã no que foi preciso. Obrigada por todas as boleias para o aeroporto fora de horas. Gosto muito de ti maninho!

Aos meus avós. Agradeço toda a preocupação e beijinhos expressos por telefone. Desculpem toda a ausência. Gosto muito de vocês.

Às babes que Coimbra uniu. Obrigada por todas as mensagens, videochamadas e telefonemas trocados. Senti-vos pertinho do meu coração.

Às amigas de sempre. Obrigada por estarem aí, e por fazerem sentir que o tempo não passa passados vinte anos.

E por último, ao Vitor. Ao companheiro que me incentivou a levantar voo e que esteve sempre lá, longe ou perto com a maior paciência e carinho do mundo. Obrigada por todo o apoio, pelas palavras de incentivo, por seres o meu porto seguro.

To all the people that somehow contributed to this work, to all the friends and family that are part of my life, THANK YOU!!

FUNDING

This work was performed at Nencki Institute of Experimental Biology, Polish Academy of Sciences, Warsaw, Poland, under the supervision of Mariusz Roman Wieckowski, PhD and at Center for Neuroscience and Cell Biology, University of Coimbra, Portugal, under the supervision of Paulo Jorge Oliveira, PhD.

This work was supported by the National Science Centre, Poland (OPUS grant UMO-2018/29/B/NZ1/00589 and ETIUDA grant UMO-2020/36/T/NZ1/00004). This work was also supported by the research grants to Prof. Paulo Jorge Oliveira PTDC/BTM-SAL/29297/2017, POCI-01-0145-FEDER-029297, PTDC/DTP-FTO/2433/2014, PO-CI-01-0145-FEDER-016659, PO-CI-01-0145-FEDER-006980,/ASP-HOR/29152/2017, PO-CI-01-0145-FEDER-029152, UIDB/04539/2020, UIDP/04539/2020, PTDC/BIA-MOL/28607/2017, POCI-01-0145-FEDER-028607 from FEDER funds through the Operational Programme Competitiveness Factors—COMPETE and national funds by FCT—Foundation for Science and Technology.

Moreover, this work was supported by FOIE GRAS project from the European Union's Horizon 2020 Research and Innovation Programme under the Marie Skłodowska-Curie Grant Agreement No. 722619 (FOIE GRAS).

PUBLICATIONS

The results presented in the following sections of this thesis have been already published in international peer-reviewed scientific journals:

Agnieszka Karkucinska-Wieckowska, **Ines C. M. Simoes**, Piotr Kalinowski, Magdalena Lebiedzinska-Arciczewska, Krzysztof Zieniewicz, Piotr Milkiewicz, Magdalena Górska-Ponikowska, Paolo Pinton, Afshan N. Malik, Marcin Krawczyk, Paulo J. Oliveira, Mariusz R. Wieckowski. "Mitochondria, oxidative stress and Non-Alcoholic Fatty Liver Disease: a complex relationship". *Eur J Clin Invest 2021 May 29, e13622. DOI: 10.1111/eci.13622. IF (2020) – 4.686; Q2 (Medicine, Research & Experimental 56/140).*

Ines C. M. Simoes, Ricardo Amorim, Jose Teixeira, Agnieszka Karkucinska-Wieckowska, Adriana Carvalho, Susana P. Pereira, Rui F. Simoes, Sylwia Szymanska, Michal Dabrowski, Justyna Janikiewicz, Agnieszka Dobrzyn, Paulo J. Oliveira, Yaiza Potes, Mariusz R. Wieckowski, "The Alterations of Mitochondrial Function during NAFLD Progression—An Independent Effect of Mitochondrial ROS Production". *Int. J. Mol. Sci. 2021, 22(13), 6848. DOI: 10.3390/ijms22136848. IF (2020) – 5.923; Q1 (Biochemistry & Molecular Biology 67/297).*

Ines C. M. Simoes, Agnieszka Karkucinska-Wieckowska, Justyna Janikiewicz, Sylwia Szymanska, Maciej Pronicki, Pawel Dobrzyn, Michal Dabrowski, Agnieszka Dobrzyn, Paulo J. Oliveira, Hans Zischka, Yaiza Potes, Mariusz R. Wieckowski. "Western diet causes obesity-induced Non-Alcoholic Fatty Liver Disease development by differentially compromising the autophagic response". *Antioxidants, 2020, 9(10), 995. DOI:10.3390/antiox9100995. IF (2020) – 6.312; Q1 (Biochemistry & Molecular Biology 60/297).*

Ines C. M. Simoes, Justyna Janikiewicz, Judith Bauer, Agnieszka Karkucinska-Wieckowska, Piotr Kalinowski, Agnieszka Dobrzyn, Andrzej Wolski, Maciej Pronicki, Krzysztof Zieniewicz, Pawel Dobrzyn, Marcin Krawczyk, Hans Zischka, Mariusz R. Wieckowski, Yaiza Potes. "Fat and Sugar—A Dangerous Duet. A Comparative Review on Metabolic Remodeling in Rodent Models of Nonalcoholic Fatty Liver Disease". *Nutrients, 2019, 11 (12), pii: E2871. DOI: 10.3390/nu11122871. IF (2019) – 4.546; Q1 (Nutrition & Dietetics 17/89).*

Afshan N. Malik, **Ines C. M. Simoes**, Hannah S. Rosa, Safa Khan, Agnieszka Karkucinska-Wieckowska, Mariusz R. Wieckowski. "A Diet Induced Maladaptive Increase in Hepatic Mitochondrial DNA Precedes OXPHOS Defects and May Contribute to Non-Alcoholic Fatty Liver Disease". *Cells, 2019, 8 (10), pii: E1222, DOI:10.3390/cells8101222. IF (2019) – 4.366; Q2 (Cell Biology 70/195).*

Carlotta Giorgi, Saverio Marchi, **Ines C. M. Simoes**, Ziyu Ren, Giampaolo Morciano, Mariasole Perrone, Paulina Patalas-Krawczyk, Sabine Borchard, Paulina Jędrak, Karolina Pierzynowska, Jedrzej Szymanski, David Q. Wang, Piero Portincasa, Grzegorz Wegrzyn, Hans Zischka, Pawel Dobrzyn, Massimo Bonora, Jerzy Duszynski, Alessandro Rimessi, Agnieszka Karkucinska-Wieckowska, Agnieszka Dobrzyn, Gyorgy Szabadkai, Barbara Zavan, Paulo J. Oliveira, Vilma A. Sardao, Paolo Pinton, Mariusz R. Wieckowski. "Mitochondria and Reactive Oxygen Species in Aging and Age-Related Diseases". *International Review of Cell and Molecular Biology, 2018, 340, pp 209-344. DOI: 10.1016/bs.ircmb.2018.05.006. IF (2018) – 3.788; Q2 (Biochemistry & Molecular Biology 96/299).*

Ines C. M. Simoes, Adriana Fontes, Paolo Pinton, Hans Zischka, Mariusz R. Wieckowski. "Mitochondria in non-alcoholic fatty liver disease". *The International Journal of Biochemistry & Cell Biology, 2017, 95, pp 93-99. DOI: 10.1016/j.biocel.2017.12.019. IF (2017) – 3.247; Q2 (Biochemistry & Molecular Biology 118/293).*

Other publications:

Ricardo Amorim, **Ines C. M. Simoes**, Caroline Veloso, Adriana Carvalho, Rui F. Simoes, Francisco B. Pereira, Theresa Thiel, Andrea Normann, Catarina Morais, Amalia S. Jurado, Mariusz R. Wieckowski, Jose Teixeira, Paulo J. Oliveira. "Exploratory Data Analysis of Cell and Mitochondrial High-Fat, High-Sugar Toxicity on Human HepG2 Cells". *Nutrients 2021, 13(5), 1723. DOI: 10.3390/nu13051723. IF (2020) – 5.717; Q1 (Nutrition & Dietetics 17/88).*

Ines C. M. Simoes, Giampaolo Morciano, Magdalena Lebiedzinska-Arciszewska, Gianluca Aguiaru, Paolo Pinton, Yaiza Potes, Mariusz R. Wieckowski. "The Mystery of Mitochondria-ER Contact Sites in Physiology and Pathology: A Cancer Perspective". *Biochimica et Biophysica Acta - Molecular Basis of Disease, 2020, 186 (10): 165834. DOI: 10.1016/j.bbadis.2020.165834. IF (2020) – 5.187; Q2 (Biochemistry & Molecular Biology 85/297).*

For publication:

Maciej K. Janik, Wiktor Smyk, Beata Kruk, Benedykt Szczepankiewicz, Barbara Górnicka, Magdalena Lebiedzińska-Arciszewska, Yaiza Potes, **Ines C. M. Simoes**, Susanne N. Weber, Frank Lammert, Mariusz R. Więckowski, Piotr Milkiewicz, Marcin Krawczyk. "MARC1 p.A165T variant is associated with decreased markers of liver injury and enhanced antioxidant capacity in autoimmune hepatitis". *Under review in Scientific reports Journal.*

Ricardo Amorim, **Ines C. M. Simoes**, Jose Teixeira, Yaiza Potes, Pedro Soares, Adriana Carvalho, Ludgero C. Tavares, Fernando Cagide, Sofia Benfeito, Susana P. Pereira, Rui F. Simoes, Agnieszka Karkucinska-Wieckowska, Ivan Viegas, Sylwia Szymanska, Michal Dabrowski, Justyna Janikiewicz, Teresa Cunha-Oliveira, Agnieszka Dobrzyn, John G. Jones, Fernanda Borges, Mariusz R. Wieckowski, Paulo J. Oliveira. "Phenolic mitochondria-targeted antioxidant AntiOxCIN4 improved simple steatosis phenotype by preventing hepatic lipid accumulation due to upregulation of fatty acid oxidation, quality

control mechanism and antioxidant defense systems in Western Diet-fed mice". *Under preparation*

The author states her major contribution to the conceptual design, experimental execution, data analysis and interpretation, and manuscript preparation of all the work presented along this thesis dissertation.

List of Figures

List of Tables

List of Abbreviations

4-HNE, 4-hydroxynonenal

4E-BP1, eukaryotic translation initiation factor 4E-binding protein 1

ABTS, 2,2'-azino-bis (3-ethylbenzothiazoline-6-sulfonic acid)

ACC, acetyl-CoA carboxylase

ACOX, acyl-CoA oxidase

ACS, acyl-CoA synthetase

ADP, adenosine diphosphate

ALT, alanine aminotransferase

AMPK, 5’ adenosine monophosphate-activated protein kinase

ANT, adenine nucleotide translocator

Apo, apolipoprotein

APS, ammonium persulfate

AST, aspartate aminotransferase

ATF, activating transcription factor

ATG, autophagy related

ATP, adenosine triphosphate

BN-PAGE, Blue native polyacrylamide gel electrophoresis

BSA, bovine serum albumin

CCL, C-C motif chemokine ligand

CEs, cholesteryl esters

CHOP, CCAAT/enhancer-binding homologous protein

CHOW, standard chow diet

CL, cardiolipin

CPT, carnitine palmitoyltransferase

CsA, cyclosporin A

CXCL10, C-X-C motif chemokine 10

DAG, diacylglycerol

DMSO, dimethyl sulfoxide

DNL, *de novo* lipogenesis

DNP, 2,4-dinitrophenyl hydrazone

DNPH, 2,4-dinitrophenylhydrazine

DTNB, 5,5'-dithio-bis-(2-nitrobenzoic acid)

EDTA, ethylenediaminotetraacetic acid

EGTA, ethyleneglycoltetraacetic acid

ER, endoplasmic reticulum

ETC, electron transport chain

$FADH_2$, flavin adenine dinucleotide

FAO, fatty acid oxidation

FAs, fatty acids

FAS, fatty acid synthase

FCCP, carbonyl cyanide-4-(trifluoromethoxy)phenylhydrazone

FFAs, free fatty acids

FXR, farnesoid X receptor

GC-MS, gas chromatography – mass spectrometry

Glut, glucose transporter

GPX, glutathione peroxidase

GR, glutathione reductase

GSH, reduced glutathione

GSSG, glutathione disulphide

H&E, hematoxylin and eosin

HCC, hepatocellular carcinoma

HDL, high-density lipoprotein

HEPES, 4-(2-hydroxyethyl)-1-piperazineethanesulfonic acid

HF, high-fat

HFD, high-fat diet

HFHS, high-fat plus high-sucrose

HMOX1, heme oxygenase 1

HRP, horseradish peroxidase

HS, high-sucrose

HSC*,* hepatic stellate cells

IMM, inner mitochondrial membrane

IRE1, X-box binding protein 1

JNK, c-Jun terminal kinase

KEAP1, Kelch-like ECH-associated protein 1

LAMP2, lysosome-associated membrane glycoprotein 2

LC-MS/MS, liquid chromatography-MS3 spectrometry

LC3, microtubule-associated protein 1A/1B light chain

LCFAs, long-chain fatty acids

LDL, low-density lipoprotein

LPL, lipoprotein lipase

mΔΨ, mitochondrial membrane potential

M6PR, cation-dependent mannose-6-phosphate receptor

MAS, mitochondrial assay solution

MCFAs, medium long-chain fatty acids

MDA, malondialdehyde

mitoQ, mitoquinone

MTBE, methyl tert-butyl ether

mPTP, mitochondrial permeability transition pore

mtDNA, mitochondrial DNA

mTORC1, mammalian target of rapamycin complex 1

MUC, mitochondrial calcium uniporter

MUFAs, monounsaturated fatty acids

NADH, β-nicotinamide adenine dinucleotide

NAFL, non-alcoholic fatty liver

NAFLD, non-alcoholic fatty liver disease

NAS, NAFLD activity score

NASH, non-alcoholic steatohepatitis

NBR1, autophagy cargo receptor

NMR, nuclear magnetic resonance

NTB, nitro tetrazolium blue chloride

NRF2, nuclear factor erythroid-derived 2 related factor 2

NQO1, NAD(P)H dehydrogenase (quinone) 1

OCR, oxygen rate measurement

OMM, outer mitochondrial membrane

OXPHOS, oxidative phosphorylation

PAS, periodic acid Schiff

PBS, phosphate-buffered saline

PC, phosphatidylcholine

PE, phosphatidylethanolamine

PERK, protein kinase RNA-like ER kinase

PGC-1α, proliferator-activated receptor-γ coactivator-1α

PHSF, primary human skin fibroblasts

PMSF, phenylmethylsulfonyl fluoride

PPAR, peroxisome-proliferator-activated receptor

PRDX, peroxiredoxin

PUFAs, polyunsaturated fatty acids

PVDF, polyvinylidene fluoride

RCR, respiratory control ratio

RNS, reactive nitrogen species

ROS, reactive oxygen species

S6K1, ribosomal protein S6 kinase β1

SCD1, stearoyl-CoA desaturase 1

SCFAs, short-chain fatty acids

SD, standard diet

SDS, sodium dodecyl sulfate

SEM, standard error of the mean

SFAs, saturated fatty acids

SIRT, sirtuin

SOD, superoxide dismutase

SQSTM1, sequestosome-1

tBHP, tert-butyl hydroperoxide

TBS, tris-buffered saline

TEMED, N,N,N',N'-tetramethylethylenediamine

TFAM, mitochondrial transcription factor A

TG, triglyceride

TLC, thin-layer chromatography

TLR, toll-like receptor

TMPD, N,N,N',N'-tetramethyl-p-phenylenediamine

TPP, triphenylphosphonium

UPR, unfolded protein response

VDAC, voltage-dependent anion channel

VLCFAs, very long-chain fatty acids

VLDL, very low-density lipoprotein

WD, Western diet

MS-proteomic related abbreviations:

ABCD, ATP-binding cassette sub-family D member (members 1, 2)

ACAA, 3-ketoacyl-CoA thiolase A (members 1A, 2)

ACACA, acetyl-CoA carboxylase 1

ACAD8, isobutyryl-CoA dehydrogenase

ACAD9, acyl-CoA dehydrogenase family member 9, mitochondrial

ACADL, long-chain specific acyl-CoA dehydrogenase, mitochondrial

ACADM, medium-chain specific acyl-CoA dehydrogenase, mitochondrial

ACADSB, short/branched chain specific acyl-CoA dehydrogenase, mitochondrial

ACLY, ATP-citrate synthase

ACOT, acyl-coenzyme A thioesterase (members 2, 3, 4, 8, 9, 12)

ACOX1, acyl-coenzyme A oxidase 1, peroxisomal

ACSL4, long-chain-fatty-acid-CoA ligase 4

ADCY9, adenylate cyclase type 9

ADPGK, ADP-dependent glucokinase

AGPAT3, glycerol-3-phosphate acyltransferase (members γ, 3)

AKT, Rac serine/threonine-protein kinase (members 1, 2)

ALDOC, fructose-bisphosphate aldolase C

ATG, autophagy-related protein (members 16L1, 2A, 2B, 3, 5, 9A)

ATG12, ubiquitin-like protein ATG12

ATG4B, cysteine protease ATG4B

ATG7, ubiquitin-like modifier-activating enzyme

ATP5, ATP synthase subunit (members C1, D, E, F1, H, I, J, J2, L, O, S)

ATPAF, ATP synthase mitochondrial F1 complex assembly factor (members 1, 2)

BAAT,bile acid-CoA:amino acid N-acyltransferase

BCS1L, ubiquinol-cytochrome c reductase complex chaperone, mitochondrial

BECN1, beclin-1

BNIP3, B-cell lymphoma 2/adenovirus E1B 19 kDa protein-interacting protein 3

BPGM, bisphosphoglycerate mutase

CAT, catalase

CCS, copper chaperone for superoxide dismutase

CD36, platelet glycoprotein 4

COA, cytochrome c oxidase assembly factor (members 3, 6, 7)

COX15, cytochrome c oxidase assembly protein COX15 homolog

COX17, cytochrome c oxidase copper chaperone

COX5A, cytochrome c oxidase subunit (members 4l1, 5A, 5B, 6A1, 6B1, 7A2, 7A2L)

CS, citrate synthase, mitochondrial

CSNK, casein kinase I isoform (members 1A1, D, 2A1, 2A2, 2B)

CTS, cathepsin (members B, D, F, O, L1, S, Z)

CTSH, pro-cathepsin H

CYC1, cytochrome c1, heme protein, mitochondrial

DEPTOR, DEP domain-containing mTOR-interacting protein

DGAT, diacylglycerol O-acyltransferase (members 1, 2)

DHTKD1, 2-oxoglutarate dehydrogenase E1 component DHKTD1, mitochondrial

DLAT, pyruvate dehydrogenase complex component E2, mitochondrial

ECH1, δ(3,5)-δ(2,4)-dienoyl-CoA isomerase, mitochondrial

ECHDC2, enoyl-CoA hydratase domain-containing protein (members 2, 3)

ECHS1, enoyl-CoA hydratase, mitochondrial

ECSIT, evolutionarily conserved signaling intermediate in Toll pathway, mitochondrial

EIF4EBP1, eukaryotic translation initiation factor 4E-binding protein 1

ELOVL, elongation of very long chain fatty acids protein (members 1, 2, 5, 6)

FABP2, fatty acid-binding protein (members 2, 4, 5)

FADS, fatty acid desaturase (members 1, 2)

FASN, fatty acid synthase

FASTKD2, FAST kinase domain-containing protein 2

FOXRED1, FAD-dependent oxidoreductase domain-containing protein 1

G6PC, glucose-6-phosphatase

GAA, lysosomal α-glucosidase

GCK, glucokinase regulatory protein

GK, glycerol kinase

GLRX, glutaredoxin (members 1, 3, 5)

GM20390, nucleoside diphosphate kinase

GPX1, glutathione peroxidase (members 1, 4)

GSK3A, glycogen synthase kinase (members 3A, 3B)

GSR, glutathione reductase, mitochondrial

GSS, glutathione synthetase

HADHA, trifunctional enzyme subunit α, mitochondrial

HCCS, cytochrome c-type heme lyase

HK, hexokinase (members 1, 3)

HMGCL, hydroxymethylglutaryl-CoA lyase, mitochondrial

IDH2, isocitrate dehydrogenase (members 2, 3A, 3B, 3G)

INSR, insulin receptor

LAMTOR1, ragulator complex protein LAMTOR (members 1, 5)

LIPE, hormone-sensitive lipase

LPIN2, phosphatidate phosphatase LPIN2

LRPPRC, leucine-rich PPR motif-containing protein, mitochondrial

MAVS, mitochondrial antiviral-signaling protein

MDH, malate dehydrogenase (members 1, 2)

MGLL, monoglyceride lipase

MLXIPL, carbohydrate-responsive element-binding protein

MPO, myeloperoxidase

MSRA, mitochondrial peptide methionine sulfoxide reductase

MSRB, methionine-R-sulfoxide reductase B (members 2, 3)

MT1, metallothionein-1

MTATP8, ATP synthase protein 8

MTCO, cytochrome c oxidase subunit (members 1, 2)

MTND, NADH-ubiquinone oxidoreductase chain (members 1, 4, 5)

MTOR, serine/threonine-protein kinase mTOR

MUL1, mitochondrial ubiquitin ligase activator of NFKB 1

NBR1, next to BRCA1 gene 1 protein

NDUFA, NADH dehydrogenase [ubiquinone] 1α subcomplex subunit (members 1, 5-10, 12, 13)

NDUFAB1, acyl carrier protein, mitochondrial

NDUFAF, NADH dehydrogenase [ubiquinone] 1α subcomplex assembly factor (members 1-4, 6, 7)

NDUFB3, NADH dehydrogenase [ubiquinone] 1β subcomplex subunit (members 3 – 11)

NDUFC2, NADH dehydrogenase [ubiquinone] 1 subunit C2

NDUFS, NADH dehydrogenase [ubiquinone] iron-sulfur protein (members 2-8)

NDUFV1, NADH dehydrogenase [ubiquinone] flavoprotein (members 1, 2, 3)

NUBPL, iron-sulfur protein - nucleotide binding protein like

NUDT14, uridine diphosphate glucose pyrophosphatase

PCX, pyruvate carboxylase, mitochondrial

PDHA1, pyruvate dehydrogenase E1 component subunit (members A1, B)

PDHX, pyruvate dehydrogenase protein X component, mitochondrial

PDIA6, protein disulfide-isomerase A6

PDPK1, 3-phosphoinositide-dependent protein kinase 1

PEX, peroxisome protein (members 1, 3, 5-7, 11A, 11B, 11G, 13, 14, 16, 19, 26)

PFKL, 6-phosphofructokinase (members L, P)

PGK2, phosphoglycerate kinase 2

PGAM1, phosphoglycerate mutase 1

PGM2, phosphoglucomutase-2

PIK3C2A, phosphatidylinositol 4-phosphate 3-kinase C2 domain-containing subunit α

PIK3C3, phosphatidylinositol 3-kinase (members C3, R1, R4)

PKLR, pyruvate kinase

PKM, isoform M1 of pyruvate kinase

PRDX, peroxiredoxin (members 1-5)

PRKAA1, 5'-AMP-activated protein kinase (members A1, A2, B1, G1)

PRKACA, cAMP-dependent protein kinase catalytic subunit (members A, B)

PRKAR1A, cAMP-dependent protein kinase regulatory subunit (members 1A, 2B)

PYGL, glycogen phosphorylase, liver form

PXMP4, peroxisomal membrane protein 4

RICTOR, rapamycin-insensitive companion of mTOR

RPS6KA1, ribosomal protein S6 kinase (members A1, A3, A4, B2)

SCAP, sterol regulatory element-binding protein cleavage-activating protein

SCD1, acyl-CoA desaturase 1

SCO1, synthesis of cytochrome c oxidase 1 homolog, mitochondrial

SDHB, succinate dehydrogenase [ubiquinone] iron-sulfur subunit, mitochondrial

SDHC, succinate dehydrogenase cytochrome b560 subunit, mitochondrial

SEPP1, selenoprotein P

SLC27A4, long-chain fatty acid transport protein 4

SLC25A20, mitochondrial carnitine/acylcarnitine carrier protein

SOAT2, sterol O-acyltransferase 2

SOD, superoxide dismutase (members 1-3)

SQSTM1, sequestosome-1

SUCLG1, succinyl-CoA ligase [GDP-forming] subunit (members 1, 2)

SURF1, surfeit locus protein 1

TACO1, translational activator of cytochrome c oxidase 1

TECR, very-long-chain enoyl-CoA reductase

TIGAR, fructose-2,6-bisphosphatase

TIMMDC1, complex I assembly factor, mitochondrial

TMEM16B, transmembrane protein 16B

TPI1, triosephosphate isomerase

TXN, thioredoxin

TXN2, thioredoxin, mitochondrial

TXNDC, thioredoxin domain-containing protein (members 5, 9, 12, 15, 17)

TXNL1, thioredoxin-like protein 1

TXNRD1, thioredoxin reductase (members 1, 3)

UQCC2, ubiquinol-cytochrome-c reductase complex assembly factor 2

UQCR10, cytochrome b-c1 complex subunit (members 10, B, C1, C2, H, FS1, Q)

ABSTRACT

Non-alcoholic fatty liver disease (NAFLD) affecting approximately 24% of the worldwide population is the main leading cause of chronic liver disease. The increased number of fatty liver cases considered as the hepatic manifestation of the metabolic syndrome, is rising in parallel with obesity and type 2 diabetes. This is mainly associated with the sedentary habits and overconsumption of hypercaloric diets. The initial stage of NAFLD - non-alcoholic fatty liver (NAFL) is characterized by a metabolic remodelling of the liver to compensate the overload of fat accumulation. Although, this compensatory event seems to be abolished during disease progression. Along this process, mitochondrial function impairment and an exacerbation of oxidative stress have been described to trigger hepatic signalling pathways associated with the initiation of inflammation, fibrosis and cirrhosis (transition to non-alcoholic steatohepatitis (NASH)). Despite the advances in the field, the primary mechanisms underlying the development of NAFL and its progression into NASH are complex and still incomplete.

In this context, my first aim was to study the hepatic and mitochondrial redox-associated alterations in a NAFL stage. I have characterized hepatic proteome, mitochondrial structure and function, reactive oxygen species (ROS) production and antioxidant defences in a mouse model of early NAFLD stage. Induction of NAFL resulted from a chronic feeding (16 weeks) of mice with different diets: high-fat, high-sucrose or high-fat plus high-sucrose diets. I have shown (see Chapter 1), that no excess of mitochondrial ROS took place in NAFL. Therefore, I have suggested that other organelles as peroxisomes rather than mitochondria contribute to hepatic oxidative stress. Moreover, I established that fat and sucrose (components of Western diet) differentially impair autophagy.

In the second aim, I investigated the specific end-points for mitochondrial dysfunction that represent “a point of no return” and which drive disease progression along time. NAFL development has been studied with the use Western diet (WD) in an early NAFLD stage mice model. The combination of high-fat and high-sucrose representing Western diet good resemble human NAFLD features of the disease development. In this part of my thesis (see Chapter 2), I demonstrated for the first time

the sequential events of mitochondrial alterations during NAFL development and progression. I showed that in a more progressive NAFL stage previously observed mitochondrial adaptation in NAFL was followed by a progressive decrease of mitochondrial respiration concomitant with a higher susceptibility to mitochondrial permeability transition pore (mPTP) opening. Importantly, it was proven that mitochondrial ROS are not the first hit causing disease progression. Instead, my findings continue to support the role of peroxisomes as possible contributors to the hepatic oxidative damage in the origin of hepatic injury and progression of the disease.

The last part of my thesis was focused on the testing of a dietary-based mitochondrially-targeted antioxidant as new therapeutics for NAFLD. In this context, I aimed to validate the effectiveness of such compound in the prevention of NAFL development (see Chapter 3). I demonstrated that AntiOxCIN$_4$ supplementation improved hepatocytes phenotype in a NAFL context. This included the stimulation of the hepatic fatty acids oxidation and the stimulation of the endogenous antioxidant defence system, as well as the prevention of autophagic flux blockage. These findings supported the idea that the AntiOxCIN$_4$ could be a new promising NAFLD therapeutics.

The unravelling of the molecular pathways involved in early events of NAFLD pathogenesis will allow the design more effective therapeutic approaches. These strategies able to delay or even revert NAFLD are urgently needed since the available NAFLD therapies are based only on lifestyles changes by implementation of exercise activity and healthy diets.

STRESZCZENIE

Niealkoholowa stłuszczeniowa choroba wątroby (ang., *Non-Alcoholic Fatty Liver Disease* - NAFLD) dotykająca około 24% światowej populacji, stała się główną przyczyną przewlekłej niewydolności wątroby. Wzrost liczby przypadków stłuszczenia wątroby jako jednego z objawów zespołu metabolicznego, rośnie równolegle z otyłością i cukrzycą typu 2. Jest to głównie związane z siedzącym trybem życia, brakiem aktywności fizycznej oraz spożywaniem wysokokalorycznego pokarmu. Początkowy etap NAFLD - niealkoholowe stłuszczenie wątroby (NAFL), charakteryzuje się zmianami w metabolizmie wątroby w celu skompensowania nadmiernej akumulacji tłuszczu. Niestety tego typu mechanizmy kompensacyjne zanikają w kolejnych stadiach choroby. Uważa się, że upośledzenie funkcji mitochondriów i nasilenie stresu oksydacyjnego mogą być odpowiedzialne za inicjację stanu zapalnego i zwłóknienia, co powoduje rozwój choroby w kierunku stłuszczeniowego zapalenia wątroby (NASH), a następnie marskości tego narządu. Pomimo postępów w badaniach nad NAFLD, złożone mechanizmy leżące u podstaw przejścia z NAFL do NASH, wciąż nie są w pełni poznane.

Dlatego też, moim pierwszym celem było zbadanie zmian związanych z zaburzeniem procesów redoks w wątrobie i mitochondriach wątroby na wczesnym etapie choroby (NAFL). Scharakteryzowałam proteom wątroby, strukturę i funkcję mitochondriów, wytwarzanie reaktywnych form tlenu (RFT) i obronę antyoksydacyjną w mysim modelu wczesnego stadium NAFLD. NAFL był wynikiem przewlekłego karmienia (16 tygodni) myszy różnymi dietami: dietą wysokotłuszczową (HF), dietą wysokocukrową (HS) oraz dietą wysokotłuszczową wzbogaconą w sacharozę (HFHS). Wykazałam (patrz Rozdział 1), że w NAFL mitochondria nie przyczyniają się do zwiększonej produkcji RFT. Zasugerowałam, że to m.in. peroksysomy przyczyniają się do stresu oksydacyjnego obserwowanego w wątrobie. Dodatkowo ustaliłam, że tłuszcze i węglowodany w różny sposób zaburzają proces autofagii.

Drugim celem mojej pracy było zbadanie specyficznych punktów końcowych dysfunkcji mitochondriów, które stanowią tak zwany „punkt bez powrotu" i kierują postępem choroby w czasie. Wykorzystując dietę wysokotłuszczową, wzbogaconą w sacharozę, która najlepiej naśladuje nawyki żywieniowe naszego społeczeństwa (ang.:

Western Diet) zbadałam mechanizmy zaangażowane w rozwój NAFLD. W tej części pracy (patrz Rozdział 2), jako pierwsza pokazałam sekwencje zaburzeń mitochondrialnych podczas rozwoju i progresji NAFL. Wykazałam, że w bardziej zaawansowanym stadium NAFL, po pierwotnej adaptacji mitochondriów, następował postępujący spadek oddychania mitochondrialnego, któremu towarzyszyła większa podatność na otwarcie mitochondrialnego megakanału. Co ważne, udowodniłam, że RFT powstające w mitochondriach nie są czynnikiem odpowiedzialnym za postęp choroby. Dodatkowo, wyniki moich badań wskazują na peroksysomy jako możliwe źródło RFT przyczyniających się do oksydacyjnych uszkodzeń wątroby, będących przyczyną narastania uszkodzenia wątroby.

Ostatnia część mojej pracy koncentrowała się na wykorzystaniu, kierowanego do mitochondriów przeciwutleniacza jako nowego środka terapeutycznego w leczeniu NAFLD. Postanowiłam sprawdzić skuteczność takiego związku w zahamowaniu rozwoju NAFL (patrz Rozdział 3). Wykazałam, że suplementacja AntiOxCIN4 poprawiła funkcjonowanie hepatocytów w kontekście rozwoju NAFL. Zjawisko to obejmowało stymulację utleniania kwasów tłuszczowych i aktywację systemu obrony antyoksydacyjnej, a także zapobieganie zahamowania procesu autofagii. Moje badania wydają się potwierdzać tezę, że AntiOxCIN4 może być nowym obiecującym lekiem na NAFLD.

Odkrywanie szlaków molekularnych zaangażowanych we wczesne etapy patogenezy NAFLD pozwoli na zaprojektowanie bardziej skutecznego podejścia terapeutycznego. Te strategie, mogące opóźnić lub nawet zahamować postęp NAFLD są niezwykle potrzebne, ponieważ dostępne obecnie terapie NAFLD oparte są jedynie na zaleceniach zmiany stylu życia poprzez wdrożenie aktywności fizycznej i zdrowej diety.

Part I: General Introduction

1. NON-ALCOHOLIC FATTY LIVER DISEASE

1.1 Description

Non-alcoholic fatty liver disease (NAFLD) is the most common liver disease worldwide, characterized by the accumulation of fat in the liver with the exclusion of alcohol consumption, chronic liver diseases or secondary causes of fat accumulation as medications. NAFLD is an abbreviation for the spectrum of different stages that NAFLD comprises (**Figure 1**). Thus, non-alcoholic fatty liver (NAFL) or simple steatosis is defined as the initial stage of NAFLD when more than 5% of hepatocytes accumulate fat. Despite benign, this condition can progress to non-alcoholic steatohepatitis (NASH), a state with evidence of hepatocyte damage. Then, the presence of significant fibrosis can further culminate in cirrhosis and/-or in hepatocellular carcinoma (HCC) (Chalasani, Younossi et al. 2012, Younossi, Koenig et al. 2016).

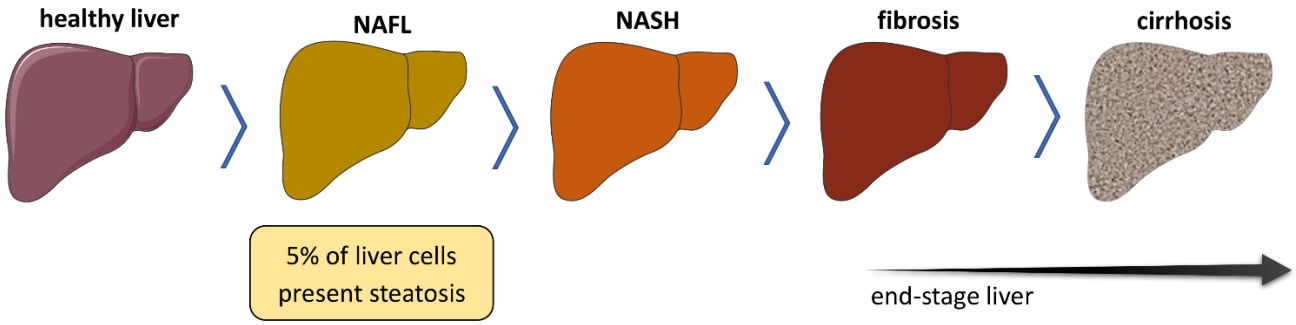

Figure 1. NAFLD spectrum. NAFLD starts with the accumulation of fat in a healthy liver. When at least 5% of hepatocytes present fat accumulation, it is called simple steatosis. This stage can progress into non-alcoholic steatohepatitis (NASH) which is characterized by inflammation in the presence or not of fibrosis. Liver injury is then associated with the development of fibrosis, with consequent cirrhosis and hepatocellular carcinoma. Abbreviations: NAFL – non-alcoholic fatty liver; NASH – non-alcoholic steatohepatitis.

1.2 Epidemiology

The prevalence of this disease has increased in the last decades, and it is estimated that approximately 24% of the worldwide population has NAFLD. The highest

prevalence of the disease has been reported in Middle East (32%), South America (31%), Asia (27%), North America (24%) and Europe (23%) (Younossi, Anstee et al. 2018). It was reported that type 2 diabetes is considered as a strongest predictor for disease progression (McPherson, Hardy et al. 2015), being estimated that 10-25% of NAFL patients progress to NASH. There is an increasing disease burden associated with NASH and more advanced stages such as cirrhosis and HCC, with fibrosis considered as the strongest predictor for NAFLD-associated mortality (Ekstedt, Hagstrom et al. 2015). In an UK cohort of patients, NAFLD-HCC patients represented 35% of all HCC patients (Dyson, Jaques et al. 2014), and cirrhosis was indicated as the most common indicator for liver transplantation (Williams, Aspinall et al. 2014). Projections for the upcoming year of 2030 estimate that NASH-associated cirrhosis and HCC will increase by 168% and 137%, respectively, and the associated mortality will increase by 178% (Bzowej 2018).

1.3 Risk factors

NAFLD is known as the hepatic manifestation of metabolic syndrome. Its development is associated with sedentary lifestyles (Chalasani, Younossi et al. 2012). Therefore, obesity, type 2 diabetes, hyperlipidaemia and hypertension have been indicated as risk factors for the development of NAFLD. It is estimated that 90% of NAFLD patients possess at least one of the above-mentioned diseases. Although NAFLD has been mostly associated with obesity-associated disorders, a subset of patients has the so-called lean NAFLD. Its prevalence has increased, being estimated to be as high as 19% in Asia (Fan, Kim et al. 2017). This condition has been underestimated, but recent findings demonstrate that lean and obese patients share a similar metabolic and cardiovascular profile (Sookoian and Pirola 2017). As risk factors, high body fat, high cholesterol and high-fructose intake and genetic predisposition are pointed as initial hits for lean NAFLD (Xu, Yu et al. 2013). In fact, it has been reported that distinct alleles also confer genetic predisposition to the development and progression of NAFLD. Patatin-like phospholipase domain-containing protein 3 (PNPLA3) is involved in the hydrolysis of triglycerides (TGs) in hepatocytes and retinyl esters in stellate cells, respectively. The p.I148M variant was associated with a loss of function with consequent hepatic lipid accumulation (Romeo, Kozlitina et al. 2008). Additionally, membrane bound O-

acyltransferase domain-containing 7 gene (MBOAT7) is associated to the regulation of arachidonic levels by its lysophosphatidylinositol acyltransferase activity. Its genetic variant rs641738 C>T causes a decrease in gene expression and function (Mancina, Dongiovanni et al. 2016). Transmembrane 6 superfamily member 2 (TM6SF2) is involved in the secretion of very low-density lipoprotein (VLDL) particles, being the variant p. E167K associated with lower secretion of VLDL particles from the liver (Krawczyk, Rau et al. 2017). However, the exact mechanisms behind genetic inheritance have not been clarified.

1.4 Clinical diagnosis and management

In the past years, NAFLD has been established as a multisystemic disease due to an increasing risk of NAFLD patients (not necessarily with hepatic failure) to suffer from cardiovascular diseases, infectious diseases and carcinoma (Adams, Anstee et al. 2017, Sinn, Kang et al. 2020). There are some blood markers that may be used as indicators of liver injury, but they can also be useful in the diagnosis, evaluation of the disease severity, and monitoring. This includes the assessment of aminotransferases (aspartate aminotransferase (ASP) and alanine aminotransferase (ALT)), alkaline phosphatase and γ-glutamyl transferase in serum. Focusing on ALT and AST, these enzymes are elevated when liver cell integrity is affected, and ALT is considered more specific than AST (Dufour, Lott et al. 2000). Nevertheless, liver biopsy is considered as the gold standard approach for hepatic histopathology, thereby enabling the differentiation between NAFL, NASH and end-liver stages (Roeb, Steffen et al. 2015, Kleiner, Brunt et al. 2019). However, due to its invasiveness and possible complications, liver biopsy is limited to selected patients. Since the definition and the distinction between no NASH, borderline and NASH have varied over time and among pathologists, it was established a list of criteria necessary for diagnostic purposes: steatosis superior to 5% and any degree of hepatocyte ballooning (characterized by Mallory-Denk bodies inclusions) and lobular inflammation (Sanyal, Brunt et al. 2011). Then, these criteria were organized in pathological scores as NAFLD activity score (NAS)(Kleiner, Brunt et al. 2005) or Steatosis activity fibrosis (SAF) score (Bedossa, Poitou et al. 2012). Of relevance, NAS is defined as the unweighted sum of semi-quantitatively analysis of steatosis (0-3), lobular

inflammation (0-2) and hepatocyte ballooning (0-2). A value inferior to 3 is not considered NASH while a value equal or superior to 5 corresponds to NASH (Kleiner, Brunt et al. 2005). Additionally, the evaluation of fibrosis is performed.

It is important to mention that alternative non-invasive methods have been developed in order to evaluate NAFLD. Abdominal sonography is a sensitive method that allows the diagnosis of NAFL (steatotic liver also called “bright liver”) but it does not permit the distinction between more severe NAFLD stages. Another method is the vibration-controlled transient elastography with controlled attenuation parameters that assess liver parameters as steatosis and fibrosis. This method has been used just as a follow up tool in NAFLD patients (Lim, Flamm et al. 2017). However, the above-mentioned methods are not accurate enough, and none of them was applied in clinical practice.

There are also lacking pharmacological therapies for this disease (Roeb and Geier 2019). Indeed, a change to healthy dietary habits and the practice of physical exercise are the unique recommended approaches to prevent and treat the disease (Romero-Gomez, Zelber-Sagi et al. 2017), being weight-loss surgeries as bariatric surgery or intragastric balloon also considered beneficial to the amelioration of liver function in obese patients (Lee, Low et al. 2012, von Schonfels, Beckmann et al. 2018). Although patients with end-liver stages such as cirrhosis can undergo liver transplantation, it is important to stress that transplantation does not cure metabolic-associated NAFLD diseases, and it is imperative to develop more effective strategies before transplant (Haldar, Kern et al. 2019).

1.5 Pathophysiology: (possible and proposed) mechanisms of NAFLD development

The pathogenesis of NAFLD is described by the multiple-hits theory. Accordingly, after a first hit constituted by the accumulation of fat in the form of lipid droplets inside hepatocytes, multiple interacting factors including insulin resistance, mitochondrial dysfunction, oxidative stress, altered gut microbiota and genetic predisposition may cause the progression of NAFL into more severe stages (Guilherme, Virbasius et al. 2008, Bugianesi, Moscatiello et al. 2010).

1.5.1 Liver structure and function

The liver constitutes the largest gland of the human body, composed by irregular structures, called lobules, composed by parenchymal and non-parenchymal cells. Parenchymal cells consist of hepatocytes, which account for approximately 78-80% of the liver volume. Non-parenchymal cells (endothelial cells, Kupffer cells and stellate cells) constitute only 5-6% of the liver volume while the remaining 14-17% correspond to other components of the hepatic extracellular space (Blouin, Bolender et al. 1977).

Hepatocytes constitute the most important type of cell in the liver. These cells have a diameter of 25 µm with cytoplasm enriched in approximately 1000 mitochondria per cell. This cellular composition is required due to the high metabolic activity of these cells in diverse functions. Hepatocytes are responsible for processing nutrients absorbed in the gastrointestinal tract, thereby synthesizing proteins, carbohydrates and lipids. Importantly, these cells are involved in the synthesis and secretion of albumin and blood coagulation factors such as fibrinogen and pro-thrombin (Heinz and Braspenning 2015). Due to the fact that the liver is a central organ receiving blood from gastrointestinal tract, spleen and other parts of the body, hepatocytes also exert a role in systemic and local inflammatory and immunological processes (MacPhee, Schmidt et al. 1992).

Endothelial cells represent 45% of non-parenchymal cells. These cells possess pores or so-called fenestrations, a distinct feature that permits the free passage of blood and solutes to the perisinusoidal space of Disse where there is direct contact with hepatocytes (Wisse, Braet et al. 1996). Additionally, these cells exert a role in immune response. In fact, it was showed that endothelial cells can efficiently become antigen-expressing cells, thereby mediating T cell activation (Knolle, Germann et al. 1999).

Kupffer cells are considered the main phagocytic population of the liver and constitute approximately 80-90% of total macrophage body population. These cells are the first to be in contact with blood constituents, being responsible for the elimination of large particles such as endotoxins, antigens and microorganisms (Naito, Hasegawa et al. 1997). Once activated, these cells are involved in the generation of pro-inflammatory mediators such as cytokines, reactive oxygen/nitrogen species (ROS/RNS) and chemokines (Tacke, Luedde et al. 2009). It was demonstrated that Kupffer cells can modulate fibrogenic response by promoting a greater activation of hepatic stellate cells

(HSC) (Nieto 2006). Moreover, these cells can migrate to other areas of infection or damage (Heymann, Hammerich et al. 2012).

Stellate cells are mainly responsible for the transport and accumulation of retinoids (vitamin A-derived compounds) in cytosolic droplets (Wake 1971), but also the secretion of apolipoprotein (Apo)E and prostaglandins (Friedman, Liu et al. 1991, Athari, Hanecke et al. 1994), insulin-like growth factors I and II (Pinzani, Abboud et al. 1990) and epithelial growth factors (Bachem, Meyer et al. 1992). HSC are involved with hepatic's response to injury. Accordingly, quiescent HSC could differentiate, developing a myofibroblast-like cell phenotype that can produce and deposit excessive amounts of extracellular matrix proteins, such as collagen types I, III and IV (Iredale 2001).

The liver plays a myriad of functions, from synthesis of molecules, defense of the organism from external insults and excretion of substances into the bile (**Figure 2**). The liver accumulates and regulates iron and copper distribution throughout the body (Doguer, Ha et al. 2018). Another important role is the detoxification of exogenous substances (e.g. food substances, chemical compounds, drugs) that if retained in the body for long periods could cause deleterious effects on human health (Grant 1991). The liver is involved in protein synthesis and degradation of proteins and other cytoplasmic macromolecules, a critical process providing free amino acids for energy production during starvation (Mortimore, Poso et al. 1989). Importantly, liver is the unique organ in the body that possesses enzymatic machinery for ammonia detoxification through urea cycle (Olde Damink, Jalan et al. 2009).

The liver is also responsible for carbohydrates and lipid metabolism. Once absorbed in the intestinal lumen, ingested glucose, fructose and lipids enter the portal circulation and are transported to the liver. In contrast to glucose, fructose is primarily metabolized in the liver by being nearly extracted from blood upon the first-pass (Mayes 1993). Glucose transporter (GLUT) 2 and GLUT8 have been demonstrated to be the main glucose and fructose transporters in the liver (Leturque, Brot-Laroche et al. 2005, Debosch, Chen et al. 2014). Because the metabolism of fructose has less steps than glycolysis, fructose generates much faster triose phosphate intermediaries that could be used to gluconeogenesis and glycogenesis, within other pathways depending on the nutritional status of the organism and long-term dietary habits (Iizuka 2017).

Importantly, the liver is the main source of glycogen in the body. Due to that fact, glucose is mobilized to systemic circulation and extra-hepatic tissues according to metabolic energy needs (Cole and Kramer 2016). Isotope tracer studies have showed that in an acute ingestion, fructose is converted mostly to glucose (29-54%) or lactate (28%), other part is oxidized (31-59%) and just a minor percentage (1%) is used in *de novo* lipogenesis (DNL) pathway (Sun and Empie 2012). However, chronic fructose exposure leads to increased availability of DNL metabolites and lipogenic transcription factors, thereby exacerbating hepatic lipid synthesis (Faeh, Minehira et al. 2005, Stanhope, Schwarz et al. 2009). In addition to the DNL pathway, there are other pathways contributing to the hepatic lipid content: lipolysis of free fatty acids (FFAs) in adipose tissue and absorbed intestinal fat. Chylomicrons can be hydrolyzed to FFAs in the presence of lipoprotein lipase (LPL) in endothelial cells of peripheral tissues (e.g. adipose tissue specialized in fat accumulation). The resultant TGs and cholesteryl esters (CE)-enriched chylomicrons remnants are taken up to the hepatocytes by interaction between ApoE and a low-density lipoprotein (LDL) receptor-mediated endocytosis process. Hepatic cholesterol pool is tightly controlled by its uptake from the intestinal tract and from remnant lipoproteins, cholesterol *de novo* synthesis and its secretion into the enterohepatic circulation in the form of bile acids. As output pathway, hepatic TGs (from DNL or re-esterification of fatty acids (FAs)) and cholesterol can be packed into VLDL particles surrounded by ApoE and ApoB-100, which are secreted into circulation. The liver is also responsible for the secretion and recycling of LDL and high-density lipoprotein (HDL) particles (Arnold and Kwiterovich 2003). In addition, carbohydrates and lipids can fuel mitochondrial-fatty acid oxidation (FAO) with energy and carbon dioxide generation. Particularly relevant in fasting conditions, mitochondrial-FAO can contribute to the production of ketone bodies preferentially oxidized by the central nervous system over glucose or fatty acids (Hawkins, Mans et al. 1986). Evidence has demonstrated that a positive energy balance between the lipid input and the output may originate excessive hepatic lipid accumulation as observed in NAFL (Fabbrini, Magkos et al. 2009)

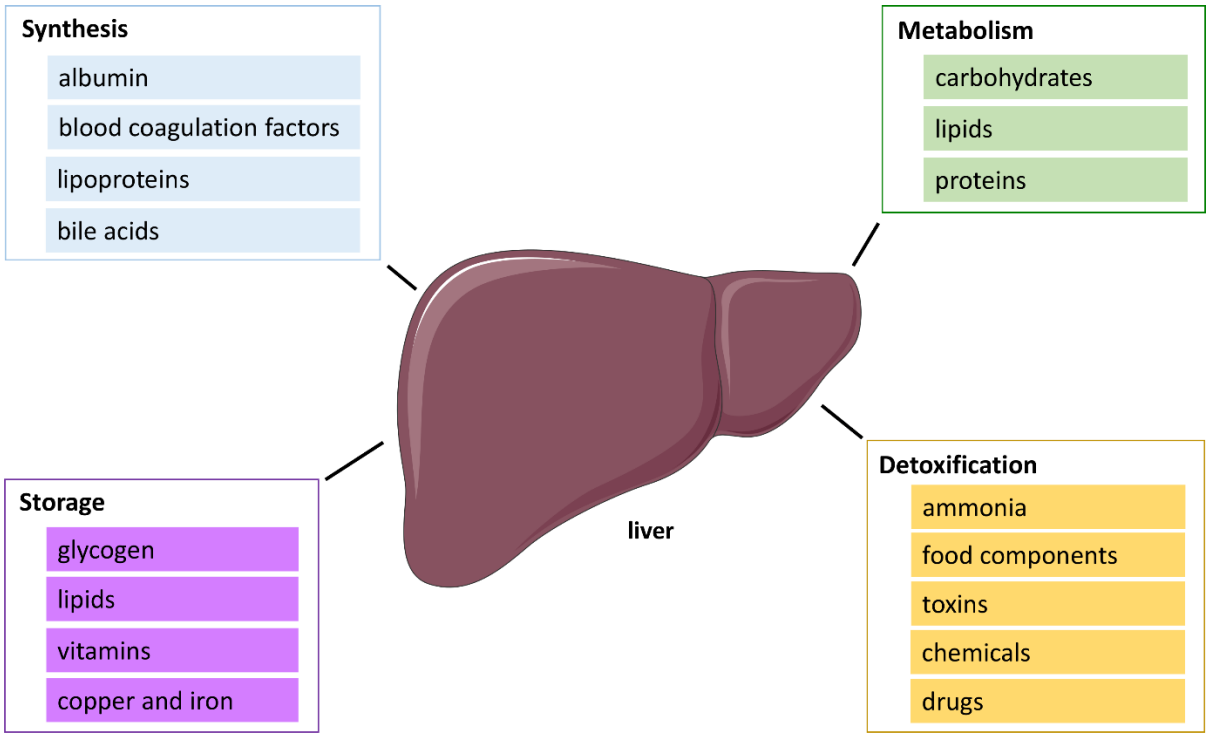

Figure 2. Liver main functions. The liver plays a critical role in the synthesis of blood components (e.g. albumin and coagulation factors), lipoproteins composed by cholesterol and triglycerides, recycling of low-density lipoproteins and high-density lipoproteins and bile synthesis. The liver is also responsible for the metabolism of carbohydrates, lipids and proteins, from which can result the storage of glycogen and lipids. The liver can accumulate vitamins and minerals such as copper and iron. Moreover, the liver is the organ responsible for detoxifying ammonia, food components, toxins, chemicals and drugs.

1.5.2 Lipid accumulation

Hepatic fat accumulation is caused by an imbalance between an increased FAs inflow and an impaired clearance of FAs in the liver (Asrih and Jornayvaz 2014). Excess calorie intake and an increased lipolysis of FFAs from adipose tissue result in high FFAs circulating levels which are taken up by hepatocytes. Once in hepatocytes, there is an increase of DNL pathway as demonstrated in patients with NAFLD (Lambert, Ramos-Roman et al. 2014) (**Figure 3**). Donnelly and colleagues have showed that 60% of hepatic TGs are derived from adipose tissue, 26% from DNL and 15% from calories intake (Donnelly, Smith et al. 2005). The high rate of DNL is stimulated by hyperglycaemic and hyperinsulinemia conditions under the activation of transcriptional factors sterol regulatory element binding protein-1c (SREBP-1), carbohydrate responsive element

binding protein (ChREBP) and peroxisome proliferator-activated receptor (PPAR)-γ (Dentin, Girard et al. 2005, Higuchi, Kato et al. 2008, Ferramosca and Zara 2014). The activation of SREBP-1 induces the expression of acetyl-CoA carboxylase (ACC) and fatty acid synthase (FAS) enzymes, both considered as rate-limiting enzymes of hepatic lipogenesis (Kohjima, Enjoji et al. 2007, Higuchi, Kato et al. 2008, Xie, Li et al. 2010). TGs accumulation has shown to have a protective role against hepatic inflammation and fibrosis (Yamaguchi, Yang et al. 2007). Although, it is important to highlight that acyl chain FAs composition may also determine disease progression. Mice knock-out of stearoyl-CoA desaturase 1 (SCD1), enzyme responsible for monounsaturated fatty acids (MUFAs) synthesis, showed to be protected from obesity-induced steatosis but possess increased hepatic apoptosis and fibrosis (Rizki, Arnaboldi et al. 2006). This demonstrates that the accumulation of saturated FAs (SFAs) is cytotoxic (Wang, Wei et al. 2006, Wei, Wang et al. 2006), being MUFAs synthesis responsible for the development of hepatic steatosis with no evidence of liver injury (Listenberger, Han et al. 2003).

Hepatic steatosis seems to be an adaptative mechanism of hepatocytes to the excess caloric supply. Nevertheless, other mechanisms seem to exacerbate hepatic lipid accumulation: FAO and the export of lipids in VLDL particles (**Figure 3**). Indeed, a decrease of FAO is described in a high-fat diet-fed animal model (Ferramosca and Zara 2014). This finding is correlated with decreased mitochondrial function and is associated with inhibition of the oxidative phosphorylation (OXPHOS) complexes and increased mitochondrial ROS production (Vial, Dubouchaud et al. 2011). However, there are some contradictory data in clinical studies, where FAO is reported to be enhanced (Sanyal, Campbell-Sargent et al. 2001, Miele, Grieco et al. 2003, Dasarathy, Kasumov et al. 2009) or either decreased (Croci, Byrne et al. 2013). Then, it is suggested that a compensatory elevation of mitochondrial- and peroxisomal-FAO during steatosis may be abolished with an increase of NAS score and disease severity (Francque, Verrijken et al. 2015, von Loeffelholz, Docke et al. 2017). Moreover, the export of VLDL particles from the liver is increased in NAFLD patients, where the secretion rate is proportional to the hepatic TGs content (Adiels, Taskinen et al. 2006, Fabbrini, Mohammed et al. 2008, Fabbrini, Magkos et al. 2009). Although, this compensatory mechanism also fails to counteract hepatic lipid accumulation when reaches more than 10% of total hepatic fat accumulation (Fabbrini, Mohammed et al. 2008).

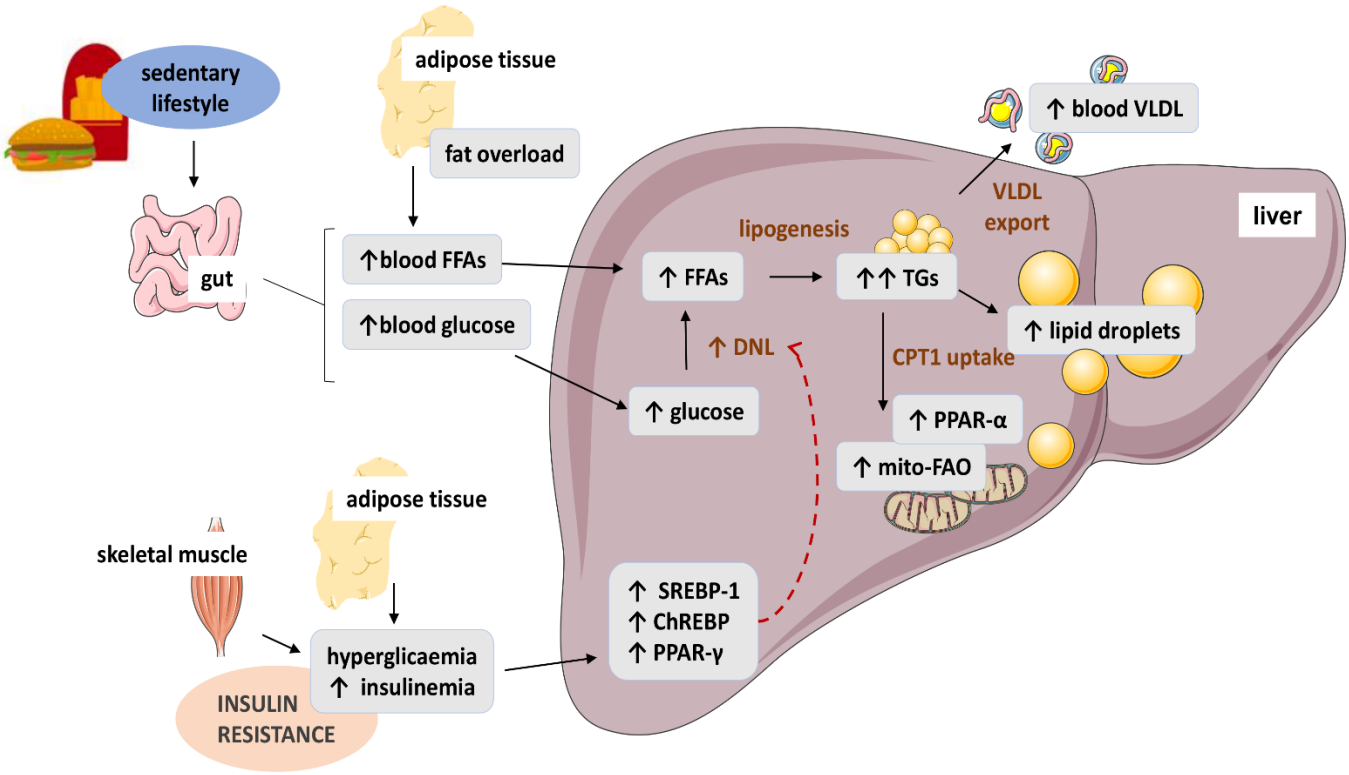

Figure 3. Hepatic lipid accumulation-associated mechanisms. Hypercaloric diets and lipolysis of FFAs from adipose tissue exacerbate the circulating levels of FFAs and glucose, with consequent uptake by the liver. Glucose is converted into FFAs by DNL, being the increased FFAs levels then converted into TGs. DNL is also promoted by insulin resistance conditions in the skeletal muscle and adipose tissue through the activation of hepatic transcriptional factors SREBP-1, ChREBP and PPAR-γ. TGs can accumulate in the liver in the form of lipid droplets, can be released in the form of VLDL particles into the blood or can be diverted to mitochondrial FAO. Abbreviations: ChREBP - carbohydrate responsive element binding protein; CPT1 - carnitine palmitoyltransferase 1; DNL – *de novo* lipogenesis; FFAs – free fatty acids; mito-FAO – mitochondrial fatty acid oxidation; PPAR- peroxisome proliferator-activated receptor; SREBP-1 - sterol regulatory element binding protein-1c; VLDL - very low-density lipoprotein.

1.5.3 Mitochondrial physiology and pathology

1.5.3.1 Mitochondrial structure and function

Mitochondria are composed by an outer (OMM) and an inner mitochondrial membrane (IMM), with an intermembrane space dividing them. Double membrane structure surrounds a matrix where mitochondrial DNA (mtDNA) and many proteins reside (Vogel, Bornhovd et al. 2006). Mitochondria possess their own circular mtDNA

which is encoding 22 tRNAs, 2 rRNAs and only 13 mitochondrial proteins. Other mitochondrial proteins are encoded by nuclear DNA (Neupert 1997, D'Erchia, Atlante et al. 2015). The IMM is constituted by two distinct domains: an inner boundary membrane contiguous with the OMM, and cristae, considered as tubular structures closely tied with inner boundary membrane at cristae junctions (Frey and Mannella 2000, Scheffler 2001). Notably, cristae invaginations allow for a significant increase of mitochondrial surface where proteins of oxidative phosphorylation are embedded.

Mitochondrial membranes are mainly composed by phospholipids (approximately 80% of phosphatidylcholine (PC) and phosphatidylethanolamine (PE); and 10-15% of cardiolipin, sterols and proteins. Although, this content quite differs between OMM and IMM. The outer membrane has higher fluidity by being composed of a higher content of phospholipids and cholesterol and a lower content of proteins compared to the inner membrane. Thus, IMM possesses a high amount of PE while anionic cardiolipin is almost exclusively present in this membrane (Horvath and Daum 2013). Cardiolipin plays not only important structural but also functional role in mitochondria, namely the stabilization of the mitochondrial carrier proteins (Noel and Pande 1986, Nury, Dahout-Gonzalez et al. 2006) and respiratory chain complexes, thereby protecting their activity (Gomez and Robinson 1999, Sedlak and Robinson 1999).

Moreover, mitochondrial membranes have different permeabilities. The IMM is highly impermeable with the transport of molecules done through multiple specific transporters, such as adenine nucleotide translocator, phosphate carrier, tricarboxylate transporter and carnitine shuttle. Moreover, the electrochemical gradient of protons generated in intermembrane space is created by the transport of protons through OXPHOS complexes inserted in the IMM (Saraste 1999). In contrast, the transport through OMM is less well regulated, and metabolites can cross this membrane through the voltage-dependent anion channel (VDAC), a transmembrane channel that allows the free transport of nearly all molecules up to 5 kDa (Colombini 2004). In this process, ions and protein transport require an electrochemical gradient across the mitochondrial membrane. The mitochondrial content in the cell is regulated by the production of new mitochondria – biogenesis; and by the degradation of damaged and non-functional mitochondria – mitophagy. Perturbations at the level of mitochondrial structure and

dynamics could have implications for their proper function (Hunter, Haworth et al. 1976).

1.5.3.1.1 Mitochondrial fatty acid oxidation

Mitochondria are involved in the oxidation of long-chain FAs (LCFAs) (C13 to C21), medium-chain FAs (MCFAs) (C6 to C12) and short-chain FAs (SCFAs) (<C6). In a fed state, hepatic LCFAs are esterified into TGs, which are accumulated in the liver or secreted in the form of VLDL to the systemic circulation. During this process, malonyl-CoA, the first intermediate of DNL, inhibits carnitine palmitoyltransferase (CPT)1, which is responsible for transferring LCFAs inside mitochondria where mitochondrial-FAO takes place (Xiao, Hsieh et al. 2011). In fasting conditions, adipose tissue lipolysis and TGs uptake by the liver provide energy and precursors for hepatic gluconeogenesis and ketogenesis that supply glucose for whole body energy homeostasis (Oh, Han et al. 2013). With low levels of malonyl-CoA, LCFAs are activated to long-chain acyl CoAs by acyl-CoA synthetase (ACS) followed by its conversion to acylcarnitines by CPT1 at OMM. In this latter form, acylcarnitines are translocated to the mitochondrial matrix by carnitine-acylcarnitine translocase and converted back to long-chain acyl-CoAs by CPT2 (Kerner and Hoppel 2000). Then, all FAs enter in four sequential reaction cycles. Each cycle of oxidation generates flavin adenine dinucleotide ($FADH_2$) and nicotinamide adenine dinucleotide (NADH), which are oxidized by the respiratory electron transport chain (ETC), and one molecule of acetyl-CoA. During fasting, the resultant acetyl-CoA molecules may enter the tricarboxylic acid (TCA) cycle or contribute to the production of ketone bodies, namely, acetoacetate and β-hydroxybutyrate that can be further transported and oxidized by the TCA cycle in other tissues (Houten, Violante et al. 2016).

Although mitochondria are considered the main site for FAO, it should be also taken into account the contribution of peroxisomes and microsomes in this process (Lazarow and De Duve 1976). Indeed, very long chain FAs (VLCFAs) (C>22) are preferentially oxidized in peroxisomes through a four-step reaction that includes acyl-CoA oxidase (ACOX), enoyl-Coa hydratase, 3-hydroxyl-acyl-Coa dehydrogenase and β-ketothiolase. In each reaction cycle, this pathway originates one acetyl-CoA and one acyl-CoA molecule with hydrogen peroxide (H_2O_2) generation. Therefore, peroxisomes

act as a FAs shortening system, being MCFAs further diverted into the mitochondria where FAO is completed (Fransen, Lismont et al. 2017)).

In alternative, LCFAs can be oxidized through microsomal ω-FAO in microsomes. LCFAs can be metabolized into dicarboxylic acids in these organelles mainly through members of oxido-reductase cytochrome P450 (CYP2E1/ CYP4A) family. In the first step of the reaction, NADPH and O_2 are converted into superoxide anion ($O_2^{\bullet-}$) and H_2O_2 as by-products. Then, the resulting dicarboxylic acids are subsequently metabolized by peroxisomes/-or mitochondria (Chitturi and Farrell 2001). Peroxisomal and microsomal FAO can be upregulated in situations of hepatic fat overload or when mitochondrial function gets compromised.

1.5.3.1.2 Electron transport chain (ETC) and energy production

Firstly described by Mitchell in 1961, the chemiosmotic theory describes that along the transfer of electrons through ETC, protons are translocated from the mitochondrial matrix across the IMM to the intermembrane space what is connected with the generation of a proton-motive force that drives ATP synthesis. (Mitchell 1961). All reducing equivalents (e.g. NADH and $FADH_2$) generated in glycolysis, TCA cycle and FAO processes are oxidized in mitochondrial ETC by different enzymes complexes (Chance and Williams 1955). ETC is constituted by four complexes containing different prosthetic groups (flavine, Fe-S groups, heme centers) and several carriers that allow the flux of electrons from Complex I to Complex IV where a four-electron transfer culminates with the conversion of molecular oxygen to water (**Figure 4**). The four multi-subunits complexes are designated as NADH-ubiquinone oxidoreductase (Complex I), succinate dehydrogenase (Complex II), ubiquinol-cytochrome c reductase (Complex III) and cytochrome c oxidase (Complex IV) (Green and Tzagoloff 1966). Complex I and II catalyze the electron transfer from NADH and succinate to ubiquinone, respectively. It is important to highlight that Complex I is the major contributor for the ETC electrons entry, and its activity is considered a rate-limiting step of oxidative phosphorylation. Ubiquinone is a mobile redox molecule localized in the IMM, and is responsible for the transfer of two electrons (in the form of ubiquinol) to Complex III. Then, electrons are transferred from Complex III to cytochrome c, a hydrophilic protein localized at the

external leaflet of IMM, that conducts electrons to Complex IV and ultimately to the final acceptor oxygen (Nicholls and Ferguson 2013).

Electron transfer through ETC is done from a lower to a higher redox potential in three of the ETC complexes - Complex I, III and IV. This causes conformational changes in the complexes, allowing the translocation of protons from the mitochondrial matrix to the intermembrane space, except Complex II which does not contribute to the protons translocation across the IMM because its redox potential is equivalent to the ubiquinone. This movement of protons generates a pH gradient and a voltage gradient (membrane potential) across IMM. Together, these two components constitute the electrochemical proton gradient. Since the IMM is a highly impermeable membrane, protons cannot diffuse back to the matrix. Instead, electrochemical gradient enables the transport of protons back to the mitochondrial matrix through ATP synthase down their concentration gradient, with the generation of ATP from ADP and inorganic phosphate (Nicholls and Ferguson 2013) (**Figure 4**). According to the "plasticity model", OXPHOS complexes are organized between free respiratory complexes and respiratory supercomplexes, which optimizes the efficiency of ETC but it can also prevent pathological derangements with increased ROS formation (Schagger and Pfeiffer 2001, Lenaz, Baracca et al. 2010, Acin-Perez and Enriquez 2014).

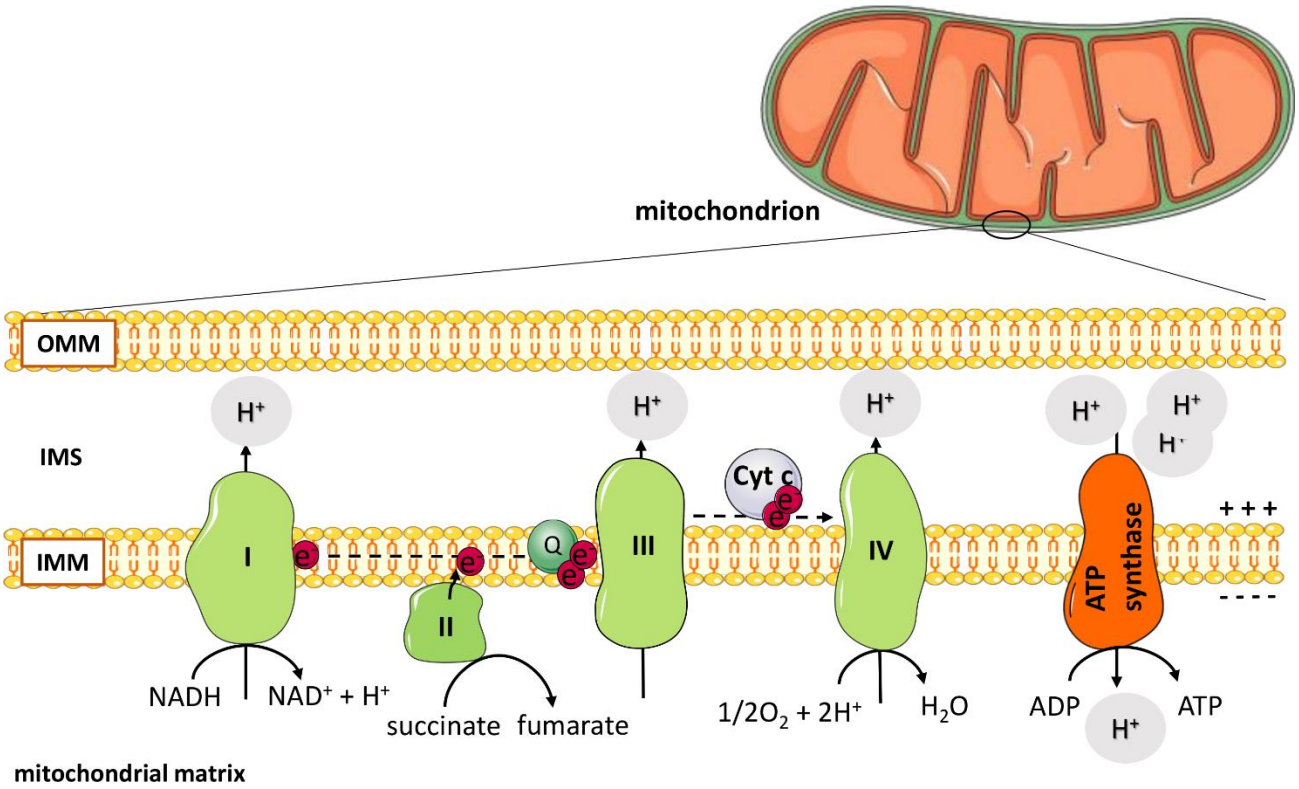

Figure 4. Mitochondrial oxidative phosphorylation. Mitochondria are composed of a double membrane, IMS and matrix. OXPHOS complexes are in the IMM. In the presence of reduced substrates, electrons are transferred along the electron transport chain to the Complex IV where electrons reduce molecular oxygen to water. During this process, protons are translocated from mitochondrial matrix to the IMS through Complex I, Complex III and Complex IV. This proton gradient enables the ATP synthesis at the level of ATP synthase, being protons pumped back to the mitochondrial matrix. Abbreviations: cyt c – cytochrome c; IMM – inner mitochondrial membrane; IMS – intermembrane space; OMM – outer mitochondrial membrane; Q – ubiquinone.

1.5.3.1.3 Ca^{2+} homeostasis

The level of Ca^{2+} inside mitochondria is critical for the mitochondrial metabolism, what causes that alterations of cellular Ca^{2+} homeostasis are detrimental for the mitochondrial function.

Mitochondrial free Ca^{2+} concentration ranges from 0.17 to 5.0 µM (Delierneux, Kouba et al. 2020). This range results from a fine-tuning between Ca^{2+} uptake from extramitochondrial space, Ca^{2+} buffering in the mitochondrial matrix and Ca^{2+} efflux to the cytosol. These processes are tightly coupled to the electrochemical gradient and to cytoplasmic free Ca^{2+} levels. Thus, in the presence of high extra-mitochondrial Ca^{2+}

concentrations, mitochondria can transiently take up Ca^{2+}, a process that activate mitochondrial enzymes, namely those involved in TCA cycle and OXPHOS, thereby stimulating ATP synthesis (Jouaville, Pinton et al. 1999). Moreover, this ion can also regulate uncoupling proteins (Graier, Trenker et al. 2008) and activate mPTP (Rasola and Bernardi 2011).

To reach the mitochondrial matrix, cytosolic Ca^{2+} can cross the OMM through the high permeable VDAC channel. Since the IMM is much less permeable, Ca^{2+} cross this membrane through the mitochondrial calcium uniporter (MCU) according the electrochemical gradient (Gunter and Pfeiffer 1990). Several mitochondrial regulators of MCU are identified (e.g. MICU1/2 and MCUR1), which act as gatekeepers of the channel (Mallilankaraman, Cardenas et al. 2012, Ahuja and Muallem 2014). At the mitochondrial matrix level, Ca^{2+} concentration is buffered by forming insoluble and relatively inert complexes in the presence of phosphates (Lehninger, Rossi et al. 1963). The calcium extrusion from mitochondria to the cytosol is regulated by $Na^+/Ca^{2+}/Li^+$ exchanger. Such mechanism was initially identified in the ER and plasma membrane. Later it was also found in the IMM, being responsible for the extrusion of one Ca^{2+} and the import of three Na^+ ions (Palty, Silverman et al. 2010). Although Na^+/Ca^{2+} antiporter is expressed in liver mitochondria, recent evidence has shown its activity mostly in brain and heart. Thus H^+/Ca^{2+} antiporter (extrusion of one Ca^{2+} and the import of two H^+) is the main responsible for Ca^{2+} extrusion in the liver (Rysted, Lin et al. 2021). Moreover, its activity has been associated with the maintenance of the cristae structure (Tamai, Iida et al. 2008, Shao, Fu et al. 2016).

1.5.3.1.4 Mitochondrial permeability transition pore

mPTP opening constitutes another potential pathway involved in Ca^{2+} efflux under certain physiological circumstances (Bernardi and Di Lisa 2015, Halestrap and Richardson 2015). However, mPTP opening has been associated with a detrimental mitochondrial function and consequently, cell damage and death. In fact, mitochondrial Ca^{2+} overload, especially during oxidative/nitrosative stress can sensitize mPTP to open (Haworth and Hunter 1979). In this state, it is formed a pore spanning IMM and OMM with high-permeability to solutes up to 1.5 kDa and water (Crompton, Costi et al. 1987).

The mPTP opening is responsible for two main consequences. Firstly, it is associated with loss of mΔΨ and uncoupling of OXPHOS, thereby causing ATPase to work in a reverse mode. Therefore, ATP depletion causes the disruption of mitochondrial metabolism and the activation of cellular necrosis (Szabo, Bernardi et al. 1992, Scorrano, Petronilli et al. 1997, Crompton 1999). Secondly, upon mPTP opening, there is an equilibrium of low molecular weight solutes between mitochondrial matrix and cytosol, while mitochondrial protein concentration is still high. This leads to a mitochondrial matrix-related osmotic pressure, and subsequent mitochondrial swelling that comprises the unfolding of cristae and the expansion of the matrix against OMM. Swelling may not affect IMM integrity but eventually, this process may result in OMM rupture with the release of cytochrome c and the initiation of pro-apoptotic cascades (Martinou and Green 2001, Crompton, Barksby et al. 2002, Green and Kroemer 2004).

The structure/composition of mPTP on IMM is highly controversial, and in fact it has evolved along the time with different hypotheses proposing adenine nucleotide translocator (ANT), VDAC, phosphate carrier, ATP synthase or spastic paraplegia 7 pointed as possible candidates for this complex structure (Halestrap and Brenner 2003, Leung, Varanyuwatana et al. 2008, Giorgio, von Stockum et al. 2013, Alavian, Beutner et al. 2014, Shanmughapriya, Rajan et al. 2015). Although this is a topic still under investigation (He, Ford et al. 2017), it was unequivocally accepted the role of cyclophilin D as the regulator of pore opening at mitochondrial matrix, being this component inhibited in the presence of cyclosporin A (CsA) (Halestrap and Davidson 1990).

1.5.4 Mitochondrial failure in NAFLD

In NAFL, a mitochondrial metabolic shift has been reported to overcome hepatic lipid accumulation (Koliaki, Szendroedi et al. 2015). This includes an increased mitochondrial mass (Mansouri, Gattolliat et al. 2018) and function, including an increased mitochondrial FAO, TCA cycle induction and stimulation of OXPHOS (Sunny, Parks et al. 2011). This is a process regulated by PPAR-α, which promotes FFAs delivery to the mitochondria, and by 5’ adenosine monophosphate-activated protein kinase (AMPK), which inhibits DNL and promotes FAO by preventing CPT-1 inhibition (Rolo, Teodoro et al. 2012). In this stage, an upregulation of UCP2 seems to protect

hepatocytes from the deleterious effect of ROS (Serviddio, Bellanti et al. 2008). Despite these early adaptative mechanisms, peroxisomes, microsomes and mitochondria cannot handle the excess of FFAs that exceeds the rate of FAO, resulting in the generation of lipid-derived intermediates such as ceramides, diacylglycerols (DAGs) and long-chain acyl-coA molecules. Importantly, the accumulation of these lipotoxic intermediates induce hepatic lipotoxicity rather the simple process of fat accumulation. Ceramides, which are involved in the biosynthesis of sphingolipids, can supress mitochondrial ETC and promote ROS production, while ceramides depletion has been shown to protect OXPHOS complexes activities (Chaurasia, Tippetts et al. 2019). Moreover, ceramides have been associated with the inhibition of mitochondrial FAO and they are responsible for the negative regulation of insulin-related pathways in different tissues involving Akt pathway (Chavez, Siddique et al. 2014). Similarly, increased levels of DAGs are reported to activate protein kinase C in skeletal muscle and liver, which subsequently decreases insulin receptor-1/-2 phosphorylation, leading to the impairment of insulin signaling pathway (Petersen, Madiraju et al. 2016). Thus, the induction of mitochondrial FAO can decrease DAGs accumulation and is reported to protect the liver from insulin resistance (Savage, Choi et al. 2006).

Along NAFLD progression, it has been reported a decrease of mitochondrial biogenesis, despite the fact that higher mitochondrial mass was found increased in NAFLD patients (Mansouri, Gattolliat et al. 2018). Despite higher mass, mitochondria are swollen with de-arrangement of cristae structure which is suggested to be linked to defective clearance of damaged and/-or malfunctioning mitochondria (Koliaki, Szendroedi et al. 2015). Moreover, an increased cellular accumulation of cholesterol is reported to induce alterations in mitochondrial membrane permeability, which may be linked to mitochondrial glutathione depletion in NASH (Mari, Caballero et al. 2006, Gan, Van Rooyen et al. 2014). Altered mitochondrial structure is in agreement with observed alterations in the mitochondrial function. Hepatic accumulation of dicarboxylic acids (predominantly due to microsomal FAO) can inhibit Complexes I and II and coenzyme Q (Passi, Picardo et al. 1984). Alterations in the level of ETC complexes and their activities have been reported in several NAFLD models (Teodoro, Rolo et al. 2008, Rector, Thyfault et al. 2010, Eccleston, Andringa et al. 2011), which is associated with decreased mitochondrial respiration, decreased mitochondrial membrane potential ($m\Delta\Psi$),

opening of the mPTP and ATP depletion (Teodoro, Rolo et al. 2008). Then, decreased cellular ATP levels could trigger endoplasmic reticulum (ER) stress and the unfolded protein response (UPR), which is linked to the activation of DNL and exacerbation of hepatic steatosis (Lee, Homma et al. 2017). Importantly, these pathways seem to play a key role in the induction of hepatocyte death and activation of inflammatory pathways (Willy, Young et al. 2015). In more advance stages of the disease, it is reported a decrease of mitochondrial DNA in hepatocytes (Aubert, Begriche et al. 2012, Garcia-Martinez, Santoro et al. 2016). Interestingly, it has been suggested by Garcia-Martinez and colleagues that such decrease is correlated with augmented levels of circulating mitochondrial DNA which further activates toll-like receptor (TLR)9 involved in the pro-inflammatory response (Garcia-Martinez, Santoro et al. 2016).

The molecular mechanisms underlying mitochondrial adaptation and dysfunction along NAFLD progression are still not fully clarified, possibly resulting from disparities in dietary composition of high-fat diets, duration of treatment, animal models, or methods to assess mitochondrial function. However, it is mainly suggested that mitochondrial ROS provokes mitochondrial oxidative stress resulting in mitochondrial impairment and hepatic oxidative injury (Begriche, Massart et al. 2013).

1.6 Imbalance of ROS homeostasis and oxidative stress

1.6.1 Mitochondrial ROS production

Mitochondria have been reported as the major ROS generator organelles in NAFLD (Begriche, Massart et al. 2013). This is due to the continuous supply of reduced substrates to the ETC which leads to the leak of electrons at Complex I from the ubiquinone-binding site, the flavin-binding site and the forward movement of electrons associated with a reduced NADH pool (Kussmaul and Hirst 2006, Treberg, Quinlan et al. 2011). By reacting with an oxygen molecule, there is a production of $O_2^{\bullet-}$ and sequentially H_2O_2. Additionally, the outer ubiquinone-binding site of Complex III also highly contribute to $O_2^{\bullet-}/H_2O_2$ production rate (Bleier and Drose 2013, Perevoshchikova, Quinlan et al. 2013). Also, glycerol 3-phosphate dehydrogenase is a site of $O_2^{\bullet-}$ production in the intermembrane space and matrix sides of the IMM. Furthermore,

other dehydrogenases responsible for NAD^+ reduction (e.g. 2-oxoglutarate dehydrogenase complex, pyruvate dehydrogenase) and for ubiquinone pool (e.g. Complex II) have been also described to contribute in $O_2^{\bullet-}/H_2O_2$ production (Brand 2016) (**Figure 5 and 6**). ROS play a crucial role as cellular second messengers (Giorgi, Marchi et al. 2018), although by being highly reactive, they can also interact with mitochondrial components, perpetuating the formation of radical products (e.g. lipid peroxyl radicals) and oxidative damage (D'Autreaux and Toledano 2007).

A tight balance between the production and degradation of ROS is coordinated by several cellular scavenging systems, which include enzymatic (**Figure 5**) and non-enzymatic antioxidants. Enzymatic mechanisms include superoxide dismutase (SOD)1 in cytosol, SOD2 in mitochondria and SOD3 in extracellular space, which converts $O_2^{\bullet-}$ into H_2O_2, which can be further converted into H_20 and O_2 by catalase, especially in mitochondria and peroxisomes (Salvi, Battaglia et al. 2007). While catalase is more efficient with high ROS levels, the glutathione system has the main action with low or mild ROS levels. Then, H_2O_2 is also converted into H_20 by the action of glutathione peroxidase (GPx) with oxidized glutathione disulphide (GSSG) converted back to its reduced form (GSH) by the action of glutathione reductase (GR). H_2O_2 can also be reduced by the action of peroxiredoxin (PRDX), using reduced thioredoxin as the electron donor. Apart from enzymes, molecules obtained through the diet (e.g. ascorbic acid, vitamin E) or produced by the organism (e.g. albumin, glutathione) may also play a role in the antioxidant defense system (Aydin, Ozturk et al. 1996).

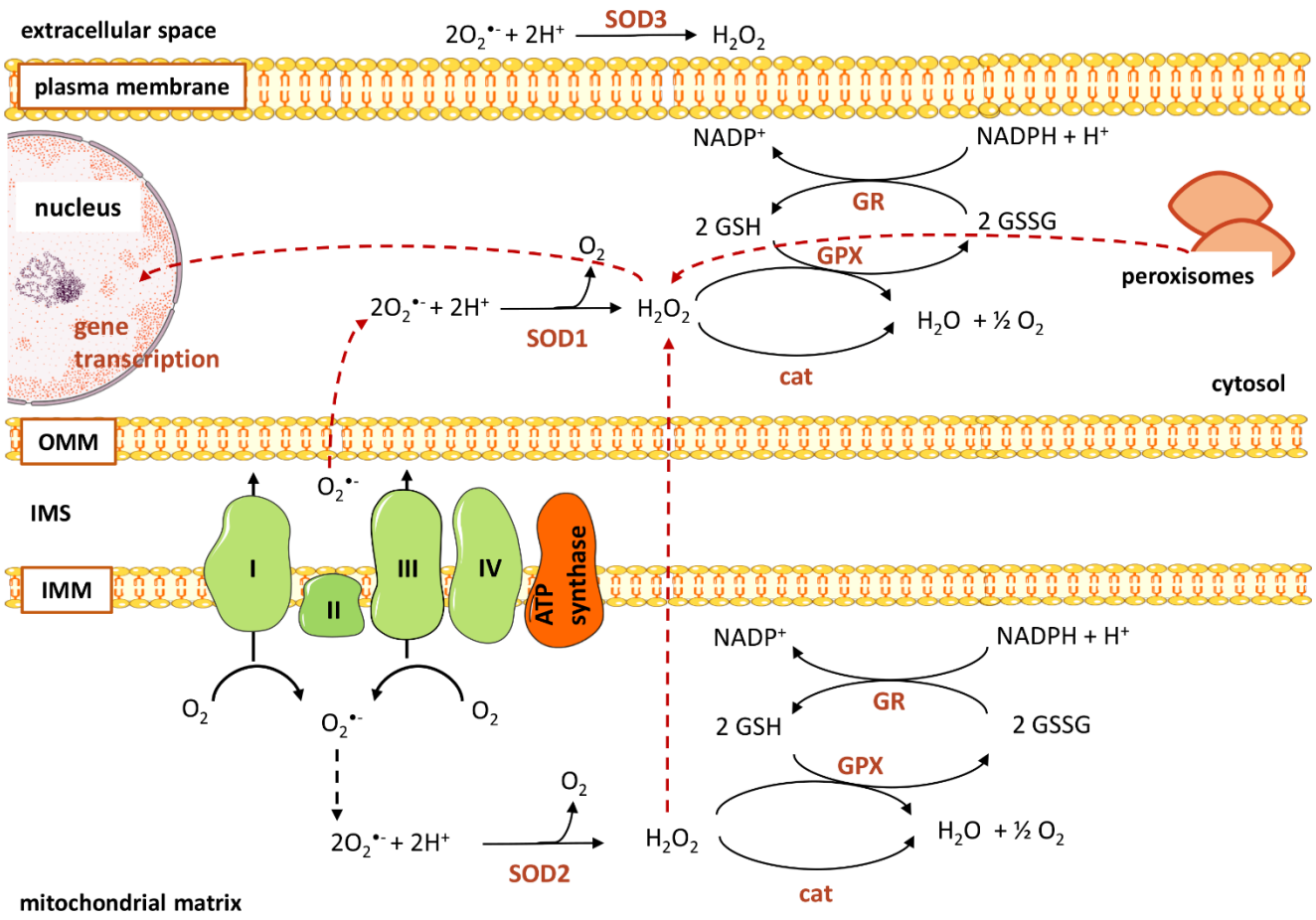

Figure 5. Main cellular antioxidant defense enzymes responsible for ROS detoxification. $O_2^{\bullet-}$ in mitochondria can be dismutated by SOD2, and H_2O_2 can be detoxified by catalase or by GPx/GR system. ROS can also diffuse into the cytosol or even to the extracellular space where cytosolic antioxidant enzymes (e.g. SOD1, catalase, GPx/GR system) or extracellular enzymes (e.g. SOD3) can act. Abbreviations: GPx – glutathione peroxidase; GR – glutathione reductase; GSH - reduced glutathione; GSSG – disulphide glutathione; IMM – inner mitochondrial membrane; IMS – inner mitochondrial space; OMM – outer mitochondrial membrane; SOD – superoxide dismutase.

1.6.2 Oxidative stress

A pro-oxidant state with increased ROS production and impaired levels/activities of ROS-detoxification mechanisms have been reported in NAFLD animal models and in NAFLD patients (Koruk, Taysi et al. 2004, Rector, Thyfault et al. 2010, Kumar, Sharma et al. 2013). Despite an increased mitochondrial activity may protect hepatocytes from lipotoxicity, increased mitochondrial activity under excess lipid influx can generate ROS in excess as observed in *in vitro* and *in vivo* models of steatosis (Eccleston, Andringa et

al. 2011, Lockman, Baren et al. 2012). Upon interaction with $O_2^{\bullet-}$, the nuclear factor erythroid-derived 2 related factor 2 (NRF2) activates the expression of a compensatory antioxidant defense response (Lohr, Pachl et al. 2016). A mitochondrial pro-oxidant state can overwhelm the mitochondrial antioxidant system (decreased *SOD*, *GPX1* activity, and *GSH*/*GSSG* ratio levels) (Rector, Thyfault et al. 2010, Gan, Van Rooyen et al. 2014) and results in oxidative modification of lipids (lipid peroxidation - malondialdehyde (MDA) and 4-hydroxy-2-nonenal (HNE)), proteins (carbonylation and nitration), and nucleic acids (mtDNA depletion and DNA damage – 8-hydroxy-2'-deoxyguanosine) during the progression of NAFL towards NASH and beyond (Valdecantos, Perez-Matute et al. 2012, Mendez, Pazos et al. 2014, Wang, Liu et al. 2015). Of relevance, it is described that oxidative stress can induce cardiolipin oxidation. This may change inner mitochondrial membrane properties with consequent destabilization of OXPHOS complexes and mPTP opening (Li, Romestaing et al. 2010). Cardiolipin oxidation may also cause the release of cytochrome c into the cytosol, activating the apoptotic cascade pathway (Kagan, Tyurin et al. 2005). Additionally, mitochondrial DNA damage is associated with a downregulation of regulatory transcription factors involved in mitochondrial biogenesis such as peroxisome proliferator-activated receptor-γ coactivator-1α (PGC-1α), mitochondrial transcription factor A (TFAM) and NRF2 (Aharoni-Simon, Hann-Obercyger et al. 2011, Koliaki, Szendroedi et al. 2015). Therefore, a pro-oxidant state is described to precede mitochondrial oxidative injury which is further linked to the impairment of mitochondrial function in NAFLD (Rector, Thyfault et al. 2010).

Despite high ROS levels and oxidative stress being associated with mitochondrial dysfunction, several studies lack direct evidence that mitochondria act as the primary site of ROS generation in NAFLD (Rector, Thyfault et al. 2010, Wang, Liu et al. 2015, Braud, Battault et al. 2017). Moreover, in a recent study, Einer and colleagues reported mitochondrial adaptation with no signs of mitochondrial oxidative stress in steatotic mice (Einer, Hohenester et al. 2018). These findings are in line with some old evidence showing that peroxisomes (mainly xanthine oxidase and ACOX (Bonekamp, Volkl et al. 2009)) and microsomes (mainly CYP2E1 (Bhattacharyya, Sinha et al. 2014)) are the main contributors for ROS generation on hepatocytes (**Figure 6**). In such a scenario mitochondria seem to be important but play a role as a secondary ROS source (Chance,

Sies et al. 1979). This is consistent with the up-regulation of peroxisomal transcription factors and higher levels of peroxisomal-related proteins in livers of HF fed-mice (Matsuzawa-Nagata, Takamura et al. 2008) and in NAFLD patients (Collins, Scheinberg et al. 1989, De Craemer, Pauwels et al. 1995), what resulted in increased peroxisomal FAO associated with an exacerbation of oxidative stress in microvesicular steatosis (Natarajan, Eapen et al. 2006). Additionally, an up-regulation of microsomal FAO was found in NAFLD (Emery, Fisher et al. 2003, Mantena, Vaughn et al. 2009, Bell, Temm et al. 2010). The upregulation of CYP2E1 levels and activity was accompanied by nitration and carbonylation of proteins, advance glycation end-products and lipid peroxidation (Abdelmegeed, Banerjee et al. 2012).

Despite mitochondria, peroxisomes and microsomes seem to contribute to oxidative stress in an early stage of NAFLD, more research studies are required to determine each ROS-generating pathway's contribution. Nonetheless, oxidative stress and the accumulation of hepatocyte oxidative damage are in the origin of the maladaptative response of hepatocytes to fat accumulation, thereby leading to hepatic metabolic impairment and NASH (Garcia-Martinez, Santoro et al. 2016, Simoes, Fontes et al. 2018).

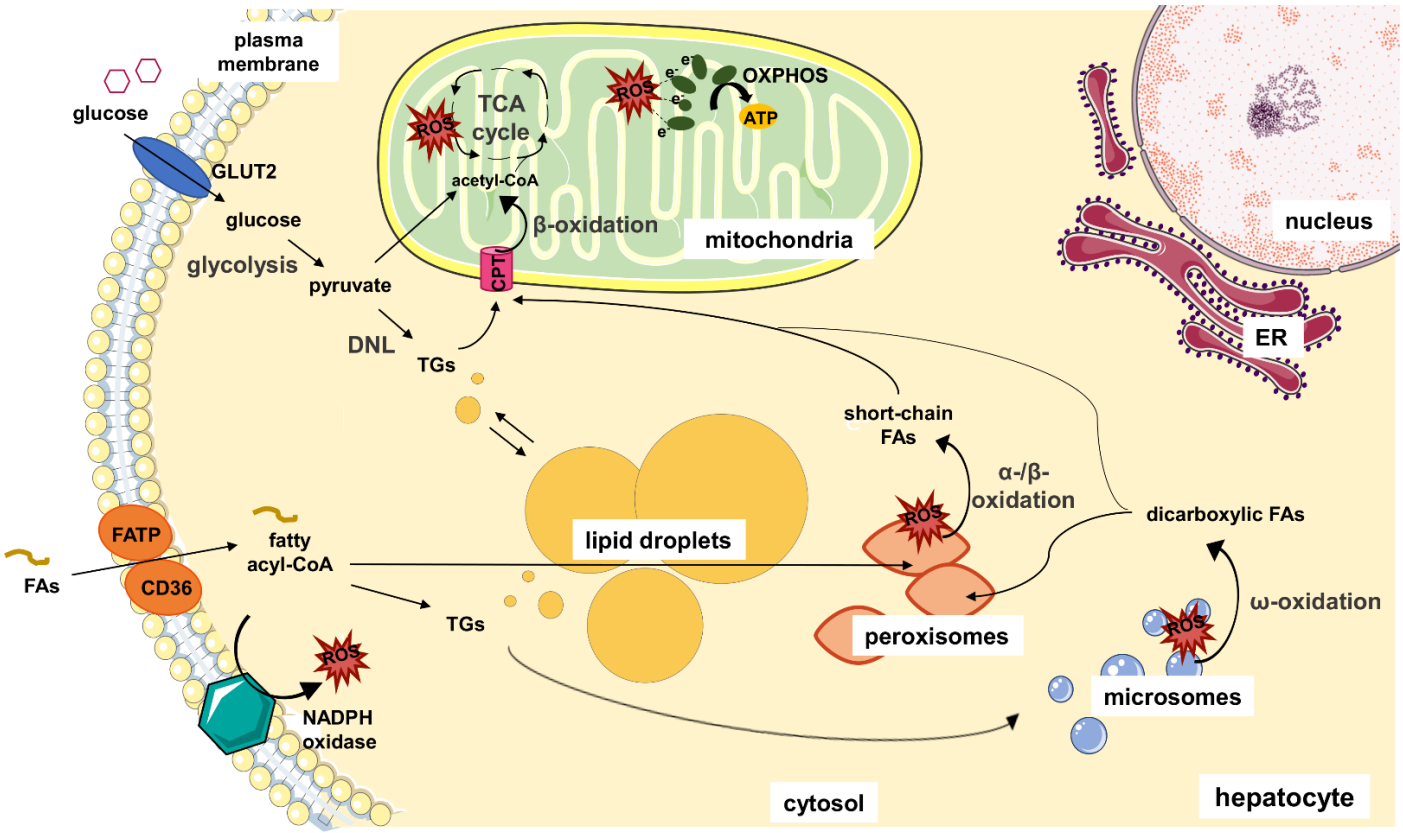

Figure 6. Contribution of distinct hepatocyte ROS sources for oxidative stress in NAFLD. Mitochondria, peroxisomes, microsomes and NADPH oxidase represent the main sources of ROS generation during the hepatic lipid overflow in an early stage of NAFLD. Abbreviations: CD36 - cluster of differentiation; CPT – carnitine palmitoyl transferase; DNL – de novo lipogenesis; ER – endoplasmic reticulum; FAs – fatty acids; FATP – fatty acid transporter protein; GLUT – glucose transporter; ROS – reactive oxygen species; TCA – tricarboxylic acid cycle; TGs – triglycerides. Adapted from (Karkucinska-Wieckowska, Simoes et al. 2021).

1.7 Endoplasmic reticulum stress

The ER is an organelle responsible for protein synthesis and folding, and the regulation of misfolded and damaged proteins (Schroder and Kaufman 2005). Perturbances in this process (e.g. hyperlipidaemia, inflammation) induce the accumulation of misfolded proteins in ER lumen and subsequent ER stress. In this context, UPR is activated to alleviate ER stress and restore protein homeostasis (Walter and Ron 2011). UPR is a well-conserved pathway that includes the activation of three ER transmembrane proteins: inositol-requiring protein 1 (IRE1), activating transcription factor (ATF)6 and protein kinase RNA-like ER kinase (PERK), once the chaperone binding

immunoglobulin protein dissociates from them (Henkel 2018). This coordinated activation ensures the reduction of protein synthesis, an increase of chaperone proteins involved in protein folding and transport, and lastly, an increase of misfolded proteins degradation (Gong, Wang et al. 2017). However, an excessive accumulation of misfolded proteins as caused by Ca^{2+} disorders or oxidative stress may induce ER-induced apoptosis, a process mediated by c-Jun terminal kinase (JNK) and CCAAT/enhancer-binding homologous protein (CHOP) (Henkel and Green 2013). Activation of ER stress in NAFLD patients has been reported to result in higher levels of downstream targets IRE1 (X-box binding protein 1), cleaved ATF6 and CHOP levels in their livers (Lee, Kim et al. 2017). Interestingly, this activation has been associated with hepatic lipid accumulation. This observation was supported by the accumulation of lipids in rodents' livers treated with ER stress inducer (Moslehi, Farahabadi et al. 2018). In other study, palmitic acid was reported to induce hepatic lipotoxicity via TLR4-IRE1 pathway (Shen, Ma et al. 2018). Under ER stress, the limited capacity of ER to degrade misfolded proteins can also induce autophagy, through the activation of PERK-ATF4 and IRE1-JNK pathways (Koh, Wang et al. 2018, Moslehi, Farahabadi et al. 2018).

1.8 Autophagy

Autophagy is a well conserved pathway which allows the degradation of proteins and cellular organelles in lysosomes, thereby regulating the turnover of cytosolic constitution (Yin, Ding et al. 2008). In the presence of limited energy supply, autophagy allows cell survival by providing energy production and degradation products for the biosynthesis of new macromolecules. Moreover, autophagy is a known quality and quantity control mechanism by removing damage molecules/organelles after oxidative injury (Ueno and Komatsu 2017). Autophagy-lysosome pathway is divided in three types: microautophagy, chaperone-mediated autophagy and macroautophagy (Yin, Ding et al. 2008). Focusing on macroautophagy, hereafter designated as autophagy, there is the formation of a double membrane structure called phagophore, its elongation and sequestration of whole cellular organelles (e.g. mitochondria) and bigger protein aggregates. Then, formed autophagosomes fuse with lysosomes for digestion of delivered material by lysosomal degradative enzymes (**Figure 7**).

In liver, mammalian target of rapamycin complex 1 (mTORC1) is one of the most known regulators of autophagy. mTORC1 activation suppresses autophagy through sequestration of ULK1 while autophagy is activated under mTORC1 inhibition. This last condition occurs during starvation when low ATP levels activate energy sensor AMPK which phosphorylates and inhibits mTORC1 (Kim and Guan 2015). This process is mediated by conserved autophagy-related (*ATG*) genes. Encoded by these genes, proteins are grouped in distinct functional groups. Serine/threonine-protein kinase complex (ULK1, FIP200/RB1CC1, ATG13L, ATG101) acts as substrates of mTORC1 for the initiation of phagophore formation. Then, class III phosphatidylinositol 3-phosphate kinase complex (VPS34, beclin-1, p115 and ATG14) is required for membrane nucleation, being ATG9 responsible for the development of the isolating membrane. In the next step, phosphatidyl-inositol 3-phosphate-binding protein complex acts at the level of membrane expansion. Lastly, E1-like or E2-like enzymes (ATG7, ATG10, ATG3) are responsible for ATG12-ATG5-ATG6 complex, which facilitates the lipidation of microtubule-associated protein 1A/1B light chain (LC3), resulting in the elongation/ enclosure of isolating membrane. The fusion between autophagosomes and lysosomes is regulated by SNARE proteins syntaxin 17, vesicle-associated membrane protein 8 and beclin-1. Autophagolysosome recycling is further mediated by ATG2, ATG9 and ATG18 proteins (Nakatogawa, Suzuki et al. 2009, Mizushima, Yoshimori et al. 2011, Schneider and Cuervo 2014).

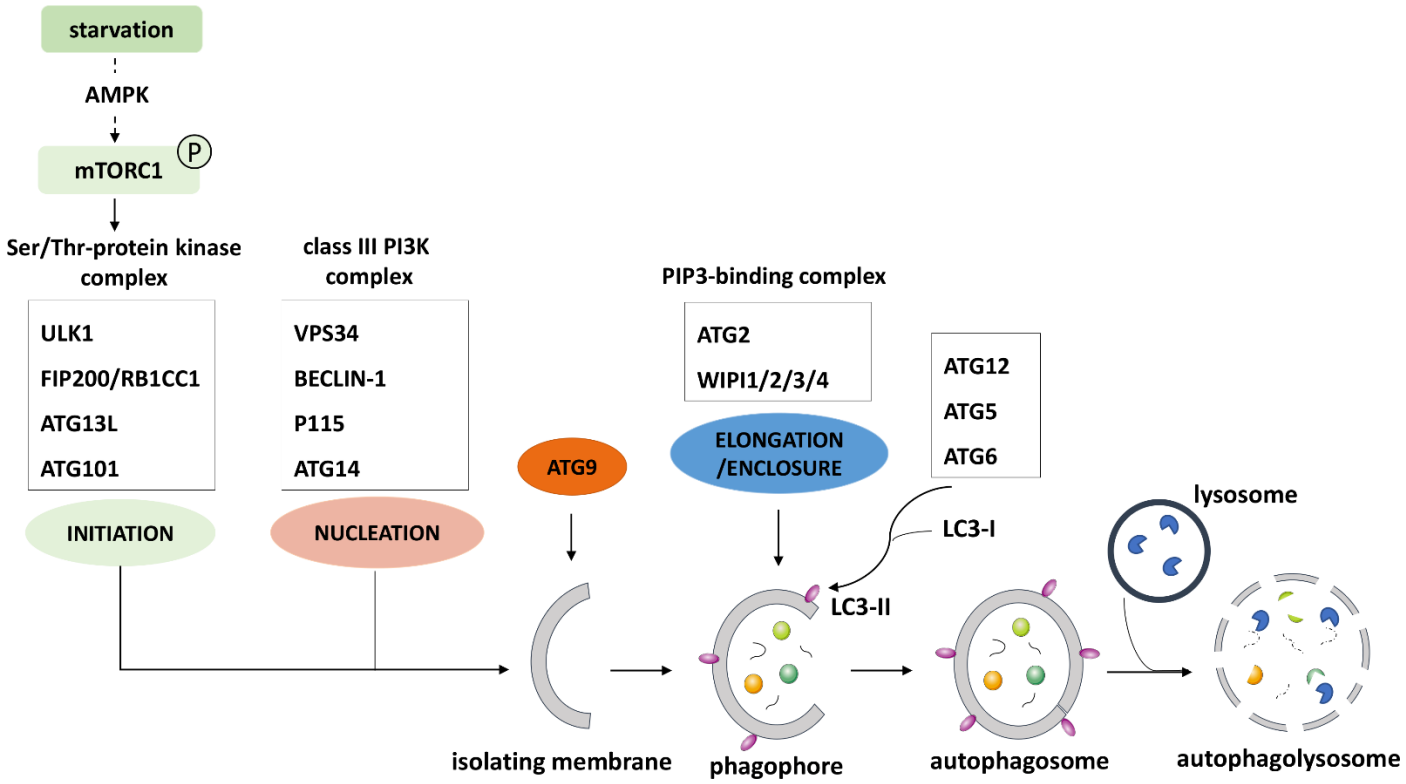

Figure 7. Different steps of macroautophagy. In the presence of low ATP levels (e.g. starvation) AMPK phosphorylates and inhibits mTORC1, thereby activating autophagy. Serine/threonine-protein kinase complex, class III PI3K complex and ATG9 are responsible for the initiation, nucleation and formation of phagophore's initiating membrane, respectively. Then, PIP3-binding complex is responsible for membrane's expansion, and ATG12-ATG5-ATG6 complex is involved in the lipidation of LC3-I into LC3-II in the autophagosome. Next, autophagosome can fuse with the lysosome and the delivered material is degraded by the action of lysosomal hydrolases. Abbreviations: AMPK – 5' AMP-activated protein kinase; LC3 - microtubule-associated protein 1A/1B light chain; mTORC1 - mammalian target of rapamycin complex 1; PI3K – phosphatidylinositol 3-phosphate kinase; PIP3 - phosphatidyl-inositol 3-phosphate; Ser – serine; Thr – threonine.

1.8.1 The role of autophagy in NAFLD

A selective form of autophagy called lipophagy has been described to enable lipid droplets turnover in mouse liver (Singh, Kaushik et al. 2009). Although the mechanisms underlying this process are still not clarified, it is postulated that lipophagy may protect the liver by contributing for hepatocytes adaptation to the excess of lipids in NAFL. However, it has been reported a decline of the autophagic pathway with conditions that predispose to the onset of NAFLD as aging (Donati, Cavallini et al. 2001, Uddin, Nishio et

al. 2012), high-calorie intake (Singh, Kaushik et al. 2009) and genetic induced-obesity (Yang, Li et al. 2010). Moreover, decreased autophagy reported in NAFLD patients was linked with the presence of hyperinsulinemia conditions (Fukuo, Yamashina et al. 2014, Gonzalez-Rodriguez, Mayoral et al. 2014, Kashima, Shintani-Ishida et al. 2014). In this scenario, a decline of autophagy further aggravates fat accumulation and associated lipotoxicity. Indeed, autophagic dysfunction is correlated with NAFLD severity in patients, according to the accumulation of autophagosomes and increased levels of LC3-II and sequestosome-1 (SQSTM1) (Gonzalez-Rodriguez, Mayoral et al. 2014, Willy, Young et al. 2017). These observations were also demonstrated by the work of Zhang and colleagues, who showed the role of chemokines in inducing an autophagic flux impairment with subsequent development of NASH. Consistently, autophagolysosome formation was restored by using C-X-C motif chemokine 10 (CXCL10) inhibitors in HepG2/ primary hepatocytes or in CXCL10-knock-out mice (Zhang, Wu et al. 2017).

Additionally, in a more severe NAFLD stage, the turnover of cytosolic composition may fail to remove non-functional/damaged mitochondria, thereby exacerbating oxidative stress (Lemasters 2005). Under oxidative stress conditions, this may culminate with the activation of SQSTM1-Kelch-like ECH-associated protein 1 (KEAP1)-NRF2 pathway (Hayes and McMahon 2009, Taguchi, Motohashi et al. 2011) As a result, phosphorylated SQSTM1 inactivates KEAP1, being both selectively degraded by autophagy while NRF2 is translocated to the nucleus, inducing the transcription of antioxidant enzymes-coding genes (Komatsu, Kurokawa et al. 2010, Taguchi, Fujikawa et al. 2012). Despite that, ROS levels may exceed NRF2-induced antioxidant proteins, thereby contributing for hepatic oxidative injury and NASH progression (Hayes and McMahon 2009, Taguchi, Motohashi et al. 2011).

It has been shown that autophagic stimulation using known autophagic inducers as rapamycin can restore autophagic flux. Importantly, this causes an improvement of NAFLD phenotype with a reduction of fat accumulation (Lin, Zhang et al. 2013) and the removal of Mallory-Denk bodies, a marker of ballooned hepatocytes consisting in cytoplasmic inclusions of ubiquitin, SQSTM1, and keratin (Harada, Hanada et al. 2008). Some studies have shown that the blockade of autophagic pathway in NAFLD may involve a reduction of ATG proteins (Yang, Li et al. 2010), alterations in membranes composition with the subsequent defective fusion between autophagosomes and

lysosomes (Koga, Kaushik et al. 2010) or a decreased activity of lysosomal degradative enzymes (Inami, Yamashina et al. 2011, Fukuo, Yamashina et al. 2014).

1.9 NASH and liver failure

Lipotoxicity, associated with the accumulation of SFAs, DAGs, ceramides and cholesterol, oxidative stress and mitochondrial dysfunction, trigger cell death mechanisms. Therefore, upon damage, hepatocyte can release danger-associated molecular pattern molecules, including free RNA, mitochondrial DNA and high-mobility group protein B1, thereby activating Kupffer cells (Zigmond, Samia-Grinberg et al. 2014, Huebener, Pradere et al. 2015). Activated Kpuffer cells release several cytokines (e.g. tumor necrosis factor α, interleukin 1β) and chemokines (e.g. C-C motif chemokine ligand (CCL)2) that severely contribute to the inflammatory response by attracting neutrophils and circulating monocytes (Holt, Cheng et al. 2008, Zigmond, Samia-Grinberg et al. 2014, Huebener, Pradere et al. 2015). CCR2-CCL2 and other chemokines pathways such as CXC3-CXCL10, CCR1-CCL5 or CCR8-CCL1 are described to attract Ly-6c$^+$ monocytes (Seki, De Minicis et al. 2009, Heymann, Hammerich et al. 2012, Zhang, Han et al. 2016). The accumulation and polarization of Ly-6c$^+$ macrophages are considered markers of NASH progression in the human liver (Reid, Reyes et al. 2016), by modulating the inflammatory (Wehr, Baeck et al. 2013), the angiogenic (Ehling, Bartneck et al. 2014) and the fibrogenic response (Ju and Tacke 2016). Accordingly, Ly-6c$^+$ macrophages can secrete cytokines that attract natural killer cells, and in another way, they also secrete transforming growth factor β and platelet-derived growth factor β that mediate the activation of HSC and subsequent fibrogenesis (Karlmark, Weiskirchen et al. 2009, Pradere, Kluwe et al. 2013, Tosello-Trampont, Krueger et al. 2016) (**Figure 8**). These cells transdifferentiate into myofibroblasts-like cells which can migrate into tissue repair sites and produce extracellular matrix (composed by collagens I, III, IV, elastin, laminin, fibronectin and hyaluronic acid) in an initiation phase (Seki and Brenner 2015). Importantly, as shown for liver damage, Ly-6c$^+$ macrophages can switch their phenotype into reparative phagocytes responsible for the expression of anti-inflammatory mediators and matrix-degrading metalloproteinases (Ramachandran, Pellicoro et al. 2012, Baeck, Wei et al. 2014). However, in the case of a chronic liver injury, HSC

activation is perpetuated by releasing cytokines, including ROS and lipid peroxides (Seki and Brenner 2015). The continuous failure of wound-healing repair processes drives the development of both cirrhosis and neoplasic lesions with subsequent loss of liver function (**Figure 8**). In HCC, a population of macrophages called tumor-associated macrophages promotes hepatic tumor cell growth and cell proliferation that favor metastasis (Wan, Zhao et al. 2014).

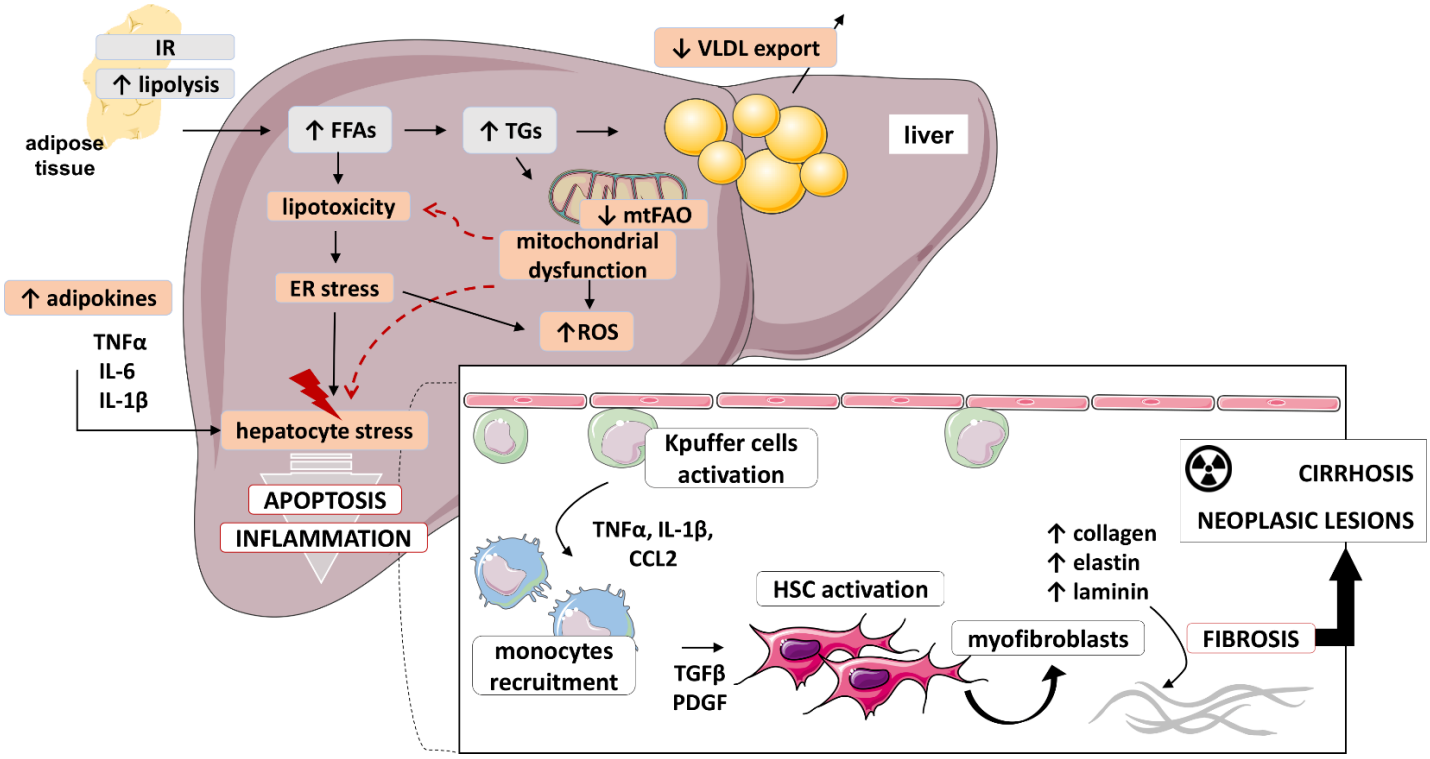

Figure 8. Molecular pathways involved in the progression of NAFL into NASH, and in the mediation of further end-liver stages. Insulin resistance, lipotoxicity, mitochondrial dysfunction, increased ROS generation and subsequent oxidative damage and ER stress are all considered insults in the origin of hepatocyte stress and injury. Upon damage, hepatocytes release pro-inflammatory molecules that activate Kpuffer cells with further monocytes recruitment and HSC activation. HSC are converted into myofibroblasts that produce fibrous matrix. Repetitive wound healing processes lead to progressive scarring and increased risk for cirrhosis and primary liver carcinoma. Abbreviations: CCL2 - C-C motif chemokine ligand; FFAs – free fatty acids; HSC – hepatic stellate cells; IL-1β – interleukin 1β; IL-6 – interleukin 6; IR – insulin resistance; mtFAO – mitochondrial fatty acid oxidation; PDGF - platelet-derived growth factor; ROS – reactive oxygen species; TGs – triglycerides; TGFβ - transforming growth factor β; TNFα – tumor necrosis factor α; VLDL – very low density lipoproteins.

1.10 Antioxidant-based therapies for NAFLD

Considering that mitochondrial dysfunction and oxidative stress are major players in the progression of NAFLD severity, antioxidant-based approaches have emerged as possible NAFLD therapeutic approaches. Among tested antioxidants, tempol by modulating gut microbiota-farnesoid X receptor (FXR) axis reduced hepatic fat accumulation and body-mass index in NASH mice (Jiang, Xie et al. 2015). Interestingly, a dietary supplement based on caffeic acid study supported the beneficial role of inhibiting intestinal FXR in improving hepatic steatosis and showed beneficial effects at mitochondrial level (Xie, Jiang et al. 2017).

Resveratrol is a polyphenol found in the diet that protects against diet-induced obesity and insulin resistance in mice (Lagouge, Argmann et al. 2006). Resveratrol demonstrated to exert its effects through the activation of sirtuin (SIRT)1-PGC-1α axis, with induction of FAO-related genes and mitochondrial uncoupling in adipose tissue and muscle. Moreover, the activation of SIRT1/SIRT3-Foxo3a-PGC-1β pathway is also described in the NAFLD-protective role of lipoic acid. This molecule prevented fatty liver and showed capacity to overcome oxidative damage through an upregulation of antioxidant defense enzymes (SOD2, GPx and GSH/GSSG ratio) (Valdecantos, Perez-Matute et al. 2012). In particular, retinoic acid protected hepatocytes from mitochondrial oxidative stress through an increase of SOD2, a decrease in mitochondrial ROS production and increase mitochondrial DNA copy number (Geng, Xu et al. 2017).

Linking mitochondria as an important source of ROS, several antioxidant molecules have been designed to target directly this organelle. Those are characterized by a lipophilic triphenylphosphonium cationic (TPP^+) group which enables the accumulation of the molecule inside mitochondria, a process driven by the negative $m\Delta\Psi$ at mitochondrial matrix (Smith, Porteous et al. 2003, Asin-Cayuela, Manas et al. 2004, Rokitskaya, Klishin et al. 2008). Moreover, an extensive hydrophobic surface and large ionic radius area of TPP^+ decreases activation energy, facilitating the transport of TPP^+-molecules through biological membranes and IMM (Porteous, Logan et al. 2010, Rodriguez-Cuenca, Cocheme et al. 2010). One example is mitoquinone (mitoQ) which has demonstrated to improve metabolic syndrome features as hypercholesterolemia, hypertriglyceridemia and hyperglycaemia in mice models of metabolic syndrome and

atherosclerosis (Mercer, Yu et al. 2012), while 8 weeks of mitoQ administration reduced body weight gain and hepatic steatosis in an obesogenic fed rat model (Feillet-Coudray, Fouret et al. 2014). Importantly, this molecule showed to reduce both nuclear and mitochondrial DNA oxidative damage, being hepatic mitochondrial function preserved with increased cardiolipin synthase expression and cardiolipin levels enriched with linoleic acid (Mercer, Yu et al. 2012, Fouret, Tolika et al. 2015). In chronic hepatitis C patients, a protective effect in liver damage by reducing AST and ALT circulating enzymes was reported (Gane, Weilert et al. 2010). Even though mitoQ has demonstrated beneficial effects in several models of NAFLD, a number of studies has also reported that mitoQ, even at low concentrations (30-100 nM), can trigger ROS production, induce apoptosis and inflammation (Doughan and Dikalov 2007, Mukherjee, Mishra et al. 2007). This was correlated with the redox cycling of the quinone group occurring at Complex I mitochondrial level. Based on its cytotoxicity, the use of mitoQ as a therapeutical strategy should be pondered.

Although a number of antioxidant molecules showed some promising results, still no approved therapy for NAFLD patients exists.

1.10.1 Novel mitochondriotropic antioxidant compound - AntiOxCIN$_4$

Due to some limitations of antioxidant-based approaches, any new compounds must be studied and validated.

Hydroxycinnamic acids are a class of phenolic compounds characterized by a phenylpropanoid backbone with nine carbons (C6-C3), known to be widely present in the human diet in the form of plants, coffee, fruits and vegetables. Importantly, these molecules (such as caffeic, p-coumaric, ferulic or sinapic acids) have been demonstrated to act as effective antioxidants in the prevention and treatment of oxidative-stress related disorders namely atherosclerosis, cancer and inflammation (Teixeira, Gaspar et al. 2013). Its scavenging efficacy is strongly dependent on its chemical structure due to hydrogen or electron-donors and to the ability to stabilize the resulting penoxyl radicals. Additionally, these molecules can inhibit ROS generating enzymes, modulate the NRF2-related antioxidant responsive pathway and act as chelators of copper or iron (Nguyen, Sherratt et al. 2003, Rodrigo, Miranda et al. 2011).

Therefore, new mitochondrial-targeted antioxidants were developed based on the conjugation of hydroxycinnamic acids with a TPP^+ group using a 6-carbon linker (Teixeira, Cagide et al. 2017, Teixeira, Oliveira et al. 2017). Then, structure-activity-toxicity based assays allowed the selection of $AntiOxCIN_4$ as a potential drug candidate. In fact, in isolated liver mitochondria and HepG2 cell line models, $AntiOxCIN_4$ accumulated inside mitochondria without signs of toxicity (no alterations in the structure and polarization of this organelle) at the concentrations needed for its antioxidant properties. Moreover, $AntiOxCIN_4$ prevented mPTP opening, and cellular and mitochondrial oxidative stress with an increase of GSH levels (Teixeira, Cagide et al. 2017) (**Figure 9**). Recently, it was demonstrated that $AntiOxCIN_4$ can also prevent cell death induced by H_2O_2 in a neuroblastoma cell line (Benfeito, Oliveira et al. 2019). Importantly, it has been confirmed that in primary human skin fibroblasts (PHSF), this mitochondriotropic compound firstly acts as a pro-oxidant, with higher ROS levels constituting the stimulus for NRF2-associated antioxidant enzymes expression such as heme oxygenase 1 (HMOX1) and NAD(P)H dehydrogenase (quinone) 1 (NQO1) (Teixeira, Basit et al. 2021). Besides, by improving cellular metabolic activity, $AntiOxCIN_4$ treatment converted PHSF from Parkinson disease patients closer to their age-matched healthy controls (Deus, Pereira et al. 2021).

However, further validation of the effect of $AntiOxCIN_4$ in oxidative stress-related metabolic diseases is desired. Based on the beneficial effects of $AntiOxCIN_4$, this compound became a good candidate for the amelioration of a NAFL phenotype of a mouse model of the disease.

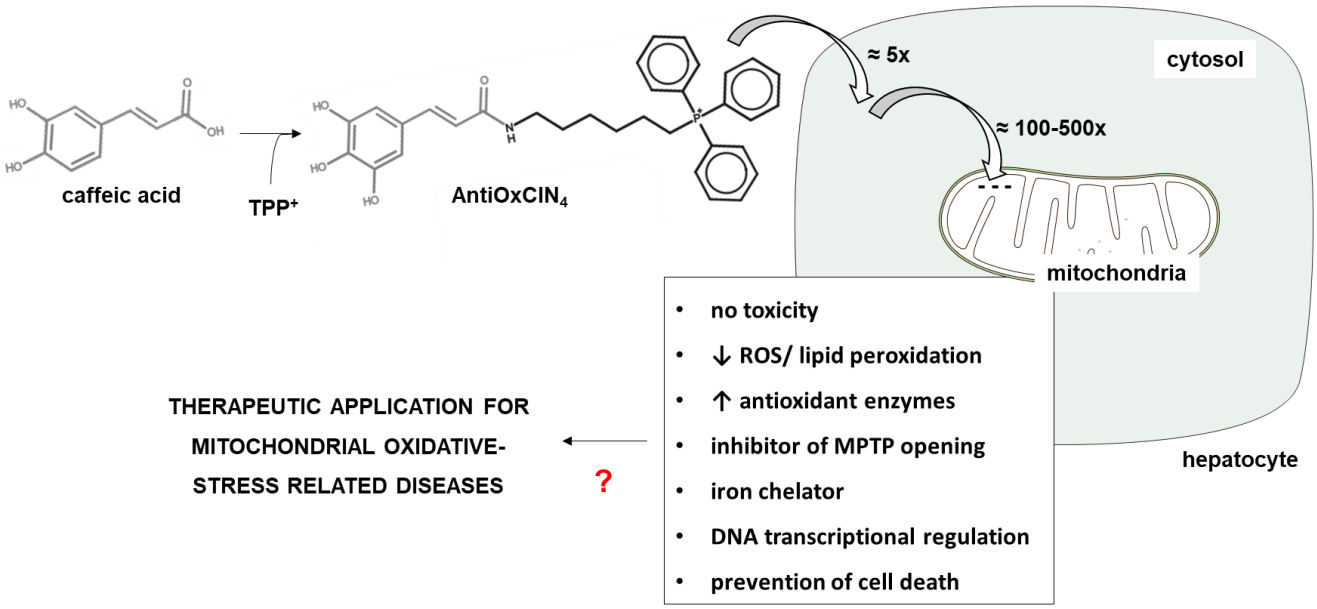

Figure 9. Cellular and mitochondrial AntiOxCIN$_4$ effects. Caffeic acid is conjugated with a mitochondriotropic TPP$^+$ group, thereby allowing AntiOxCIN$_4$ accumulation inside cytosol (5x) and inside mitochondria (100-500x) according to the negative mitochondrial membrane potential. AntiOxCIN$_4$ has several beneficial effects which enables its potential use as a therapy in mitochondrial oxidative stress-associated diseases. Abbreviations: mPTP – mitochondrial permeability transition pore; ROS – reactive oxygen species; TPP – triphenylphosphonium.

Part II: Hypothesis and Objectives

NAFLD prevalence has dramatically increased over the last decades, with NAFLD being considered as the most common cause of chronic liver disease and predictably, one of the leading causes of liver transplantation. Despite all the research work focusing on cellular and molecular mechanisms involved in NAFLD pathophysiology, there is a lack of certainty about the molecular pathways underlying the development of an early stage of the disease. Indeed, the alterations that occur in such an early stage seem to be critical to the progression of the disease and should be taken into consideration in the design of novel pharmacologic therapies, which are urgently needed.

An excessive production of ROS levels and mitochondrial dysfunction are associated with NAFLD development. However, the link between the effect of ROS on mitochondria and the underlying consequences for hepatocytes function and NAFLD pathophysiology are still not completely understood. Based on that, it was hypothesized that a pro-oxidant state is the trigger of mitochondrial-related alterations that culminate in NAFLD progression. On this basis, I established three main objectives in my thesis:

1) study of the hepatic and mitochondrial redox-associated alterations in a NAFL stage;

2) investigation of the specific end-points for mitochondrial dysfunction that represent a point of no return and which drive NAFL progression along time;

3) validation of a next generation of therapeutics for NAFL based on smart antioxidant delivery to mitochondria.

These objectives were divided in three main chapters:

1) My first objective was to study the hepatic and mitochondrial redox-associated alterations in a NAFL stage. Previous studies have focused on the effect of fat and sucrose but not on the individual effect of each diet component in the metabolic pathways involving the onset of NAFLD. Therefore, I evaluated the distinct effects of both a high-fat, a high-sucrose and a high-fat plus high-sucrose diets on developing NAFL using a mice model. The results are presented and discussed in detail in Chapter 1. Obtained data have been already published in “Western Diet Causes Obesity-Induced Nonalcoholic Fatty Liver Disease Development by Differentially Compromising the Autophagic Response”, *Antioxidants* 2020 (Simoes, Karkucinska-Wieckowska et al.

2020). In this first part of the work, an *in vivo* NAFL model that was used to assess the remaining objectives presented in this thesis was validated.

2) My second objective was to investigate the specific end-points for mitochondrial dysfunction that represent a point of no return and which drive NAFL progression along time. Previously, the progression of the disease from an early into a more severe stage has been reported to involve a pro-oxidative state with the generation of mitochondrial ROS generation. Although, it has been questioned whether mitochondrial ROS are the cause or just an accompanying event during mitochondrial dysfunction along NAFLD progression. Then, to understand how mitochondrial-related alterations and ROS homeostasis may drive by a non-reversible way NAFL progression towards NASH, I have studied disease progression by feeding mice with so-called Western diet up to 24 weeks. The results are presented and discussed in detail in the Chapter 2. Presented data has been already published in "The Alterations of Mitochondrial Function during NAFLD Progression-An Independent Effect of Mitochondrial ROS Production", *International Journal of Molecular Sciences* 2021 (Simoes, Amorim et al. 2021).

3) My third objective was to validate the effectiveness of a new mitochondrially-targeted antioxidant-based compound in the prevention of NAFL development. The complex pathophysiology of NAFLD encouraged drug discovery efforts in the search for new therapeutical candidates, mostly presenting mitochondrial-specific affinity and ability to control several cellular processes severely affected in NAFLD pathophysiology, as is the case of oxidative stress status and quality control mechanisms. While other mitochondriotropic antioxidants failed to reach the cellular target or had minimal beneficial effects, AntiOxCIN$_4$ showed to protect cells from oxidative stress, thereby increasing antioxidant defenses, triggering autophagy and stimulating mitochondrial biogenesis in several cell line models. Based on that, for the first time, I have tested the potential effect of AntiOxCIN$_4$ supplementation in NAFL stage of mice model. The results are presented and discussed in the Chapter 3. Obtained data will be published in the manuscript "Phenolic mitochondria-targeted antioxidant AntiOxCIN$_4$ improved simple steatosis phenotype by preventing hepatic lipid accumulation due to upregulation of fatty acid oxidation, quality control mechanism and antioxidant defense systems in Western Diet-fed mice" (Amorim, Simoes et al. under preparation).

With these complementary objectives, I aim to provide new insights and clarify the cellular mechanism underlying the pathophysiology of NAFL- from its development and in a progressing state into the severe stage of NASH. Furthermore, my work can contribute in finding potential novel biomarkers for disease staging and new dietary-based pharmacological approaches for NAFLD intervention.

Part III: Materials and Methods

3.1 Materials/chemicals

Diets for animals were purchased from Ssniff (Soest, Germany) (ref. V1534 and E15126) and ENVIGO Teklad (Madison, MI, USA) (ref. 2014S). Sugar free jelly was purchased from Royal, NJ, USA.

AntiOxCIN$_4$ compound was provided by Prof. Fernanda Borges's group from CIQUP/Department of Chemistry and Biochemistry, Faculty of Sciences, University of Porto (Porto 4169-007, Portugal) (Teixeira, Soares et al. 2012, Teixeira, Cagide et al. 2017).

All other remaining reagents/chemicals were purchased according to the following: β-mercaptoethanol, β-nicotinamide adenine dinucleotide (NADH), 10% neutral buffered formalin, 1,1,3,3-tetramethoxypropane, 2,2'-Azino-bis(3-ethylbenzothiazoline-6-sulfonic acid) diammonium salt (ABTS), 4-(2-hydroxyethyl)piperazine-1-ethanesulfonic acid (HEPES), 5,5'-dithio-bis-(2-nitrobenzoic acid) (DTNB), acetic acid, acetyl-coenzyme A (acetyl-coA), acid methanesulfonic, adenosine triphosphate (ATP), antimycin-A, Bouin's solution, essentially free fatty acids bovine serum albumin (BSA), calcium chloride ($CaCl_2$), carbonyl cyanide-4-(trifluoromethoxy)phenylhydrazone (FCCP), catalase, chloroform, cupric sulfate, cytochrome c, dimethyl sulfoxide (DMSO), ECL Prime Western Blotting System, ethylenediaminotetraacetic acid (EDTA), ethyleneglycoltetraacetic acid (EGTA), glycerol, glycine, glutamate, heptane, horseradish peroxidase (HRP), hydrogen peroxide (H_2O_2), isocitrate dehydrogenase, isopropyl ether, KCN, magnesium chloride ($MgCl_2$), MgSO4x $7H_2O$, malate, malic dehydrogenase, mannitol, methanol, nitro tetrazolium blue chloride (NTB), N-methyl-2-phenylindole, $Pb_2(NO_3)_2$, phenazine methosulphate, phenylmethylsulfonyl fluoride (PMSF), phosphoric acid, Ponceau S, potassium chloride (KCl), potassium phosphate monobasic (KH_2PO_4), RIPA lysis buffer, rotenone, safranin-O, sodium chloride (NaCl), sodium phosphate monobasic (NaH_2PO_4) and dibasic (Na_2HPO_4), succinate, sucrose, tert-butyl hydroperoxide (tBHP), TLC silica gel-60 plates, Trichrome Stain kit, Triton X-100, Trizma base and Weigert's iron hematoxylin solution were obtained from Sigma-Aldrich (Saint Louis, MO, USA). Oxaloacetate, amplex red and protease/phosphatase inhibitor cocktail were obtained from Thermo Fisher Scientific (Waltham, MA, USA). Acrylamide, ammonium persulfate (APS), Bis-Tris, Bradford

reagent, glycine, Laemmli buffer, N,N,N',N'-tetramethylethylenediamine (TEMED), polyvinylidene fluoride (PVDF) membranes, sodium dodecyl sulfate (SDS) and Tween 20 were obtained from BioRad (Hercules, CA, USA). Oligomycin was obtained from Santa Cruz Biotechnology (Dallas, TX, USA). Protein carbonyl assay kit, lipid peroxidation assay kit, GPx activity kit, SOD activity kit, goat anti-rabbit and anti-mouse were purchased from Abcam (Cambridge, UK). GR and catalase activity kits were purchased from Cayman Chemical (Ann Arbor, MI, USA).

Secondary IRDye®800CW and IRDye®680CW antibodies were obtained from Li-COR Biosciences (Lincoln, NE, USA). Ethylenediaminotetraacetic acid (EDTA) KE-coated microtubes were obtained from Sarsted (Nümbrecht, Germany). Low pH target retrieval solution was obtained from DAKO (Glostrup, Denmark). ECF detection kit was obtained from Healthcare Life Sciences (Buckinghamshire, UK).

All the reagents and chemicals were used with the highest grade of purity commercially available. Moreover, in the preparation of solutions, ultrapure distilled water was used to minimize any contamination with metal ions.

3.2 Animals

This section is divided in three distinct sub-sections according to the experimental design of each animal study performed. Experimental group 1, experimental group 2 and experimental group 3 correspond to the animal model/ approach presented in Chapter 1, Chapter 2 and Chapter 3.

3.2.1 Experimental group 1 (results presented in Chapter 1)

In this *in vivo* animal study, all the procedures were performed after approval by Local Ethical Committees (Resolution No. 200/2016 on December 11th, 2016). Moreover, these procedures were done according to the January 15th 2015 Act on the Protection of Animals Used for Scientific Purposes in Poland, which agree with the European Union's directive 2010/63/EU.

Four-week-old C57BL/6J male mice 20-30 g were obtained from CMD Bialystok (Bialystok, Poland). After arrival, animals were left to acclimatize for two weeks at the

animal house of Nencki Institute of Experimental Biology. Mice were housed in laboratory cages under controlled temperature (21-23ºC) and humidity (50-60%, with 10-15 exchanges per hour), with 12 h light/dark cycles and free access to tap water and food. Starting at the 7th week age, mice were randomly divided in four groups, being each group fed with standard chow diet (CHOW), high-fat diet (HF), high-sucrose diet (HS) or high-fat plus high-sucrose diet (HFHS) for 16 weeks (**Figure 10**). The detailed composition of CHOW (V1534) and HF (E15126) diets is represented below in the **Table 1**. CHOW diet was composed by 3% of fat and 5% of sucrose, with its metabolizable energy derived 9% from fat, 58% from carbohydrates and 33% from protein. HF diet was composed by 30% of fat (14% SFAs, 12% MUFAs and 1% polyunsaturated fatty acids (PUFAs)) and 6% sucrose, with its metabolizable energy derived 51% from fat, 26% from carbohydrates and 23% from protein. HS diet was composed by the standard diet in which drinking water was supplemented with 30% of sucrose. HFHS diet was composed by the HF diet supplemented with 30% of sucrose in the drinking water. In this experimental study, CHOW mice group was established as the control group of the experiment.

Table 1. Composition of standard diets and high-fat diet. Detailed information about the content in terms of protein, fibre, N free extracts, starch, sugar, fat (in percentage %) and cholesterol (mg/kg) content.

Composition	Standard diet (Ssniff V1534)	Standard diet (ENVIGO 2014S)	High-fat diet (Ssniff E15126)
Protein (%)	19.00	14.30	20.70
Fibre (%)	4.90	4.10	5.00
N free extracts (%)	54.10	-	34.30
Starch (%)	36.50	48.00	17.20
Sugar (%)	4.70	-	16.30
Fat (%)	3.30	4.00	30.00
C 12:0	-	-	0.03
C 14:0	0.01	-	0.99
C 16:0	0.47	0.50	7.49
C 16:1	0.01	-	0.74
C 17:0	-	-	0.36
C 18:0	0.08	0.10	5.29
C 18:1	0.62	0.70	10.98
C 18:2	1.80	2.00	0.75
C 18:3	0.23	0.10	0.13
C 20:0	0.01	-	0.03
C 20:1	0.02	-	0.01
C 20:4	-	-	0.07
Cholesterol (mg/kg)	-	-	284.00
Metabolizable Energy (MJ/kg)	12.80	12.10	20.10

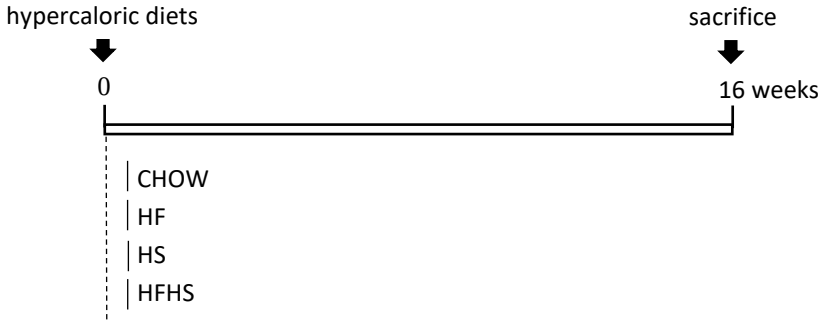

Figure 10. Schematic representation of the mice groups constituting the experimental group 1.

3.2.2 Experimental group 2 (results presented in Chapter 2)

This animal study was approved by animal welfare regulations of the Center for Neuroscience and Cell Biology/ University of Coimbra - ORBEA_131_2016/24032016; and the Portuguese authority for food and veterinary management (DGAV) - 0421/000/000/2016. Moreover, these procedures were performed according to the European Union directive – 2010/63/EU.

Four-week old C57BL/6J male mice were purchased from Charles River Laboratories (Charles River, Lyon, France). After arrival, animals were housed at the animal house of the University of Coimbra (UC) – Biotech (Portugal) under controlled conditions of temperature (20-24ºC), humidity (45-65%) and 12 h light/dark cycles. Mice were left to acclimatize for one week with free access to food and water. Next, mice were randomly divided in eight groups, four of them fed with standard diet (SD) and the other four with the so-called Western diet (WD) (**Figure 11**).

The detailed composition of the SD (2014S, ENVIGO) and WD (E15126, Ssniff; supplemented with 30% of sucrose in the drinking water) diets is presented in **Table 1**. In this experimental study, SD diet was composed by 48% of carbohydrates and 4% of fat, while WD was composed as the HF diet described in the previous sub-section of Experimental group 1. Mice were fed with SD or with WD for: 16 weeks (SD16w and WD16w), 20 weeks (SD20w and WD20w), 22 weeks (SD22w and WD22w) and 24 weeks (SD24w and WD24w). The group SD16w was established as the control group of the experiment.

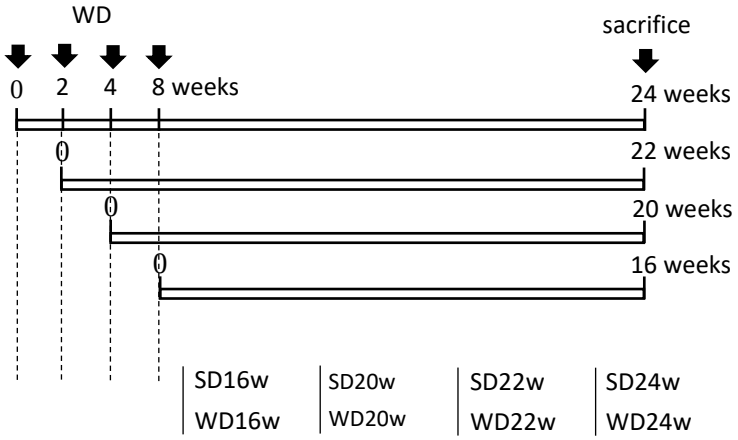

Figure 11. Schematic representation of the mice groups constituting the experimental group 2.

3.2.3 Experimental group 3 (results presented in Chapter 3)

This animal study was approved by the same regulations as Experimental group 2. Four-week-old male C57BL/6J mice were obtained from Charles River Laboratories. Mice were housed at the animal house of the University of Coimbra (UC) – Biotech

(Portugal) under controlled conditions of temperature (20-24ºC), humidity (45-65%) and 12 h light/dark cycles. Mice were left to acclimatize for one week with free access to food and water. Next, animals were divided into two groups: in the first group, mice were fed with SD supplemented with a vehicle sugar-free jelly (daily) (SD + vehicle), while in the second group mice were fed with SD supplemented with a sugar-free jelly containing AntiOxCIN$_4$ (2.5 mg/mouse/day) (SD + AntiOxCIN$_4$). This first part of the approach lasted two weeks. Then, each group was divided into two more groups: half of the group maintained the same diet/treatment regimen (SD + vehicle and SD + AntiOxCIN$_4$), and in the other half, SD was replaced by the WD (WD + vehicle and WD + AntiOxCIN$_4$) (**Figure 12**). WD feeding was performed during 16 weeks, while AntiOxCIN$_4$ treatment was performed during a total of 18 weeks. The detailed composition of SD and WD was described in Experimental group 1 and 2 sub-sections, respectively and in **Table 1**. In this approach, SD + vehicle was established as the control group of the experiment.

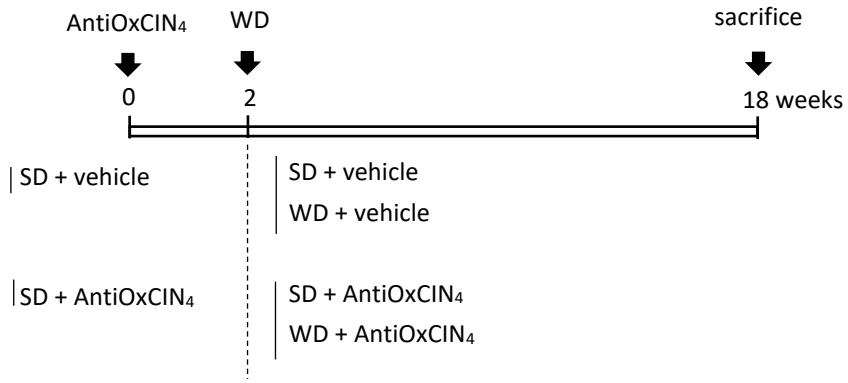

Figure 12. Schematic representation of the mice groups constituting the experimental group 3.

3.2.4 Euthanasia

After the time of feeding, mice were anesthetized with isoflurane inhalation and sacrificed by cervical dislocation. Systemic blood was collected into EDTA KE-coated microtubes and centrifuged at 2,000x g for 10 minutes at 4ºC. Next, plasma was collected and saved for further analyses at -80ºC.

Livers were excised, weighed and washed in ice-cold phosphate-buffered saline (PBS) 1x (137 mM NaCl, 2.7 mM KCl, 10 mM Na_2HPO_4, 1.8 mM KH_2PO_4). Livers were either divided for fresh mitochondrial isolation, 10% neutral buffered formalin fixation or stored for further analyses at -80ºC.

3.3 Plasma analysis

Liver injury along NAFLD development and progression is associated with increased transaminase levels in the systemic circulation. Therefore, AST and ALT enzymatic activities in plasma are used as indicators of the loss of hepatocyte integrity (Nallagangula, Nagaraj et al. 2018). In experimental group 1, ALT and AST enzymatic activities were measured with a Reflotron Plus System (Roche Diagnostics, Basel, Switzerland). In experimental groups 2 and 3, enzymatic activities were assessed using kits (ALT, ref. A-R0200001001; AST, ref. A-R0200001101; I.S.E. S.r.l., Guidonia, Italy), according to the manufacturer's protocol in a fully-automated analyzer Miura 200 (I.S.E. S.r.l.).

3.4 Histological analysis

Histochemical and immuno-stainings are routinely performed in medical liver biopsies. In this study, a set of standard stains was applied to the liver mice samples. Hematoxylin and eosin (H&E) was used to analyse tissue morphology, oil red-O to stain neutral lipids accumulation (marker of steatosis) and Masson Trichrome to stain collagen deposition (marker of fibrosis and cirrhosis). Additionally, Periodic Acid Schiff (PAS) was also used in conjugation with diastase to assess hepatic glycogen content, and reticulum II to study hepatocytes architecture by detecting reticulin fibers. Lastly, inflammation was evaluated by using a combination of distinct inflammatory markers: CD3 for T cells, CD4 for T helper cells, and CD68 for Kpuffer cells and mononuclear phagocytes (Clark and Torbenson 2017).

For oil red-O staining, liver tissue was placed in tissue embedding media and frozen in isopentane by using liquid nitrogen. For H&E, Masson trichrome, inflammatory markers (CD3, CD4 and CD68), PAS and diastase, and reticulum II stainings, livers were

fixed with 10% neutral buffered formalin (HT 50-1-1) for 24-48 h at room temperature. Next, tissues were trimmed to the appropriate size and shape and positioned inside proper cassettes for paraffin embedding. The protocol with a total duration of 16 h, comprised the following steps: 70% ethanol (two changes with 1 h each), 80% ethanol (one change with 1 h), 95% ethanol (one change with 1 h), 100% ethanol (three changes with 1.5 h each), xylene (three changes with 1.5 h each) and paraffin wax at 58-60ºC, with two changes of 2 h each for the final embedding of tissues into paraffin blocks.

a) Frozen liver tissues were cut in 8 µm thick slices for oil red-O staining and mounted on SuperFrost microscope slides (Gerhard Menzel GMBH, Braunschweig, D-38116 Germany). Next, slices were stained with oil red soluble dye, which by possessing highly solubility against lipoid substances allowed the detection of neutral lipids accumulation (lipid droplets) (Szymanska-Debinska, Karkucinska-Wieckowska et al. 2015).

b) For H&E and Masson Trichrome stainings, paraffin blocks were cut into 3 µm thick slices and mounted on microscope slides. Initially, slices were deparaffinized and rehydrated and then, stained with H&E staining or with Masson's staining (Bouin's solution (HT10132), Weigert's iron hematoxylin solution (HT1079-1SET) and Trichrome Stain kit (HT15-1KT), according to standard protocols (Szymanska-Debinska, Karkucinska-Wieckowska et al. 2015). In H&E, nuclei were visualized in blue and cytoplasm and extracellular matrix display different shades of pink. Masson staining enabled visualization of collagen fibers (in blue), muscle (in red) and nuclei (in black) (Bancroft and Layton 2019).

c) For PAS, PAS diastase and reticulum II, stainings were performed on the BenchMark Special Stains platform. After automatic deparaffinization and rehydration, ready-to-use Ventana Staining kits were used: PAS staining (ref. 860-014), diastase kit (ref. 860-004) and reticulum II (ref. 860-024). PAS staining was visualized by the violet color which can acquire a light violet after diastase degradation (glycogen digestion). Reticulum II stains fibers with a black color against a pink background.

d) For CD3, CD4, CD45 and CD68 inflammatory markers, paraffin blocks were firstly processed for antigen retrieval with low pH target retrieval solution at 99.5ºC for 30 minutes. Antibodies of CD3 (A0452, Agilent, Santa Clara, USA), CD4 (orb4830, Biorbyt, St Louis, USA), CD45 (GTX65913 GeneTex, CA, USA) and CD68 (GTX37743, GeneTex, Alton Pkwy Irvine, USA) were used.

Stainings were visualized in a Hamamatsu NanoZoomer 2.0 RS scanner (Hamamatsu Photonics, Hamamatsu, Japan) at an original magnification of 40x.

1.4.1 NAS score

Based in H&E, Masson Trichrome and inflammatory immunostainings, it is possible to calculate NAFLD activity score (NAS) score. Firstly described by Kleiner et al. (Kleiner, Brunt et al. 2005), this score allows the staging of the disease based in the histopathological evaluation of four criteria: steatosis (grade 0-3), hepatocellular ballooning (grade 0-2), lobular inflammation (grade 0-3) and fibrosis (S0-4). Steatosis grade: grade 0 = < 5%; grade 1 = 5–33%; grade 2 = 34–66%; and grade 3 = > 66%. Ballooning grade: grade 0 = absent; grade 1 = few ballooned hepatocytes; and grade 2 = many ballooned hepatocytes. Lobular inflammation grade: grade 0 = absent; grade 1 = up to two foci per field of view (200x magnification); grade 2 = two to four foci per field of view; and grade 3 = more than four foci per field of view (note: lipogranulomas are included in the category of inflammation). Fibrosis grade: S0 = no fibrosis; S1a = zone 3, perisinusoidal fibrosis; S1b = zone 3, perisinusoidal fibrosis, can be detected with H&E; S1c = only periportal/portal fibrosis; S2 = zone 3, plus portal/periportal fibrosis; S3 = zone 3, plus portal/periportal fibrosis with bridging fibrosis; and S4 = cirrhosis. [&]NAS score: sum of the steatosis, hepatocyte ballooning, lobular inflammation and fibrosis grades. HF, high-fat; HFHS, high-fat plus high-sucrose; HS, high-sucrose. NAS score was evaluated by a pathologist from The Children's Memorial Health Institute (Warsaw, Poland).

3.5 Isolation of liver mitochondria

Liver mitochondria were isolated according to a differential centrifugation approach. All materials and solutions were kept on ice during all the procedures.

Livers with excised gallbladder were washed with ice-cold PBS 1x and minced before homogenization with ice-cold isolation buffer I (50 mM Tris-HCl (pH 7.4), 75 mM sucrose, 225 mM mannitol, 0.5 mM EGTA, 0.5% essentially FAs free bovine serum albumin (BSA)). Livers were homogenized with a Potter-Elvehjem homogeneizer with a motor-driven Teflon pestle, followed by an initial centrifugation at 740x g at 4ºC for 3 minutes. The supernatant was collected and centrifuged again at 740x g at 4ºC but in this second time for 5 minutes. Pellet was discarded and supernatant was centrifuged at 10,000x g, 4ºC for 10 minutes to pellet mitochondria. Supernatant was saved as the cytosolic fraction of hepatocytes and pellet was resuspended in isolation solution II (50 mM Tris-HCl, pH 7.4, 75 mM sucrose, 225 mM mannitol, 0.5% essentially FAs free BSA) followed by another centrifugation at 10,000x g, 4ºC for 10 minutes. Pellet was resuspended in isolation solution III (50 mM Tris-HCl, pH 7.4, 75 mM sucrose, 225 mM mannitol) and centrifuged again at 10,000x g, 4ºC for 10 minutes. Final pellet was resuspended in a small volume of isolation solution III and kept on ice until further use. Mitochondrial protein content was determined according to the Bradford method (Bradford 1976).

3.6 Measurement of oxygen consumption

3.6.1 Clark oxygen electrode

Oxygen consumption of isolated mitochondria in Experimental group 1 was assessed using a classical Clark electrode (Estabrook 1967), in which oxygen electrode control system (5300A Biological Oxygen Monitor, YSI model; Rye Brook, NY, USA) was connected to a suitable recorder. Measurements were performed by adding 1 mg of freshly isolated mitochondria into the chamber containing under constant stirring 1.4 mL of respiratory medium (50 mM Tris-HCl, pH 7.4, 225 mM mannitol, 75 mM sucrose, 0.5 mM EGTA, 1 mM $MgCl_2$, 10 mM KCl) supplemented with 5 mM glutamate and 5 mM

malate at 25ºC. State 4 respiration was measured followed by the addition of 0.5 mM of adenosine diphosphate (ADP), which induced State 3 respiration. State 3 and State 4 respiration are expressed as nmol of O_2 per minute per mg of protein. State 3/State 4 ratio was used to calculate the respiratory control ratio (RCR). This ratio is used as an indicator of mitochondrial coupling between oxygen consumption and the efficiency of ADP phosphorylation.

3.6.2 Using a Seahorse XFe96 analyzer

3.6.2.1 Oxygen consumption rate

Oxygen consumption rate (OCR) in Experimental groups 2 and 3 was measured by using a Seahorse XFe96 Extracellular Flux Analyzer (Agilent Technologies, Santa Clara, CA, USA). On the day previous to the experiment, a sensor cartridge for each experiment was placed in a 96-well calibration plate with 200 µL of calibration buffer and left to hydrate at 37ºC. On the day of the experiment, 2.5 µg of freshly isolated mitochondria was added to mitochondrial assay solution 1x (70 mM sucrose, 220 mM mannitol, 10 mM KH_2PO_4, 5 mM $MgCl_2$, 2 mM HEPES, 1 mM EGTA and 0.2% free fatty acid BSA, pH 7.2) containing 10 mM glutamate/10 malate; 10 mM succinate and 2 mM rotenone; and 10 mM pyruvate. 25 µL of diluted mitochondria were loaded in a 96-well assay plate which was centrifuged at 2,000x g for 20 minutes at 4ºC in order to allow the adherence of mitochondria to the bottom of the well's plate. Then, 125 µL of pre-warmed MAS 1x supplemented with substrates was added to the plate, which was incubated at 25ºC for 10 minutes to allow the temperature and the pH of the medium to reach the equilibrium before the measurement. The mitochondria were visualized under a microscope (20x magnification) to ensure consistency in the adherence.

For the measurement assays, substrates and ADP were diluted in MAS 3x. Inhibitors (rotenone, oligomycin, antimycin A and FCCP were prepared in 95% ethanol. For OCR measurement, the sensor cartridge was loaded with 4 mM ADP, 2 µg/µL oligomycin, 4 µM FCCP and 2 µM antimycin A into port A, B, C and D, respectively. The compounds were pneumatically injected into each well, and measurements were performed using 3 minutes mix and 5 minutes of measurement cycle. Results were

analyzed using Software Wave Desktop Version 2.2. Using this measurement approach, several respiratory parameters were evaluated: State 2, State 3, State 4o and State 3u. Firstly, State 2 which represents the respiration of the mitochondria in the presence of substrates but no ADP – basal respiration, was measured. Then, State 3, a state in which the addition of ADP allows the formation of ATP, was measured. Next, the addition of oligomycin induced shift to the State4o, which represents the proton leak measured after the inhibition of ATP synthase. Lastly, State 3u which represents the maximal respiratory capacity due to the addition of the FCCP uncoupler was measured. State 3 and State 4o ratio was used to calculate the RCR.

3.6.2.2 Electron flow assay

Electron flow assay in Experimental groups 2 and 3 was performed by using a Seahorse XFe96 Extracellular Flux Analyzer. This assay allowed the evaluation of electron transport flow through the different complexes of the ETC. Based on that, it is considered as an indirect way to measure maximal complexes activities using depolarized mitochondria.

On the day previous to the experiment, a sensor cartridge was prepared as previously described. On the day of the experiment, 2.5 µg of freshly isolated mitochondria was added to mitochondrial assay solution 1x. 25 µL of diluted mitochondria were loaded in a 96-well assay plate which was centrifuged at 2,000x g for 20 minutes at 4ºC in order to allow the adherence of mitochondria to the bottom of the well's plate. Then, 125 µL of pre-warmed MAS 1x supplemented with 10 mM pyruvate, 10 mM malate and 4 µM FCCP was added to the plate. XFe96 sensor cartridge was loaded with 2 µM rotenone, 10 mM succinate, 2 µM antimycin A and 10 mM ascorbate/100 µM N,N,N',N'-tetramethyl-p-phenylenediamine (TMPD) into port A, B, C and D, respectively. Results were analyzed using Software Wave Desktop Version 2.2.

3.7 Measurement of aconitase activity

Aconitase is a mitochondrial enzyme susceptible to oxidation of its iron-sulfur cluster. In order to determine its activity, physiological and reactivated activities were

measured. Physiological activity was determined using the method of Quirós P. (Quiros 2018), based on the conversion of citrate into α-ketoglutarate, coupled to the reduction of $NADP^+$ to NADPH at 340 nm. Accordingly, 200 µL of reaction buffer (50 mM Tris-HCl, 21.25 mM sodium citrate, 0.60 mM $MnCl_2$, 0.61 mM NADP, 0.2% Triton X-100 and 2U/mL isocitrate dehydrogenase) was added to a 96 well plate, being the reaction initiated by adding 80 µg of frozen isolated mitochondria (2 µg/µL) per well. Absorbance was measured for 30 minutes. Negative controls were prepared by incubating mitochondria with reaction buffer with no isocitrate dehydrogenase enzyme.

The activity of reactivated aconitase form was performed according to Razmara A. and colleagues' method (Razmara, Sunday et al. 2008). Firstly, frozen isolated mitochondria (2 µg/µL) were incubated in the presence of 12 mM dithiothreitol and 1.2 mM iron chloride for 5 minutes. After 200 µL of reaction buffer (50 mM Tris-HCl, 21.25 mM sodium citrate, 0.60 mM $MnCl_2$, 0.61 mM NADP, 0.2% Triton X-100 and 2U/mL isocitrate dehydrogenase) and 80 µg of frozen isolated mitochondria (2 µg/µL) were added to a 96 well plate. The reaction with the formation of NADPH was monitored at 340 nm along 30 minutes.

Aconitase activity was expressed as % of inhibition, determined by the difference between 100% and the ratio of mitochondrial aconitase activity before and after its reactivation:

$$\%\ inhibition = 100 - \frac{physiological\ aconitase\ activity}{reactivated\ aconitase\ activity}$$

3.8 Determination of mitochondrial membrane potential

One of the most often used dyes to indicate mΔΨ in isolated mitochondria and in digitonin-permeabilized cells is safranine-O (Figueira, Melo et al. 2012). Safranine-O constitutes a lipophilic dye with a positive charge, and therefore this dye can accumulate between extramitochondrial medium and intramitochondrial compartment upon mitochondrial energization. mΔΨ was measured at 495 nm and 586 nm excitation and emission wavelengths, respectively, at 25ºC using a cuvette assay in Shimadzu model RF 5000 spectrofluorometer (Shimadzu Corporation, Kyoto, Japan) for Experimental group

1 approach and using a 96-well plate in Biotek Cytation 3 reader (Biotek Instruments, Winooski, VT, USA) for Experimental group 2 and 3 approaches.

For experimental group 1 approach, 3 mL of reaction buffer (50 mM Tris-HCl (pH 7.4), 225 mM mannitol, 75 mM sucrose, 0.5 mM EGTA, 1 mM $MgCl_2$) containing 5 mM glutamate/5 mM malate and 8.3 µM safranine-O was added to the cuvette. After baseline measurement, the reaction was initiated by adding 1 mg of freshly isolated mitochondria. After the absorbance reached a plateau, 2 µM FCCP was added to the cuvette.

For experimental group 2 and 3 approaches, 150 µL of reaction buffer (50 mM Tris-HCl (pH 7.4), 75 mM sucrose, 225 mM mannitol, 10 mM KCl, 1 mM EGTA, 0.5 mM KH_2PO_4, 1 mM $MgCl_2$) supplemented with 5 mM glutamate/5 mM malate was added to a 96 well plate. Next, 150 µg of freshly isolated mitochondria was added to each well. The reaction was initiated by the addition of 25 µL of safranine-O (final concentration 10 µM). After the absorbance reached the plateau, 2 µM FCCP was added to each well. $m\Delta\Psi$ was calculated as the difference between the maximal mitochondrial membrane potential (considered the minimal absorbance reached after mitochondrial addition) and the minimal mitochondrial membrane potential (the maximal absorbance reached after FCCP addition). $m\Delta\Psi$ was expressed in % respective to the control of each experiment.

3.9 Measurement of the mitochondrial permeability transition pore opening

The opening of mPTP was monitored through changes in the light scattering of mitochondrial suspension at 540 nm (Palmeira and Wallace 1997) in a Biotek Cytation 3 reader.

For experimental groups 2 and 3, the experiment was performed by addition of 150 µL of reaction buffer (225 mM mannitol, 75 mM sucrose, 1 mM KH_2PO_4, 3 mM HEPES and 10 µM EGTA) supplemented with 10 mM succinate/2 µM rotenone to a 96 well plate. After the addition of 150 µg of freshly isolated mitochondria, a basal absorbance measurement was performed during 2 minutes at 25ºC. mPTP opening was induced with mPTP inducers: 200 µM tert-butyl hydroperoxide (tBHP) and 150 µM $CaCl_2$. The concentrations of mPTP inducers used in the assay were chosen based on previous

assays in which increasing $CaCl_2$ concentrations (12.5 µM-300 µM range) were tested with mitochondrial preparations. Once chosen the most appropriate concentration (150 µM $CaCl_2$), assay was performed for 20 minutes. Negative controls of mPTP opening were performed without mPTP inducers or by adding 1 µM cyclosporine-A (mPTP inhibitor) before mPTP inducers into the well plate.

3.10 Mitochondrial OXPHOS complexes

Blue native polyacrylamide gel electrophoresis (generally termed BN-PAGE) followed by in-gel activity assays are techniques that allow the evaluation of OXPHOS complexes activities in their native state. This is based on non-denaturing gradient gel conditions in which complexes negatively charged by Coomassie blue-G250 are separated according to their molecular weight (Schagger and von Jagow 1991). The assay was performed for Experimental group 1.

3.10.1 Separation of mitochondrial OXPHOS complexes

Frozen liver samples with approximately 8 mg were homogenized and mitochondria were isolated as previously described in the methodological sub-section "Isolation of liver mitochondria". In parallel, heart mitochondria were also isolated, to be used as an internal standard for OXPHOS complexes separation. Then, the resulting mitochondrial pellets were resuspended in 100 µL of ice-cold ACBT buffer (75 mM Bis-Tris, pH 7.0, 1.5 mM epsilon-aminocaproic acid) and 20 µL of 10% (w/v) β-lauryl maltoside. Pellets were incubated on ice for 10 minutes, followed by centrifugation at 10,000x g for 30 minutes at 4ºC. Supernatant was collected, and protein content was measured according to the Bradford method. Then, 10 µg of heart and 20 µg of liver mitochondrial samples were prepared with BN sample buffer (50 mM Bis-Tris, pH 7.0, 750 mM aminocaproic acid, 0.5 mM EDTA and 5% (w/v) Coomassie Blue G 250 in a ratio 1:10 of sample per BN sample buffer.

3.10.2 Non-denaturing PAGE (Blue Native PAGE)

Freshly prepared native mitochondrial and heart OXPHOS samples (20 µg/lane and 10 µg/lane, respectively) were loaded and separated on polyacrylamide native gels with a gradient concentration of 4-15%. In non-denaturing conditions, gel ran with a constant voltage of 75 V until the blue front migrated up to the middle of the gel. Then, cathode buffer with Coomassie Blue G 250 was replaced by cathode buffer without this compound. At that time, the voltage was increased up to 150 V until the blue front has reached the bottom of the gel. After, gels were disassembled and incubated for the evaluation of each OXPHOS complex activity.

3.10.3 In-gel activity assay

In order to evaluate Complex I activity, gel was incubated in a solution containing 3 mM Tris-HCl, pH 7.4, 113 µM β-nicotinamide adenine dinucleotide (NADH) and 245 µM of nitro tetrazolium blue chloride (NTB) for 20 minutes at 37ºC. To assess Complex II activity, gel was incubated in a solution containing 1.5 mM phosphate buffer, pH 7.4, 5 mM EDTA, 0.8 mM KCN, 50 mM succinate, 0.2 mM phenazine methosulphate and 245 µM NTB for 20 minutes at 37ºC. To evaluate Complex IV activity, gel was incubated in a solution containing 30 mM phosphate buffer, pH 7.4, 0.24 M sucrose, 2.3 mM diamino benzidine tetrachloride, 24 mM cytochrome c and 0.04 mg/mL catalase for 2 h at 37ºC. Lastly, to assess ATP synthase activity, gel was incubated in a solution containing 35 mM Tris-HCl, pH 7.8, 0.3 M glycine, 14 mM $MgSO_4x7H_20$, 9 mM ATP and 3.7 mM $Pb_2(NO_3)_2$ overnight at 37ºC. Next, gels were scanned and band intensities were analyzed using ImageJ software (version 1.53e).

3.11 Evaluation of mitochondrial reactive oxygen species generation level

The determination of mitochondrial ROS (H_2O_2) production from mitochondria was based on the formation of the fluorescent compound resofurin (7-hydroxy-3H-phenoxazin-3-one) caused by the reaction of amplex red (N-acetyl-3,7-dihydroxyphenoxazine) with horseradish peroxidase (HRP)-hydrogen peroxide (H_2O_2).

Resofurin is a stable molecule that accumulates in the extramitochondrial space once H_2O_2 is released from mitochondria. The increase of resofurin levels was monitored kinetically at 560 nm and 590 nm excitation and emission wavelengths, respectively (Quinlan, Perevoschikova et al. 2013), using an Infinite M200 (Tecan, Männedorf, Switzerland) for experimental group 1 and a Biotek Cytation 3 reader for experimental groups 2 and 3.

The assay was started by adding reaction buffer (50 mM Tris-HCl (pH 7.4), 75 mM sucrose, 225 mM mannitol) with 5 mM glutamate/5 mM malate or with 10 mM succinate/2 µM rotenone supplemented with 5 µM amplex red, 20 U/mL HRP and 40 U/mL SOD to the wells plate. In this experiment, exogenous SOD was added to ensure that all $O_2^{\bullet-}$ released from mitochondria was converted to H_2O_2. The reaction was initiated with the addition of 100 µg of freshly isolated mitochondria and the absorbance was followed for 30 minutes at 25ºC.

3.12 Oxidative damage analysis

ROS species can interact with biological molecules inside the cells, thereby originating oxidative damage of proteins, lipids and DNA. Oxidative damage of proteins was assessed by measuring protein carbonyls and nitrotyrosine levels while oxidative damage of lipids was evaluated by the measurement of lipid peroxidation end-products MDA and 4-HNE levels.

3.12.1 Protein carbonylation and protein nitration

The direct oxidation of side-chains of aminoacids (primary source) and the oxidation of lipid derivatives (secondary source) originate reactive aldehydes/ ketones that by reacting with 2,4-dinitrophenylhydrazine (DNPH) produce 2,4-dinitrophenyl hydrazone (DNP)-derivatized proteins which can be measured by using an anti-DNP antibody in Western blotting (Suzuki, Carini et al. 2010). Here, the levels of carbonylated proteins were assessed by following the manufacturer's protocol of a protein carbonyl assay kit (ab178020). Accordingly, liver homogenate samples, mitochondrial and cytosolic fractions from experimental groups 1, 2 and 3 were incubated with extraction

buffer, incubated on ice for 20 minutes and centrifuged at 18,000x g for another 20 minutes. After supernatant collection, extracted protein was quantified by the Bradford method. 20 µg of protein was used to proceed with the assay. Next, samples were denatured with 1% (w/v) SDS solution followed by the addition of DNPH to each sample and addition of derivatization control solution to the negative control of each sample. After 15 minutes of incubation at room temperature, neutralization solution was added to the samples. Then, samples and negative controls were electrophoretically separated on a 10% SDS polyacrylamide gel and transferred to PVDF membranes. Membranes were blocked with 5% (w/v) non-fat dry milk in tris-buffered saline (TBS) (50 mM Tris-HCl, pH 8.0, 154 mM NaCl) for 1 h at room temperature, and after incubated with anti-DNP primary antibody (1:1000 dilution) overnight at 4ºC under constant agitation. On the day after, membranes were washed three times for 5 minutes with TBS-T (TBS with 0.1% Tween-20) prior to the incubation with the correspondent IRDye®800CW secondary antibody for 1 h at room temperature. Membranes were then washed three times for 10 minutes with TBS-T, and membranes were imaged with an Odyssey infrared imaging system (LI-COR Biosciences). Band intensities were analyzed using Image Studio Lite (version 5.2) and band intensities wee normalized with 0.01% (w/v) Ponceau staining.

In order to have a more complete picture of protein oxidative damage, it was also assessed nitrotyrosine levels in mitochondria and liver homogenate samples from experimental group 1. In this assay, the occurrence of 3-nitrotyrosine, a common and stable post-translational modification caused by the action of nitration agents on tyrosine residues preferentially located at the protein surface (Ahsan 2013), was determined. To evaluate the levels of 3-nitrotyrosine, 50 µg of samples were electrophoretically separated on a 10% SDS polyacrylamide gel. Protocol of Western blotting performed as similar to the one described in the above paragraph, but using 3-nitrotyrosine antibody (189542, Cayman) (1:1000).

3.12.2 Lipid peroxidation

The reaction of oxidants with lipids containing carbon-carbon double bonds, especially PUFAs generate lipid peroxyl radicals and hydroperoxides as primary

products, and MDA and 4-hydroxynonenal (4-HNE) as secondary products. While MDA can be easily detected, 4-HNE is used due to its high cellular toxicity by acting as a second messenger of free radicals (Ayala, Munoz et al. 2014).

For the experimental group 1, lipid peroxidation products (MDA and 4-HNE) were evaluated using a lipid peroxidation assay kit (ab118970). According to the manufacturer's protocol, 10 mg of frozen liver and 500 µg of liver mitochondria were homogenized in MDA lysis buffer supplemented with butylated hydroxytoluene. Samples were centrifugated at 13,000x g for 10 minutes and supernatant was collected. A calibration curve with known concentrations of MDA was prepared: 0, 20, 40, 60, 80 and 100 µM. Next, 600 µL of thiobarbituric acid (TBA) reagent was added to the samples and to the MDA standard curve. After incubation at 95ºC for 1 h, samples were left to cool down. To remove some insoluble material, samples were centrifugated and 200 µL of supernatant was loaded into a 96-well plate. The absorbance of MDA-TBA adducts was measured at 532/553 nm emission and excitation wavelengths, respectively using an Infinite M200.

For experimental group 2 and 3, lipid peroxidation end-products were determined following the method described by Gérard-Monnier et al. (Gerard-Monnier, Erdelmeier et al. 1998). Accordingly, this is based in the reaction of MDA and 4-HNE with 1-methyl-2-phenylindole that yields a stable chromophore with absorbance at 586 nm. The assay was performed by using 230 µg of cytosolic and 460 µg of mitochondrial protein. In parallel, a standard curve was prepared with the following concentrations: 0.25, 0.5, 0.75, 1.0, 1.5, 2.5, 5, 10, 15 and 20 µM of 1,1,3,3-tetramethoxypropane. Next, to 200 µL of samples/standards, it was added 650 µL of 10.3 mM N-methyl-2-phenylindole in methanol: acetonitrile (3:1) solution and 150 µL of methanesulfonic acid. Samples were firstly incubated at 45ºC for 40 minutes, being left to cool down for 15 minutes on ice. Next, samples were centrifuged at 10,000x g for 5 minutes at 4ºC. The supernatant was transferred to a new tube and 200 µL of samples were loaded into a 96-well plate. Absorbance was measured in an Infinite M200. Results were expressed in terms of nmol MDA + 4-HNE per g of protein.

3.13 Total antioxidant activity

Total antioxidant activity is a parameter used to evaluate the total amount of antioxidants in biological samples. This study used an adapted method originally described by Arnao and colleagues (Arnao, Cano et al. 2001). According to this adaptation (de Gonzalo-Calvo, Neitzert et al. 2010), total antioxidant activity is directly proportional to the sample's capacity to neutralize the quite stable 2,2'-azino-bis (3-ethylbenzothiazoline-6-sulfonic acid) (ABTS) radical. This radical was freshly prepared a few hours prior to the starting of the assay by incubating 50 mM ABTS with a reaction mixture containing 50 mM sodium phosphate buffer (0.2 M NaH_2PO_4; 0.2 M Na_2HPO_4), pH 7.5, 10 mM H_2O_2 and 1 mM HRP for 4 h in the darkness at 4ºC. Once radical absorbance was stable, 90-150 µg of cytosolic and 150-300 µg of mitochondrial fractions from experimental study 2 and 3 were added to a 96 wells plate (final volume of 10 µL). Next, 240 µL of stabilized radical were added to the each well and the absorbance was measured at 730 nm for 15 minutes using an Infinite 200 Pro. Results were expressed in mg of Trolox per g of protein, being 1 mole of Trolox (molecular weight = 250.29 g/mol) correspondent to 2 moles of ABTS.

3.14 Antioxidant enzymatic activities

The activities of antioxidant enzymes (SOD, catalase, GPx and GR) were evaluated in frozen cytosolic and mitochondrial fractions extracted according to the above sub-section "Isolation of liver mitochondria". Apart from when it is referred, samples were prepared in ice-cold lysis buffer (50 mM Tris, pH 8.0, 150 mM NaCl, 1% (v/v) IGEPAL, 0.5% (w/v) sodium deoxycholate) containing protease and phosphatases inhibitors cocktail, and after incubation on ice for 30 minutes, samples were centrifugated at 16,000x g for 15 minutes at 4ºC. Supernatant was collected and samples were quantified following the Bradford method.

3.14.1 SOD activity

Superoxide dismutase (generally termed as SOD) converts $O_2^{\bullet-}$ into H_2O_2, and it comprises three different isoforms distinctively expressed in cytosol (SOD1), mitochondria (SOD2) and extracellular matrix (SOD3). In this work, it was evaluated the activity of SOD1 in cytosol and SOD2 in mitochondria for all experimental studies 1, 2 and 3. Cytosolic (1:100 dilution) and mitochondrial samples (1:10 dilution) were used to assess SOD activity according to SOD assay kit (ab65354). Therefore, it was added to a 96 well plate: 20 µL of sample, 200 µL of WST working solution and 20 µL of working solution. Plate was mixed and incubated at 37ºC, with absorbance measured at 450 nm for 20 minutes, in an Infinite M200.

3.14.2 Catalase activity

After SOD, catalase can further decompose H_2O_2 into H_20 and O_2. Moreover, catalase may also decompose H_2O_2 through its peroxidatic activity by using aliphatic alcohols as substrates. In this work catalase activity was evaluated in both fractions: cytosol and mitochondria.

For experimental study 1 and 3, catalase activity was assessed according to catalase assay kit (707002). Thus, 20 µL of each sample (1:800 dilution) was loaded into a 96 well plate. A standard curve of formaldehyde standards (0, 5, 15, 30, 45, 60 and 75 µM) was prepared in parallel with samples of interest. Next, it was added 100 µL of diluted assay buffer, 30 µL of methanol and 20 µL of H_2O_2 to each well. Plate was incubated on a shaker for 20 minutes, protected from light, followed by adding 30 µL of potassium hydroxide and 30 µL of catalase purpald. After a 10 minutes incubation on a shaker, 10 µL of catalase potassium periodate was added and the absorbance was read at 540 nm in an Infinite M200.

For experimental study 2, catalase activity was assessed according to the method described by Grilo and colleagues (Grilo, Martins et al. 2020). Accordingly, frozen liver tissue was homogenized in 50 mM phosphate buffer, pH 7.8. Samples were further sonicated two times for 30 seconds each using a 2 mm probe. After protein quantification, 20 µL of sample containing 10 mg of total protein or mitochondrial

protein and 180 µL of phosphate buffer were added to a 96 well plate. Basal absorbance was measured at 240 nm. Then, 100 µL of 10 mM H_2O_2 solution was added and absorbance was followed for 2 minutes and 30 seconds in a Biotek Cytation 3 reader. In this measurement, purified catalase of bovine liver was used as a positive control and sodium azide was used as negative control of the assay.

3.14.3 GPx and GR activities

An increased GSH/GSSG ratio is critical for the protection against oxidative stress. GPx catalyzes the reduction of various peroxides by oxidizing reduced glutathione (GSH) into GSSG. To keep a tight balance of GSH redox cycle, GR regenerates GSH levels by catalyzing GSSG reduction in a NADPH-dependent reaction (Valko, Leibfritz et al. 2007).

Both GPx and GR activities were assayed as indicated in manufacturer's protocol, ab102530 and 703202, respectively. For GPx activity, 100 µL of standard NADPH (0, 20, 40, 60, 80, 100 nmol/well) and 50 µL of samples (1:50 dilution) were added to each 96 well's plate. Additionally, a GPx positive control was performed. Next, 40 µL of reaction mix (33 µL assay buffer, 3 µL 40 mM NADPH solution, 2 µL GR solution, 2 µL GSH solution) were added to samples and control wells. After 15 minutes of incubation at room temperature with agitation, 10 µL of cumene hydroperoxide solution was added to samples and control wells. Absorbance was read at 340 nm for 5 minutes in an Infinite M200. For GR activity, 20 µL of samples (1:2 dilution) were added to a 96 well's plate, followed by 100 µL of assay buffer and 20 µL of GSSG. The reaction was initiated by adding 50 µL of NADPH, and the absorbance was further measured at 340 nm for 5 minutes in an Infinite M200.

3.15 Assessment of cathepsin B activity

Cathepsin B, localized in lysosomes, is responsible for the turnover and the degradation of proteins at neutral and acidic pH. Cathepsin B activity was measured using 10 mg of frozen liver tissue. Liver tissue was homogenized in 50 mM phosphate buffer, pH 7.8. Then, 50 µL of sample aliquots at a concentration of 0.2 mg/mL were added to 70 µL of 100 mM sodium acetate, pH 5.5, 1 mM EDTA, 5 mM DTT and 0.05%

(v/v) Brij-35 at 37ºC. The reaction assay started by the addition of 70 µL of 40 µM Z-Arg-Arg-N-methyl-coumarin at 40 µM, and the fluorescence was measured at 460 nm/360 nm emission/excitation, respectively for 20 min in a Biotek Cytation 3 reader. A calibration curve with known concentrations of N-methyl-coumarin was prepared. Then, cathepsin B activity was calculated based on the slope of the linear regression of samples, being values normalized according to the protein concentration of each sample.

3.16 Western blotting analysis

The levels of proteins were analyzed using sodium dodecyl sulfate-polyacrylamide gel electrophoresis (SDS-PAGE), which allows the separation of proteins by molecular weight in denaturing/reducing conditions (Mahmood and Yang 2012).

Frozen liver tissue (50 mg) was homogenized in 1 mL of 50 mM sodium phosphate buffer (0.2 M NaH_2PO_4, 0.2 M Na_2HPO_4, pH 7.5) containing 1 mM NaF, 1 mM Na_3VO_4, 0.1% (v/v) Triton X-100, 1 mM PMSF and supplemented with a cocktail of inhibitors of proteases and phosphatases. Samples were homogenized by applying two cycles of homogenization with 15 seconds each using a homogenizer. Then, liver homogenates were centrifuged at 1,500x g for 6 minutes at 4ºC. Supernatants were collected. Cytosolic and mitochondrial fractions were incubated with ice-cold RIPA buffer (50 mM Tris, pH 8.0, 150 mM NaCl, 1% (v/v) IGEPAL, 0.5% (w/v) sodium deoxycholate, 0.1% (w/v) SDS) also supplemented with the cocktail of inhibitors for 30 minutes on ice. Samples were centrifuged at 15,000x g for 15 minutes at 4ºC, and the supernatants were collected.

All the samples (liver homogenates, cytosol, and mitochondria) were quantified according to the Bradford method and using BSA as a standard. Then, an equivalent amount of 30-75 µg of protein was added to Laemmli buffer (62.5 mM Tris-HCl, pH 6.8, 10% (v/v) glycerol, 1% (w/v) SDS, 0.005% (w/v) bromophenol blue, 355 mM β-mercaptoethanol), and samples were denatured at 95ºC for 5 minutes with the exception of the samples for the determination of OXPHOS levels. Next, samples were loaded on 7 - 14% SDS polyacrylamide gels. After gel electrophoresis, samples were transferred to PVDF membranes. Membranes were blocked with 5% (w/v) non-fat dry

milk or with 5% (w/v) BSA in TBS (50 mM Tris-HCl, pH 8.0, 154 mM NaCl) for 1 h at room temperature, and after incubated with primary antibodies overnight at 4ºC under constant agitation. The list of primary antibodies used is presented in **Table 2**. On the day after, membranes were washed three times for 5 minutes with TBS-T prior to the incubation with the correspondent HRP-secondary antibodies (goat anti-rabbit (1:10000 dilution) and goat anti-mouse (1:10000)) for 1 h at room temperature. Membranes were then washed three times for 10 minutes with TBS-T, and membranes were incubated with ECL Prime Western Blotting System. Proteins of interest were visualized in a GBOX Chemi XT4 system (Frederik, MD, USA) with GeneSys software (version 1.2.5.0). Band intensities were analyzed using Image Studio Lite (version 5.2), being band intensities normalized with β-actin for liver homogenate, with VDAC1 for mitochondria and GAPDH or β-actin for cytosol.

Table 2. List of primary antibodies (antibody name, specie, dilution, supplier and reference) used in the studies.

Antibody	Specie	Dilution	Supplier	Reference
AKT	Rabbit	1:1000	Cell Signaling	4691
^{Ser473}p-AKT	Rabbit	1:1000	Cell Signaling	4060
mTOR	Rabbit	1:500	Cell Signaling	2972
^{Ser2448}p-mTOR	Rabbit	1:500	Cell Signaling	2971
AMPKα	Rabbit	1:1000	Cell Signaling	2603
^{Thr172}p-AMPKα	Rabbit	1:1000	Cell Signaling	2531
p70s6k1	Mouse	1:1000	Santa Cruz Biotechnology	8418
^{Thr389}p-p70s6k1	Rabbit	1:1000	Cell Signaling	9205
4EBP1	Mouse	1:1000	Santa Cruz Biotechnology	9977
^{Thr45}p-4EBP1	Mouse	1:1000	Santa Cruz Biotechnology	271947
SQSTM1	Mouse	1:1000	Santa Cruz Biotechnology	PM045
eIF4E	Mouse	1:1000	Santa Cruz Biotechnology	271480
LC3	Rabbit	1:1000	Cell Signaling	12741
Beclin1	Rabbit	1:1000	Cell Signaling	3495
Pink1	Rabbit	1:1000	Abcam	65232
Parkin	Mouse	1:1000	Cell Signaling	4211
Aconitase 2	Rabbit	1:1000	Cell Signaling	6571

Catalase	Rabbit	1:1000	Abcam	1877
PGC1-α	Mouse	1:1000	Sigma-Aldrich	ST1202
SIRT3	Rabbit	1:1000	Cell Signaling	5490
SOD2	Mouse	1:1000	Santa Cruz Biotechnology	13334
OXPHOS	Mouse	1:1000	Abcam	110413
MT-CO1	Mouse	1:1000	Abcam	14705
GAPDH	Mouse	1:1000	Cell Signaling	365062
VDAC1	Rabbit	1:1000	Abcam	34726
β-actin	Mouse	1:5000	Sigma-Aldrich	A5441

3.17 Proteomic analysis

Liquid chromatography-MS3 spectrometry (LC-MS/MS) was performed at the Thermo Fisher Center for Multiplexed Proteomics (Department of Cell Biology, Harvard Medical School, Cambridge, MA, USA). Peptide fractions were analyzed by using an LC-MS3 data collection strategy on an Orbitrap Fusion mass spectrometer (Thermo Fisher Scientific Inc., Waltham, MA, USA).

3.17.1 Quantitative mass spectrometry

Frozen liver samples were homogenized with an ice-cold lysis buffer (50 mM Tris, pH 8.5, 8 M urea, 1% (w/v) SDS supplemented with protease and phosphatase inhibitors (Roche, Basel, Switzerland) in order to have liver samples with a protein concentration between 2-8 mg/mL. Protein quantification of liver lysates was assessed using a micro-BCA assay (Pierce Biotechnology Inc., Rockford, IL, USA). Then, proteins were reduced, alkylated, and further precipitated using methanol/chloroform mixture: four volumes of methanol, one volume of chloroform, and three volumes of water. The mixture was vortexed and centrifuged to separate the chloroform phase and the aqueous phase. Then, the precipitated protein was washed with one volume of ice-cold methanol. The washed precipitated protein was allowed to air dry. Next, the precipitated protein was resuspended in 50 mM Tris, pH 8.5, 4 M urea. Then, proteins were firstly digested with LysC (1:50 - enzyme:protein) for 12 h at 25°C. The LysC digestion was diluted to 50 mM Tris, pH 8.5, 1 M urea and further digested with trypsin (1:100 - enzyme:protein) for 8 h

at 25°C. Next, the peptides were desalted using C18 solid phase extraction cartridges and the dried peptides resuspended in 200 mM EPPS, pH 8.0. Peptide quantification was performed using a microBCA assay (Pierce). The same amount of peptide from each condition was labelled with tandem mass tag (TMT) reagent (1:4 -peptide: TMT label, Pierce). The 10-plex labelling reactions were performed for 2 h at 25°C. Modification of tyrosine residues with TMT was reversed by the addition of 5% hydroxyl amine for 15 minutes at 25°C. The reaction was quenched with 0.5% (v/v) TFA, and samples were combined at a 1:1:1:1:1:1:1:1:1:1 ratio for 10-plex experiments, being desalted and fractionated offline into 24 fractions as previously described (Weekes, Tomasec et al. 2014).

3.17.2 Liquid chromatography-mass spectrometry

12 out of 24 peptide fractions from the basic reversed-phase step (every other fraction) were analyzed with an LC-MS3 data collection strategy (McAlister, Nusinow et al. 2014) on an Orbitrap Fusion mass spectrometer (Thermo Fisher Scientific Inc.) equipped with a Proxeon Easy nLC 1000 for online sample handling and peptide separations. 5 µg of peptide in 5% (v/v) formic acid and 5% (v/v) acetonitrile (ACN) was loaded onto a 100 µm inner diameter fused-silica micro capillary with a needle tip pulled to an internal diameter inferior to 5 µm. The column was packed in-house to a length of 35 cm with a C18 reversed-phase resin (GP118 resin, 1.8 µm, 120 Å, Sepax Technologies Inc., Newark, DE, USA). The peptides were separated using a 120-minute linear gradient from 3% to 25% of 100% (v/v) ACN/0.125% (v/v) formic acid and equilibrated with 3% (v/v) ACN and 0.125% (v/v) formic acid at a flow rate of 600 nL per minute. The scan sequence for the Fusion Orbitrap began with an MS1 spectrum (Orbitrap analysis; resolution, 120,000; 400−1400 m/z scan range; AGC target, 2 × 105; maximum injection time, 100 ms; dynamic exclusion, 75 seconds). ‘Top speed’ (2 seconds) was selected for MS2 analysis, which consisted of CID (quadrupole isolation set at 0.5 Da and ion trap analysis; AGC, 4 × 103; NCE, 35; maximum injection time, 150 ms). The top ten precursors from each MS2 scan were selected for MS3 analysis (synchronous precursor selection), in which HCD fragmented precursors prior to Orbitrap analysis (NCE, 55; max

AGC, 5 × 104; maximum injection time, 150 ms; isolation window, 2.5 Da; resolution, 60,000).

A suite of in-house software tools was used for RAW file processing and controlling peptide and protein level false discovery rates, assembling proteins from peptides, and protein quantification from peptides. MS/MS spectra were searched against a UniProt mouse database (2014) with both forward and reverse sequences. The database search criteria were as follows: tryptic with two missed cleavages, a precursor mass tolerance of 50 ppm, fragment ion mass tolerance of 1.0 Da, static alkylation of cysteine (57.02146 Da), static TMT labelling of lysine residues and N-termini of peptides (229.162932 Da), and variable oxidation of methionine (15.99491 Da). TMT reporter ion intensities were measured using a 0.003 Da window around the theoretical m/z for each reporter ion in the MS3 scan for 10-plex data (0.03 for 6-plex data). Peptide spectral matches with poor quality MS3 spectra were excluded from quantitation (<200 summed signal-to-noise across 10 channels, <100 for 6-plex and <0.5 precursor isolation specificity).

3.17.3 Mass spectrometry data analysis

Protein data (ProteinQuant) from all independent quantification experiments were uploaded into the mysql database and merged using Protein ID (SwissProt/UniProt ID). Each quantification run consisted of several plexes (groups of 10 samples analyzed together), with each plex including the same reference sample. Separately, the data for each plex were normalized by dividing the quantification result for each protein (protein ID) in a particular sample by the (nonzero) quantification result for the same protein in the reference sample. If the quantification result for a protein in the reference sample of a given plex had a value of zero or null, then the normalization result for this protein in this plex was set to null. The dataset was split into two parts: data that contained no null values and data that contained one or more null values. The data with no null values were clustered with the number of significant clusters determined by the gap statistics. The mean difference data (between every group and the control group) were loaded into KeggAnim for visualization of specific pathways (Adler, Reimand et al. 2008). The final expression of selected groups of proteins was visualized by heatmaps.

3.18 Lipidomic analysis

Neutral lipids content of total frozen liver tissue and phospholipids content of frozen isolated liver mitochondria were assessed using thin-layer chromatography (TLC). Moreover, the acyl-chains FAs composition of each class of lipids was assessed using Gas Chromatography-Mass Spectrometry (GC-MS) technique.

3.18.1 Lipid extraction

Lipids were extracted using Bligh and Dyer method (Bligh and Dyer 1959). Approximately 1.8 mg of frozen liver tissue and 500 µg of frozen isolated mitochondria were used to extract neutral lipids and phospholipids, respectively. Each sample was added to a glass tube containing 1 mL of chloroform:methanol (2:1) containing 0.01% (w/v) of butylated hydroxytoluene, followed by homogenization for 1 minute for mitochondria and 2 minutes for tissue. Next, 0.5 mL of distilled water was added to each tube which was vortexed for 20 or 30 seconds, for mitochondria and tissue respectively. Samples were centrifugated at 3,000x rpm for 10 minutes at 4ºC. After centrifugation, the resulting two-phase system was separated, with the bottom phase composed by lipids collected to a new glass tube and saved at -20ºC until further analysis.

3.18.2 Analysis of mitochondrial phospholipids

A TLC silica gel-60 plate was firstly pre-activated in an oven at 110ºC for 90 minutes. Meanwhile, a mixture composed by chloroform/methanol/acetic acid/water (50/37.5/3.5/2 (v/v/v/v)) was added to a tank container. Then, tubes containing mitochondrial lipid samples were placed under a N_2 flow at 37ºC until they evaporate completely. 100 µL of chloroform:methanol (2:1) was added to each tube. After TLC silica plate cooling down, each sample was loaded into the silica plate by using glass Pasteur pipettes and left to dry for 10 minutes. Silica plate was placed inside the tank container, and phospholipid species were left to separate by the action of the mobile solvent. After 2 h, silica plate was taken out and left to evaporate under the hood for another 10 minutes. Next, silica plate was soaked in 10% (w/v) cupric sulfate/8% (v/v)

phosphoric acid. Plate was placed inside the oven at 140ºC for 20 minutes, until phospholipid bands were visualized. Plate was scanned and bands were quantified using Image Studio Lite (version 5.2).

3.18.3 Neutral lipids in hepatocytes

A mixture composed by heptane/isopropyl ether/glacial acetic acid (60/40/3 (v/v/v)) was added to a tank container. Then, tubes containing liver lipid samples were placed under a N_2 flow at 37ºC until they evaporate completely. After 100 µL of chloroform:methanol (2:1) was added to each tube, each sample was loaded into the silica plate by using glass Pasteur pipettes. Plate was left to dry for 10 minutes, and placed inside the tank container. After 50 minutes, the silica plate was taken out and left to evaporate under the hood for another 10 minutes. Next, silica plate was soaked in 10% (w/v) cupric sulfate/8% (v/v) phosphoric acid. Plate was placed inside the oven at 140ºC for 20 minutes, until phospholipid bands were visualized. Plate was scanned and bands were quantified using Image Studio Lite (version 5.2).

3.18.4 Gas chromatography - mass spectrometry

For experimental study 1, liver neutral lipids and mitochondrial phospholipids were extracted and assessed according to the above-described protocols: lipid extraction; mitochondrial phospholipids analysis and neutral lipids analysis. After running TLC, instead of soaking the plates in 10% (w/v) cupric sulfate/8% (v/v) phosphoric acid, plates were visualized under an ultraviolet lamp after spraying with 0.2% (w/v) 2,3-dichlorofluorescein and incubation with NH_3 solution for 10 minutes. Then, bands of interest were identified with a pencil. For neutral lipids: TGs. For mitochondrial phospholipids: phosphatidylcholine (PC), phosphatidylethanolamine (PE) and cardiolipin. Each band was scraped off into a tube, followed by addition of 100 µL of internal standard (C19:0/R40) and 2 mL of chloroform:methanol (4:1) mixture containing 0.01% (w/v) of butylated hydroxytoluene. After overnight incubation in the dark, liquid fraction was collected and transferred into a new tube. Samples were placed under a N_2 flow at 37ºC until they evaporate completely. Next, samples were

transmethylated in the presence of 1 mL of 14% (v/v) boron trifluoride in a methanol solution at 100ºC, for 10 minutes for PC, PE and cardiolipin and 30 minutes for TGs. After, samples were taken out and left to cool down. Two-phase systems were obtained after adding 2 mL of hexane and 1 mL of water, followed by vortex and centrifugation at 3,000x rpm for 10 min at 4ºC. The fatty acid methyl esters present in the upper phase (hexane) were collected into new tubes and evaporated again in a N_2 flow at 37ºC. Tubes were resuspended in 110 µL of hexane, being 100 µL of this solution transferred to the final tubes of analysis. Analysis was performed by GC-MS with an Agilent 7890A-5975C GC-MS system (Agilent Technologies, Santa Clara, CA) equipped with an Agilent 19091N-205 capillary column. Nonadecanoic acid was used as an internal standard. The mass-to-charge ratios of the FA methyl esters were quantified by selected ion monitoring.

3.19 Metabolomic analysis

A metabolomic hepatic analysis was performed by obtaining ^{1}H and ^{13}C nuclear magnetic resonance (NMR) spectra of natural abundance in frozen liver samples for experimental groups 2 and 3. According to the Folch method (Folch, Lees et al. 1957), frozen liver tissue was homogenized in methanol (6.7 mL/g) followed by the addition of chloroform (13.3 mL/g). After 1 h of incubation on ice with agitation, samples were centrifuged at 13,000x g for 10 minutes. While pellet was saved, supernatant was collected and phase separation was induced by the addition of distilled water. After a new centrifugation at 13,000x g for 10 minutes, aqueous phase (water soluble metabolites) and organic phase (mostly TGs) were separated. While aqueous phase was lyophilized, organic samples were air dried for two days. Both fractions were stored at -80ºC until further use.

3.19.1 Triglycerides purification

Organic fractions were purified according to the method previously described by Hamilton & Comai (Hamilton and Comai 1988), using discovery solid phase extraction DSC-Si silica columns (2 g/12 mL). Firstly, columns were washed with 8 mL of hexane/methyl tert-butyl ether (MTBE) (96/4 (v/v)) and with 24 mL of hexane. Next,

dried lipid samples were resuspended with 500 µL of hexane/MTBE (200/3 (v/v)) and added to the column; this step was repeated once again to transfer total lipid fraction into the column. Then, column was eluted with 32 mL of Hexane/MTBE (96/4 (v/v)), being the eluted fraction collected in different flasks, further pooled together and air dried. Purified TGs were saved at -20ºC until NMR analysis.

3.19.2 Nuclear magnetic resonance

NMR spectra of aqueous samples and purified TGs samples were obtained at 25ºC with an Agilent V600 spectrometer (12.1 T, 600 MHz), equipped with a 3 mm broadband probe. Aqueous samples were dissolved in 180 µL of D_2O (99.8%) and 45 µL of buffer (50 mM phosphate, pD 7.4, 4.91 mM D_2O) and placed in 3 mm NMR tubes. Spectra were processed and peaks were integrated using an ACD/NMR Processor Academic Edition from ACD\Labs 12.0 software (Advanced Chemistry Development, Inc.). Spectra were set with tetramethylsilane (TMS) as a reference standard (0 ppm). Then, peaks of lactate, alanine, α-glucose and acetate were integrated (Fan 1996).

TGs samples were dissolved in 0.2 mL of CDCl3 and 10 µL of pyrazine standard and placed in 3 mm NMR tubes. Spectra were acquired with a 70º pulse, 2.5 seconds of acquisition time, 0.5 seconds of pulse delay, with the collection of 2,000-4,000 fid. Spectra were processed and peaks were integrated using an ACD/NMR Processor Academic Edition. ^{13}C spectra were set with chloroform as a reference standard (77.36 ppm) while ^{1}H spectra were set with pyrazine as the reference (8.6 ppm). As an internal control of TGs extraction, FA/glycerol ratio (between 2.85 and 3.10) was calculated (Duarte, Carvalho et al. 2014). FA profile (in percentage) of SFAs, MUFAs, palmitoleate acid and linoleate acid were estimated from the ^{13}C spectra, while ω-3 FAs and non ω-3 FAs were estimated from ^{1}H spectra described by Duarte et al. (Duarte, Carvalho et al. 2014). Even though it is a small correction, data collected from ^{1}H spectra were corrected for the presence of ^{13}C-^{1}H, which provides more precise estimates of ^{1}H signals for lipidomic analyses.

3.20 Principal component analysis (PCA)

Computational data analysis and visualization was performed for Experimental Group 2 with R program and for Experimental Group 3 with Orange 3.27.1. The parameters used for each PCA are defined in **Table 3**.

Table 3. List of parameters used for PCA analysis. PCA was performed in Experimental Group 2 and 3, focusing on the categories: fatty acids metabolism, Ca^{2+}-induced mPTP opening, oxidative stress, oxidative metabolism and autophagy.

Experimental Group 2	
Fatty acids metabolism	MS-proteomic data: ACLY, ACACA, FASN, ACSL4, AGPAT9, AGPAT3, LPIN2, DGAT1, DGAT2, SCAP, MLXIPL, SLC27A4, CD36, FABP2, FABP4, FABP5, SCD1, TECR, ELOVL5, ELOVL6, ELOVL1, ELOVL2, FADS1, FADS2, LIPE, MGLL, ACSL4, SLC27A4, SLC25A20, ACAD8, ACAD9, ACADL, ACADM, ACADSB, ECHDC2, ECHDC3, ACAA2, ECH1, HADHA, ACOT2, ACOT9, ABCD1, ABCD2, ACOX1, ACAA1A, ACOT3, ACOT4, ACOT8, ACOT12.
Ca^{2+}-induced mPTP opening	Ca^{2+}-induced mPTP opening; cardiolipin, phosphatidylcholine, sphingomyelin, phosphatidylethanolamine, phosphatidylinositol, phosphatidylserine.
Oxidative stress	H_2O_2 generation; lipid peroxidation; protein carbonylation; total antioxidant activity; SOD activity; catalase activity; GR activity; GPx activity; MS-proteomic data: SOD1, SOD2, SOD3, GSR, GSS, CAT, PRDX1, PRDX2, PRDX3, PRDX4, PRDX5, GPX1, GPX4, GLRX, GLRX3, GLRX5, MPO, CCS, PDIA6, SEPP1, MSRA, MSRB2, MSRB3, TXN, TXN2, TXNDC12, TXNDC15, TXNDC17, TXNDC5, TXNDC9, TXNL1, TXNRD1, TXNRD3.
Oxidative metabolism	MS-proteomic data: NDUFA10, NDUFA12, NDUFA13, NDUFA2, NDUFA5, NDUFA6, NDUFA7, NDUFA8, NDUFA9, NDUFAB1, NDUFB10, NDUFB11, NDUFB3, NDUFB4, NDUFB5, NDUFB6, NDUFB7, NDUFB8, NDUFB9, NDUFC2, NDUFS2, NDUFS3, NDUFS4, NDUFS5, NDUFS6, NDUFS7,

	NDUFS8, NDUFV1, NDUFV2, NDUFV3, MTND1, MTND4, MTND5, NDUFAF1, NDUFAFA2, NDUFAF3, NDUFAF4, NDUFAF7, TIMMDC1, TMEM16B, ECSIT, NUBPL, ACAD9, FOXRED1, NDUFAF6, SDHB, SDHC, CYC1, UQCR10, UQCRB, UQCRC1, UQCRC2, UQCRFS1, UQCRH, UQCRQ, UQCC2, BCS1L, HCCS, MTCO1, MTCO2, COX4I1, COX5A, COX5B, COX6A1, COX6B1, COX7A2, COX7A2L, COX17, COX15, SURF1, SCO1, LRPPRC, TACO1, FASTKD2, COA3, COA6, COA7, ATP5C1, ATP5D, ATP5E, ATP5F1, ATP5H, ATP5I, ATP5J, ATP5J2, ATP5L, ATP5O, ATP5S, MTATP8, ATPAF1, ATPAF2, HK1, HK3, GCK, ADPGK, GCKR, G6PC, PGM2, PFKL, PFKP, ALDOC,TPI1, PGK2, BPGM, PGAM1, PKLR, PKM, ADCY9, PRKACA, TIGAR, MDH1, MDH2, PGK2, GK, G6PC, PCX, PDHA1, PDHB, PDHX, DLAT, CS, IDH2, IDH3A, IDH3B, IDH3G, DHTKD1, SUCLG1, SUCLG2, GM20390, SDHB, SDHC, MDH2, PGM2, NUDT14, GSK3A, GSK3B, GAA, PYGL, CSNK1A1, CSNK1D, CSNK2A1, CSNK2A2, CSNK2B, LIPE, MGLL, ACSL4, SLC25A20, ACAD8, ACAD9, ACADL, ACADM, ACADSB, ECHDC2, ECHDC3, ECHS1, ECH1, HADHA, ACOT2, ACOT9.
Autophagy	LC3-II/LC3-I ratio; p-mTOR/mTOR ratio; p-AKT/AKT ratio; MS-proteomic data: INSR, PIK3C2A, PIK3C3, PIK3R1, PIK3R4, PDPK1, AKT1, AKT2, DEPTOR, LAMTOR1, LAMTOR5, MTORC, RICTOR, RPS6KA1, RPS6KA3, RPS6KA4, RPS6KB2, EIF4EBP1, BECN1, ATG12, ATG16L1, ATG2A, ATG3, ATG4B, ATG5, ATG7, SQSTM1, NBR1, BNIP3, PRKAA1, PRKAA2, PRKAB1, PRKACA, PRKACB, PRKAG1, PRKAR1A, PRKAR2B, CTSD, CTSO, CTSF, CTSZ, CTSS, CTSL, CTSB, CTSH.
Experimental Group 3	
Physiological parameters	body weight; liver weight; AST and ALT; lipid accumulation; TGs; DAGs; SFAs; MUFAs; palmitoleate; linoleate; ω-3 fatty acids.

1.21 Statistical analysis

Statistical analysis was performed using GraphPad Prism (version 8.0.2) for Windows (GraphPad Software, Inc., San Diego, CA USA).

Data were expressed as the mean ± standard error of the mean (SEM). Normality of the data was assessed with Shapiro–Wilk normality test. Then, non-normally distributed datasets were analyzed using the nonparametric Mann–Whitney test (two groups) or Kruskal–Wallis test (more than two groups) followed by Dunn's test for multiple comparisons. Normally distributed datasets were analyzed according to parametric tests. For experimental study 1 showed in Chapter 1, it was used Student's *t*-test and one-way ANOVA followed by Welch's correction or Bonferroni's multiple comparisons test, respectively. For experimental study 2 (showed in Chapter 2) and 3 (showed in Chapter 3), it was used two-way ANOVA followed by Fisher's LSD test. The level of significance considered was $P < 0.05$.

Part IV: Results and Discussion

CHAPTER 1: FAT AND SUCROSE INDUCE THE DEVELOPMENT OF FATTY LIVER WITH THE IMPAIRMENT OF AUTOPHAGIC FLUX IN MICE.

4.1 Results

4.1.1 HFHS-diet induces body and liver weight gain with increased ALT levels.

The hypercaloric consumption of HF- and HFHS-diets induced a progressive increase of body weight of mice during the sixteen weeks of feeding time, when compared to the CHOW-fed group (**Figure 12A, C**). These differences in body weight gain were maintained until the time of mice euthanasia (**Figure 12A**). No alterations were observed in body weight gain of HS-fed mice in comparison with the control group (**Figure 12A, C**).

Curiously, all hypercaloric diet regimens induced visceral fat accumulation in the abdominal cavity of the animals (**Figure 12C**). These alterations were accompanied by an augment of wet liver weight in HF- and HFHS-fed mice, being this effect especially increased in the latter (**Figure 12B, C**). Additionally, I observed not only an increase of the liver size but also an alteration of its color, indicative of hepatic lipid accumulation in mice fed with HF-, HS- and HFHS-diets (**Figure 12C**).

Although no significant differences were reported in the levels of AST enzyme activity, an upward trend in ALT enzyme activity in HF-fed mice and an increased activity in the HFHS-fed mice group were showed (**Figure 12D**).

Altogether, these results suggest at all hypercaloric diets induce hepatic fat accumulation, and this effect was accompanied by hepatocyte liver damage in HF- and HFHS-fed mice.

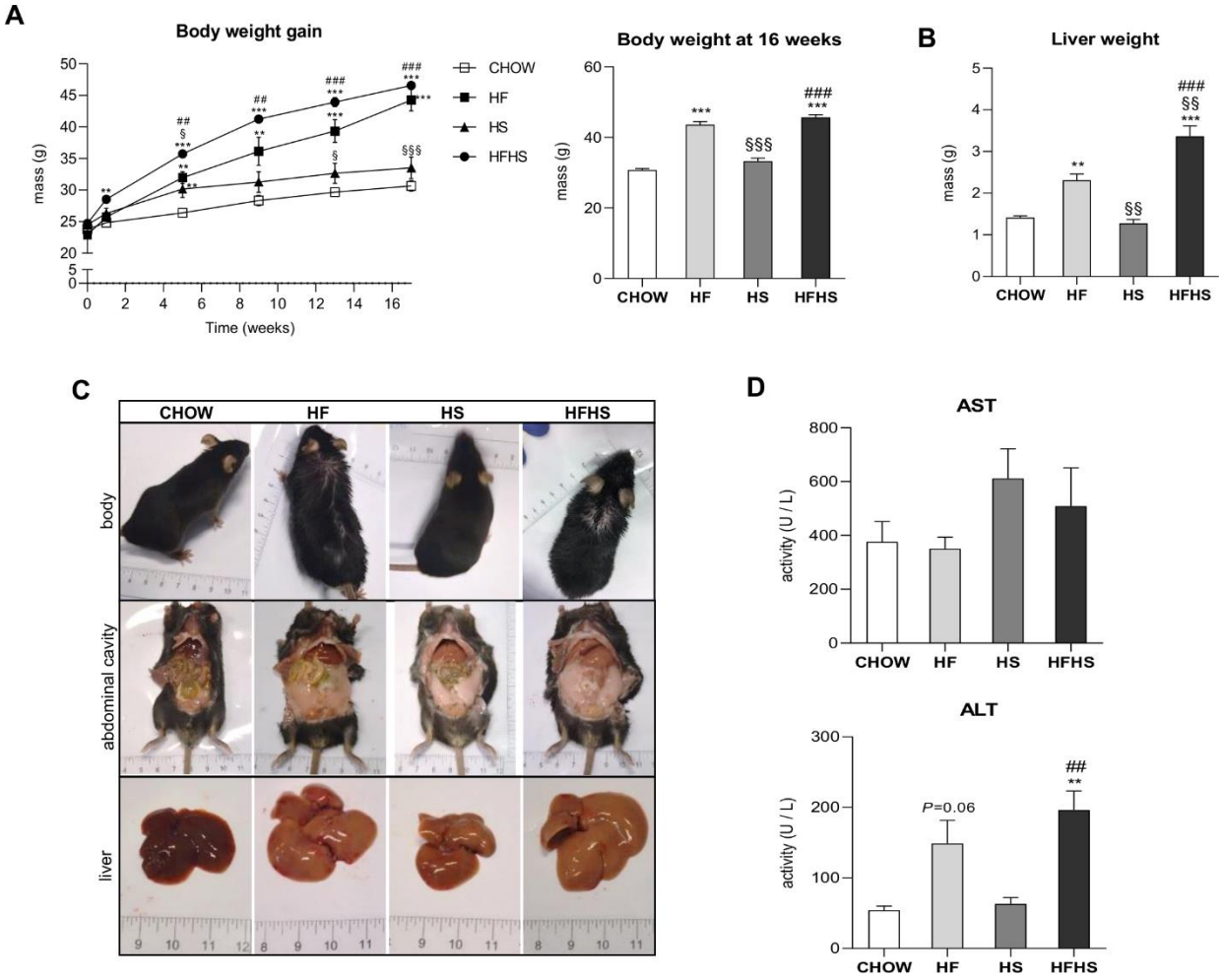

Figure 12. HF-, HS- and HFHS-diets increase body and liver weight of mice. (A) Body weight gain along the 16-weeks feeding period (left panel) and body weight at the time or mice euthanasia (right panel). **(B)** Liver weight at the time of mice euthanasia. **(C)** Representative images of body, abdominal cavity and livers of mice at euthanasia time. **(D)** Plasma aspartate aminotransferase (AST) and alanine aminotransferase (ALT) enzymes activity levels. All data are expressed as the mean ± SEM. (§) vs. the HF diet ($P < 0.05$); (**) vs. the CHOW diet, (§§) vs. the HF diet and (##) vs. the HS diet ($P < 0.01$); (***) vs. the CHOW diet, (§§§) vs. the HF diet and (###) vs. the HS diet ($P < 0.001$); *P* values were determined using one-way ANOVA followed by Bonferroni's post hoc test. HF, high-fat; HS, high-sucrose; HFHS, high-fat plus high-sucrose; AST, aspartate aminotransferase; ALT, alanine aminotransferase.

4.1.2 Hepatic lipid accumulation is induced by HF- or HS-diet intake, being early signs of fibrosis observed with HFHS-diet.

An increase in body weight is well correlated with the development of simple steatosis, which is diagnosed when at least 5% of hepatocytes present fat accumulation

(Fan, Wang et al. 2018). Therefore, to evaluate the effect of all hypercaloric diets in the mice livers, I assessed different hepatic parameters: steatosis, inflammation and fibrosis. These parameters were measured by performing distinct histological stainings. H&E staining revealed that all hypercaloric diets induce similar levels of steatosis, with this parameter staged as grade 3 according to the NAS score (**Figure 13A; Table 4**). Importantly, a more detailed analysis of hepatic lipid accumulation in oil-red staining showed that among the HF-, HS- and HFHS-diets, it was the HFHS-diet that caused the highest lipid accumulation (six-fold increase) (**Figure 13A, B**). Additionally, while HF- and HFHS-diets were characterized by inducing macrosteatosis, HS-diet was characterized to induce a microsteatosis phenotype (**Figure 13A**).

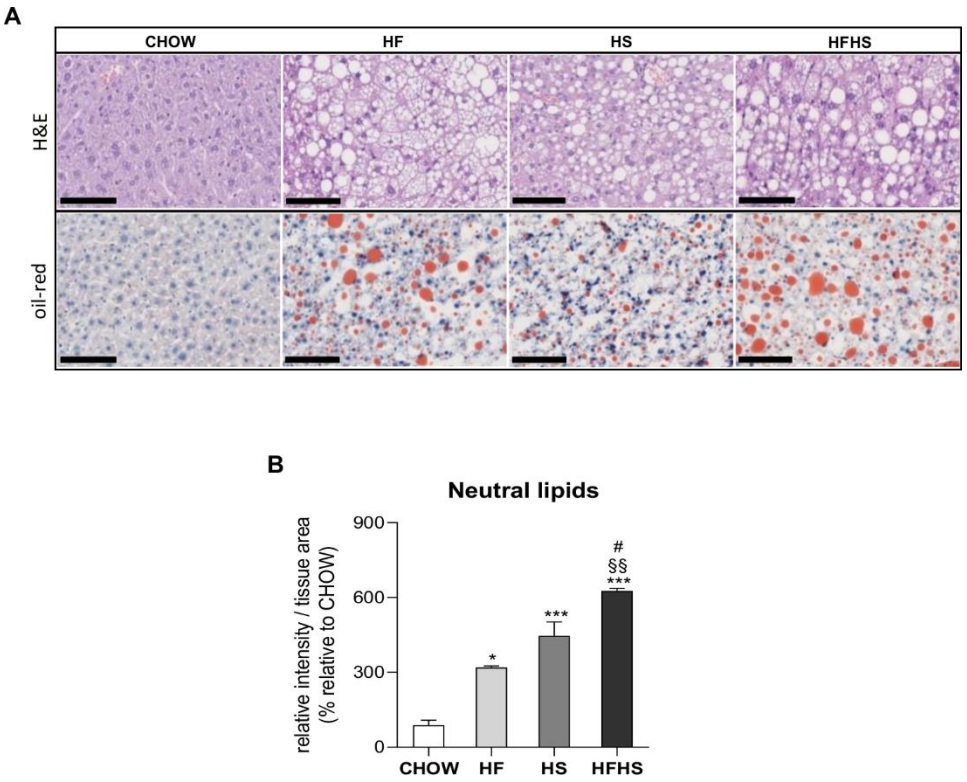

Figure 13. HF-, HS- and HFHS-diets induce simple steatosis with HFHS-diet inducing the highest lipid accumulation. (A) Representative images of paraffin-embedded mice liver sections with H&E and oil-red O stainings. Scale bar, 250 µm and magnification, 10×. **(B)** Hepatic neutral lipids accumulation of oil-red O staining, obtained from three independent images (per animal) from the experimental conditions shown in (A). All data are expressed as the mean ± SEM. (*) vs. the CHOW diet and (#) vs. the HS diet ($P < 0.05$); (§§) vs. the HF diet ($P < 0.01$); (***) vs. the CHOW diet ($P < 0.001$); *P* values were determined using one-way ANOVA followed by Bonferroni's post hoc test. H&E, hematoxylin and eosin; HF, high-fat; HFHS, high-fat plus high-sucrose; HS, high-sucrose.

Table 4. Histopathological evaluation of the NAS in NAFL mice.

NAFLD Activity Score (NAS)					NAS value[&]
Groups	**Steatosis**	**Ballooning**	**Inflammation**	**Fibrosis**	
CHOW	grade 0	grade 0	grade 0	S 0	0
HF	grade 3	grade 2	grade 0	S 0	5
HS	grade 3	grade 2	grade 0	S 0	5
HFHS	grade 3	grade 2	grade 0	S 1a	6

Abbreviations: CHOW, standard; HF, high-fat; HFHS, high-fat plus high-sucrose; HS, high-sucrose.

HF-, HS- and HFHS-diets also induced a decrease of glycogen levels in comparison with the CHOW-fed mice control group (**Figure 14A, B**).

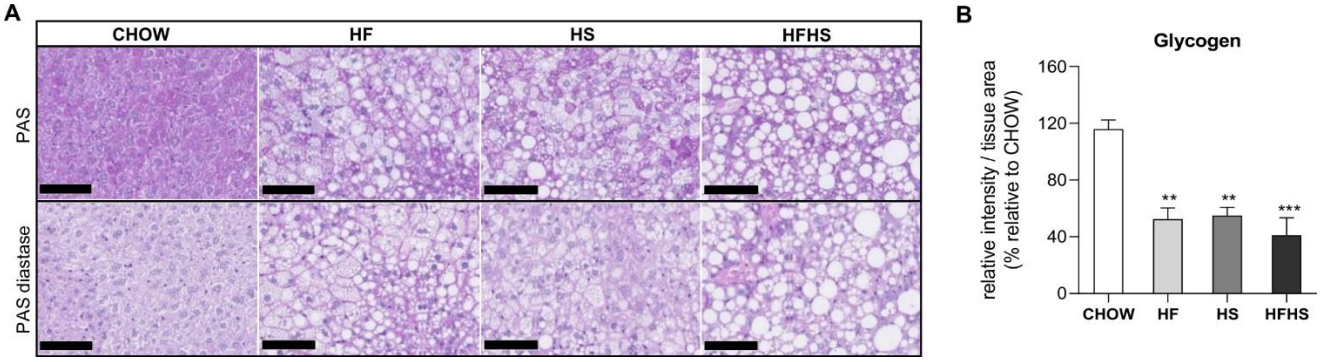

Figure 14. HF-, HS- and HFHS-diets decrease hepatic glycogen content in mice. (A) Representative images of paraffin-embedded mice liver sections with periodic acid–Schiff (PAS) and PAS diastase stainings. Scale bar, 250 µm and magnification, 10×. **(B)** Glycogen content in the liver, obtained from three independent images (per animal) from the experimental conditions shown in (A). All data are expressed as the mean ± SEM. (**) vs. the CHOW diet ($P < 0.01$); (***) vs. the CHOW diet ($P < 0.001$); *P* values were determined using one-way ANOVA followed by Bonferroni's post hoc test. HF, high-fat; HFHS, high-fat plus high-sucrose; HS, high-sucrose; PAS, periodic acid–Schiff.

Regarding the inflammatory state, I observed that all hypercaloric conditions led to a similar degree of hepatocyte ballooning (grade 2) and inflammation (grade 0) (**Table 3**). Additionally, I did not find significant alterations in the levels of CD3 and CD4 inflammatory markers, but an upward trend for CD68 marker was observed for all hypercaloric diets, especially for HF-fed mice (**Figure 15A, B**). Then, Masson's trichrome staining showed signs of perisinusoidal fibrosis in the HFHS-fed mice (**Figure 15A, Table**

13). By assessing the hepatic content of type 3 reticular fibers, I showed a decrease in the deposition of these fibers in HF- and HFHS-fed conditions (**Figure 15A, C**), suggesting alterations in the normal architecture of hepatic cells in these mice groups.

Considering that the NAFLD activity score is the sum of the steatosis, inflammation and fibrosis criteria (Kleiner, Brunt et al. 2005), I can conclude that HFHS is the diet that induces the highest NAS score, while HF- and HS-diets induces an equivalent grade.

These observations confirmed that all HF-, HS- and HFHS-diets induced an early stage of NAFLD, so called NAFL which is characterized by simple steatosis and absence of inflammatory markers. Although, HFHS-diet induced a more severe NAFL stage with early signs of fibrosis.

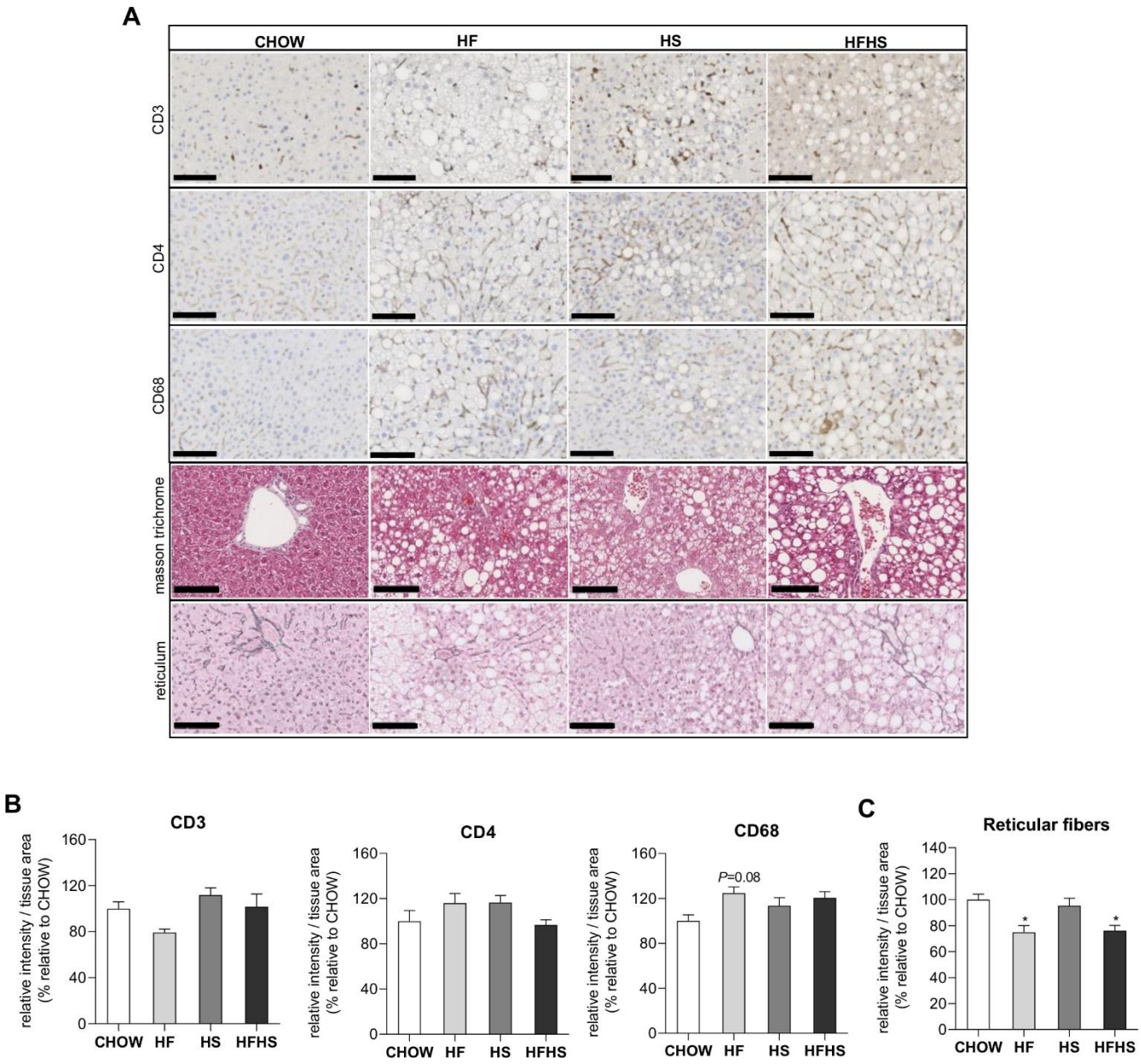

Figure 15. HF-, HS- and HFHS-diets induce an upward trend in CD68 marker, while HF- and HFHS-diet cause an abnormal architecture of hepatocytes. (A) Representative images of paraffin-embedded mice liver sections with CD3, CD4 and CD68 immunostaining, Masson's trichrome and reticular fibers stainings. Scale bar, 250 µm and magnification, 10×. **(B)** CD3, CD4 and CD68 quantification; **(C)** Reticular fibers quantification, obtained from three independent images (per animal) from the experimental conditions shown in (A). All data are expressed as the mean ± SEM. (*) vs. the CHOW diet ($P < 0.05$); *P* values were determined using one-way ANOVA followed by Bonferroni's post hoc test. HF, high-fat; HFHS, high-fat plus high-sucrose; HS, high-sucrose.

4.1.3 The consumption of fat, sucrose or the combination of both exacerbates hepatic TGs content enriched with monounsaturated fatty acids.

Next, I characterized hepatic lipid accumulation by performing TLC and GC-MS analysis. I observed that in the presence of HF-, HS- and HFHS-diets, the primary form of neutral lipids accumulated inside hepatocytes were TGs and CEs (**Figure 16A**). Additionally, these diets also induced higher levels of DAGs, especially in HF-fed mice (**Figure 16A**). No significant alterations were observed in the levels of FFAs while an upward trend in free cholesterol levels was observed for all hypercaloric diets in comparison to CHOW-fed group (**Figure 16A**). Accordingly, higher levels of TGs were in agreement with an augmented expression of proteins involved in the DNL pathway, such as ATP-citrate synthase (ACLY), acetyl-CoA carboxylase 1 (ACACA), fatty acid synthase (FASN) and glycerol-3-phosphate acyltransferase 3 (AGPAT9) in mice fed with HS- and HFHS-diets (**Figure 16B**). These observations seem to be correlated with an increased carbohydrates availability present in HS- and in HFHS-diets, and not in HF-diet. Moreover, HS- and HFHS-diets also induced higher levels of proteins responsible for the elongation of FAs such as ELOVL5 and 6 (**Figure 16C**).

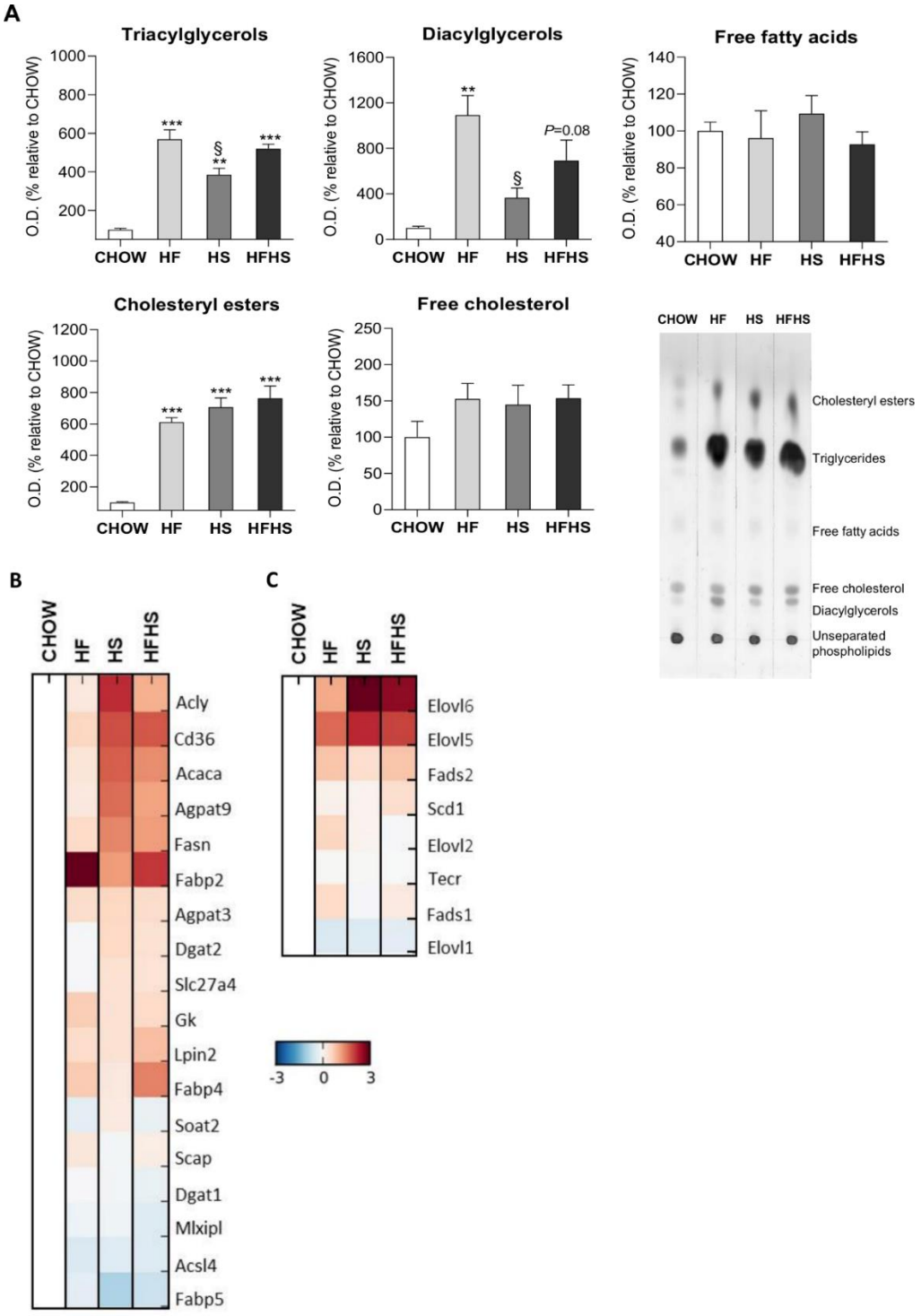

Figure 16. HF-, HS- and HFHS-diets induce hepatic lipid accumulation in the form of triglycerides and cholesteryl esters, with an increased protein expression of *de novo* lipogenesis pathway and elongases in HS- and HFHS-fed groups. (A) Optical density (in arbitrary units) of hepatic triglycerides, diacylglycerols, free fatty acids, cholesteryl esters and free cholesterol and representative thin-layer chromatography image of a replicate showing all neutral lipid species. **(B)** Hepatic protein expression levels involved in the *de novo* lipogenesis pathway. **(C)** Hepatic protein expression levels involved in the elongation of fatty

acids. The blue color represents decreased levels, and the red color represents increased levels. All data are expressed as the mean ± SEM. (§) vs. the HF diet ($P < 0.05$); (**) vs. the CHOW diet ($P < 0.01$); (***) vs. the CHOW diet ($P < 0.001$); *P* values were determined using one-way ANOVA followed by Bonferroni's post hoc test. HF, high-fat; HFHS, high-fat plus high-sucrose; HS, high-sucrose.

Next, GC-MS analysis revealed that the distinct hypercaloric diets induced a different pattern in accumulating saturated fatty acids (SFAs) and unsaturated fatty acids (USFAs) in the TGs fraction accumulated inside hepatocytes. Even though the HF-diet had a quite similar percentage of SFAs (14%) and USFAs (12%) (**Table 1**), I observed a higher accumulation of monounsaturated fatty acids (MUFAs) than SFAs levels in HF- and HFHS-fed mice (**Figure 17A**). Although to a lower extent, I also observed increased MUFAs levels in HS-fed group (**Figure 17A**). In terms of polyunsaturated fatty acids (PUFAs), I just found an increase in its levels in the HF condition (**Figure 17A**).

Additionally, a more detailed analysis showed an augmented accumulation of C14:0, C16:0 and C18:0 in TGs of all hypercaloric diets fed mice, in comparison with the CHOW-fed group (**Figure 17B**). MUFAs, specially C16:1, C18:1 and C20:1 were also enriched in HF-, HS- and HFHS-fed groups, being these species more abundant than PUFAs such as C20:2, C20:3n6, C20:4 and C22:6n3, which were just slightly increased in HF- and HFHS-fed groups (**Figure 17B**). These findings are in agreement with higher protein levels of elongases but particularly desaturases such as acyl-CoA desaturase 1 (SCD-1) and fatty acid desaturase (FADS)2 (**Figure 17B**). No significant alterations in protein levels of ELOVL1/2 and FADS1 could explain a lower content of PUFAs in lipid droplets of hepatocytes (**Figure 17B**). Overall, these results demonstrate that both HF- and HS-diets induce a higher and comparable enrichment of hepatic MUFAs.

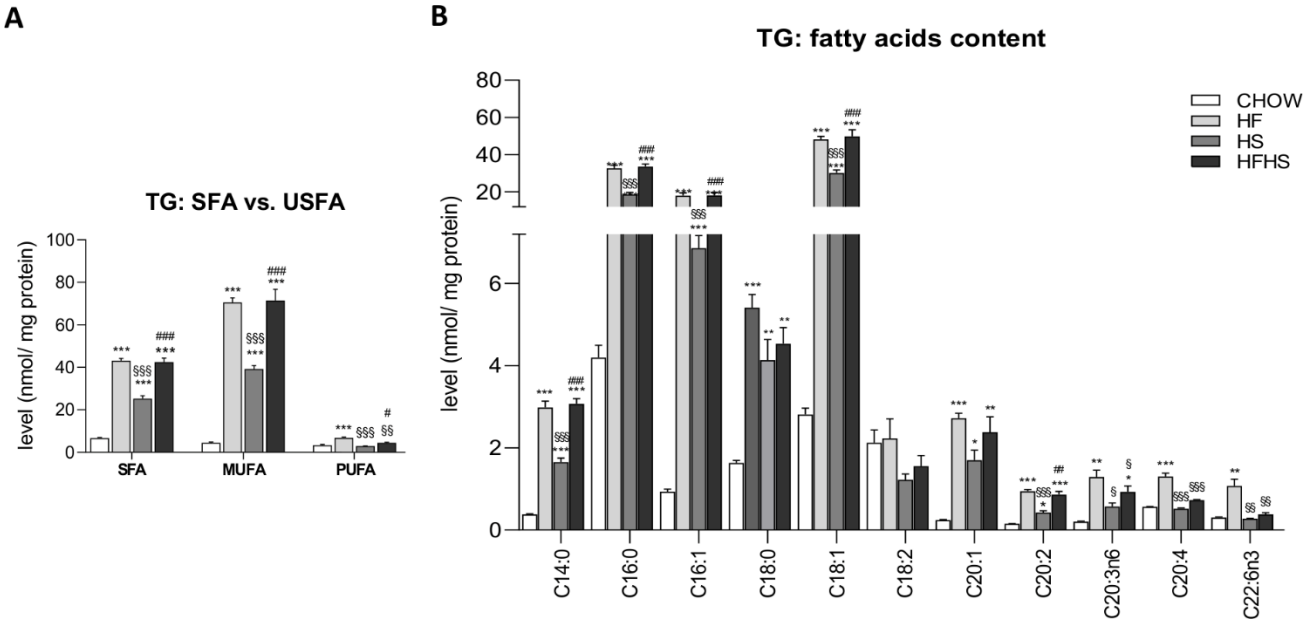

Figure 17. HF-, HS- and HFHS-diets induce an enrichment of saturated and monounsaturated fatty acids in triglycerides of fatty mice livers. (A) Saturated, monounsaturated and polyunsaturated fatty acids levels in triglycerides fraction of mice livers. **(B)** Detailed acyl chain fatty acids composition of triglycerides fraction of mice livers. All data are expressed as the mean ± SEM. (*) vs. the CHOW diet, (§) vs. the HF diet and (#) vs. the HS diet ($P < 0.05$); (**) vs. the CHOW diet, (§§) vs. the HF diet and (##) vs. the HS diet ($P < 0.01$); (***) vs. the CHOW diet, (§§§) vs. the HF diet and (###) vs. the HS diet ($P < 0.001$); *P* values were determined using one-way ANOVA followed by Bonferroni's post hoc test. HF, high-fat; HFHS, high-fat plus high-sucrose; HS, high-sucrose; MUFA, monounsaturated fatty acid; PUFA, polyunsaturated fatty acid; SFA, saturated fatty acid; TGs, triglycerides; USFA, unsaturated fatty acid.

4.1.4 HS- and HFHS-diets increase cardiolipin and decrease phosphatidylcholine/ phosphatidylethanolamine (PC/PE) ratio in liver isolated mitochondria.

Then, I examined the physiology and the function of the mitochondria in my NAFL mice model. Firstly, I investigated whether hypercaloric diets modulate mitochondrial membrane composition of mice livers. Using TLC analysis, I did not report alterations in the levels of phosphatidylcholine (PC) however I have observed an upward trend of phosphatidylethanolamine (PE) levels in isolated mitochondria of HS- and HFHS-fed mice when compared with CHOW-fed mice (**Figure 18**). Considered as the most abundant phospholipid species in mitochondrial membranes, PC/PE ratio is normally used as a measure of mitochondrial fluidity and integrity. Then, I have shown an upward trend of PC/PE ratio in the group of HF-fed mice, while a downward trend of this ratio

could be observed in HS- and HFHS-fed groups in comparison with the control group (**Figure 18**).

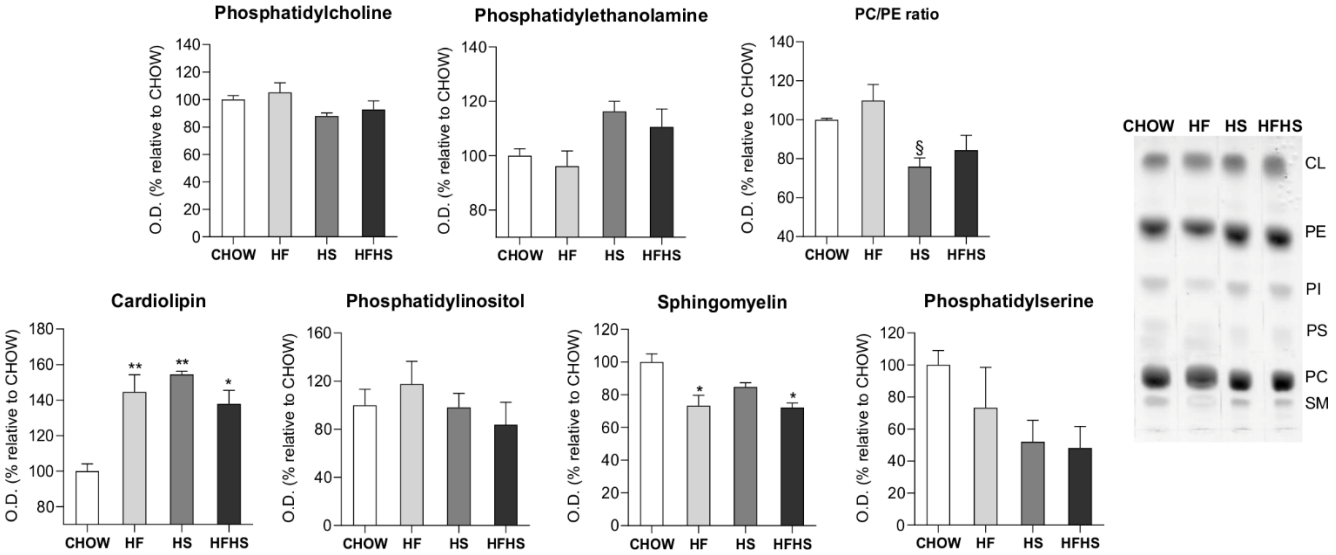

Figure 18. HF-, HS- and HFHS-diets induce phosphatidylethanolamine, cardiolipin, phosphatidylserine and sphingomyelin remodeling on mitochondrial membranes of liver mice. Optical density (arbitrary units) of phosphatidylethanolamine, phosphatidylcholine, cardiolipin, phosphatidylinositol, sphingomyelin and phosphatidylserine. Phosphatidylcholine/phosphatidylethanolamine (PC/PE) ratio was calculated. Representative image of thin-layer chromatography showing a replicate of mitochondrial phospholipid species. All data are expressed as the mean ± SEM. (*) vs. the CHOW diet and (§) vs. the HF diet ($P < 0.05$); (**) vs. the CHOW diet ($P < 0.01$); *P* values were determined using one-way ANOVA followed by Bonferroni's post hoc test or Kruskal–Wallis test followed by Dunn's post hoc test. CL, cardiolipin; HF, high-fat; HFHS, high-fat plus high-sucrose; HS, high-sucrose; PC, phosphatidylcholine; PE, phosphatidylethanolamine; PI, phosphatidylinositol; PS, phosphatidylserine; PUFA, polyunsaturated fatty acid; SFA, saturated fatty acid; SM, sphingomyelin; USFA, unsaturated fatty acid.

Regarding fatty acyl chain composition, I observed no major alterations in SFAs in PC phospholipid (**Figure 19A**). However, an upward trend in the MUFAs levels (C18:1) was found in HF-, HS- and HFHS-fed groups while a downward trend in PUFAs (C18:2 and C20:4) was reported in HS- and HFHS-fed mice (**Figure 19A**). Then, a different FAs acyl chain saturation/unsaturation profile was shown for PE phospholipid. In fact, there was an upward trend in SFAs (C18:0) in HFHS-fed group (**Figure 19B**). In this case, I did not report significant differences in MUFAs levels, however an upward trend of PUFAs levels particularly in HS- and HFHS-fed mice, with an enrichment of C20:3n6 and C22:6n3

species could be observed. Interestingly, both HF- and HFHS-diets also induced a decrease of C18:2 in PE (**Figure 19B**).

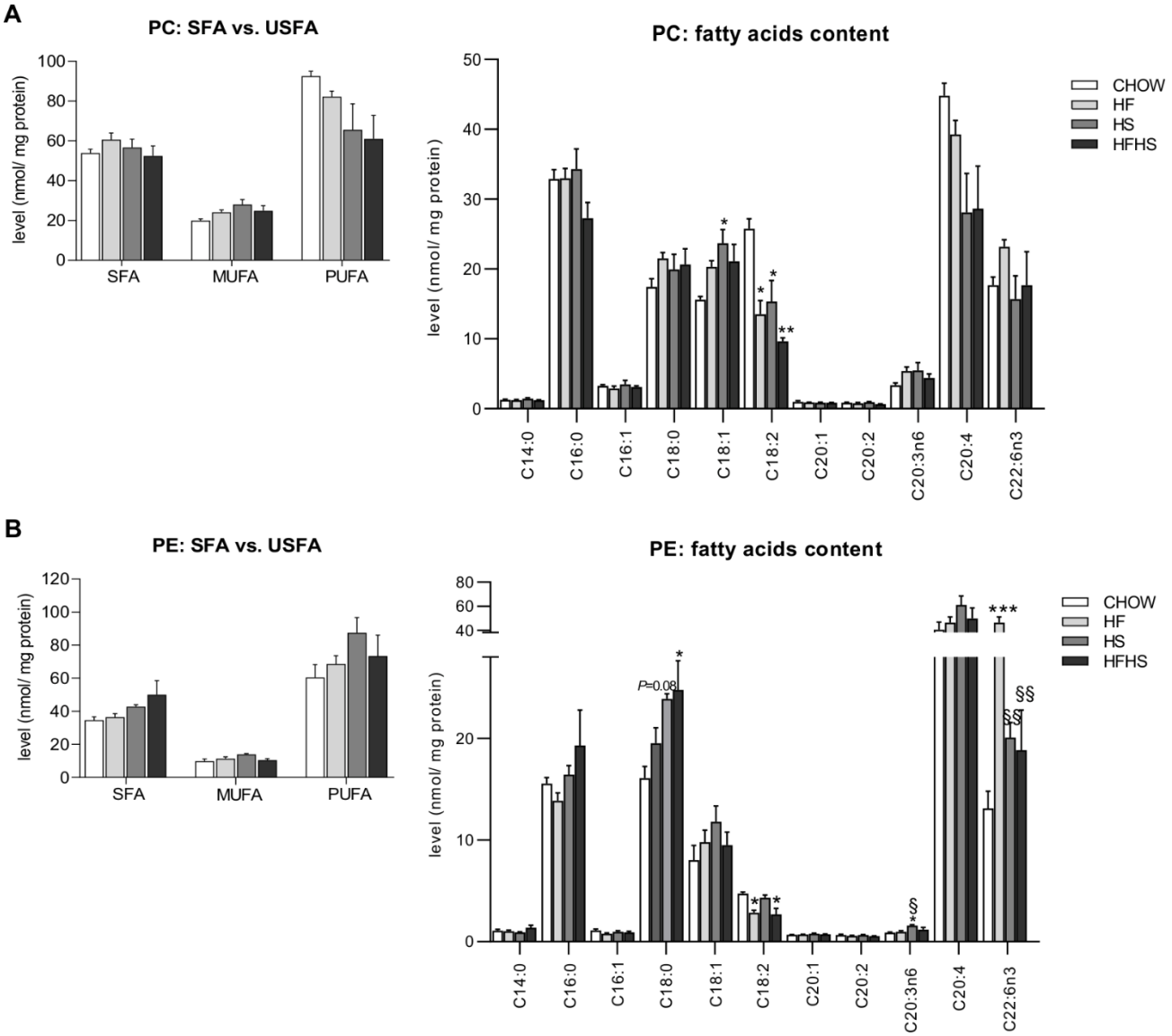

Figure 19. Hypercaloric diets trigger saturation/unsaturation of PC and PE fatty acyl chain composition in liver isolated mitochondria of NAFL mice. (A) Levels of SFAs, MUFAs and PUFAs in PC phospholipid (left panel) and the detailed fatty acyl chain composition of PC (right panel). **(B)** Levels of SFAs, MUFAs and PUFAs in PE phospholipid (left panel) and the detailed fatty acyl chain composition of PE (right panel). All data are expressed as the mean ± SEM. (*) vs. the CHOW diet and (§) vs. the HF diet ($P < 0.05$); (**) vs. the CHOW diet and (§§) vs. the HF diet ($P < 0.01$); (***) vs. the CHOW diet ($P < 0.001$); *P* values were determined using one-way ANOVA followed by Bonferroni post hoc test or Kruskal-Wallis test followed by Dunn post hoc test. HF, high-fat; HFHS, high-fat plus high-sucrose; HS, high-sucrose; PC, phosphatidylcholine; PE, phosphatidylethanolamine; PUFA, polyunsaturated fatty acid; SFA, saturated fatty acid; USFA, unsaturated fatty acid.

Additionally, I also evaluated the content of other mitochondrial phospholipids. Cardiolipin, a phospholipid signature of mitochondrial membranes, was found to be increased (40-50%) in all hypercaloric diets-fed groups compared to the CHOW-fed group (**Figure 18**). The cardiolipin levels of SFAs were not significantly altered, but an upward trend in the MUFAs levels (C16:1 and C18:1) was found for HF-, HS- and HFHS-fed mice (**Figure 19, Figure 20**). In respect to cardiolipin PUFAs, a detailed analysis revealed a reduction of C18:2, C20:2 in HF- and HFHS-fed groups, C22:6n3 in HS- and HFHS-fed groups and C20:4 in all treated groups (**Figure 20**). In contrast, I found augmented levels of C20:3n6 in all hypercaloric diets conditions (**Figure 20**).

Performed analysis of other phospholipids less abundant in mitochondrial membranes revealed a downward decrease of phosphatidylserine levels in HS- and HFHS-fed groups and a decrease of sphingomyelin levels just in mice fed with fat solely or in combination with sucrose. Additionally, I did not detect alterations in phosphatidylinositol levels (**Figure 18**).

These findings demonstrate that hypercaloric diets induce the remodelling of mitochondrial phospholipids species and their saturated/unsaturated fatty acyl chains composition in the liver of mice after sixteen weeks of feeding period.

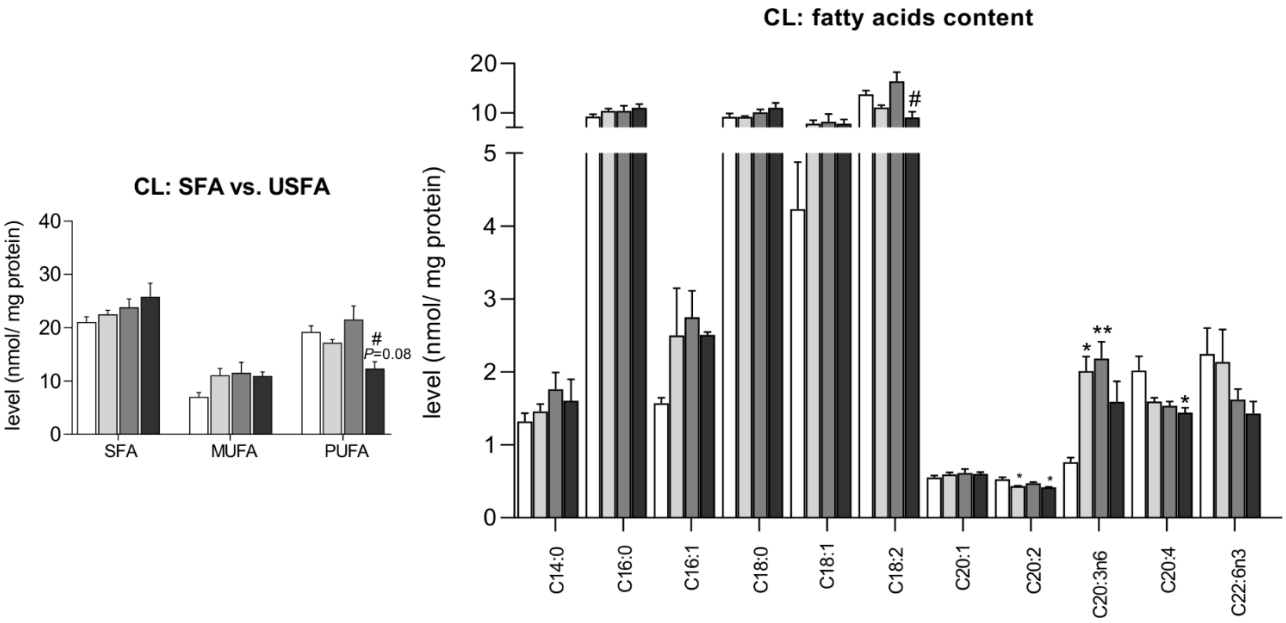

Figure 20. Hypercaloric diets trigger saturation/unsaturation of cardiolipin fatty acyl chain composition in liver isolated mitochondria of NAFL mice. Levels of SFAs, MUFAs and PUFAs in cardiolipin (left panel) and the detailed fatty acyl chain composition of cardiolipin (right panel). All data are expressed as the mean ± SEM. (*) vs. the CHOW diet and (#) vs. the HS diet ($P < 0.05$); (**) vs. the CHOW diet ($P < 0.01$); *P* values were determined using one-way ANOVA followed by Bonferroni's post hoc test or Kruskal–Wallis test followed by Dunn's post hoc test. CL, cardiolipin; HF, high-fat; HFHS, high-fat plus high-sucrose; HS, high-sucrose; MUFA, monounsaturated fatty acid; PUFA, polyunsaturated fatty acid; SFA, saturated fatty acid; USFA, unsaturated fatty acid.

4.1.5 HF- and HS-diets induce OXPHOS complexes remodelling but HFHS-diet decreases mitochondrial respiration.

It has been described that alterations in mitochondrial membrane composition could compromise its integrity and permeability with subsequent loss of OXPHOS complexes function inserted at the IMM level (Lu and Claypool 2015). Therefore, I assessed OXPHOS complexes subunits by Western blot technique. Despite no significant alterations among Complex I, II, IV and V subunits, I observed that all hypercaloric diets feeding regimens induced a significant reduction of Complex III subunit – UQCRC2 (18-25%) in comparison with CHOW-fed group (**Figure 21A**).

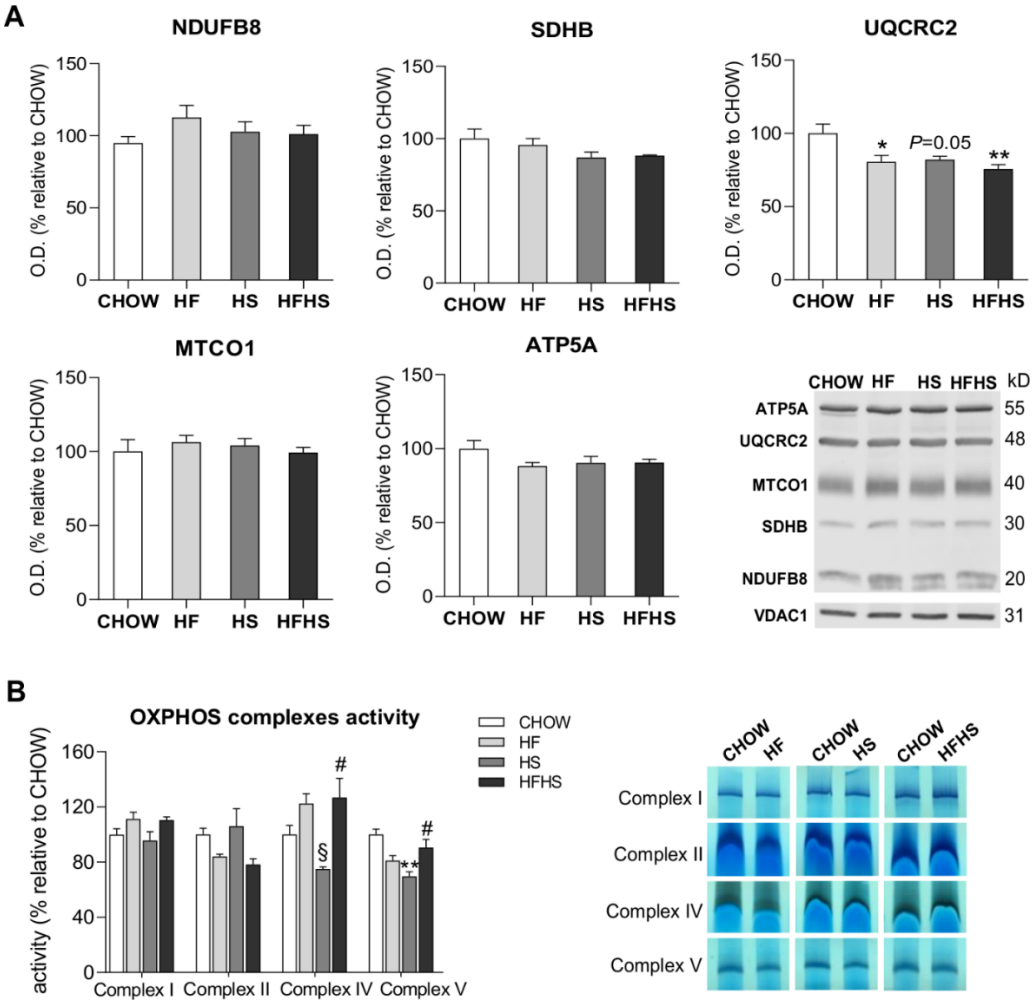

Figure 21. HF-, HS- and HFHS-diets cause alterations of mitochondrial OXPHOS complexes levels and activities. (A) Optical density (arbitrary units) of OXPHOS complexes subunits levels: NDUFB8 - Complex I; SDHB - Complex II; UQCRC2 - Complex III; MTCO1 - Complex IV; ATP5A – ATP synthase. Representative Western blot image using VDAC1 as the loading control. **(B)** OXPHOS complexes in gel activities and the representative image of in-gel activity assay for Complex I, II, IV and V. All data are expressed as the mean ± SEM. (*) vs. the CHOW diet, (§) vs. the HF diet and (#) vs. the HS diet ($P < 0.05$); (**) vs. the CHOW diet ($P < 0.01$); *P* values were determined using one-way ANOVA followed by Bonferroni's post hoc test or Kruskal–Wallis test followed by Dunn's post hoc test. HF, high-fat; HFHS, high-fat plus high-sucrose; HS, high-sucrose.

Moreover, using comparative mass spectrometry - proteomic analysis approach, I have shown a global reduction in the levels of several subunits and assembly factors of all OXPHOS complexes in the presence of HF-, HS- and HFHS-diets (**Figure 22A-E**).

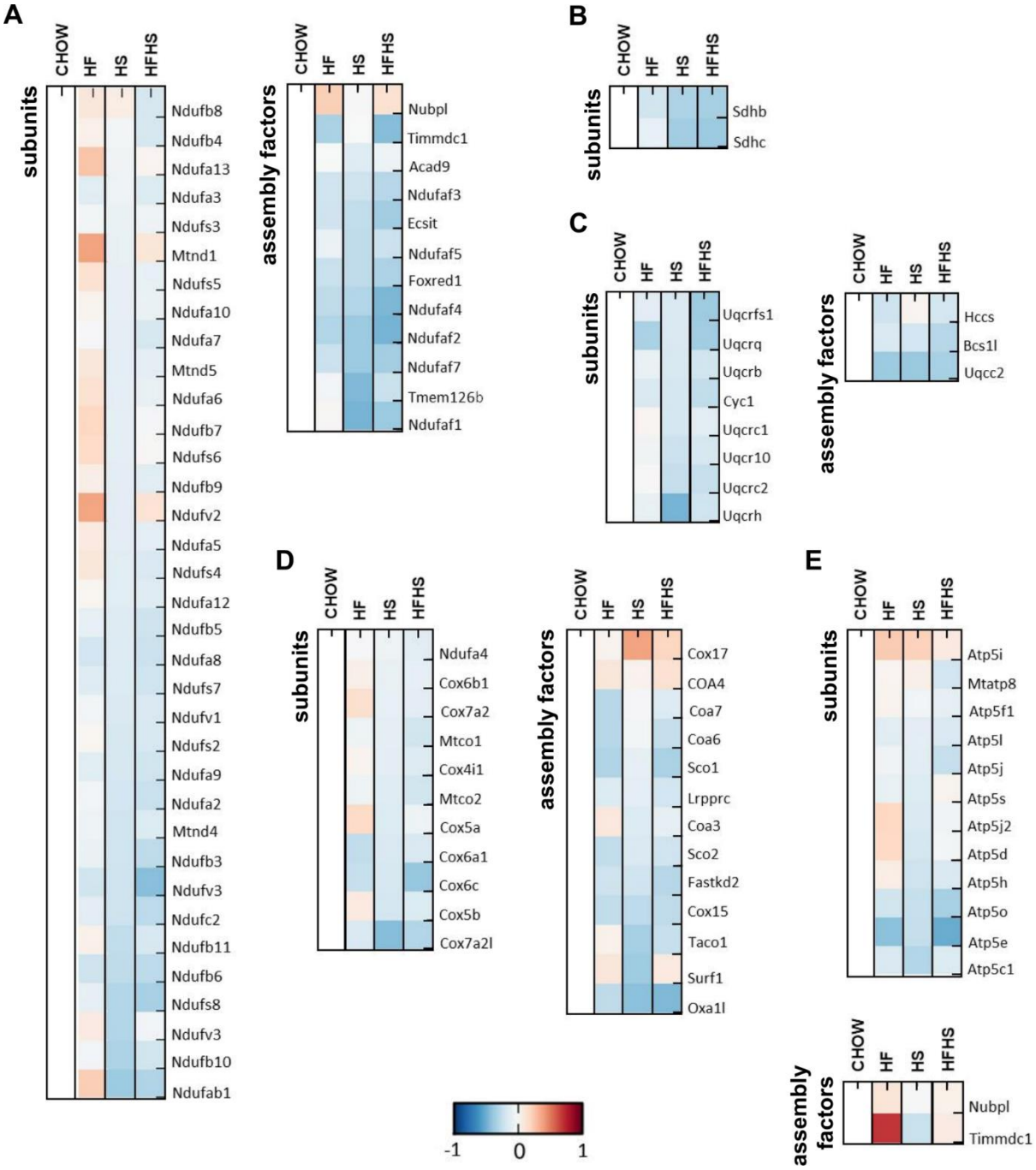

Figure 22. HF-, HS- and HFHS-diets decrease OXPHOS complexes composition in terms of their subunits as well as assembly factors in liver isolated mitochondria. (A) Protein levels of Complex I (subunits and assembly factors). **(B)** Protein levels of Complex II (subunits). **(C)** Protein levels of Complex III (subunits and assembly factors). **(D)** Protein levels of Complex IV (subunits and assembly factors). **(E)** Protein levels of ATP synthase (subunits and assembly factors). The blue color represents decreased protein levels while the red color represents increased protein levels. HF, high-fat; HFHS, high-fat plus high-sucrose; HS, high-sucrose.

Then, I separated OXPHOS complexes by BN-PAGE and measured their activities by in-gel activity assay. I have shown an upward trend for Complex I and IV activities in HF- and HFHS-fed mice. The activity of Complex II was slightly decreased in the same mice groups (**Figure 21B**). Additionally, I have found that HS-diet induced a downward trend in Complex IV activity, with HS- but also HF-diet triggering a decrease in ATP synthase activity (**Figure 21B**). It is important to note that OXPHOS complexes activities were measured independently and not in their native environment in a supercomplexes structure. Based on alterations of mitochondrial phospholipids, OXPHOS levels and their respective activities, I suggested that Western-like diets could impair mitochondrial function. Therefore, next, I evaluated mitochondrial oxygen consumption. HFHS-diet induced a decrease of oxygen consumption in State 4 (no ADP stimulated respiration) (46%) and in State 3 (ADP stimulated respiration) (38%) in comparison with CHOW-fed mice (**Figure 23A**).

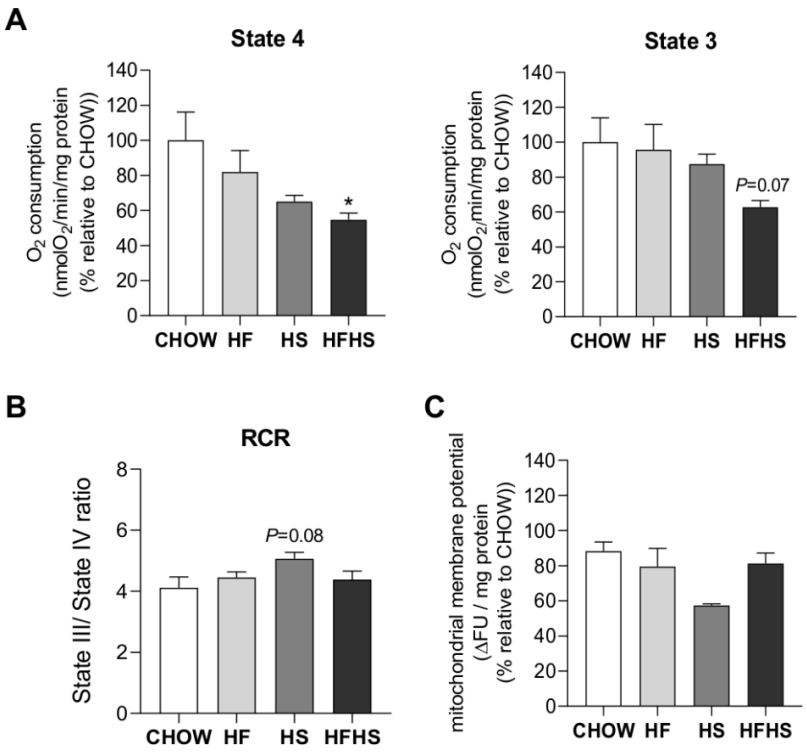

Figure 23. HFHS-diet decreases mitochondrial respiration but respiratory control ratio is sustained in the same group. (A) Oxygen consumption rate in State 4 and in State 3 of fresh liver isolated mitochondria. **(B)** Respiratory control ratio (State 3/State 4) of fresh liver isolated mitochondria. **(C)** Mitochondrial membrane potential of fresh liver isolated mitochondria. All data are expressed as the mean ± SEM. (*) vs. the CHOW diet ($P < 0.05$); *P* values were determined using one-way ANOVA followed by Bonferroni's

post hoc test or Kruskal–Wallis test followed by Dunn's post hoc test. mΔΨ, mitochondrial membrane potential; HF, high-fat; HFHS, high-fat plus high-sucrose; HS, high-sucrose; RCR, respiratory control ratio.

Despite such a decrease, respiratory control ratio (RCR) of HFHS-fed mice was not altered (**Figure 23B**). Curiously, an upward trend of RCR in HS-fed group in comparison with CHOW-fed group was observed, suggesting a higher mitochondrial coupling efficiency in this condition (**Figure 23B**). Moreover, I measured the capacity of mitochondria to generate mΔΨ. Even though no significant alterations were reported between the distinct dietary regimens tested and the CHOW control group, ΔΨm was slightly diminished in HS-fed condition (**Figure 23C**).

Altogether, these findings showed that alterations in mitochondrial phospholipids and OXPHOS complexes do not impair mitochondrial coupling efficiency, despite a decrease of mitochondrial respiration in the presence of HFHS-diet.

4.1.6 HF- and HS-diets decrease mitochondrial oxidative damage while increase cytosolic oxidative damage linked to a peroxisomal dependent pathway.

Then, I investigated whether mitochondrial alterations at the level of oxidative phosphorylation are somehow correlated with mitochondrial ROS production and signs of oxidative damage. Therefore, I assessed H_2O_2 production in liver isolated mitochondria. Surprisingly, HF-diet induced a decrease in H_2O_2 production while no significant alterations were observed when HS- or HFHS-diets were compared with CHOW-fed group (**Figure 24A**). In line with previous findings, I found no signs of mitochondrial oxidative damage in proteins or in lipids. In fact, HF-, HS- or the combination of both diets induced a reduction of DNP and nitrotyrosine levels (**Figure 24B**). In the case of mitochondrial lipids, HF- and HS-diets caused a reduction of lipid peroxidation (**Figure 24C**).

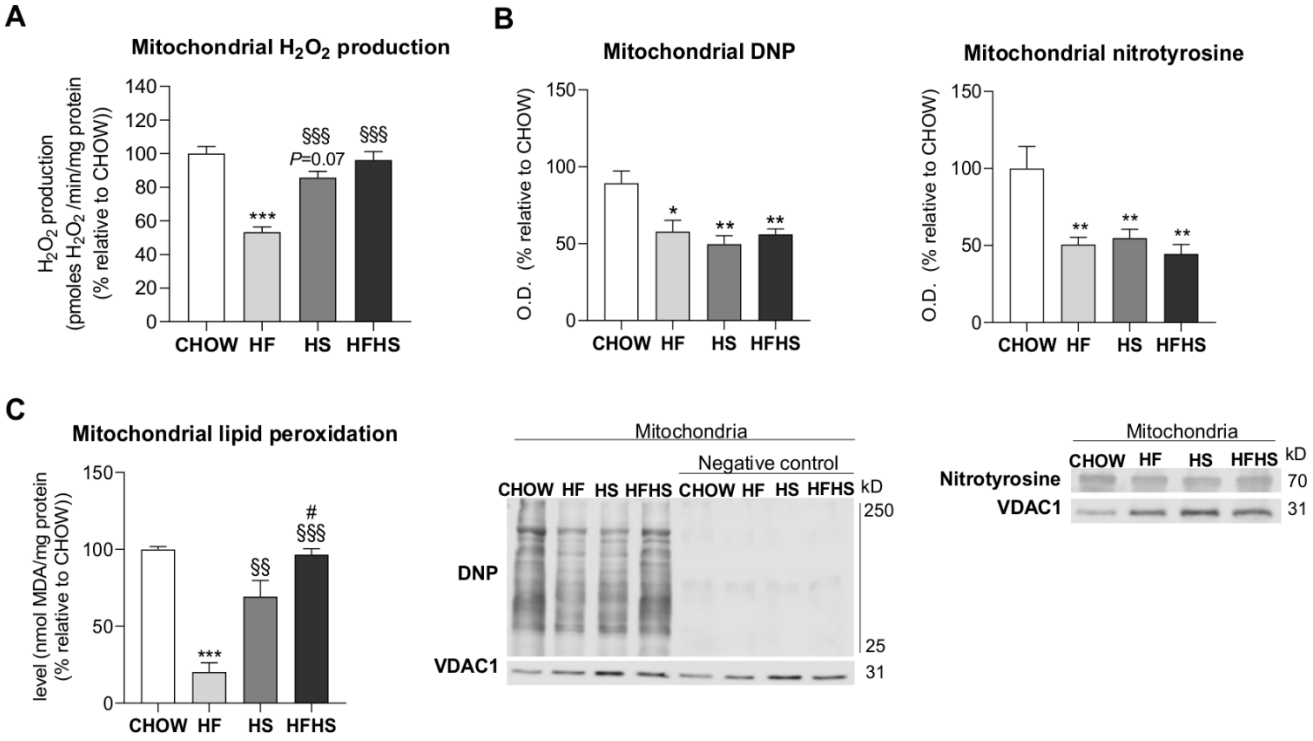

Figure 24. No excess of ROS generation neither oxidative damage was observed in liver isolated mitochondria of HF-, HS- or HFHS-fed mice. (A) Mitochondrial H_2O_2 production rate of fresh liver isolated mitochondria. **(B)** Optical density (arbitrary units) of mitochondrial DNP and nitrotyrosine levels, with representative Western blot image. VDAC1 protein was used as mitochondrial loading control. **(C)** Levels of malondialdehyde in liver mitochondria. Data are expressed as the mean ± SEM. (*) vs. the CHOW diet and (#) vs. the HS diet ($P < 0.05$); (**) vs. the CHOW diet and (§§) vs. the HF diet ($P < 0.01$); (***) vs. the CHOW diet and (§§§) vs. the HF diet ($P < 0.001$); *P* values were determined using one-way ANOVA followed by Bonferroni's post hoc test. DNP, dinitrophenyl; HF, high-fat; HFHS, high-fat plus high-sucrose; HS, high-sucrose; MDA, malondialdehyde.

Next, I performed the same studies with the use of whole liver lysates. In this case, I observed a decrease of DNP and nitrotyrosine levels in livers of mice fed with HS- or with the combined HFHS-diet (**Figure 25A**). In contrast, HFHS diet-induced an upward trend while HF- and HS-diets induced a significant increase (50%) of lipid peroxidation compared to the CHOW-fed group (**Figure 25B**).

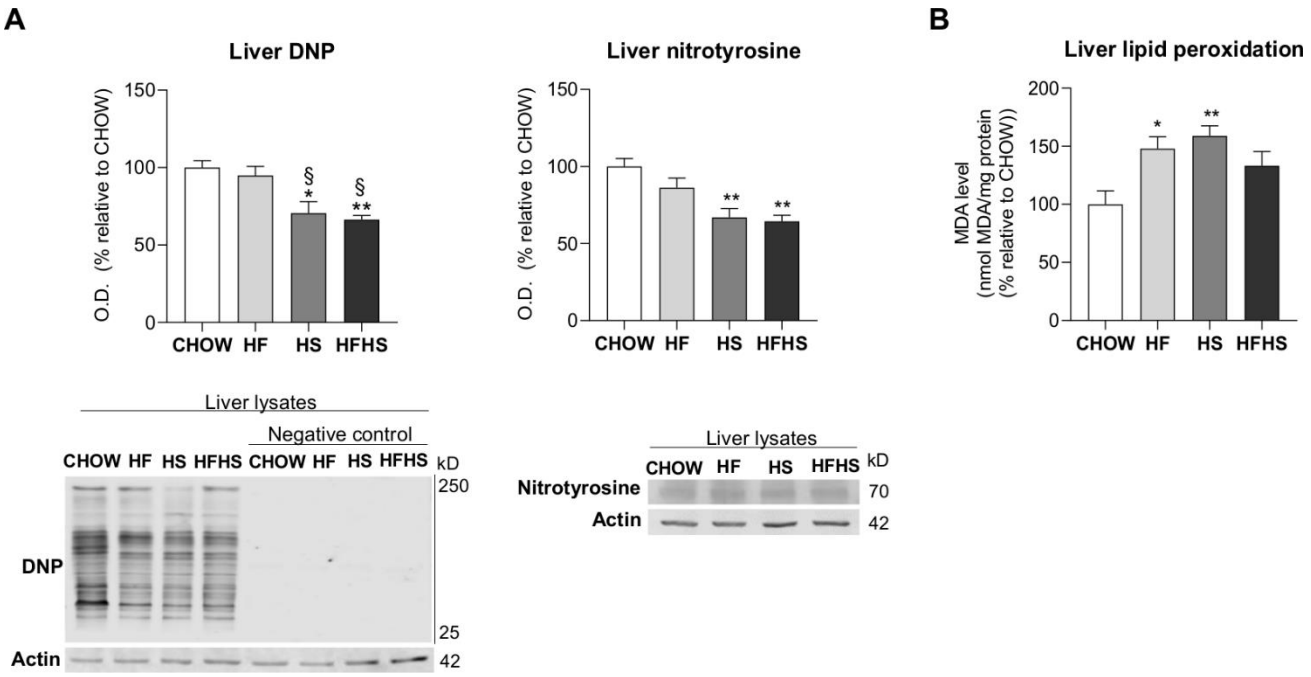

Figure 25. HF- and HS-diets induced higher hepatic lipid peroxidation. (A) Optical density (arbitrary units) of total liver homogenate DNP and nitrotyrosine levels, with the representative Western blot image. Actin was used as cytosolic loading control. **(B)** Levels of malondialdehyde in total liver homogenate. Data are expressed as the mean ± SEM. (*) vs. the CHOW diet and (§) vs. the HF diet ($P < 0.05$); (**) vs. the CHOW diet ($P < 0.01$); *P* values were determined using one-way ANOVA followed by Bonferroni's post hoc test. DNP, dinitrophenyl; HF, high-fat; HFHS, high-fat plus high-sucrose; HS, high-sucrose; MDA, malondialdehyde.

Furthermore, I investigated the possible source of ROS generation associated with the observed cytosolic oxidative damage. Among the possible sources, I focused on FAO, particularly on mitochondrial and peroxisomal-dependent pathways. Using MS-proteomic analysis, I reported an increase of acyl-coenzyme A thioesterase (ACOT)2 protein level. The other proteins involved in mitochondrial FAO were not significantly altered in comparison to CHOW-fed group (**Figure 26A**). Opposingly, peroxisomal FAO-related proteins such as ACOT3, ACOT4, and ATP-binding cassette subfamily D member (ABCD)2 were found extremely augmented in all hypercaloric diets tested (**Figure 26B**). To support the role of peroxisomal FAO in a NAFL stage, I have also found an increase (from 2- up to 4-fold) in the levels of peroxisomal proteins such as membrane-related (PEX11a, PEX13, PEX14 and PEX16), assembly-related (PEX19 and PEX6) and biogenesis-related (PEX1 and PEX3) proteins on the same hypercaloric diet-fed groups versus

CHOW-fed group (**Figure 26B**). These results suggest that HF-, HS- or in combination induce not only higher peroxisomal number but also higher peroxisomal FAO activity.

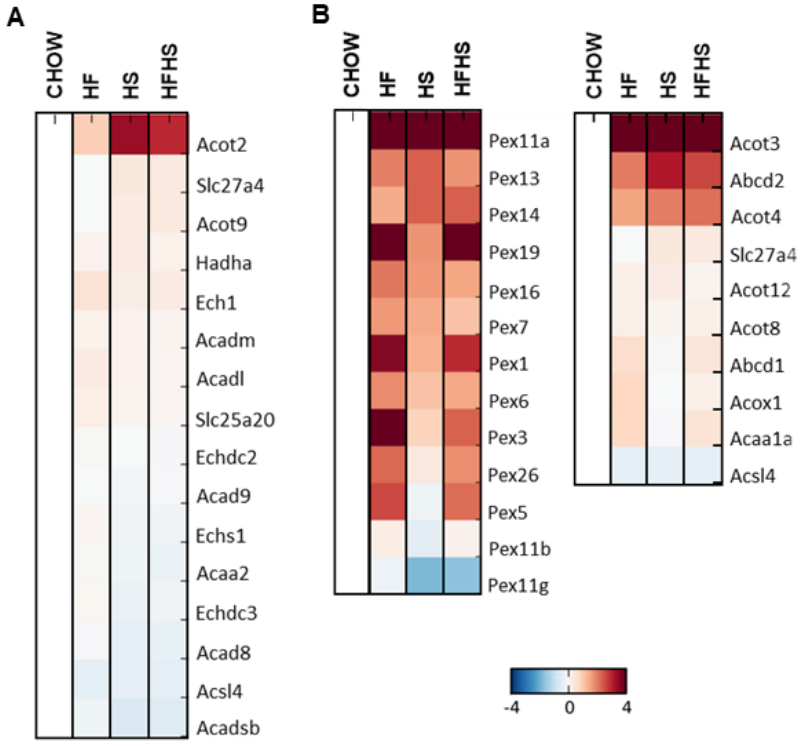

Figure 26. A higher protein expression of fatty acid oxidation-related pathways, specially peroxisomal-dependent pathway was reported for HF-, HS- and HFHS-feeding regimens. (A) Hepatic protein levels of mitochondrial fatty acid oxidation-related pathway. **(B)** Hepatic protein levels of peroxisomal-related markers and peroxisomal fatty acid oxidation-related pathway. The blue color represents decreased protein levels while the red color represents increased protein levels. HF, high-fat; HFHS, high-fat plus high-sucrose; HS, high-sucrose.

Based on the signs of hepatic oxidative damage, in the next step, I analyzed the cellular antioxidant defense system. The levels of antioxidant defense enzymes were assessed through MS-proteomic analysis, being revealed augmented levels of metallothionein-1 (MT1) in mice fed with HS- and HFHS-diets and increased SOD3 and selenoprotein P (SEPP1) protein levels in mice fed with HF- and HFHS-diets (**Figure 27**). Additionally, HF-diet induced an increase of glutaredoxin (GLXR) protein level and the combined HFHS-diet induced an increase of myeloperoxidase (MPO) and GPX4 protein levels (**Figure 27**).

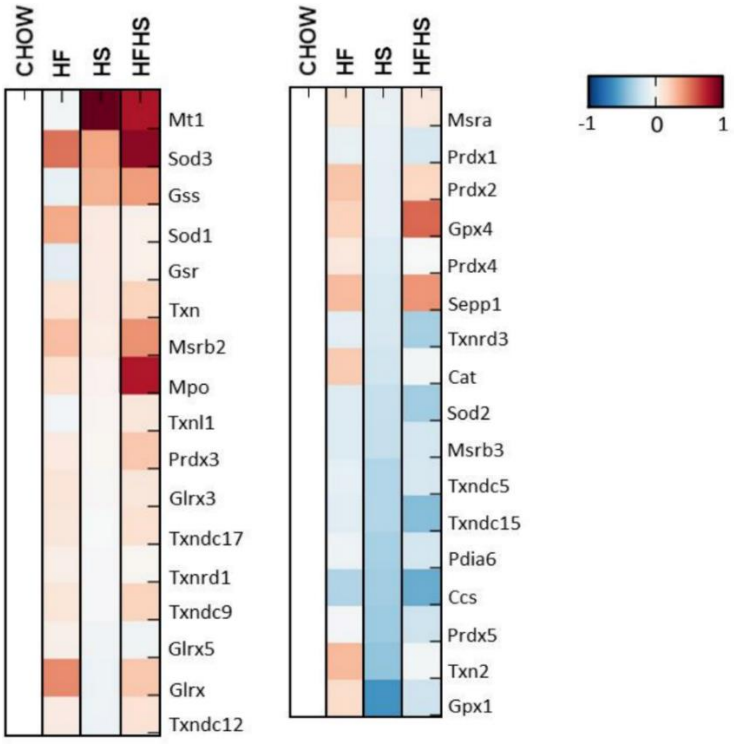

Figure 27. Hypercaloric diets induce alterations in the levels of hepatic antioxidant enzymes. Hepatic protein expression levels of antioxidant defense enzymes. The blue color represents decreased protein levels while the red color represents increased protein levels. HF, high-fat; HFHS, high-fat plus high-sucrose; HS, high-sucrose.

Additionally, I determined the activities of antioxidant enzymes in two distinct fractions: cytosol and mitochondria. The purity of both cytosolic and mitochondrial fractions was shown in **Figure 28A**. Actin and GAPDH were considered as cytosolic markers and VDAC1 as a mitochondrial marker.

I observed an increase of cytosolic SOD activity in HS-fed group. The activity of this enzyme was also found slightly elevated in mice fed with HF- and HFHS-diets (**Figure 28B**). Curiously, cytosolic SOD activity is in line with the hepatic lipid peroxidation profile shown in **Figure 25B**. However, an increase of SOD activity was not accompanied by any increase in catalase activity (**Figure 28B**), which indicates a de-regulation of the hepatic antioxidant defense system in animals fed with hypercaloric diets tested. At cytosolic level, I also reported a reduction in GPx and a downward trend in GR activities in HF-fed mice in comparison with CHOW-fed group (**Figure 28B**). Then, at mitochondrial level, no alterations were reported in SOD or catalase activities. I observed just a slight decrease

in GPx and GR activities in HF-, HS- and HFHS-fed mice when compared with CHOW-fed group (**Figure 28C**).

Altogether, these observations demonstrate the absence of mitochondrial ROS generation in steatotic livers and suggest that hepatic oxidative damage could have origin in another ROS generating organelle such as peroxisomes, known to be involved in FAO-related pathway. Moreover, an imbalance of cytosolic antioxidant defense system seems to contribute/exacerbate the hepatic oxidative damage found in the presence of hypercaloric diets.

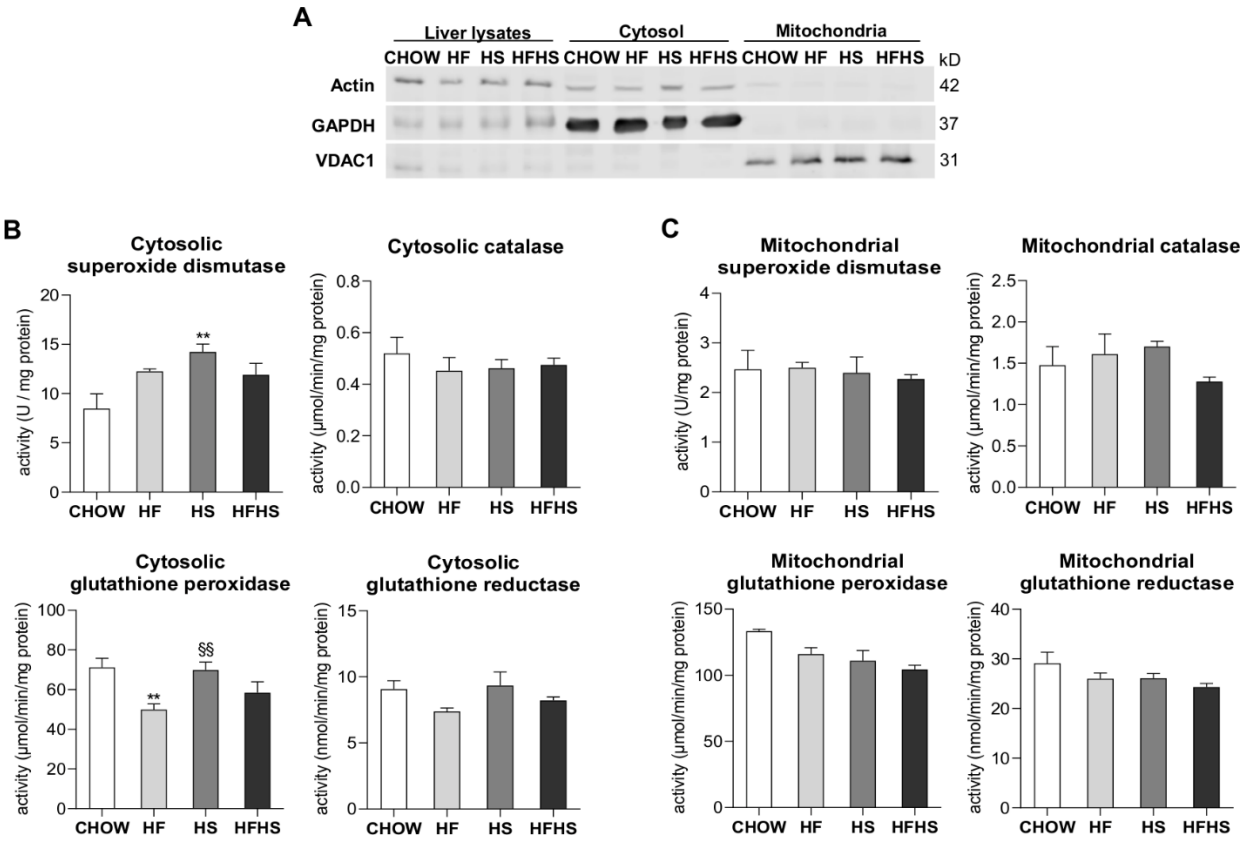

Figure 28. HF- and HS-diets induced higher hepatic lipid peroxidation. (A) Representative image of Western blot showing the purity of cytosolic and mitochondrial fractions of mice livers. Actin and GAPDH were used as cytosolic protein markers while VDAC1 was used as a mitochondrial protein marker. **(B)** Cytosolic activities of superoxide dismutase, catalase, glutathione peroxidase and glutathione reductase. **(C)** Mitochondrial activities of superoxide dismutase, catalase, glutathione peroxidase and glutathione reductase. Data are expressed as the mean ± SEM. (**) vs. the CHOW diet and (§§) vs. vs. the HF diet ($P < 0.01$); *P* values were determined using one-way ANOVA followed by Bonferroni's post hoc test. HF, high-fat; HFHS, high-fat plus high-sucrose; HS, high-sucrose.

4.1.7 Hypercaloric diets induce alterations in hepatic autophagic flux.

PI3K/AKT/mTOR signaling pathway is involved in the regulation of protein homeostasis and in the cellular adaptative response to oxidative stress. In this part of the work, I analyzed the levels of proteins involved in this pathway. MS-proteomic analysis did not reveal major differences between the feeding regimens evaluated (**Figure 29A**).

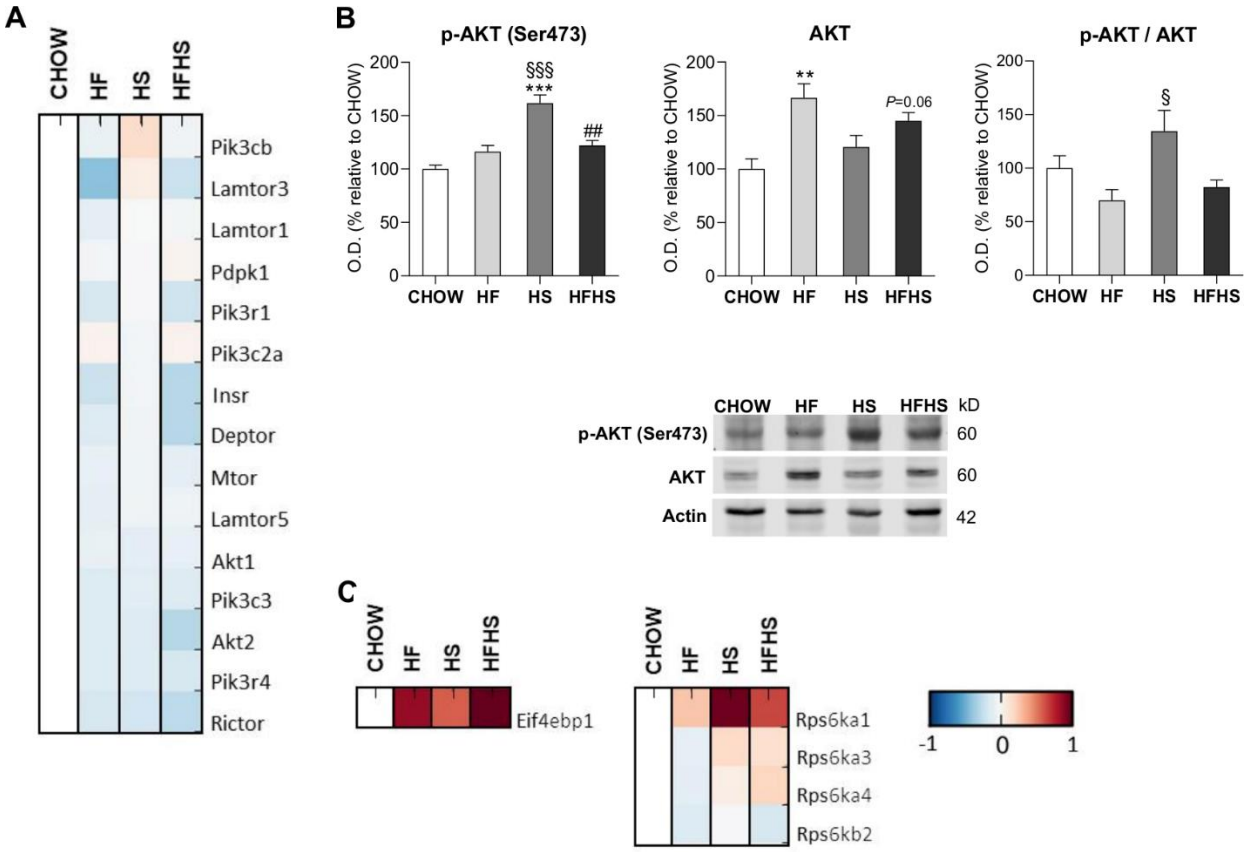

Figure 29. HF-, HS- and HFHS-diets induced higher levels of proteins involved in downstream mTOR-related pathways. (A) Hepatic protein levels of PI3K/AKT/mTOR pathway. **(B)** Optical density (arbitrary units) of ^{Ser473}p-AKT, total AKT and p-AKT/AKT levels, with the representative Western blot image. Actin was used as a loading control. **(C)** Hepatic protein levels of EIF4EBP1, RPS6KA1, RPS6KA3, RPS6KA4 and RPS6KB2. The blue color represents decreased protein levels while the red color represents increased protein levels. Data are expressed as the mean ± SEM. (§) vs. HF diet ($P < 0.05$); (**) vs. the CHOW diet and (##) vs. the HS diet ($P < 0.01$); (***) vs. the CHOW diet and (§§§) vs. the HF diet ($P < 0.001$); *P* values were determined using one-way ANOVA followed by Bonferroni's post hoc test. AKT, protein kinase B; HF, high-fat; HFHS, high-fat plus high-sucrose; HS, high-sucrose.

Even though higher total AKT levels were found in HF- and HFHS-fed mice, I have just observed a slight increase in ^{Ser473}p-AKT in these mice groups (**Figure 29B**). A significant increase in AKT phosphorylation and higher p-AKT/AKT ratio was reported in the group of mice fed with HS-diet (**Figure 29B**), which indicates the activation of the AKT/mTOR pathway. These findings are in agreement with augmented protein levels of downstream pathways of the mTOR pathway such as EIF4EBP1 (involved in protein translation inhibition) and RPS6KA1 and RPS6KA3 (involved in protein synthesis) in all hypercaloric diets tested (**Figure 29C**). Another pathway regulated by PI3K/AKT/mTOR axis is autophagy, a key pathway regulating cellular stress response and quality control. My MS-proteomic analysis revealed a downward trend of autophagic-related proteins (ATGs) and beclin-1 levels in HF-, HS- and HFHS-fed groups compared to the CHOW control group (**Figure 30 A**). These findings suggest possible alterations in the autophagic flux. Increased sequestosome-1 (SQSTM1) protein levels together with an increased accumulation of LC3-II and higher LC3 II/LC3 I ratio confirmed the blockade of the autophagic flux in HFHS-fed mice (**Figure 30A, B**). Moreover, I have also reported a slight increase in autophagy cargo receptor (NBR1) and LC3-II protein levels with a significant increase in the LC3 II/LC3-I ratio in HF-fed mice (**Figure 30A, B**). Supporting previous findings, I have found diminished levels of cathepsins, the lysosomal hydrolases responsible for cargo degradation in autophagolysosomes. Indeed, a reduction of cathepsin D was reported in HF-fed mice while cathepsins B, L, F and H were found reduced in both HF- and HFHS-fed mice in comparison with liver of CHOW-fed group (**Figure 30C**). Even though all hypercaloric diets seem to affect protein homeostasis, these results suggest that HF feeding is more detrimental to the autophagic clearance of proteins/organelles in the hepatocytes.

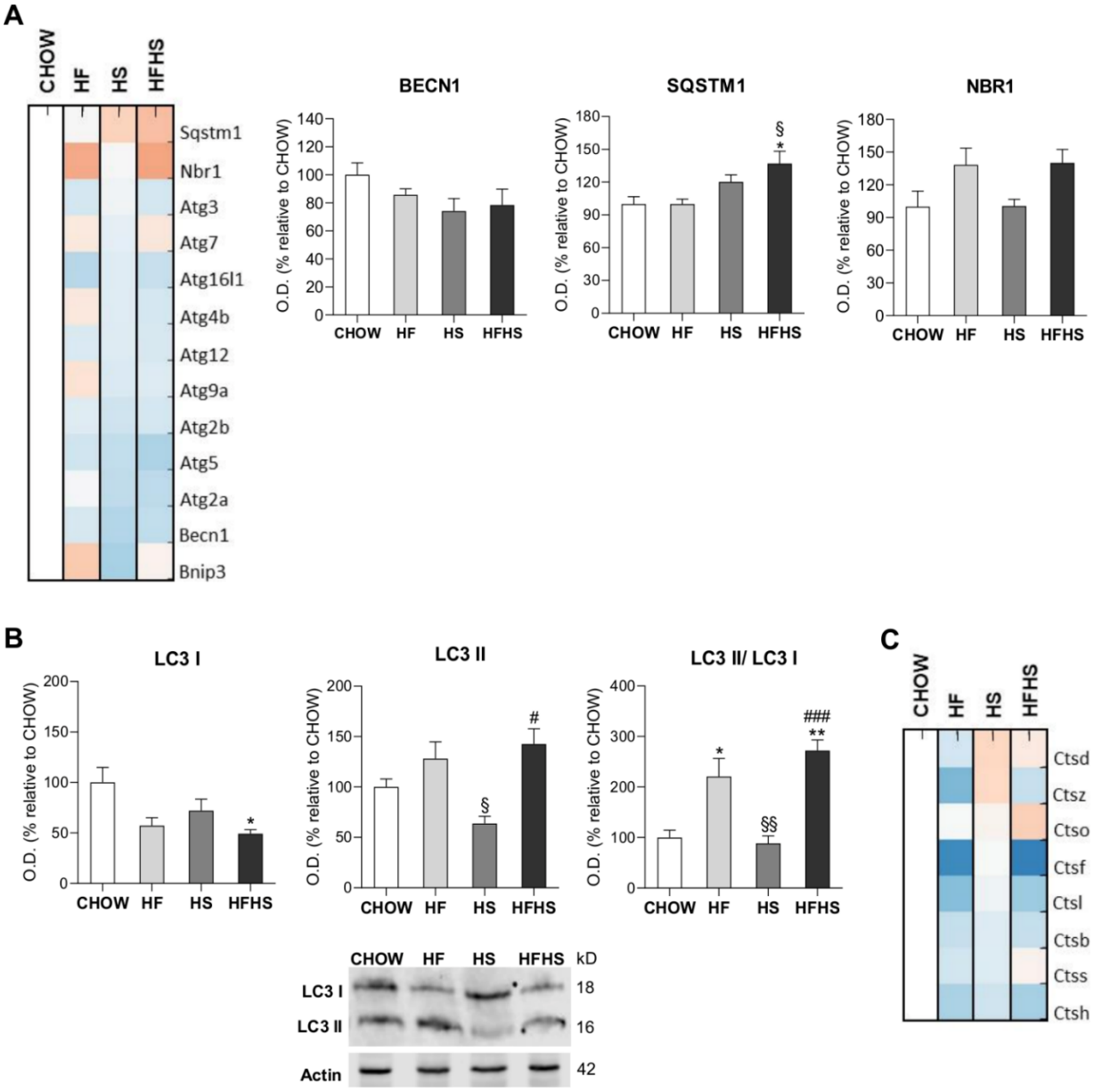

Figure 30. HFHS-diet induce accumulation of SQSTM1 and LC3-II levels in livers of mice. (A) Hepatic protein levels of autophagy-related pathway, with BECN1, SQSTM1 and NBR1 protein levels represented in the graph. **(B)** Optical density (arbitrary units) of LC3 I, LC3 II and LC3 II/LC3 I ratio levels, with the representative Western blot image. Actin was used as a loading control. **(C)** Hepatic protein levels of cathepsins. The blue color represents decreased protein levels while the red color represents increased protein levels. Data are expressed as the mean ± SEM. (*) vs. CHOW diet, (§) vs. the HF diet and (#) vs. the HS diet ($P < 0.05$); (**) vs. the CHOW diet and (§§) vs. the HF diet ($P < 0.01$); (###) vs. the HS diet ($P < 0.001$); *P* values were determined using one-way ANOVA followed by Bonferroni's post hoc test. BECN1, beclin 1; HF, high-fat; HFHS, high-fat plus high-sucrose; HS, high-sucrose; LC3, microtubule-associated protein 1A/1B-light chain 3; NBR1, next to BRCA1 gene 1; SQSTM1, sequestosome 1.

4.2 Discussion of the data presented in Chapter 1

The overconsumption of hypercaloric diets containing fat and sucrose is considered as the main risk factor for the onset of metabolic disorders, including NAFLD with an early accumulation of fat in the liver. Then, simple steatosis is correlated with further development and progression of the disease, which includes mechanisms such as oxidative stress, mitochondrial function impairment, lipotoxicity, ER stress, secretion of inflammatory cytokines and activation of programmed cell death. Importantly, these mechanisms are responsible for the disease progression into NASH (Friedman, Neuschwander-Tetri et al. 2018). Despite the large evidence about the mechanisms underlying NAFLD pathophysiology, there are still some discrepancies, namely those related with ROS generation and mitochondrial function. It remains still to be clarified the exact sequence of events for the development of NAFLD. In this first part of my dissertation, I presented evidence that hepatocyte damage is not caused by mitochondrial-related oxidative stress but probably due to peroxisomal FAO-induced ROS generation and the impairment of hepatic proteolysis. Thus, the blockage of the autophagic flux could play an important role in the aggravation of fat accumulation and subsequent hepatic-associated lipotoxicity during a NAFL stage.

Diet-induced obesity with liver enlargement and hepatocyte damage was observed in mice fed with HF- and HFHS-diets. Moreover, histological analysis confirmed the onset of simple steatosis with all hypercaloric regimens tested. Despite the observations of fat-induced TGs and CEs accumulation, it has been described the beneficial role of TGs accumulation in protecting hepatocytes against the accumulation of toxic-lipid intermediates such as FFAs, ceramides or DAGs. Thus, it was demonstrated that hepatic fat accumulation protects the liver from oxidative injuries, inflammation and fibrosis, known markers of the more severe NASH stage (Yamaguchi, Yang et al. 2007).

Donelly and colleagues have demonstrated that hepatic lipids which accumulate inside lipid droplets have 59% origin in re-esterification of FAs from adipose tissue lipolysis while 15% are derived from diet intake (Donnelly, Smith et al. 2005). Moreover, dietary sugars such as fructose, are used as substrates of DNL and strongly contribute to the hepatic lipid accumulation in NAFLD clinical cohorts (Lambert, Ramos-Roman et al.

2014). Accordingly, my work showed that dietary intake of sucrose is correlated with an increase of DNL and subsequently, it causes hepatic fat accumulation. It is important to highlight that the presence of sucrose in the dietary regimen is associated with a higher NAS severity as observed by histological assessment of livers from animals fed with HF-plus HS-diets. Other studies have also suggested that the degree of saturation/unsaturation of FAs acyl chain could compromise TGs esterification and this is in the origin of hepatic lipotoxicity. SFAs have a lower capacity to be esterified and induce higher toxicity than MUFAs, which are easily esterified into TGs. Consequently, MUFAs accumulation protects from initiation of cellular apoptosis and autophagy impairment both in *in vitro* and *in vivo* models of the disease (Li, Berk et al. 2009, Mei, Ni et al. 2011). Additionally, I have shown that an increased protein expression of elongases and desaturases is in agreement with a higher content of MUFAs in TGs of mice fed with HF-, HS- and with HFHS-diets, suggesting that this can be a protective mechanism in the adaptation against fat accumulation in NAFL.

Western diet-like regimens have also been linked to a deregulation of phospholipids content in the livers of NAFLD cohorts (Arendt, Ma et al. 2013). Gonçalves and co-workers have reported a decrease of PC/PE ratio and a reduction of cardiolipin levels in liver isolated mitochondria of HF-fed rats (Goncalves, Maciel et al. 2014). Likewise, I have shown that PC/PE ratio is diminished in HS-fed mice but we found that HF- and/or- HS feeding increases cardiolipin levels. Considering the role of mitochondrial phospholipids such as PC and PE in maintaining the proper structure and stability of mitochondrial membranes (Einer, Hohenester et al. 2018), these findings indicate that HS-diet *per se* or its combination with HF-diet may compromise mitochondrial structure and subsequent function. Then, *in vitro* studies demonstrated that an increase of PE contributed for the maintenance of the mitochondrial membrane fluidity by increasing membrane viscosity (Dawaliby, Trubbia et al. 2016). In my study, increasing amounts of PE suggest that there is a modulation of mitochondrial membrane properties in a NAFL stage.

One of the main functions of mitochondria on hepatocytes is its involvement on the regulation of hepatic lipid accumulation through mitochondrial FAO and oxidative phosphorylation. In fact, several works have shown that FAs stimulate mitochondrial remodelling with up-regulation of mitochondrial FAO and oxygen consumption (Sunny,

Parks et al. 2011, Rolo, Teodoro et al. 2012). However, it has been also proposed that the continuous influx of FAs may be in the origin of mitochondrial proton leak and excessive ROS generation which can ultimately impair mitochondrial respiration (Koliaki, Szendroedi et al. 2015, Patterson, Kalavalapalli et al. 2016). This is considered as a key event in NAFLD progression. Opposingly, I have demonstrated no significant alterations in mitochondrial FAO pathway. Despite a decrease in OXPHOS subunits levels as well as in its in-gel activities, oxygen consumption was not significantly altered in basal and in ADP-stimulated states in HF- or HS-fed mice. It is important to highlight that the HFHS-diet induced a decrease of mitochondrial respiration when compared to the same diets *per se*. I have also observed higher cardiolipin levels enriched with MUFAs in all hypercaloric fed groups while a lower content of PUFAs (namely C18:2, C20:2, C20:4 and C22:6n3) was detected just in HFHS-fed mice. Interestingly, a similar reduction of C18:2 levels and/-or a defective cardiolipin remodelling has been linked to a decrease of mitochondrial oxygen consumption and OXPHOS complexes activities (Yamaoka, Urade et al. 1990, Vreken, Valianpour et al. 2000). Cardiolipin is a phospholipid mostly found at IMM, where it is involved in stabilizing mitochondrial OXPHOS proteins thereby enabling mitochondrial respiratory efficiency (Fouret, Gaillet et al. 2018). Accordingly, my findings suggest that augmented cardiolipin levels may act as a mitochondrial adaptative mechanism under FAs insult. Nevertheless, I hypothesized that the alterations in PC/PE ratio and in the levels of unsaturated FAs acyl chain of cardiolipin may induce changes in mitochondrial structure, thereby compromising mitochondrial OXPHOS function.

Mitochondrial oxidative stress and subsequent oxidative injury have been pointed as the main cause of mitochondrial impairment in a NAFLD context (Koliaki, Szendroedi et al. 2015, Besse-Patin, Leveille et al. 2017). I have performed a very comprehensive characterization of oxidative stress-related parameters in mitochondria and in cytosol of hepatocytes. My studies revealed that there is no increase in mitochondrial ROS generation neither any alterations in mitochondrial antioxidant defense system up to 16 weeks of hypercaloric diets feeding. This is in line with the findings of Einer and colleagues (Einer, Hohenester et al. 2018). Additionally, no mitochondrial oxidative stress is in agreement with absence of mitochondrial oxidative damage. Since a reduction of cardiolipin levels is associated with an exacerbation of ROS

levels (Paradies, Petrosillo et al. 2000), higher cardiolipin levels found in my study also support the lack of mitochondrial oxidative stress in fatty livers.

Despite the fact that mitochondria are considered as the major organelles responsible for ROS generation in pathological conditions, it has been suggested that other cellular organelles namely peroxisomes and microsomes can contribute to ROS generation. Indeed, peroxisomal FAO-related enzymes can contribute for ROS production (Antonenkov, Grunau et al. 2010). In my study, I have assessed the levels of proteins considered as markers of peroxisomal number and peroxisomal-related FAO and it was found an upregulation of both pathways. These observations agree with similar findings reported in livers of NAFLD mice models (Knebel, Hartwig et al. 2015, Knebel, Goddeke et al. 2018). Interestingly, Elsner and colleagues have showed that higher FAs levels stimulate peroxisomal-dependent FAO rather mitochondrial FAO, with a parallel increase of peroxisomal ROS formation. These ROS can easily cross the peroxisomal membrane, with further oxidative injury that is known as a cause of lipotoxicity in β-pancreatic cells (Elsner, Gehrmann et al. 2011). In a similar way, I have proposed that a higher peroxisomal abundance together with an increase of peroxisomal-dependent FAO pathway constitute cellular adaptative mechanisms in order to overcome the excess of hepatic lipid accumulation. Even though, these mechanisms likely also contribute for augmented ROS levels that may overwhelm cytosolic antioxidant capacity. This is corroborated by increased levels of lipid peroxidation, which contribute to liver oxidative injury in NAFL stage.

Remarkably, elevated peroxisomal ROS generation together with oxidative damage have been associated with an impairment of the autophagic function with subsequent accumulation of damaged/dysfunctional peroxisomes (Vasko and Goligorsky 2013). The PI3K/AKT/mTOR constitutes a cellular stress response pathway, intimately related with quality control mechanisms such as autophagy. In hepatocytes, autophagy is described to be involved not only at the removal of damaged proteins/organelles but also in the elimination of lipid droplets by so-called lipophagy (Singh, Kaushik et al. 2009). Although, accumulated evidence has demonstrated the activation of mTOR-related pathway with further autophagic inhibition in both obese mice and in NAFLD patients (Yang, Li et al. 2010, Gonzalez-Rodriguez, Mayoral et al. 2014). Likewise, I have observed a blockage of autophagy, being this effect dependent

on the diet used. Thus, diminished levels of autophagic-related proteins, namely ATG4, ATG12-ATG5-ATG16-complex and beclin-1 were found in mice fed with HS- and with HFHS-diets, with the lack of these proteins associated with a compromised autophagosomal formation (Liu, Han et al. 2009, Yang, Li et al. 2010). On other hand, my data showed a reduction of cathepsins B, L and D in animals fed with a HF-diet. This latter effect indicates that fat intake induces a decrease of lysosomal hydrolases (Inami, Yamashina et al. 2011, Fukuo, Yamashina et al. 2014). Therefore, I suggest that HF-diet intake impairs autophagic flux due to a reduction of lysosomal enzymes activities and a defective autophagolysosomal acidification while HS-diet intake impairs autophagolysosomal formation. A defective acidification is correlated with an impairment of autophagolysosomal degradation and consequent blockage of the autophagic flux (Huynh, Eskelinen et al. 2007, Button, Roberts et al. 2017). Autophagolysosomal accumulation is supported by an increased accumulation of SQSTM1/NBR1 and LC3-II proteins in mice fed with HF-diet *per se* or with its combination with HS-diet.

Overall, my results show that a high intake of fat and/-or sucrose induce simple steatosis with an accumulation of FAs in its saturated form but importantly also in the form of MUFAs. This mechanism could protect hepatocytes from SFAs-induced lipotoxicity. Additionally, I have also observed that hepatic fat accumulation induced mitochondrial phospholipids remodelling with increased cardiolipin levels. At mitochondrial level, no increase in ROS generation and no signs of oxidative damage have been observed. Then, I reported a higher number of peroxisomes that together with an increase of peroxisomal-FAO related proteins, likely suggest a role of peroxisomes as cellular ROS producers. Accordingly, this may be in the origin of hepatic oxidative damage in early NAFLD stage. In addition, I have shown that fat and sucrose impair autophagic response at different steps of the regulatory pathway. While fat impair lysosomal acidification, sucrose causes defective autophagolysosomal formation. Thus, a defective autophagic flux contributes to the accumulation of damaged/malfunctioning organelles, which can exacerbate hepatocyte injuries and hasten for NAFLD progression (results are summarized in the **Figure 31**).

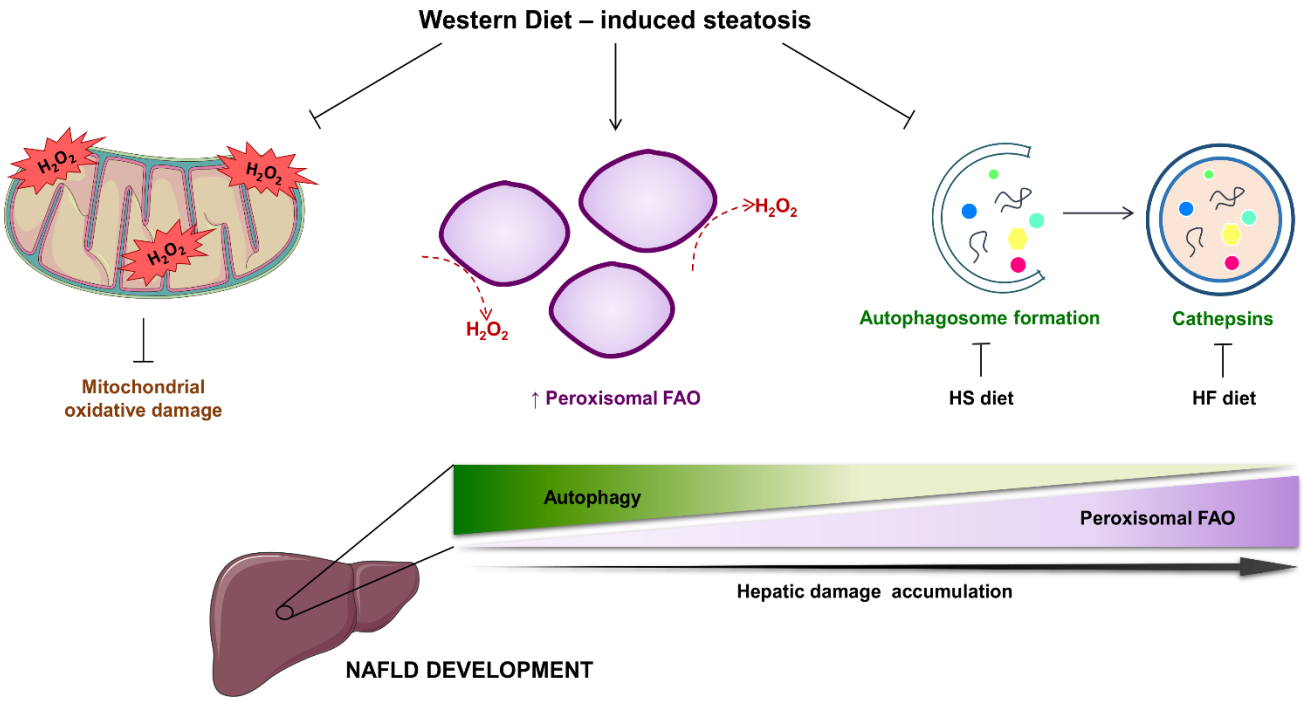

Figure 31. Schematic diagram summarizing the role of hypercaloric diets in the development of NAFL. FAO, fatty acid oxidation; H_2O_2, hydrogen peroxide; HS, high-sucrose; HF, high-fat; NAFLD, non-alcoholic fatty liver disease.

CHAPTER 2: NON-ALCOHOLIC FATTY LIVER DEVELOPMENT AND FURTHER PROGRESSION IS INDEPENDENT OF MITOCHONDRIAL OXIDATIVE STRESS GENERATION.

5.1 Results

5.1.1 WD increases body weight and hepatic lipid accumulation, thereby causing hepatic damage with early signs of ballooning and fibrosis.

Mice fed with WD showed a progressive increase of body weight gain when compared with SD-fed mice along 16, 20, 22 and 24 weeks (**Figure 32A**). Detailed information of body weight progression in SD- and WD-fed animals is provided in **Table 5**. At euthanasia time, WD-fed mice presented an increase of 25-50% of body weight versus each respective control group (**Figure 32B**). At the hepatic level, I observed an augment of liver size (**Figure 33A**), with 100-200% of wet liver weight gain in WD-fed animals up to 24 weeks of feeding (**Figure 32C**). Moreover, plasmatic ALT and AST activity levels were increased (**Figure 32C**), which confirmed hepatocyte damage in WD-fed mice.

Increased liver size and weight in WD-fed mice was found to be correlated with hepatic fat accumulation (**Figure 33B, C**). Curiously, H&E relative intensity quantification of lipid droplets revealed that this accumulation occurred at a similar extent in all WD feeding timepoints (**Figure 33C**) as confirmed by a blind histopathological evaluation presented in **Table 5**. These findings suggest that WD-fed animals reached their maximal hepatic capacity to accumulate lipids even if fed for longer periods. Additionally, steatotic livers presented higher hepatocyte ballooning (grade 1-2) in comparison with SD-fed mice (grade 0) (**Table 6**). In terms of lobular inflammation, I did not observe any differences between WD- and SD-fed animals in immunohistological assessment of CD3, CD45 and CD68 inflammatory markers (**Figure 34**).

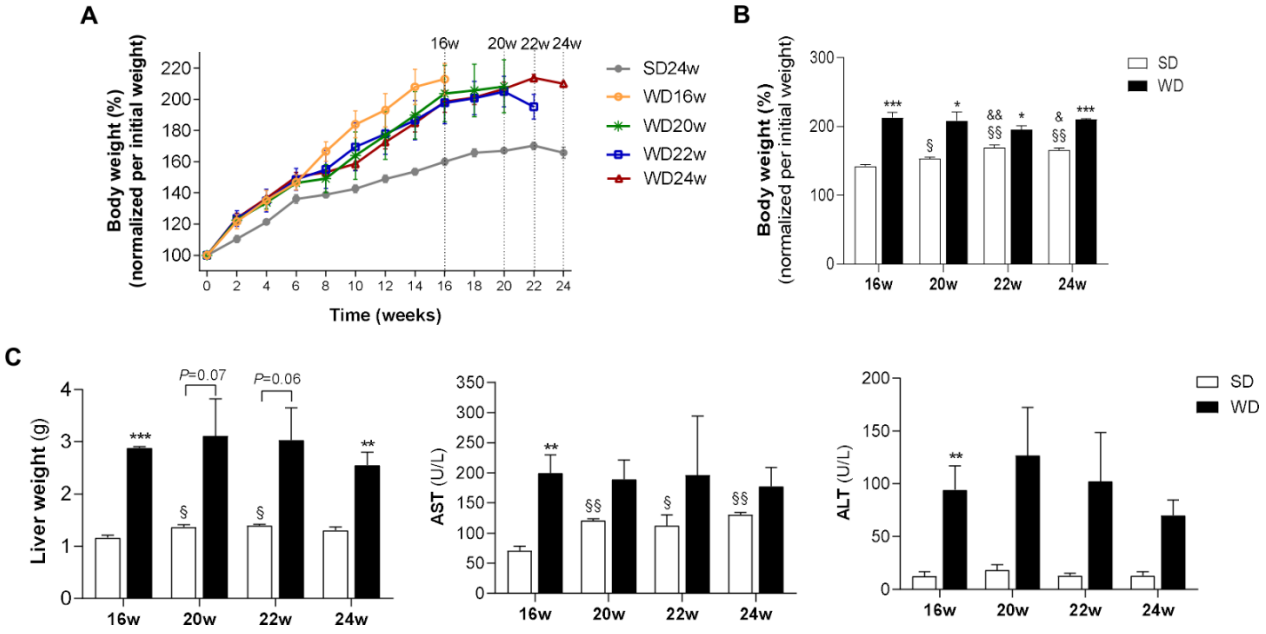

Figure 32. WD induces body and liver weight gain with the development of hepatic associated damage along 24 weeks of feeding. (A) Body weight profile along 16, 20, 22, and 24 weeks of WD feeding. **(B)** Body weight at the end of the study, before euthanasia time. **(C)** Wet liver weight after mice euthanasia; and aspartate aminotransferase (AST) and alanine aminotransferase (ALT) plasmatic activity levels. All data are expressed as the mean ± SEM. (*) vs. SD, (§) vs. 16w, (&) vs. 20w ($P < 0.05$); (**) vs SD, (§§) vs. 16w, (&&) vs. 20w ($P < 0.01$); (***) vs. SD ($P < 0.001$); *P* values were determined using two-way ANOVA. SD, standard diet; WD, Western diet.

Table 5. Body weight progression along 16, 20, 22 and 24 weeks of SD and WD feeding. SD, standard diet; WD, Western diet.

Body weight progression

		Time (weeks)																							
		1	2	3	4	5	6	7	8	9	10	11	12	13	14	15	16	17	18	19	20	21	22	23	24
16W	SD	106.0 ± 3.2	108.3 ± 2.3	114.8 ± 2.9	120.7 ± 3.8	123.0 ± 2.7	122.4 ± 3.3	128.4 ± 4.1	131.9 ± 4.7	131.9 ± 3.5	137.9 ± 4.5	135.2 ± 2.8	136.0 ± 2.6	139.9 ± 2.2	140.7 ± 2.9	143.5 ± 4.5	142.2 ± 3.3								
	WD	105.0 ± 0.1	121.5 ± 4.6	131.7 ± 5.4	135.2 ± 6.3	137.9 ± 6.1	146.8 ± 5.1	158.3 ± 6.8	166.6 ± 6.4	172.9 ± 9.7	184.0 ± 8.7	188.9 ± 10.4	193.0 ± 10.8	200.4 ± 12.3	208.0 ± 11.5	208.3 ± 11.3	212.9 ± 10.2								
20W	SD	108.0 ± 0.2	115.7 ± 1.5	117.7 ± 2.8	123.3 ± 3.9	128.6 ± 2.9	133.9 ± 3.8	134.0 ± 2.4	140.4 ± 3.2	139.4 ± 3.2	144.3 ± 3.0	143.5 ± 4.8	148.1 ± 3.5	149.0 ± 2.9	151.8 ± 2.7	157.4 ± 2.8	157.7 ± 3.7	155.37 ± 3.4	157.1 ± 3.6	159.6 ± 2.9	153.2 ± 3.3				
	WD	117,6 ± 2.0	122.5 ± 2.0	129.7 ± 2.2	133.7 ± 3.8	143.0 ± 3.5	146.4 ± 3.2	144.6 ± 3.1	149.2 ± 9.1	155.3 ± 12.8	163.9 ± 15.3	170.3 ± 15.3	176.9 ± 15.5	184.5 ± 14.4	189.8 ± 15.3	196.0 ± 15.2	203.7 ± 18.1	196.6 ± 16.6	205.8 ± 16.9	210.7 ± 15.2	208.3 ± 17.1				
22W	SD	110.5 ± 2.9	118.0 ± 4.0	121.2 ± 5.7	125.7 ± 6.3	134.7 ± 8.8	139.4 ± 7.8	139.2 ± 6.9	142.0 ± 7.8	143.4 ± 6.5	149.4 ± 6.9	150.7 ± 6.3	154.5 ± 8.0	154.7 ± 8.5	155.5 ± 6.6	164.8 ± 6.4	164.8 ± 7.0	163.0 ± 6.8	164.9 ± 7.5	165.3 ± 8.6	169.6 ± 7.7	174.5 ± 6.8	169.1 ± 5.3		
	WD	116.1 ± 4.5	123.5 ± 5,1	132.2 ± 6.6	135.1 ± 7.2	141.9 ± 8.2	148.6 ± 7.1	149.5 ± 8.3	155.1 ± 12.2	161.7 ± 14.5	169.5 ± 15.4	174.7 ± 16.6	177.9 ± 13.2	183.0 ± 12.9	186.7 ± 12.5	192.0 ± 12.1	197.7 ± 13.5	199.2 ± 12.8	200.8 ± 10.8	204.4 ± 9.3	205.1 ± 9.8	207.1 ± 8.4	195.3 ± 7.8		
24W	SD	98.6 ± 1.2	110.4 ± 2.3	117.2 ± 2.9	121.3 ± 2.0	128.1 ± 2.3	136.1 ± 2.8	138.5 ± 3.4	138.8 ± 2.1	141.5 ± 2.2	142.7 ± 2.5	150.4 ± 2.8	149.0 ± 2.3	153.3 ± 3.5	153.6 ± 2.2	157.9 ± 3.7	159.9 ± 2.4	163.8 ± 3.1	165.8 ± 2.6	166.6 ± 1.2	167.0 ± 1.2	169.0 ± 1.5	170.2 ± 2.5	173.8 ± 1.6	165.8 ± 3.6
	WD	112.1 ± 2.3	123.7 ± 3.3	129.6 ± 2.0	136.6 ± 1.8	143.0 ± 1.0	150.4 ± 2.8	153.0 ± 3.4	153.0 ± 1.7	155.0 ± 2.7	158.7 ± 4.0	170.2 ± 2.0	172.7 ± 4.4	179.1 ± 5.2	184.9 ± 6.0	190.2 ± 6.2	198.5 ± 7.1	204.3 ± 6.9	201.1 ± 4.3	204.0 ± 7.3	206.7 ± 4.3	209.5 ± 1.8	213.7 ± 2.4	216.6 ± 3.2	210.1 ± 1.9

These results were confirmed by the pathologist evaluation (**Table 6**). Lastly, I reported early periportal/portal fibrosis signs in mice fed with WD for the distinct timepoints tested (**Table 6**). These parameters indicated the development of simple steatosis with no disease progression into a more severe NASH stage up to 24 weeks of feeding. Moreover, NAS score, based on steatosis, ballooning, inflammation and fibrosis parameters supported the absence of histological disease progression from 16th up to the 24th week of feeding (**Table 6**).

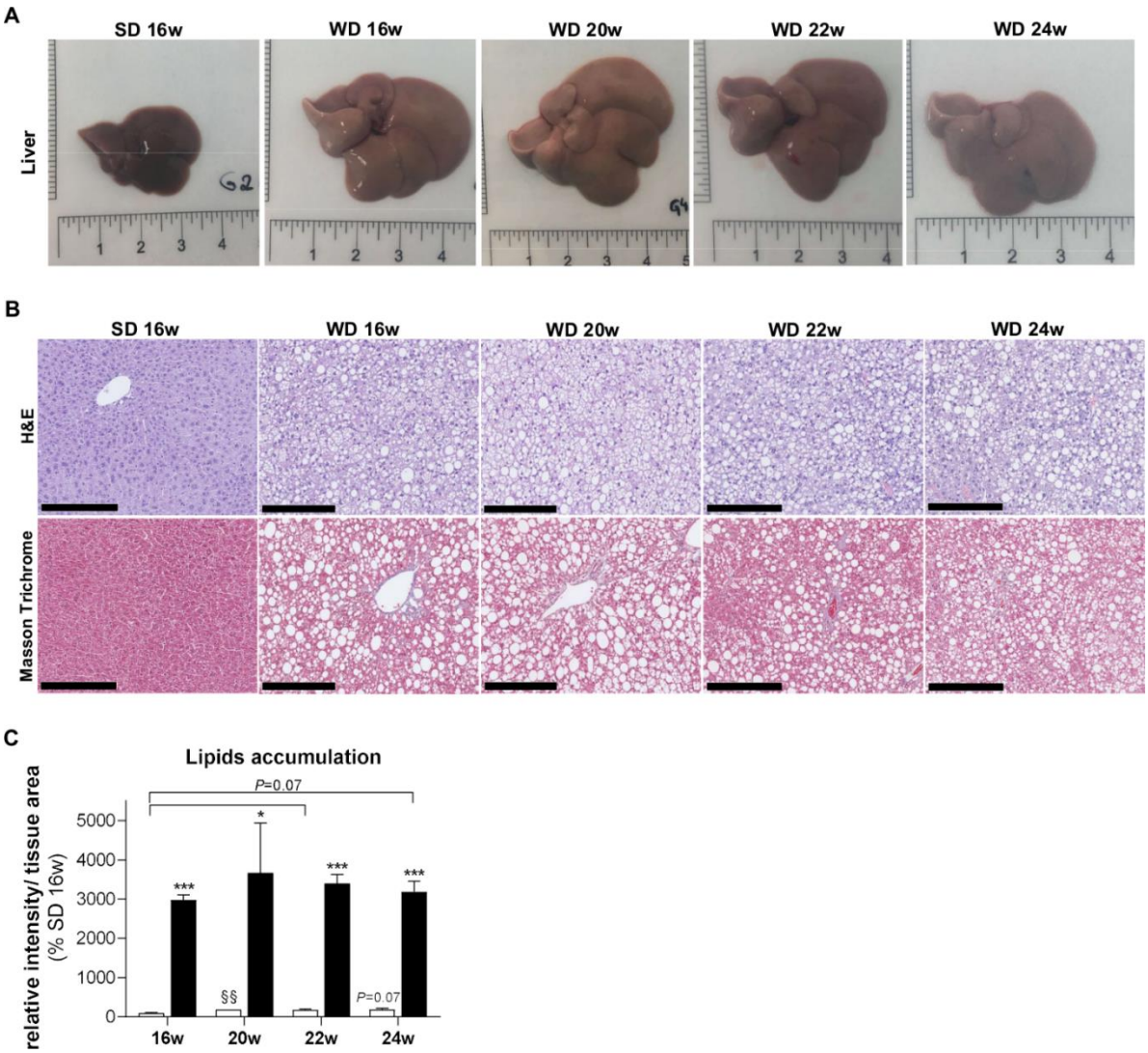

Figure 33. WD induces hepatic lipid accumulation in mice fed for 16, 20, 22 and 24 weeks of feeding. (A) Representative images of liver appearance/size after euthanasia of mice. **(B)** Representative images of paraffin-embedded liver sections after Hematoxylin & Eosin (H&E) and Masson Trichrome stainings; Scale bar: 250 µm; 10x magnification. **(C)** Hepatic lipid content, quantified from H&E staining of three independent images per mouse, and per feeding condition with results expressed in % of SD16w group. Data is expressed as the mean ± SEM. (*) vs. SD ($P < 0.05$); (§§) vs. 16w ($P < 0.01$); (***) vs. SD ($P < 0.001$); *P* values were determined using two-way ANOVA. SD, standard diet; WD, Western diet.

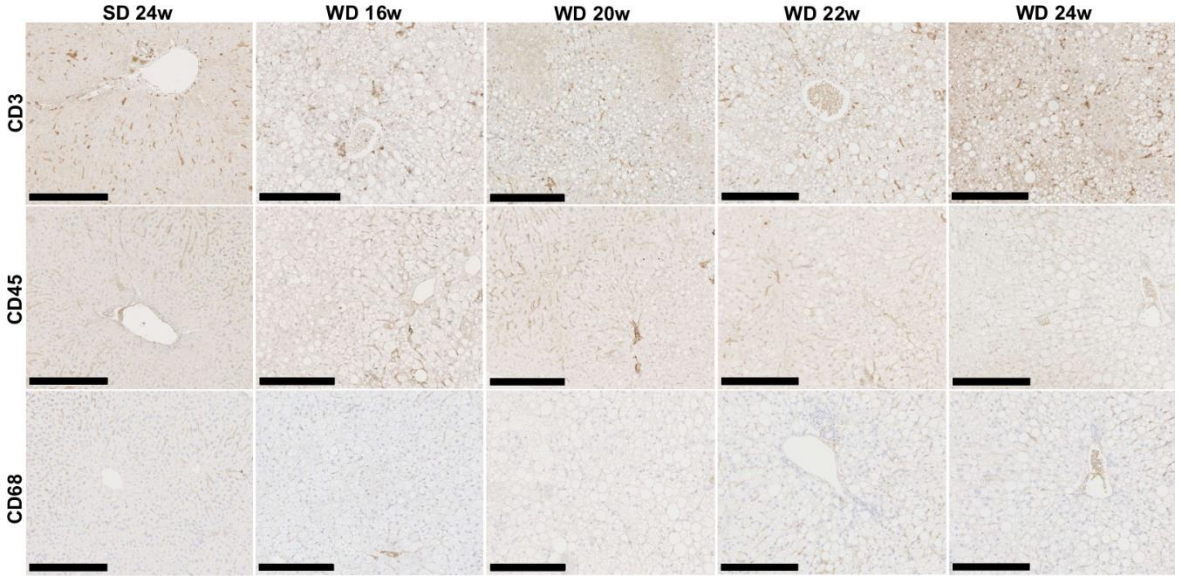

Figure 34. WD do not cause signs of lobular inflammation. Representative images of paraffin-embedded liver sections after immunohistochemistry of CD3, CD45, and CD68 inflammatory markers. Scale bar: 250 µm; 10x magnification.

Table 6. WD induces hepatic steatosis and ballooning with early signs of fibrosis but with absence of lobular inflammation. NAFLD activity score (NAS) calculated based of Hematoxylin & Eosin (H&E), Masson Trichrome and immunohistochemistry of CD3, CD45 and CD68 markers. Steatosis grade: 0 ≤ 5%; grade 1 = 5-33%; grade 2 = 34-66%; grade 3 ≥ 66%. Ballooning grade: 0 = absent; 1 = a few ballooned hepatocytes; 2 = many ballooned hepatocytes. Inflammation grade (magnification 200x): 0 = absent; 1 = up to two foci per field of view; 2 = two to four foci per field of view; 3 = more than four foci per field of view (lipogranulomas are counted in this category). Fibrosis grade: S0 = absent; S1a = zone 3, perisinusoidal fibrosis; S1b = zone 3, perisinusoidal fibrosis; S1c = only periportal/ portal fibrosis; S2 = zone 3, plus portal/ periportal fibrosis; S3 = zone 3, plus portal/ periportal fibrosis with bridging fibrosis; S4 = cirrhosis. NAS value[&] is considered as the sum of the grades obtained for steatosis, ballooning, inflammation and fibrosis parameters. H&E,Hematoxylin & Eosin. SD, standard diet; WD, Western diet.

		NAFLD Activity Score				NAS value[&]
Groups		Steatosis	Ballooning	Inflammation	Fibrosis	
16w	SD	Grade 0	Grade 0	Grade 0	S 0	0
	WD	Grade 3 mixed	Grade 2	Grade 0	S 1c	5
20w	SD	Grade 0	Grade 0	Grade 0	S 1c	1
	WD	Grade 2	Grade 2	Grade 0	S 1c	5
22w	SD	Grade 0	Grade 0	Grade 0	S 1c	1
	WD	Grade 3	Grade 1	Grade 0	S 1c	4
24w	SD	Grade 0	Grade 0	Grade 0	S 0	0
	WD	Grade 3	Grade 2	Grade 0	S 1c	5

5.1.2 WD induces hepatic lipid accumulation in the form of TGs and CEs with enrichment of MUFAs.

The accumulation of fat inside lipid droplets of hepatocytes occurs as neutral lipids. In fact, by using TLC, I have demonstrated that WD caused an accumulation of 2-fold of TGs and higher than 6-fold of CEs compared to SD after a feeding period of 16, 20, 22 and 24 weeks (**Figure 35**).

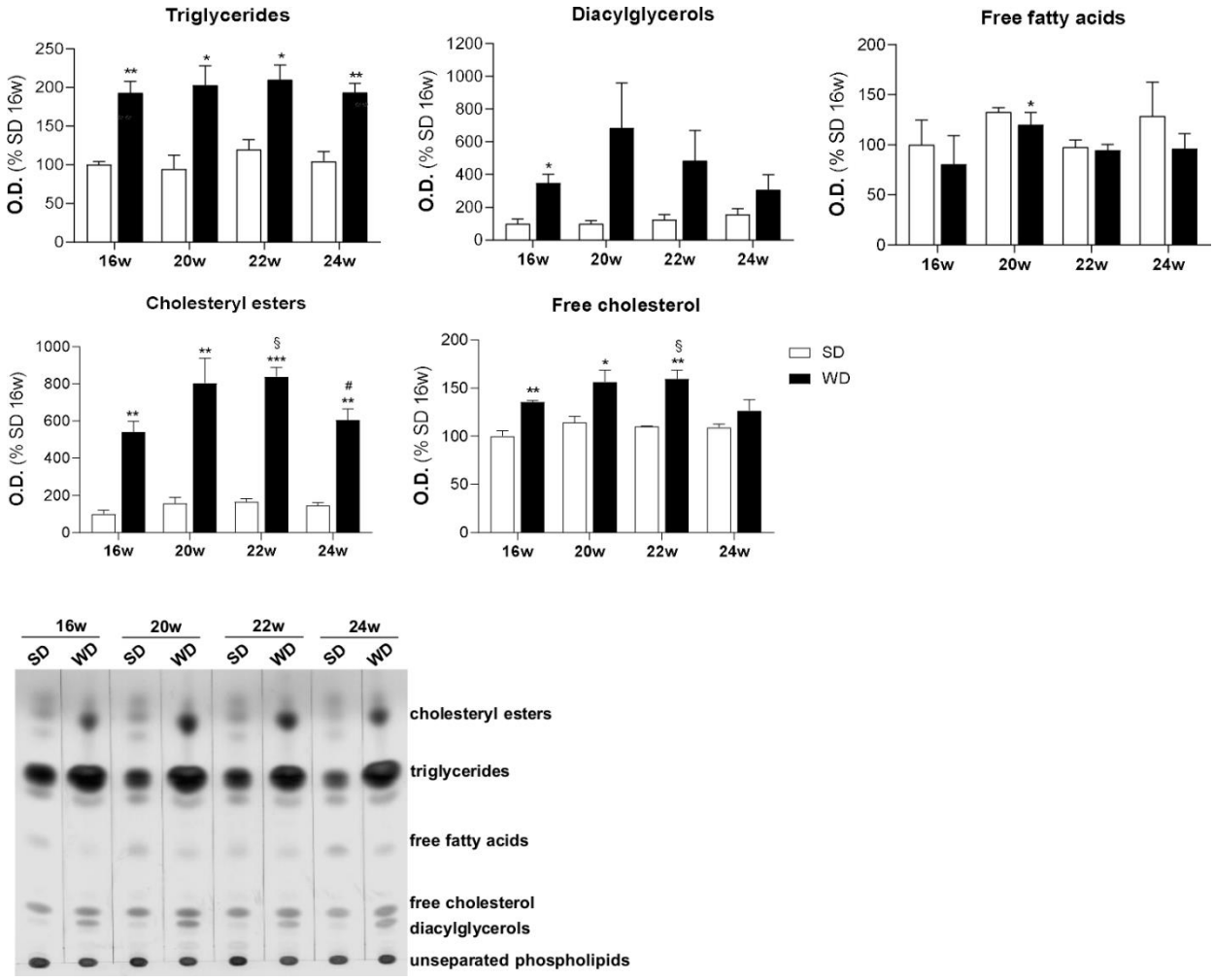

Figure 35. Hepatic lipid accumulation is characterized by triglycerides and cholesteryl esters. Quantification of triglycerides, diacylglycerols, free fatty acids, cholesteryl esters and free cholesterol in SD- and WD-fed mice for 16, 20, 22 and 24 weeks; and representative image of thin-layer chromatography of hepatic neutral lipids. All data are expressed as the mean ± SEM. (*) vs. SD, (§) vs. 16w, (#) vs. 22w ($P < 0.05$); (**) vs. SD ($P < 0.01$); (***) vs. SD ($P < 0.001$); P values were determined using two-way ANOVA. SD, standard diet; WD, Western diet.

As a result of the stimulation of anabolic and catabolic lipid metabolism reported in my previous work (Simoes, Karkucinska-Wieckowska et al. 2020), I have also found augmented levels of DAGs and free cholesterol in WD-fed mice versus the respective SD-fed mice (**Figure 35**). Regarding FFAs levels, no major alterations were reported in WD feeding along time (**Figure 35**). Then, I evaluated the capacity of lipid accumulation-related parameters to discriminate between SD- and WD-fed groups. After applying principal component analysis (PCA), I verified that: 1) samples belonging to the same feeding period cluster close to each other; and 2) samples belonging to WD-fed mice cluster far away from SD-fed mice (**Figure 36**).

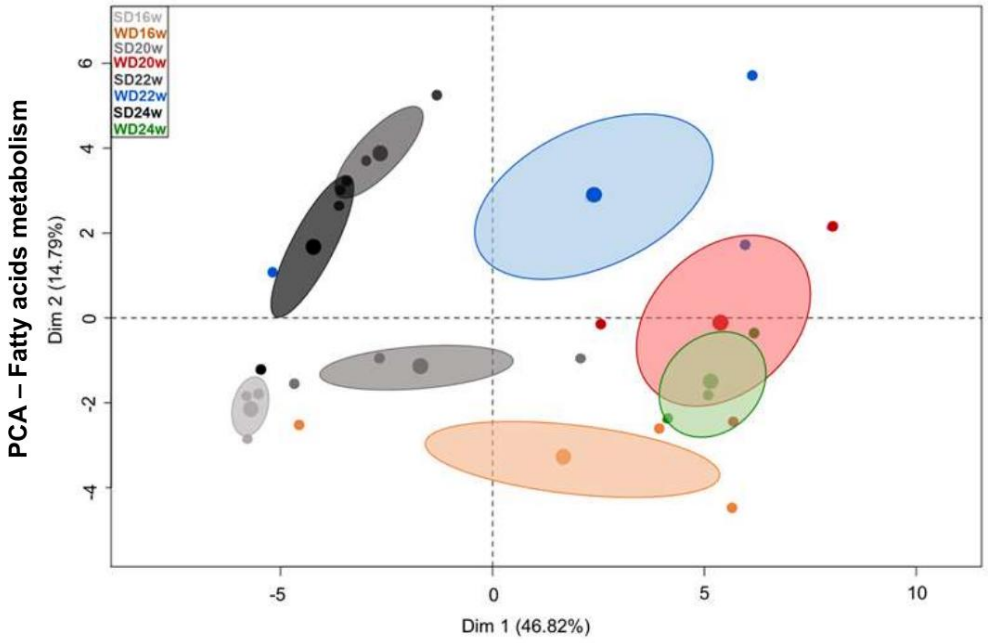

Figure 36. WD feeding promotes good discrimination between SD- and WD-fed groups in lipid accumulation parameters. Principal component analysis (PCA) of lipid metabolism-related parameters. SD, standard diet; WD, Western diet.

Additionally, WD induced fatty acyl chain composition remodelling in the TGs fraction. Using NMR analysis, I verified that although WD feeding did not induce major alterations in SFAs levels, it provoked a 2-fold increase of MUFAs relative to the SD-fed group (**Figure 37**). Moreover, I also showed a reduction of linoleate levels in WD-fed group in comparison with respective controls (**Figure 37**). Of note, I did not observe significant WD-induced changes in lipid accumulation within the timepoints studied.

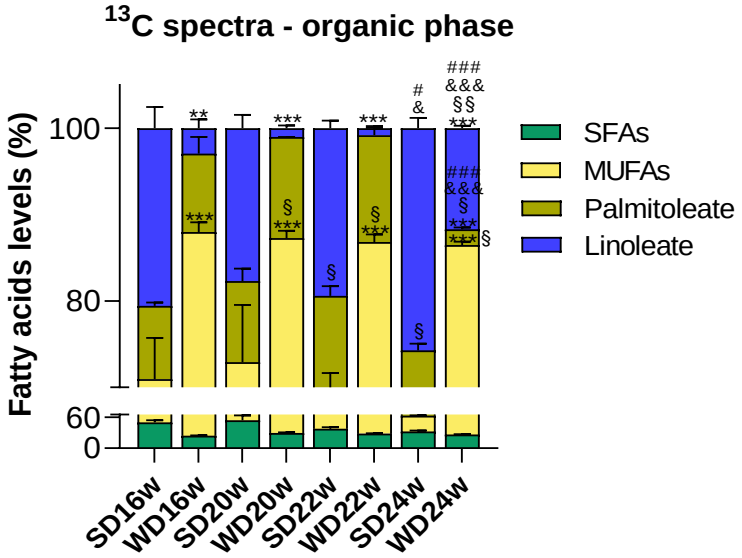

Figure 37. WD induces higher content of MUFAs and reduces linoleate levels, both in triglycerides of WD-fed mice. Fatty acyl chain composition of purified triglycerides, in terms of saturated fatty acids, monounsaturated fatty acids, palmitoleate and linoleate levels in livers of animals fed with SD and WD for 16, 20, 22 and 24 weeks. All data are expressed as the mean ± SEM. (§) vs. 16w, (&) vs. 20w, (#) vs. 22w ($P < 0.05$); (**) vs. SD, (§§) vs. 16w ($P < 0.01$); (***) vs. SD, (&&&) vs. 20w, (###) vs. 22w ($P < 0.001$); *P* values were determined using two-way ANOVA. MUFAs, monounsaturated fatty acids; SD, standard diet; SFAs, saturated fatty acids; WD, Western diet.

5.1.3 WD induces a progressive decrease in mitochondrial function along the time of feeding.

Mitochondria are the main cellular organelles responsible for FAO, thereby allowing hepatocytes to eliminate the excess of FAs inflow and its accumulation inside lipid droplets (Begriche, Massart et al. 2013). In order to evaluate mitochondrial function under such circumstances, OXPHOS proteins and phospholipid membrane levels were evaluated using isolated mitochondrial fractions. Regarding OXPHOS protein levels, I observed that WD induced an upward trend of Complex I (NDUFB8), Complex II (SDHB), Complex IV (MTCO1) and ATP synthase (ATP5A) subunits at 16th week of feeding (**Figure 38**). Despite that, I have found a decrease of Complex III (UQCRC2) and ATP5A subunits at 20th week, SDHB and UQCRC2 subunits at 22nd week, and lastly, a decrease of UQCRC2 subunit at 24th week (**Figure 38**).

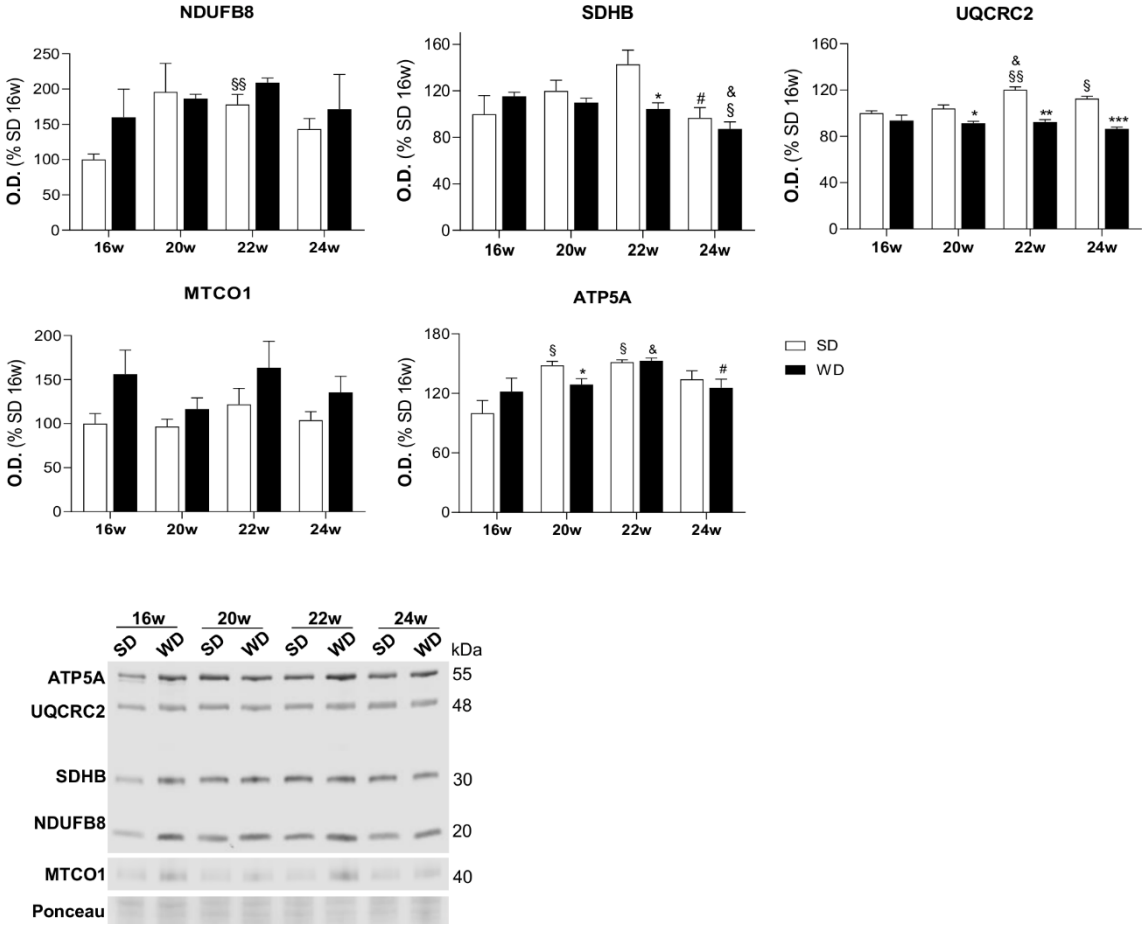

Figure 38. WD induces OXPHOS subunits remodelling along time of feeding. OXPHOS subunits protein levels (NDUFB8, Complex I; SDHB, Complex II; UQCRC2, Complex III; MTCO1, Complex IV; ATP5A, ATP synthase) expressed as optical density (arbitrary units), in which Ponceau was used for normalization of the data; and representative image of OXPHOS subunits Western blot. All data are expressed as the mean ± SEM. (*) vs. SD, (§) vs. 16w, (&) vs. 20w, (#) vs. 22w ($P < 0.05$); (**) vs. SD, (§§) vs. 16w ($P < 0.01$); (***) vs. SD ($P < 0.001$); *P* values were determined using two-way ANOVA. SD, standard diet; WD, Western diet.

In parallel with OXPHOS subunits remodelling, I have also observed alterations in phospholipid membrane composition with an upward trend of cardiolipin and phosphatidylinositol levels in mitochondria from WD-fed mice, being this increase statistically significant at 22th week (**Figure 39**). No major changes were detected in the other phospholipid species (**Figure 39**).

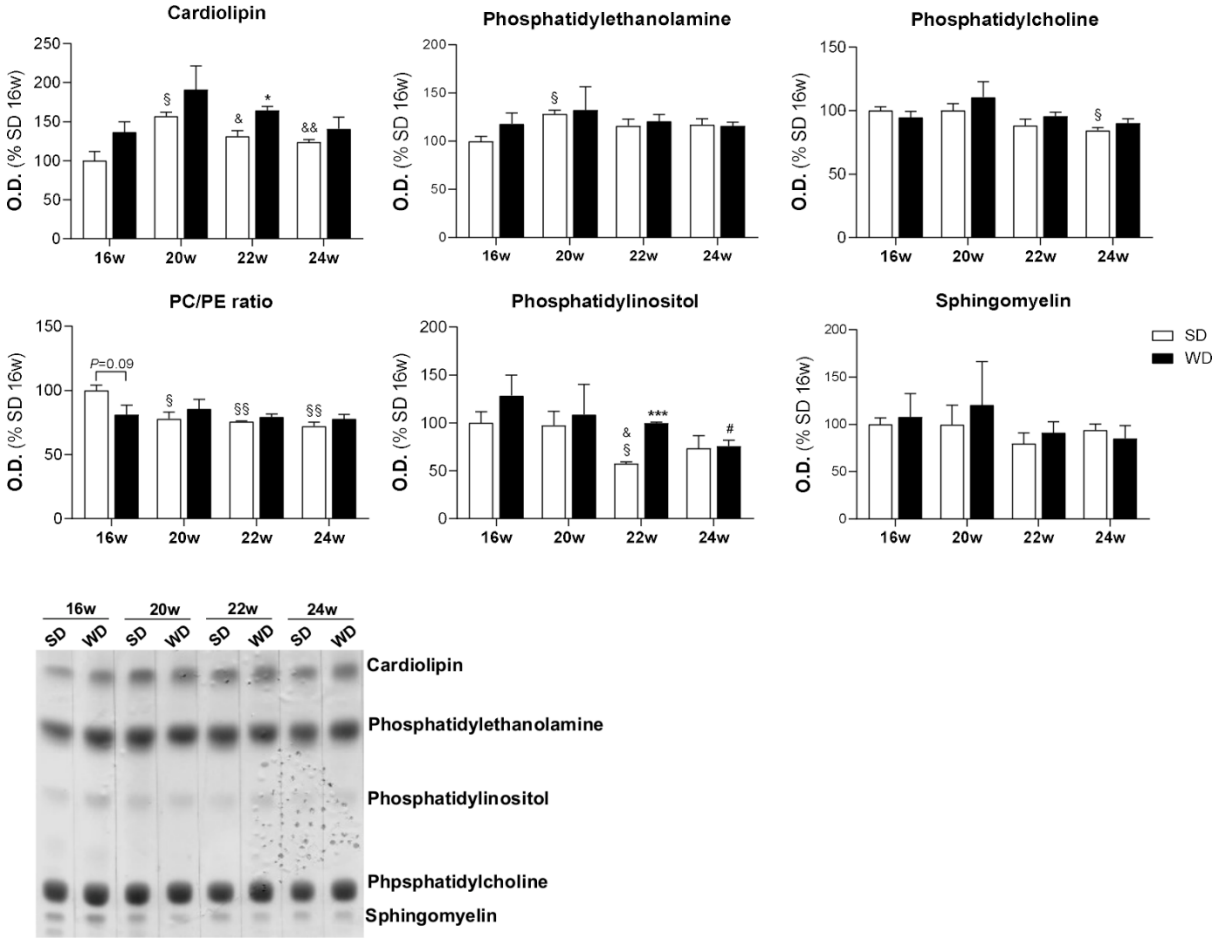

Figure 39. WD induces phospholipid membrane remodelling along the time of feeding. Mitochondrial phospholipids levels - cardiolipin, phosphatidylethanolamine (PE), phosphatidylcholine (PC), phosphatidylinositol, sphingomyelin and PC/PE ratio expressed as optical density (arbitrary units); and a representative image of thin-layer chromatography. All data are expressed as the mean ± SEM. (*) vs. SD, (§) vs. 16w, (&) vs. 20w ($P < 0.05$); (§§) vs. 16w, (&&) vs. 20w ($P < 0.01$); (***) vs. SD ($P < 0.001$); *P* values were determined using two-way ANOVA. SD, standard diet; WD, Western diet.

Based on the previous findings, I next investigated whether the mitochondrial function of WD-fed mice along time could be compromised. Therefore, the OCR was firstly evaluated in the presence of Complex II substrate - succinate. Considering the fact that no significant alterations were found between OCR values of SD-fed mice along the distinct timepoints (**Figure 40A**), OCR values of WD-fed mice were represented just in comparison with SD16w group (**Figure 40B**).

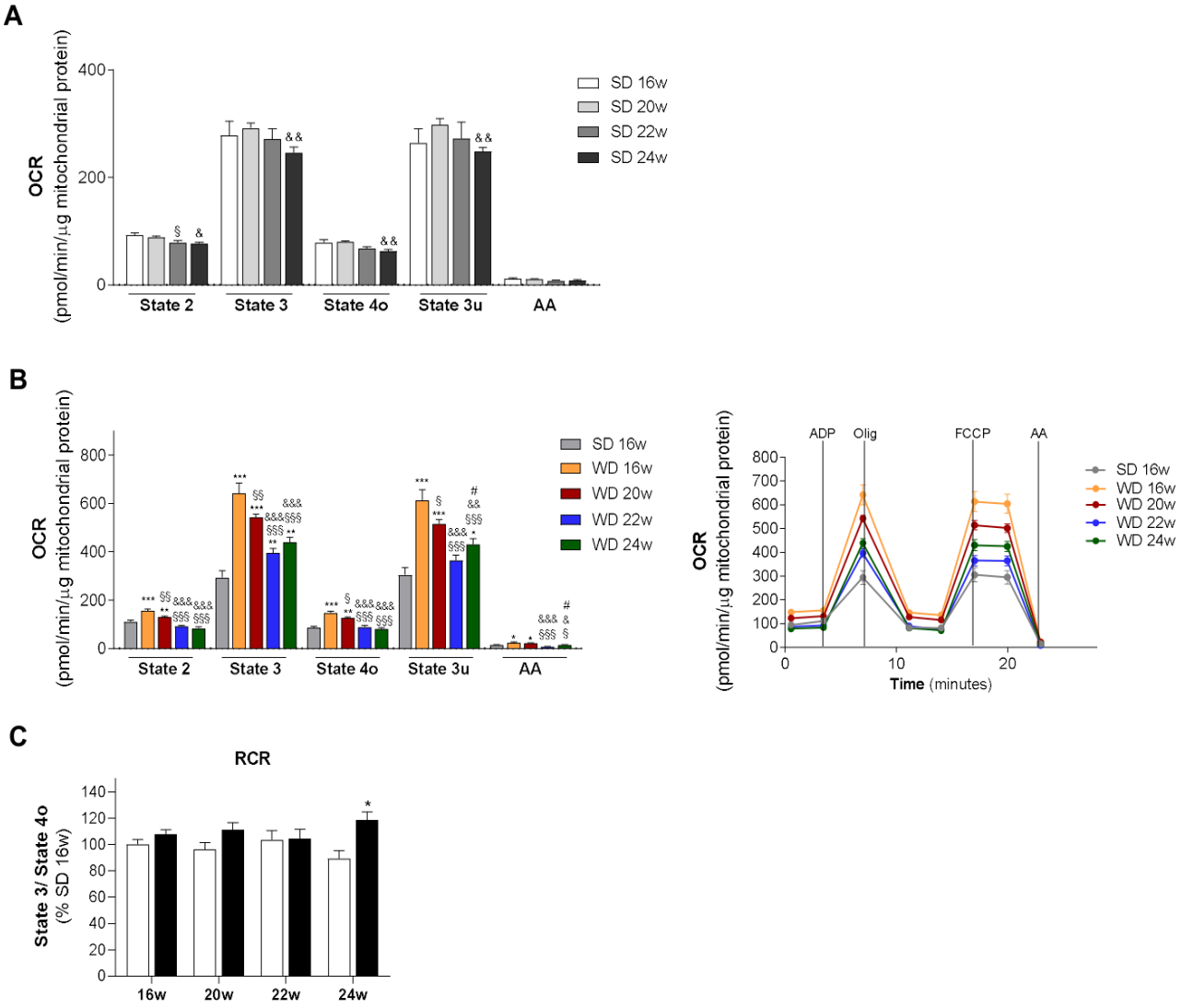

Figure 40. WD causes an increase of oxygen consumption rate at 16th week followed by a progressive decrease for longer timepoints. (A) Oxygen consumption rate of hepatic mitochondria from SD-fed mice among the distinct time points studied, using succinate as energizing substrate. **(B)** Oxygen consumption rate of hepatic mitochondria from SD16w group versus WD-fed groups, using succinate as energizing substrate; and representative oxygen consumption rate profile. **(C)** Respiratory control ratio (RCR) (State 3/State 4o) using succinate. All data are expressed as the mean ± SEM. (*) vs. SD, (§) vs. 16w, (&) vs. 20w, (#) vs. 22w ($P < 0.05$); (**) vs. SD, (§§) vs. 16w, (&&) vs. 20w ($P < 0.01$); (***) vs. SD, (§§§) vs. 16w, (&&&) vs. 20w ($P < 0.001$); *P* values were determined using two-way ANOVA. AA, antimycin A; FCCP, carbonyl cyanide-p-trifluoromethoxyphenylhydrazone; Olig, oligomycin; SD, standard chow diet; WD, Western diet.

An increase of OCR was measured in basal respiration (State 2), ADP-stimulatd respiration (State 3), non-ADP stimulated respiration also known as proton leak (State 4o), FCCP-induced maximal respiration (State 3u) and after Antimycin-A addition in mice

fed with WD-fed mice for 16 and 20 weeks, when compared with SD-fed group (**Figure 40B**). Importantly, this increase was followed by a progressive decrease of OCR values for longer WD feeding periods: 22 and 24 weeks (**Figure 40B**). Despite no significant alterations in RCR at 16, 20 and 22 weeks of feeding, an increase of RCR was found at the 24th week of WD feeding (**Figure 40C**). These findings suggest a lower proton leak and/-or a higher phosphorilative efficiency at this last timepoint studied. Moreover, I have also assessed electron flow assay. Again, to facilitate graphical representation, I demonstrated no significant differences between SD-fed groups at different timepoints studied (**Figure 41A**). Then, electron flow characteristic for SD16w group was compared with WD-fed groups (**Figure 41B**). I observed a higher transport of electrons through Complex I, II and III at 20th week and through Complex II at 22th and 24th weeks of WD feeding (**Figure 41B**).

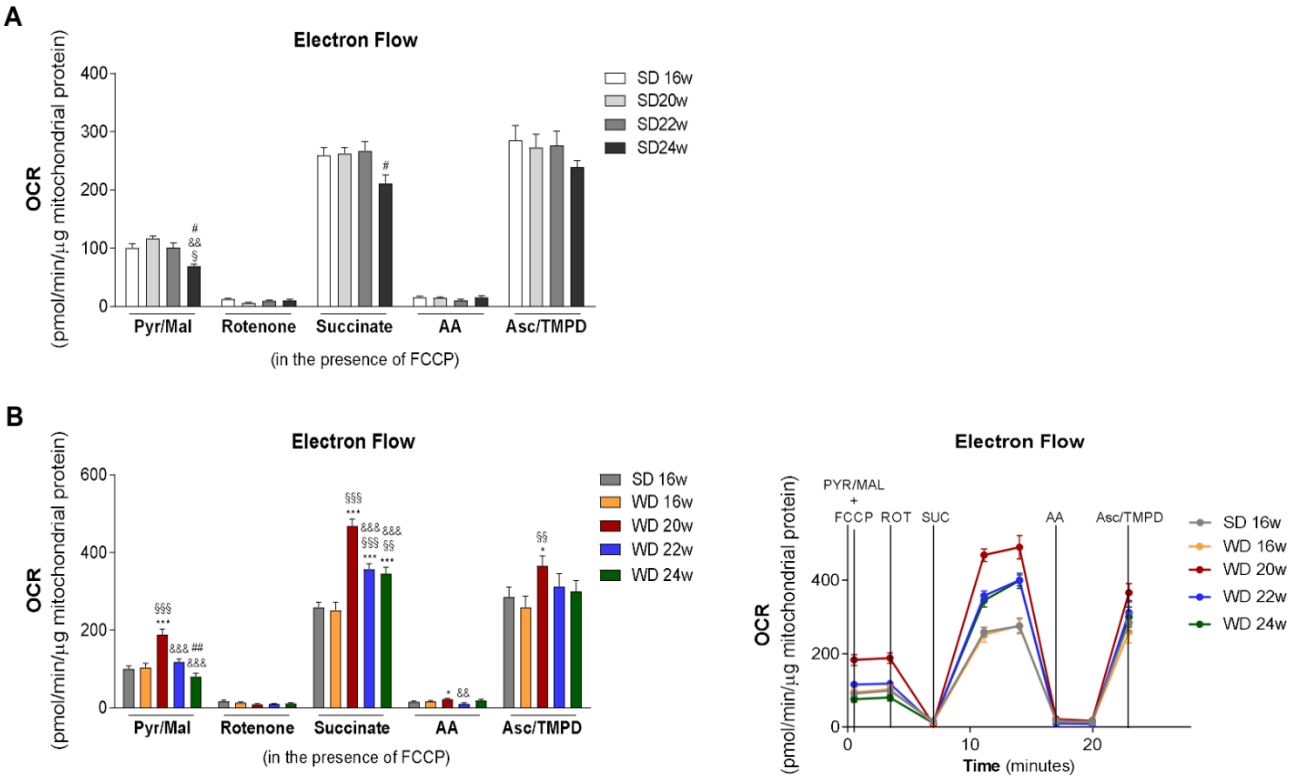

Figure 41. WD causes a higher electron transport through Complex I, II and III after 20 weeks of feeding. **(A)** Electron flow assay of hepatic isolated mitochondria from SD-fed mice at 16, 20, 22 and 24 weeks of feeding. **(B)** Electron flow assay of hepatic isolated mitochondria from SD16w group versus WD-fed groups; and representative Electron flow profile. All data are expressed as the mean ± SEM. (*) vs. SD, (§) vs. 16w, (#) vs. 22w ($P < 0.05$); (§§) vs. 16w, (&&) vs. 20w, (##) vs. 22w ($P < 0.01$); (***) vs. SD, (§§§) vs.

16w, (&&&) vs. 20w ($P < 0.001$); *P* values were determined using two-way ANOVA. AA, antimycin A; Asc, ascorbate; FCCP, carbonyl cyanide-p-trifluoromethoxyphenylhydrazone; OCR, oxygen consumption rate; Olig, oligomycin; Mal, malate; Pyr, pyruvate; Rot, rotenone; SD, standard chow diet; Suc, succinate; TMPD, N, ,N,N',N'-tetramethyl-p-phenylenediamine; WD, Western diet.

Next, I also evaluated the susceptibility of mitochondrial permeability transition pore (mTPT) opening in the presence of mPTP inducers e.g. Ca^{2+} and tBHP. Accordingly, hepatic isolated mitochondria from WD-fed mice showed a significant increase in the susceptibility for mPTP opening at 20 and 24 weeks of feeding (**Figure 42A**). This enables a good discrimination among WD-fed groups for 20, 22 and 24 weeks from the respective SD-groups as observed in PCA analysis represented in the **Figure 42B**.

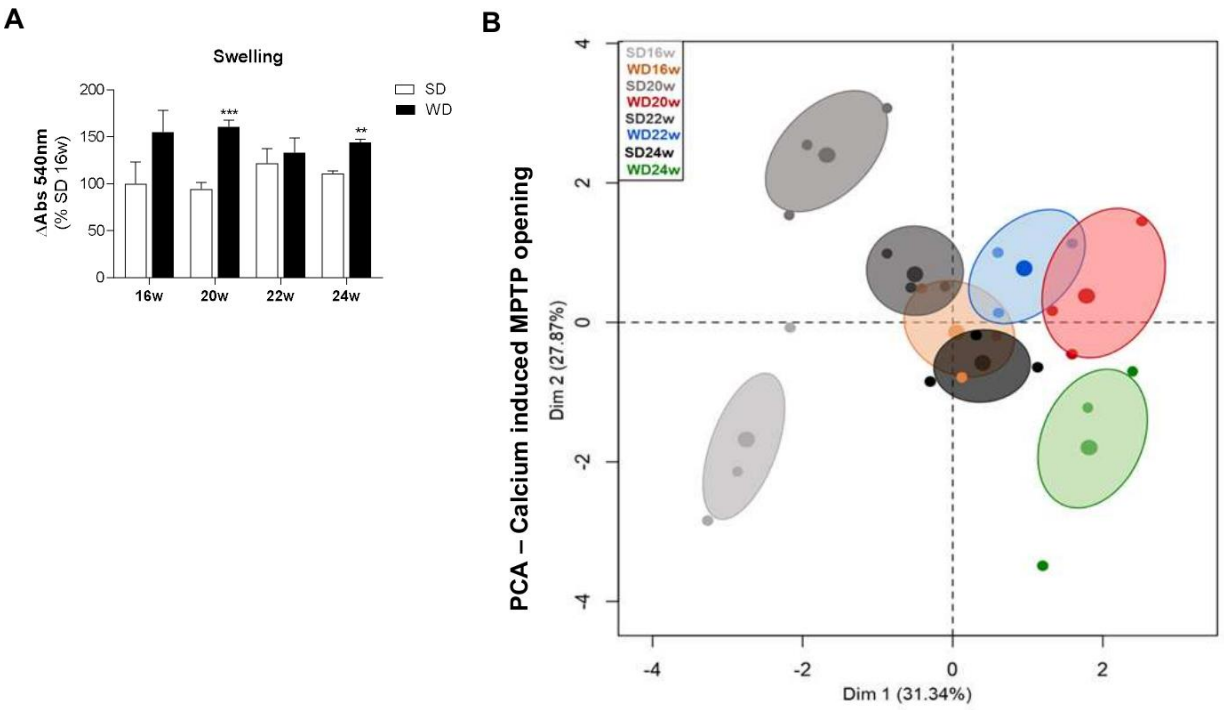

Figure 42. WD causes a higher susceptibility for mitochondrial permeability transition pore opening. (A) Mitochondrial permeability transition pore (mPTP) opening after 16, 20, 22 and 24 weeks of feeding. **(B)** Principal component analysis (PCA) of mPTP opening. All data are expressed as the mean ± SEM. (**) vs. SD ($P < 0.01$); (***) vs. SD ($P < 0.001$); *P* values were determined using two-way. SD, standard chow diet; WD, Western diet.

Overall, increased OXPHOS subunits protein levels together with cardiolipin levels support the higher OCR rate observed at the 16th week, while the decrease of OCR

is possibly correlated with higher susceptibility of mitochondria to mPTP opening, starting from the 20th week of WD feeding.

5.1.4 A decreased mitochondrial ROS production is accompanying NAFLD progression.

Mitochondia are considered as a major source for ROS generation in the cell under pathological conditions. Based on that, I investigated whether the above described mitochondrial alterations could be associated with increased ROS generation and subsequent mitochondrial oxidative injury during NAFL progression. Interestingly, no differences in mitochondrial H_2O_2 production were observed between WD16w and SD16w groups (**Figure 43A**).

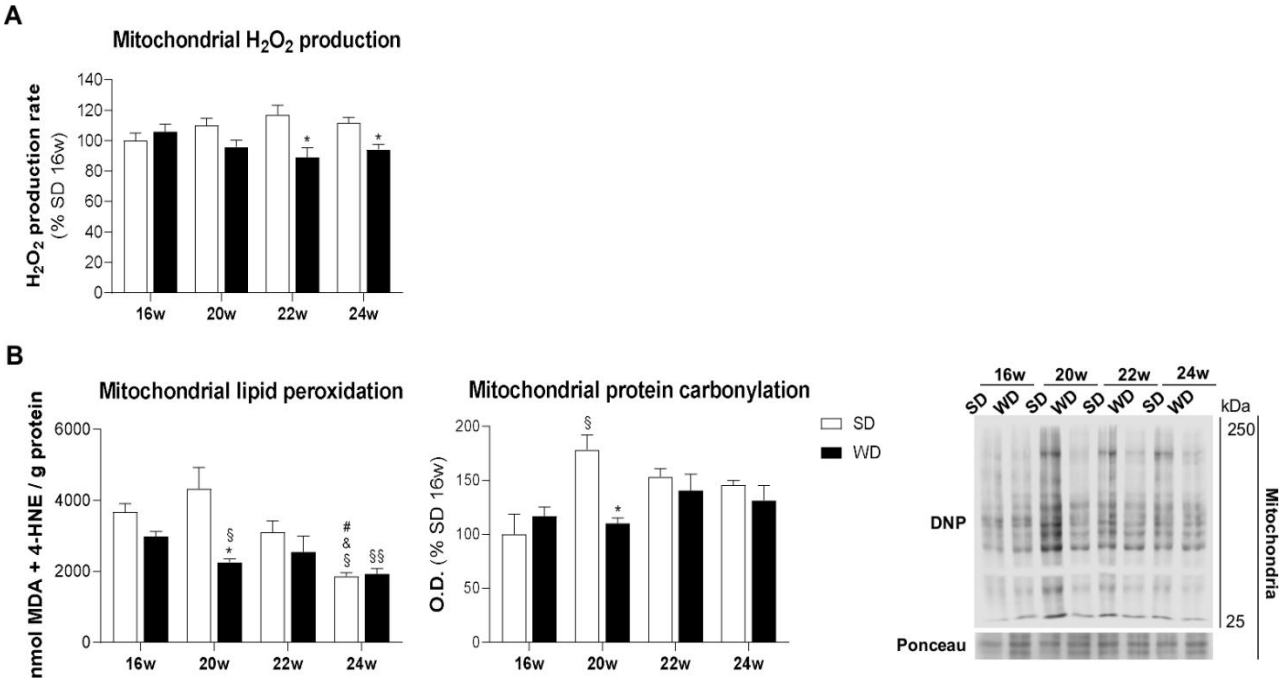

Figure 43. WD reduces hepatic mitochondrial reactive oxygen generation with no evidence of mitochondrial oxidative damage along NAFL progression. (A) Mitochondrial H_2O_2 generation in hepatic isolated mitochondria of WD-fed mice for 16, 20, 22 and 24 weeks. **(B)** Mitochondrial lipid peroxidation and protein carbonylation with a representative image of Western blot showing protein carbonylation (DNP) levels, using Ponceau as a loading control. All data are expressed as the mean ± SEM. (*) vs. SD, (§) vs. 16w, (&) vs. 20w, (#) vs. 22w ($P < 0.05$); (§§) vs. 16w ($P < 0.01$); *P* values were determined using two-way ANOVA. SD, standard chow diet; WD, Western diet.

Nevertheless, from the 20th until the 24th week timepoints, I observed a progressive decline in mitochondrial H_2O_2 production. In fact, this decline was shown to be statistically significant in WD22w and WD24w groups versus the respective SD-fed groups (**Figure 43A**). Hepatic isolated mitochondria from WD-fed mice showed lower levels of lipid peroxides and carbonylated proteins when compared with SD-fed mice (**Figure 43B**). However, no clear trend in mitochondrial oxidative damage was observed along WD feeding. Then, I decided to check the same oxidative damage markers but in hepatic cytosolic fraction. I did not observe any significant alteration in carbonylated proteins. I have just observed an upward trend in lipid peroxides between WD- and SD-fed mice at the 22nd week (**Figure 44A**).

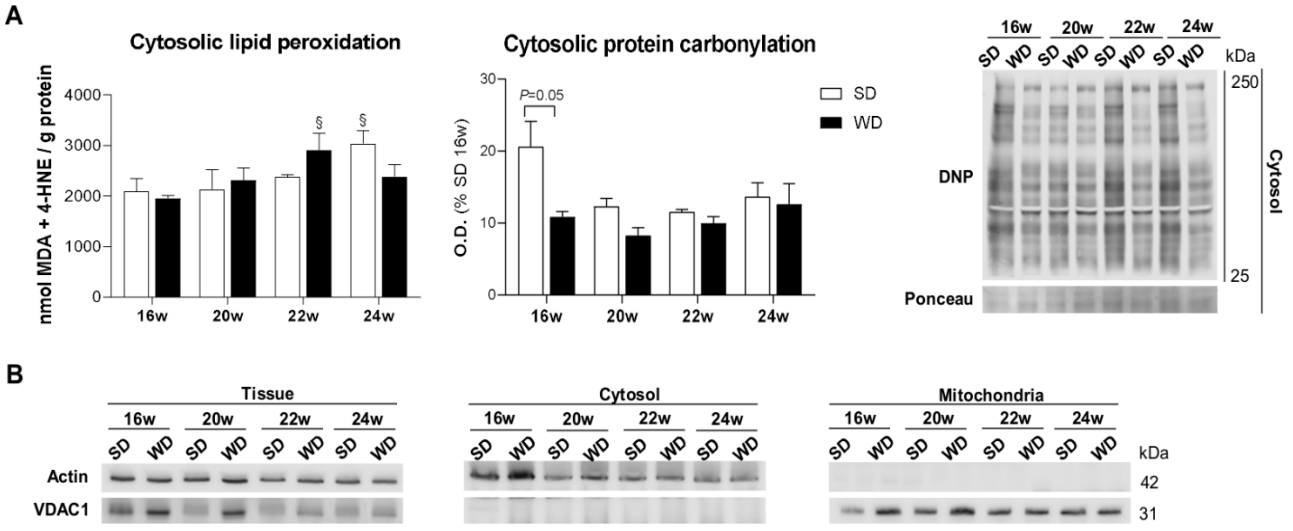

Figure 44. Absence of oxidative damage in hepatic cytosolic fractions of non-alcoholic fatty liver mice along with disease progression. (A) Cytosolic lipid peroxidation and protein carbonylation with a representative image of Western blot showing protein carbonylation (DNP) levels, using Ponceau as a loading control. **(B)** Representative image of Western blot showing total liver homogenate and the purity of cytosolic and mitochondrial fractions. Actin was used as cytosolic and VDAC1 as mitochondrial loading control. All data are expressed as the mean ± SEM. (§) vs. 16w ($P < 0.05$). *P* values were determined using two-way ANOVA. SD, standard chow diet; WD, Western diet.

In order to strengthen the validity of the above described findings, I have evaluated the purity of mitochondrial and cytosolic fractions (the representative images presented in the **Figure 44B**). Accordingly, I demonstrated that obtained results were not affected by the low purity of the analyzed organelles/fractions. Altogether, WD

feeding showed to induce a decrease in mitochondrial ROS production, with no signs of hepatic oxidative damage.

5.1.5 WD induces a de-regulation of the antioxidant defense system and exacerbates peroxisomal-FAO in hepatic cytosol along NAFLD progression.

Considering that oxidative stress is a balance between ROS production and ROS scavenging system, next I investigated the status of the antioxidant defense system again in both isolated liver fractions: mitochondria and cytosol. At the mitochondrial level, I observed a downward trend of SOD and an increase of catalase activities in WD16w group versus SD16w group (**Figure 45**).

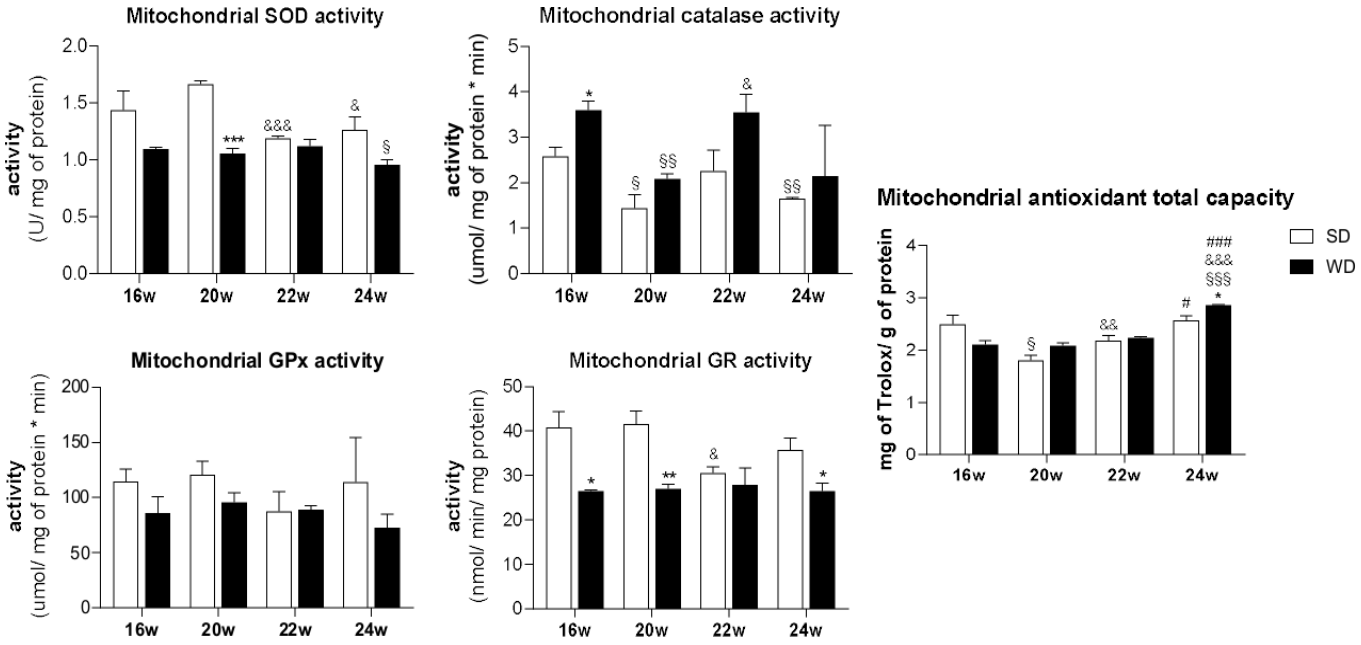

Figure 45. Alterations in mitochondrial antioxidant defense enzymes activities induced by WD feeding along time. Mitochondrial superoxide dismutase (SOD), catalase, glutathione peroxidase (GPx), glutathione reductase (GR) activities, and mitochondrial antioxidant total activity in hepatic mitochondria isolated from WD-fed mice for 16, 20, 22 and 24 weeks. All data are expressed as the mean ± SEM. (*) vs. SD, (§) vs. 16w, (&) vs. 20w, (#) vs. 22w ($P < 0.05$); (**) vs. SD, (§§) vs. 16w, (&&) vs. 20w ($P < 0.01$); (***) vs. SD, (§§§) vs. 16w, (&&&) vs. 20w, (###) vs. 22w ($P < 0.001$). *P* values were determined using two-way ANOVA. SD, standard chow diet; WD, Western diet.

Although a decrease in SOD activity was still visible at WD20w group, both differences (SOD and catalase) disappear for longer feeding timepoints. Regarding the other enzymes analyzed, I observed a downward trend for GPx activity and a significant decrease in GR activity for WD-fed mice for 16, 20 and 24 weeks of WD feeding. Of note, mitochondrial total antioxidant activity was significantly augmented at 24th week of WD-fed mice when compared with respective SD group (**Figure 45**).

In the cytosolic fraction, I observed an upward trend of SOD activity in WD16w and WD20w groups followed by a progressive increase for longer WD feeding timepoints tested (**Figure 46**).

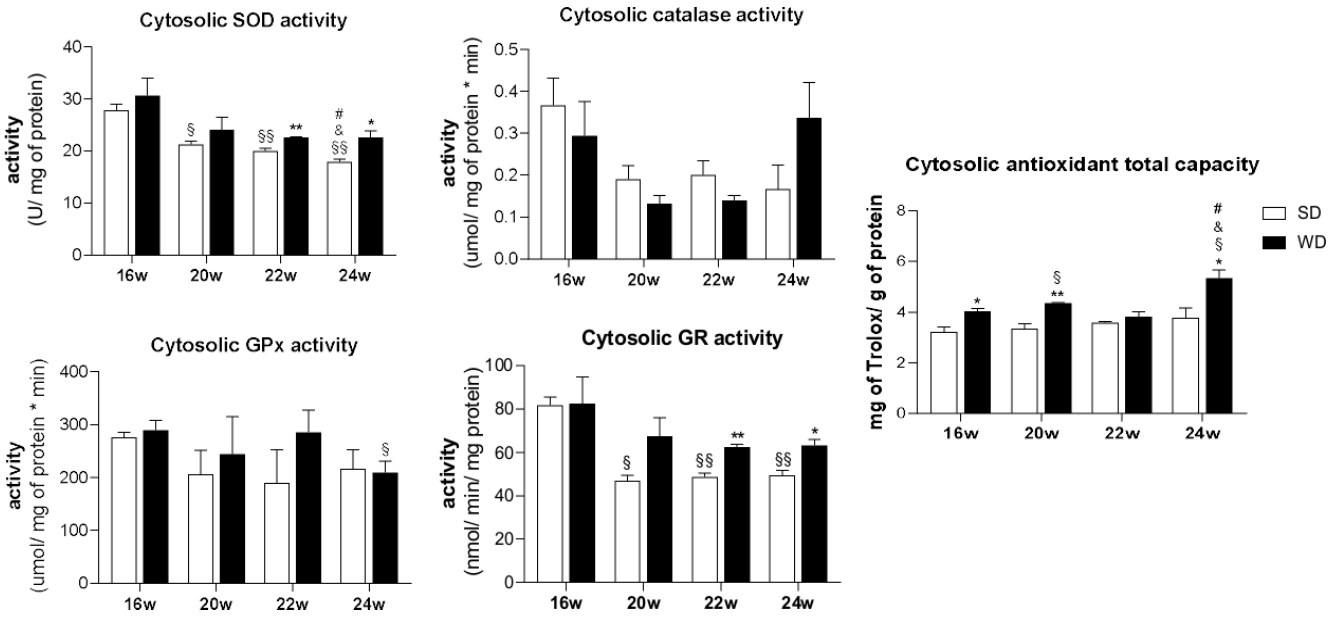

Figure 46. Alterations in cytosolic antioxidant defense enzymes activities induced by WD feeding along time. Cytosolic superoxide dismutase (SOD), catalase, glutathione peroxidase (GPx), glutathione reductase (GR) activities, and mitochondrial antioxidant total activity in hepatic mitochondria isolated from WD-fed mice for 16, 20, 22 and 24 weeks. All data are expressed as the mean ± SEM. (*) vs. SD, (§) vs. 16w, (&) vs. 20w, (#) vs. 22w ($P < 0.05$); (**) vs. SD, (§§) vs. 16w ($P < 0.01$). *P* values were determined using two-way ANOVA. SD, standard chow diet; WD, Western diet.

I have found a similar trend for GR activity, starting from the 22nd week of feeding (**Figure 46**). Interestingly, I observed that the significant increase in SOD and GR activities at 22nd of WD feeding coincided with an upward trend in cytosolic lipid peroxide levels. Despite the previous findings, no significant differences were observed in catalase and GPx

activities between WD- and SD-fed mice (**Figure 46**), suggesting a possible de-regulation of cytosolic antioxidant defense system along NAFLD progression. In addition, total antioxidant activity was found to increase in the cytosol of mice livers fed for 16, 20 and 24 weeks (**Figure 46**). Then, I also assessed the levels of antioxidant defense enzymes in liver homogenates. Thanks to mass spectrometry-proteomic analysis, I observed augmented levels of myeloperoxidase (MPO), selenoprotein P (SEPP1), thioredoxin reductase (TXNRD1) and thioredoxin domain-containing protein (TXNRD17) in all WD-fed groups versus SD-fed mice (**Figure 47A**). These results enabled me a distinct separation between SD and WD regimens in oxidative stress-related data as shown in PCA analysis represented in the **Figure 47B**.

According to an upward trend of cytosolic lipid peroxides and a de-regulation of cytosolic antioxidant defense system, next I examined possible pathways contributing for cytosolic ROS generation. In a steatotic liver context, FAO occurs not only at mitochondrial level, but it could also take place in cooperation with peroxisomes. In my work, mitochondrial FAO-related proteins such as ACOT2 and ACOT9 were found to be increased 2-fold and 1-fold, respectively (**Figure 48A**). Nevertheless, many peroxisomal FAO-related proteins were found elevated (**Figure 48A**), which supports the idea that peroxisomes are the main organelles responsible for hepatocyte FAO in a fatty liver context. Of note, my findings showed increased levels (1- to 2-fold) of proteins responsible for the import of VLCFAs into the peroxisome – ABCD1 and ABCD2, lipid metabolism - ACOT3, ACOT4 and ACOT8, and oxidation of FAs - ACOX1 in livers of mice fed with a WD for 16 up to 24 weeks (**Figure 48A**). These findings are well correlated with upregulated peroxisomal-related protein markers, namely proteins involved in peroxisomal biogenesis (PEX1/3), peroxisomal assembly (PEX6/7/26) and peroxisomal membrane composition (PXMP4, PEX11a/14/16) (**Figure 48B**). Therefore, WD contributes for a distinct oxidative metabolism phenotype in steatotic livers of mice fed up to 24 weeks (**Figure 49**).

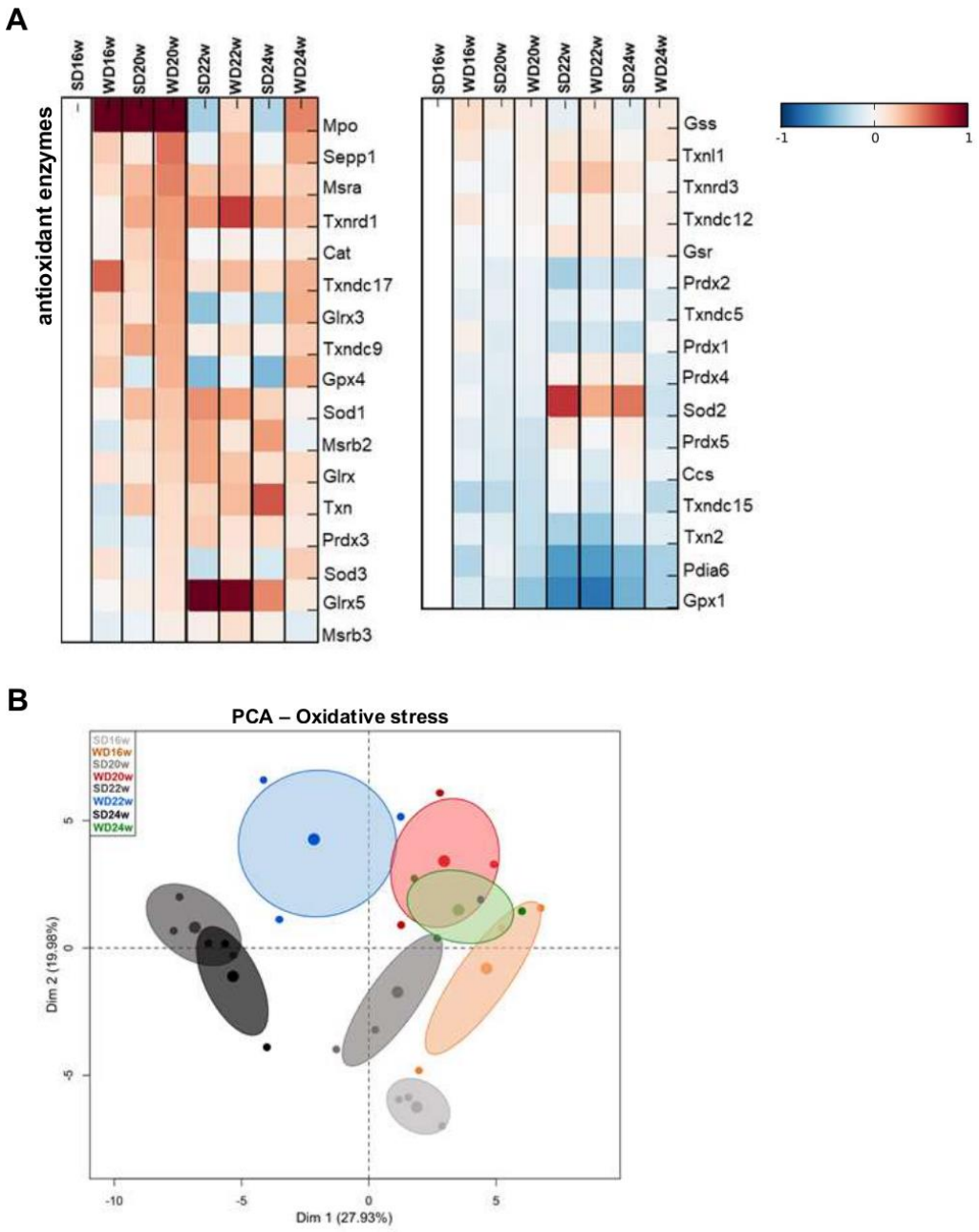

Figure 47. WD induced changes in antioxidant defense protein levels and a distinct signature of oxidative stress-related data along NAFL progression. (A) Mass spectrometry-proteomic analysis of hepatic antioxidant defense enzymes protein levels of SD and WD-fed mice for 16, 20, 22 and 24 weeks of feeding. The blue color represents decreased, and the red color represents increased levels. **(B)** Principal component analysis (PCA) of oxidative stress-related data. SD, standard chow diet; WD, Western diet.

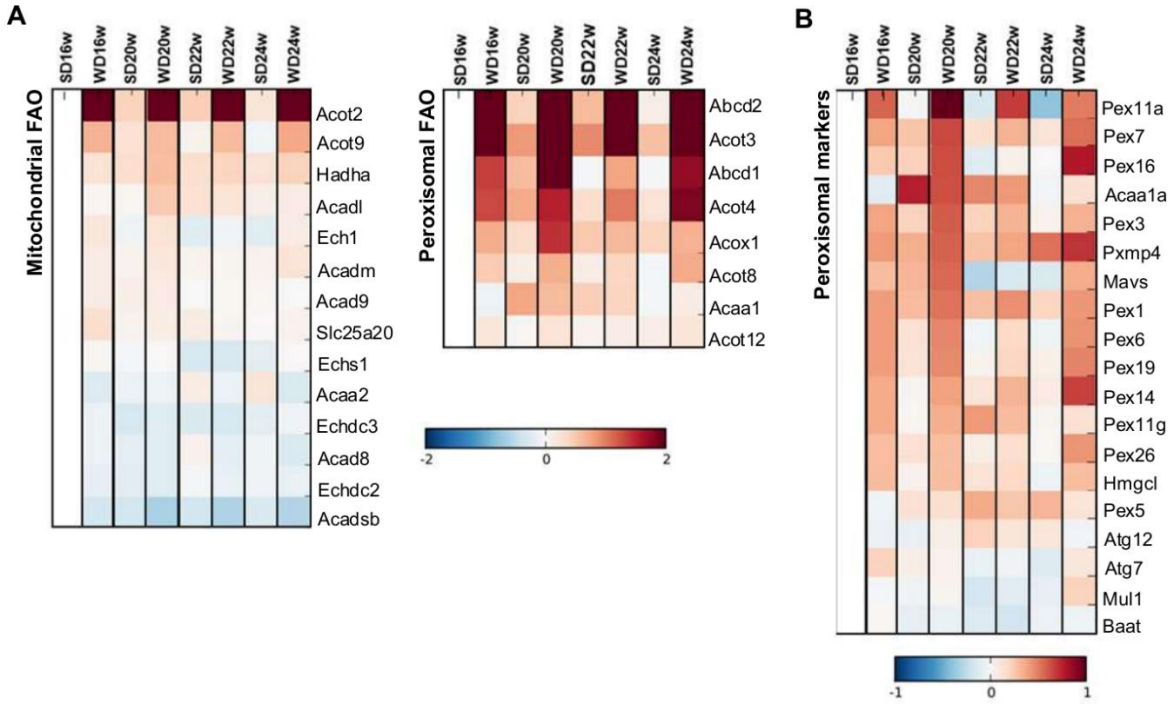

Figure 48. WD increased hepatic oxidative metabolism at both mitochondrial and peroxisomal levels. (A) Mass spectrometry analysis of hepatic mitochondrial and peroxisomal-related fatty acid oxidation (FAO) protein levels of SD and WD-fed mice for 16, 20, 22 and 24 weeks of feeding. **(B)** Mass spectrometry analysis of hepatic peroxisomal-related protein markers of SD and WD-fed mice for 16, 20, 22 and 24 weeks of feeding. The blue color represents decreased, and the red color represents increased levels. SD, standard chow diet; WD, Western diet.

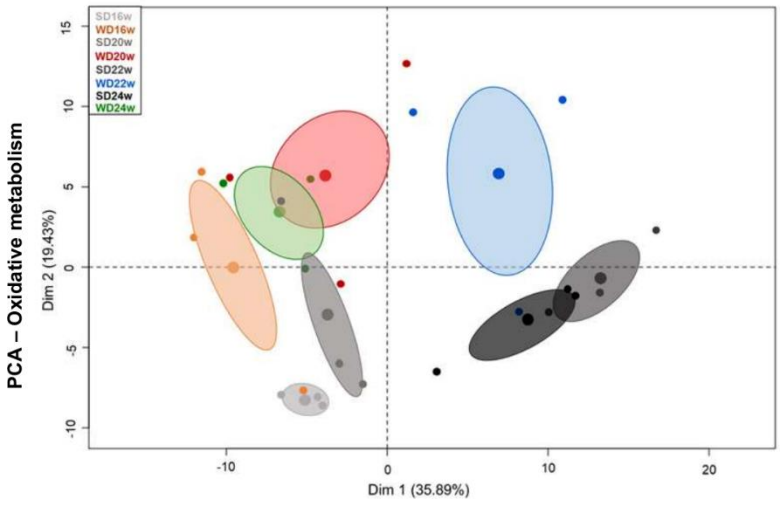

Figure 49. WD induced a distinct clustering of oxidative metabolism-related parameters in SD- and WD-fed mice. Principal component analysis (PCA) of oxidative metabolism-related parameters in mice fed with SD- and WD-diets for 16, 20, 22 and 24 weeks. SD, standard chow diet; WD, Western diet.

My findings highlight that mitochondrial and cytosolic alterations above do not correlate with mitochondrial ROS generation but rather have a cytosolic origin. Then, WD feeding induces an imbalance between cytosolic ROS generation and the endogenous antioxidant defense system along NAFLD progression.

5.1.6 WD induces the accumulation of autophagic-associated proteins LC3-II, SQSTM1 and NBR1 along NAFLD progression.

According to the impairment of autophagic pathway observed in early-stage NAFL model fed with distinct hypercaloric diets (Chapter 1), I have also investigated whether such impairment is regulated in a time-dependent manner along NAFLD progression. Therefore, my first step was to investigate the regulation of the pathway by PI3K/AKT/mTOR axis. Regarding the upstream proteins involved in the pathway, I did not observe any significant alteration in the ^{Ser473}p-AKT at neither in p-AKT/AKT ratio along the WD versus SD timepoints studied (**Figure 50A**). Despite an increase in ^{Ser2448}p-mTOR in WD24w compared with the SD24w group, no other significant alterations were observed for the remaining WD feeding timepoints (**Figure 50B**). Although, mass spectrometry analysis revealed increased levels of proteins involved in downstream pathways under mTOR regulation, namely protein synthesis. In fact, upregulation of RPS6KA1 and RPS6KA3 was found in WD-fed mice up to the 24th week of feeding (**Figure 50C**).

Another pathway under the regulation of mTOR is autophagy, a cellular quality control mechanism. In this regard, no major alterations were observed at the level of ATG proteins (**Figure 50C**). Despite of that, I observed increased Beclin-1 (BECN1) levels in WD16w and WD20w groups (**Figure 50C**). Additionally, I showed a progressive increase of 100-150% in LC3-II levels in WD-fed mice for longer periods of feeding, being LC3-II/LC3-I ratio also augmented by 170-360% when WD-fed groups were compared with respective SD-fed groups (**Figure 51A**).

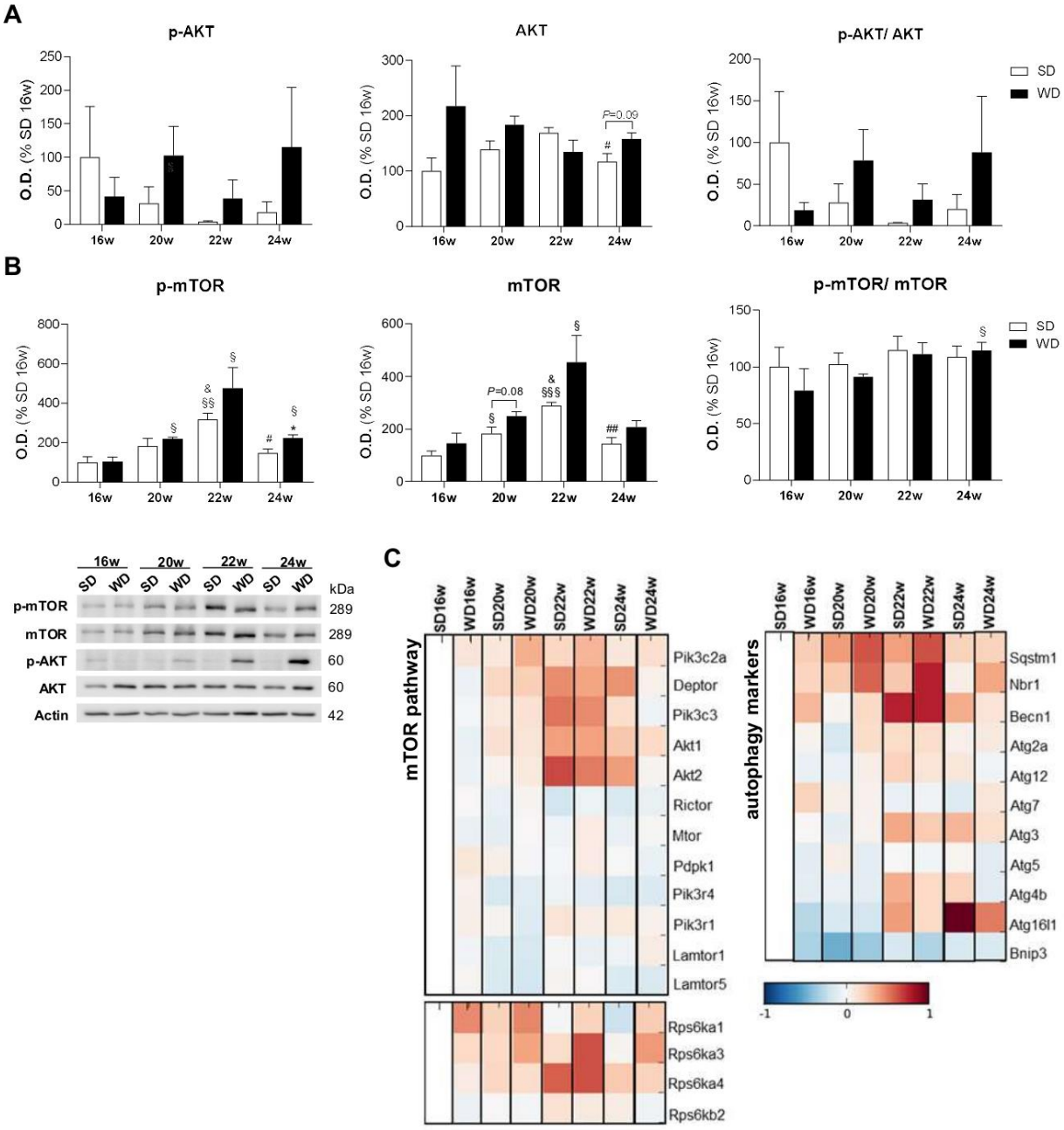

Figure 50. WD increased the accumulation of autophagic-related markers up to the 24th week of feeding. **(A)** Protein levels of ^{Ser473}p-AKT, AKT and p-AKT/AKT ratio. **(B)** Protein levels of ^{Ser2448}p-mTOR, mTOR and p-mTOR/mTOR ratio. Representative Western blot images of (A) and (B) are represented below. Actin was used as loadig control. **(C)** Mass spectrometry-proteomic analysis of mTOR-related protein levels and autophagic-related protiens of SD- and WD-fed mice for 16, 20, 22 and 24 weeks of feeding. The blue color represents decreased, and the red color represents increased levels. All data are expressed as the mean ± SEM. (*) vs. SD, (§) vs. 16w, (&) vs. 20w, (#) vs. 22w ($P < 0.05$); (§§) vs. 16 w, (##) vs. 22w ($P < 0.01$); (§§§) vs. 16w ($P < 0.001$). *P* values were determined using two-way ANOVA. SD, standard chow diet; WD, Western diet.

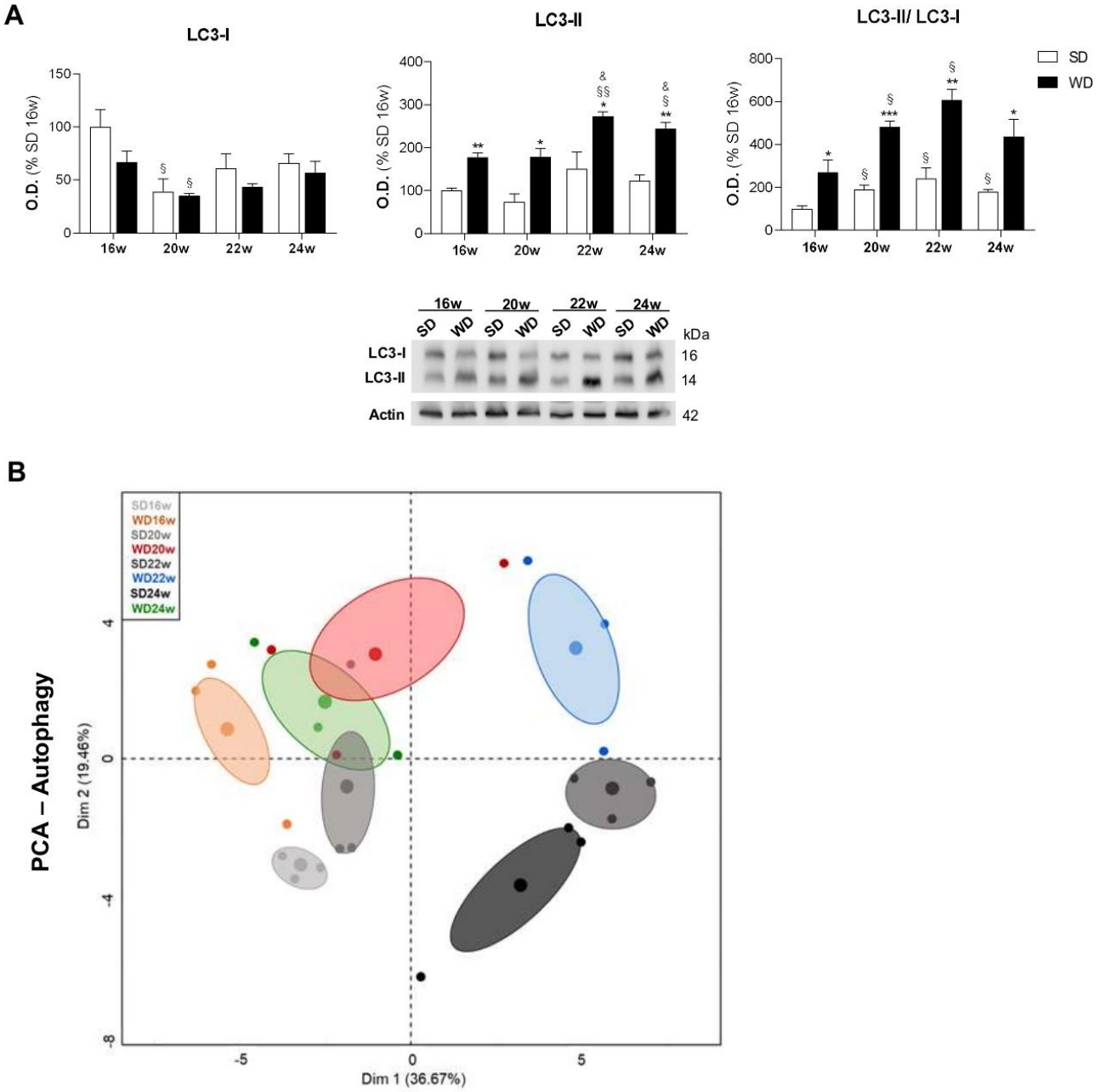

Figure 51. WD induced an increased accumulation of LC3-II protein levels along NAFLD progression. (A) Protein levels of LC3-I, LC3-II and LC3-II/LC3-I ratio, with representative Western blot images. Actin was used as a loadig control. **(B)** Principal component analysis (PCA) of autophagy-related parameters in mice fed with SD- and WD-diets for 16, 20, 22 and 24 weeks. All data are expressed as the mean ± SEM. (*) vs. SD, (§) vs. 16w, (&) vs. 20w ($P < 0.05$); (**) vs. SD, (§§) vs. 16w ($P < 0.01$); (***) vs. SD ($P < 0.001$). *P* values were determined using two-way ANOVA. SD, standard chow diet; WD, Western diet.

In paralel with the accumulation of LC3-II and the respective ratio, I also reported an accumulation of 16-18% of SQSTM1 and 34-60% of NBR1 in WD-fed groups for all WD-feeding periods studied (**Figure 50C**). Even though autophagic flux was not directly monitored in my experiments, the accumulation of SQST1M and NBR1 suggests a

possible blockage of the autophagic pathway, with impairment of autophagossomal formation and/-or a deficit of its clearance. Indeed, this is supported by a distinct clustering of autophagic-related data between WD- and SD-fed groups (**Figure 51B**).

5.2 Discussion of the data presented in Chapter 2

The development of NAFL, followed by a possible progression into a more severe NAFLD stage depends on the capacity of hepatocytes and mitochondria to adapt to nutrients overload. It is established that structural and molecular mitochondrial modifications are associated with a decline of mitochondrial function in a NASH context (Koliaki, Szendroedi et al. 2015). In this chapter of my thesis, I revealed the sequence of events that precedes mitochondrial-associated alterations during the development and progression of NAFL. Additionally, I also clarified the role of mitochondrial ROS by following disease progression from 16 up to 24 weeks of WD feeding, using the mice model established in the previous chapter. In this part of the work, I showed that WD feeding induced a time-dependent mitochondrial remodelling with increased OCR, higher OXPHOS protein expression levels and higher content of cardiolipin in NAFL. However, I also showed that for longer timepoints of feeding, WD decreased mitochondrial OCR and increased the susceptibility of mPTP opening. Importantly, I demonstrated that the above-described findings are independent of mitochondrial ROS production, that in fact was found to be diminished in animals exposed to WD for longer timepoints. Moreover, an accumulation of autophagic-related markers may also indicate a blockage of the autophagic flux, contributing to hepatic damage accumulation and subsequent NAFLD progression.

The intake of hypercaloric diets enriched in fat and sucrose, which mimic the eating habits of the Western society induced higher body weight and the accumulation of fat in the liver of mice when fed for 16, 20, 22 and 24 weeks. A more detailed histological assessment confirmed the development of simple steatosis with early signs of hepatocyte ballooning and fibrosis but no further disease progression even at the longest timepoint studied. Focusing on hepatic lipid accumulation, I demonstrated that lipids accumulate inside hepatocytes in lipid droplets, in the form of TGs and CEs, with enrichment of MUFAs even for longer WD feeding timepoints. This lipid profile ensures

a protective mechanism against lipotoxicity-associated damage characteristic of NAFLD pathophysiology (Yamaguchi, Yang et al. 2007). NAS score showed that there is no significant disease progression between the 16th and the 24th week of feeding. Considering that dietary studies that last more than 20 weeks are scarce, it is difficult to establish direct comparisons between my findings and the existing literature. Nevertheless, a work of Satapati *et al.* showed a continuous increase of simple steatosis with no signs of lobular inflammation up to 32 weeks of HF feeding (Satapati, Sunny et al. 2012). This is in line with my findings, suggesting that longer WD feeding timepoints and/-or extra insults would be needed to trigger NASH stage. Alternatively, a more advanced NAFLD stage should be induced with other animal model fed with appropriate NASH-inducing diets such as choline and/-or methionine deficient diets (Simoes, Janikiewicz et al. 2019).

Accumulating evidence has shown that mitochondria play a key role in the initiaton and progression of NAFLD. Accordingly, alterations in mitochondrial function have been reported in both NAFL and in NASH stage (Grattagliano, de Bari et al. 2012), such as dearrangement of mitochondrial structure and alteration of mitochondrial proteome (Eccleston, Andringa et al. 2011) as well as changes in citrate synthase (Rector, Thyfault et al. 2010) and in OXPHOS complexes activities (Fouret, Gaillet et al. 2018, Lee, Haddad et al. 2018). Nevertheless, the sequence of mitochondrial alterations driving the progression of NAFLD is still not clarified. Here, I demonstrated that NAFLD progression is correlated with differential response of mitochondrial respiration along WD feeding. While OCR started to be augmented in NAFL (up to 20 weeks of WD feeding), longer WD feeding timepoints induced a decrease of OCR in the presence of Complex II substrate. At an initial stage, an augmented OCR is well correlated with higher protein levels of OXPHOS complexes subunits belonging to Complex I, II, IV and ATP synthase. Then, mitochondrial bioenergetic efficiency started to decrease at 22 and 24 weeks timepoints. An initially augmented OCR can be attributed to the hepatic nutrient overload. In other studies, diet-induced disorders and the associated nutrient overload have been correlated with mitochondrial bioenergetic deregulation with an impaired metabolic flexibility (Muoio 2014). Accordingly, Koliaki and co-workers have reported that a cohort of obese patients (with or without NAFL) presented higher mitochondrial respiration while a cohort of NASH patients had lower mitochondrial respiration despite

presenting higher mitochondrial mass (Koliaki, Szendroedi et al. 2015). Based on that, my findings support the evidence of an early adaptative response of hepatocytes, and specially mitochondria to nutrients overload with an increased mitochondrial function. Then, this stage is followed by a progressive loss of mitochondrial respiration along disease progression.

In agreeement with the data presented in the previous chapter focusing on the effect of hypercaloric diets in NAFL, cardiolipin levels were found to be increased up to the 22nd week of WD feeding. This is also in line with other reports showing higher cardiolipin levels in NAFL rather in NASH stage (Aoun, Fouret et al. 2012, Fouret, Gaillet et al. 2018, Peng, Watt et al. 2018). Cardiolipin is a mitochondrial phospholipid signature with fulcral roles in mitochondrial membrane fluidity, osmotic stability and OXPHOS complexes assembly and phosphorilative efficiency (Schlame 2008, Prola, Blondelle et al. 2021). In my study, I demonstrated that despite a reduction in OCR along NAFLD progression, mitochondria are still functionally coupled at 24 weeks of WD feeding. This is supported by sustained cardiolipin levels and RCR values reported at this timepoint in WD-fed group versus the respective control. Consistently, Satapati and colleagues have just showed a decrease of RCR in obese mice after 32 weeks of feeding (Satapati, Sunny et al. 2012).

However, I have shown deleterious effects of hepatic fact accumulation at mitochondria level over time. In parallel with a decrease of mitochondrial respiration, I observed a higher susceptibility to Ca^{2+} ant tBHP-induced mPTP opening. Mitochondrial structure and the intrinsic stability/ fluidity properties seem to be regulated by the accumulation of cholesterol inside hepatocytes. In fact, the deposition of cholesterol in mitochondria was shown to induce JNK1 activation with consequent mPTP opening, mitochondrial swelling and decline of ATP production (Gan, Van Rooyen et al. 2014). On other hand, an increasing amount of cholesterol in hepatocyte's membranes can impair the transport of cytoslic glutathione inside mitochondria (Colell, Garcia-Ruiz et al. 2003, Fernandez-Checa and Kaplowitz 2005). The subsequent mitochondrial GSH depletion can therefore predispose these cells to the inflammatory cytokine TNF-α and Fas sensitization (Mari, Caballero et al. 2006). These alterations possibly contribute to the severity of NAFLD progression.

Another pathway that strongly modulates NAFL development is FAO. A reduced mitochondrial FAO has been associated with disease progression (Eccleston, Andringa et al. 2011, Perfield, Ortinau et al. 2013). Curiously, I did not find any significant changes in mitochondrial FAO-related protein levels. This was accompanied by higher levels of peroxisomal FAO-related proteins as well as peroxisomal-related markers along WD feeding. These findings suggest that a higher number and higher FAO activity of peroxisomes would counteract hepatic lipid accumulation. In line with that, other studies have reported an upregulation of PPAR-α and ACOX genes, along with augmented peroxisomal abundance in dietary NAFLD mice models (Matsuzawa-Nagata, Takamura et al. 2008, Knebel, Hartwig et al. 2015) and in NAFLD clinical cohorts (Collins, Scheinberg et al. 1989, De Craemer, Pauwels et al. 1995). An increased peroxisomal FAO activity was shown to protect A/J mice from the development of simple steatosis (Hall, Poussin et al. 2020). Based on the previous reports, my study supports the emerging role of peroxisomes in NAFLD, which by increasing hepatic FAO can compensate mitochondrial oxidative capacity and protect it against the harmful effects of fat overload (Knebel, Goddeke et al. 2018). Although mitochondrial oxidative metabolism has been correlated with ROS production (Natarajan, Eapen et al. 2006, Begriche, Massart et al. 2013), I have not found increased mitochondrial ROS production or augmented mitochondrial oxidative stress markers in NAFL (Simoes, Karkucinska-Wieckowska et al. 2020). These findings agree with Einer *et al.* (Einer, Hohenester et al. 2018), but in contrast with the majority of previous studies that point mitochondrial ROS generation as the trigger for mitochondrial alterations that drive hepatocyte injury and further NAFLD progression. However, it is important to highlight that mitochondrial ROS generation/ oxidative damage was not been directly monitored (Chen, Tian et al. 2020). Here, my work directly demonstrates that mitochondrial ROS seem to be not crucial during an early NAFLD stage and what is more important, I demonstrated that the mitochondrial ROS levels gradually decrease up to investigated 24th week of WD feeding. An excessive amount of lipids has been described to up-regulate FAO, resulting in higher mitochondrial proton leak and an incomplete substrate coupling. This has been pointed as a possible mitochondrial protective strategy against the deleterious effects of oxidative damage (Turner, Bruce et al. 2007, Toime and Brand 2010). In my study, WD feeding induced higher OCR and higher proton leak up to 20 weeks of WD feeding, with

no signs of mitochondrial ROS production. Moreover, no major alterations were found in the mitochondrial antioxidant defense system. Such findings may indicate a mitochondrial adaptative response which may protect hepatocytes from FAs insult, but again it also reinforces that mitochondria may not be a primary source of ROS generation in a NAFLD context (Rector, Thyfault et al. 2010, Wang, Liu et al. 2015, Braud, Battault et al. 2017).

Notably, there is evidence that endoplasmic reticulum and peroxisomes are the main organelles contributing for H_2O_2 generation in liver of rodents (Boveris, Oshino et al. 1972). In a more recent study, influx of FAs in pancreatic cells caused H_2O_2 production in peroxisomes rather than in mitochondria (Elsner, Gehrmann et al. 2011). Accordingly, I have suggested in the previous chapter of my thesis that in order to compensate hepatocyte FAs overload, peroxisomes increase their FAO-related activity thereby contributing to ROS generation during NAFL (Simoes, Karkucinska-Wieckowska et al. 2020). This is also in agreement with my observation that WD feeding causes higher levels/activities of cytosolic antioxidant defense enzymes as well as increased total antioxidant activity up to the 24th week of this study. Despite these findings were not accompanied by a direct evidence of ROS generation or signs of oxidative damage, it is suggested that peroxisomal ROS may sensitize mitochondria and hepatocytes for further oxidative injury. Koliaki and co-workers have reported a lower expression of genes encoding mitochondrial biogenesis transcription factors (namely PGC1-α and TFAM) in NAFL. With disease progression, an augmented mitochondrial mass which likely indicate an accumulation of damaged and/-or dysfunctional mitochondria in NASH was verified (Koliaki, Szendroedi et al. 2015). This agrees with increased LC3-II, NBR1 and SQSTM1 protein levels. The accumulation of these autophagic-related markers along 24 weeks of WD feeding suggests a time-dependent blockage of autophagy with an impaired clearance/ recycling of damaged hepatic structures, which likely may exacerbate disease progression.

Here, I demonstrated the chronological features, focusing on mitochondrial and hepatic-related alterations of NAFL development and progression along 24 weeks of WD feeding. It is important to stress that the most pronounced effects in terms of liver steatosis and liver damage occur up to 16 weeks of WD feeding. Then, from 16th up to the 24th week, no major differences were found in these parameters. On the other hand,

I observed an increased mitochondrial respiration in NAFL followed by a time-dependent decrease in mitochondrial respiration up to 24 weeks of feeding. Altogether, my findings suggest that hepatic alterations observed up to the 16th week may play a key role in the modulation of NAFLD progression. Then, during this progressing state, there are accompanying events contributing to mitochondrial and hepatic metabolism malfunction. My work lays the foundations for the mechanisms involved in an initial NAFLD stage. Despite that, future research work should be performed using more advanced disease models to clarify how the above described alterations will affect disease progression.

In summary, I have shown that a Western-like diet feeding for 16 up to 24 weeks induces the development of NAFL with initiation of disease progression to NASH. In this part of my work, I demonstrated a remodelling of the mitochondrial function, with an initial higher mitochondrial respiration being followed by a progressive decrease at 22 and 24 weeks of feeding. In paralel, I observed augmented cholesterol and cardiolipin levels with a time-dependent susceptibility to mPTP opening. Moreover, I have shown evidence that mitochondrial ROS does not drive such mitochondrial-related alterations. In fact, it was undoubtedly proven that mitochondrial ROS do not constitute the first hit for NAFLD progression. Following the evidence shown on the first part of my thesis, I reinforced the hypothesis that a higher peroxisomal abundance together with higher peroxisomal-FAO activity may overcome fat accumulation at the expense of hepatic oxidative stress. An impairment of autophagic flux may be also fulcral for hepatocyte injury that hasten for NAFLD progression (results summarized in the **Figure 52**).

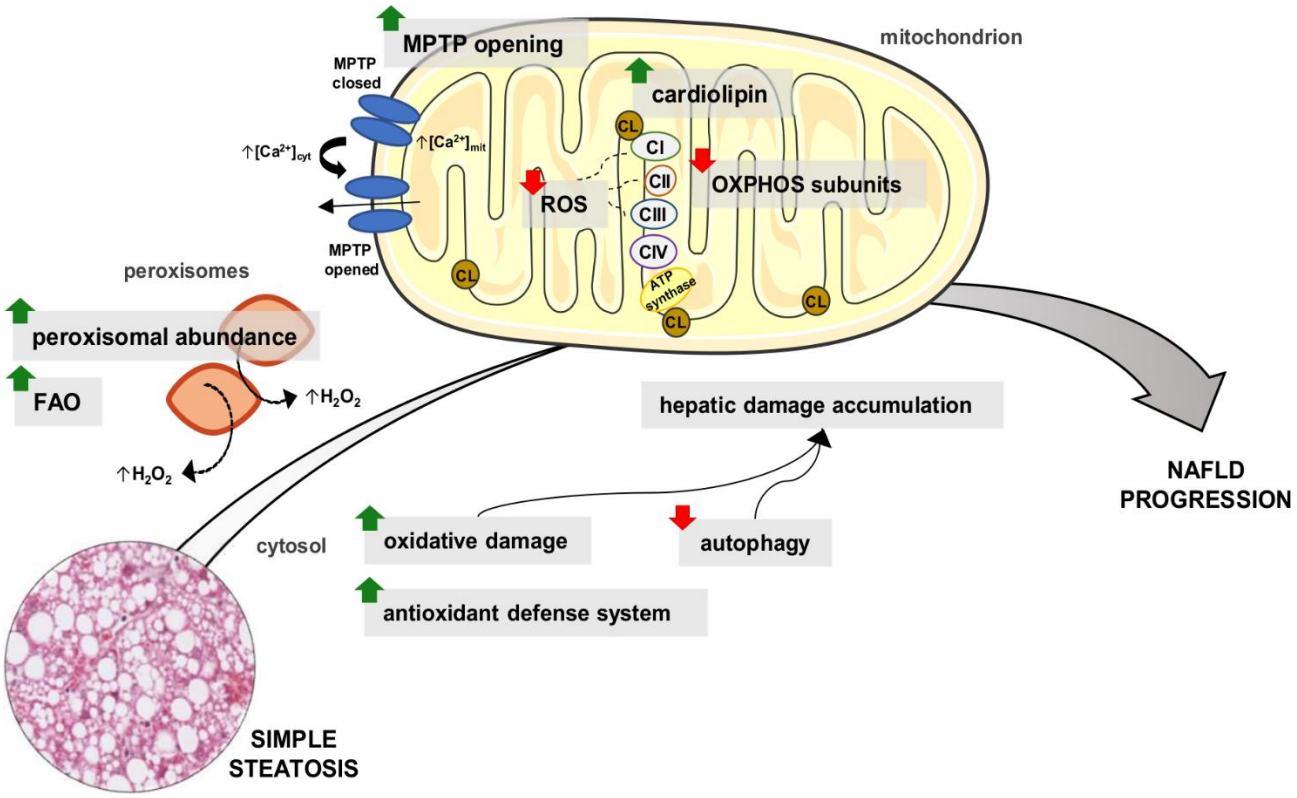

Figure 52. Schematic diagram summarizing the effect of WD in the development and progression of NAFL up to 24 weeks of feeding. CI, Complex I; CII, Complex II; CIII, Complex III; CIV, Complex IV; CL, cardiolipin; FAO, fatty acid oxidation; H_2O_2, hydrogen peroxide; mPTP, mitochondrial permeability transition pore; OXPHOS, oxidative phosphorylation; ROS, reactive oxygen species.

CHAPTER 3: ANTIOXCIN$_4$ - A NEW MITOCHONDRIALLY TARGETED ANTIOXIDANT THAT PREVENTS THE DEVELOPMENT OF NON-ALCOHOLIC FATTY LIVER PHENOTYPE.

6.1 Results

6.1.1 AntiOxCIN$_4$ reduces body weight gain and ameliorates hepatic-related parameters in NAFL-induced mice.

As I have already shown in the previous parts of my thesis (chapters 1 and 2), excess dietary intake of fat and sucrose in the form of a Western-like diet induced an increase (212%) of the body weight of mice after 16 weeks of feeding, in comparison with SD + vehicle group (138%) (**Figure 53A**). No significant alterations were induced by AntiOxCIN$_4$ supplementation in SD + AntiOxCIN$_4$ group. Despite of that, AntiOxCIN$_4$ supplementation induced a downward trend in the body weight gain of mice fed with WD, an effect statistically significant between WD + vehicle and WD + AntiOxCIN$_4$ groups from the 15th week of feeding (**Figure 53A**). Of note, such a decrease of body weight is not correlated with a decrease in food or water intake in the above-mentioned groups (**Figure 53B**). In fact, my data suggest that AntiOxCIN$_4$ supplementation may induce a higher food and water intake in both SD- and WD-fed groups (**Figure 53B**). Detailed data about body weight as well as the weight of all collected organs after mice euthanasia are provided in **Table 7**.

Focusing exclusively at the hepatic level, I observed that WD intake is associated with an increase of liver size and weight (164%), effects that were prevented when WD was supplemented with AntiOxCIN$_4$ (125%) (**Figure 54A, B**). Again, no significant differences were found between SD + vehicle versus SD + AntiOxCIN$_4$ groups (**Figure 54A, B**).

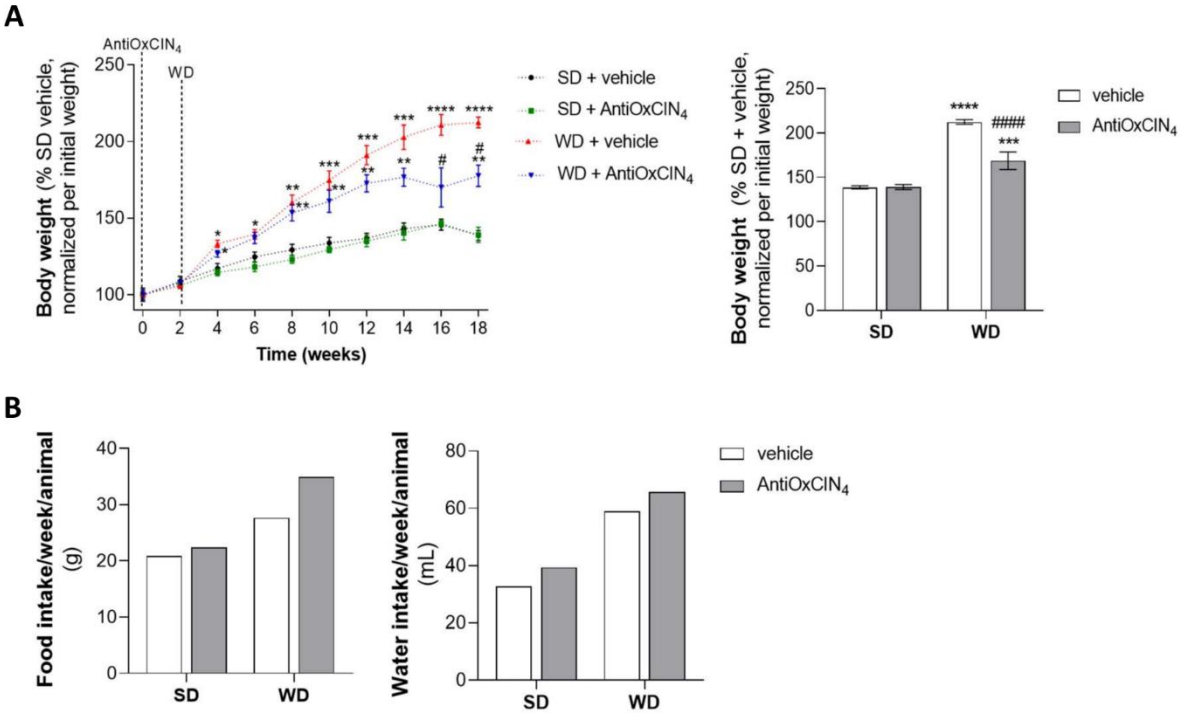

Figure 53. AntiOxCIN$_4$ induces a decrease on body weight of mice-induced NAFL phenotype. (A) Body weight progression along 18 weeks of AntiOxCIN$_4$ regimen or vehicle and 16 weeks of diet (SD or WD) (left). Body weight after mice euthanasia at the 18th week (right). **(B)** Average food intake and water consumption of mice. All data are expressed as the mean ± SEM. *P* values were determined using two-way ANOVA followed by Fisher's LSD test for multiple comparisons. (**P* < 0.05, ***P* < 0.01, ****P* < 0.0005, *****P* < 0.0001 vs. SD + vehicle); ($^{\#}$*P* < 0.05, $^{\#\#\#\#}$*P* < 0.0001 vs. WD + vehicle). SD, standard chow diet; WD, Western diet.

Table 7. Physiological parameters of mice fed with SD or with WD and additionally supplemented with AntiOxCIN4 or vehicle. SD, standard chow diet; WD, Western diet.

Parameter (Units, g)	SD + vehicle	SD + AntiOxCIN$_4$	WD + vehicle	WD + AntiOxCIN$_4$
Body weight initial	21.6 ± 0.9	24.0 ± 0.9	20.6 ± 0.5	22.6 ± 0.8
Body weight final	29.9 ± 1.8	33.4 ± 1.0	43.8 ± 1.4	38.2 ± 3.6
Liver	1.18 ± 0.11	1.25 ± 0.05	2.88 ± 0.03	1.90 ± 0.37
Adipose tissue				
Epididymal$^{\&}$	0.50 ± 0.13	0.94 ± 0.30	2.12 ± 0.24	2.00 ± 0.26
Mesenteric$^{\&}$	0.21 ± 0.06	0.36 ± 0.09	0.85 ± 0.08	0.63 ± 0.10
Kidneys	0.35 ± 0.04	0.35 ± 0.01	0.36 ± 0.00	0.34 ± 0.02
Heart	0.16 ± 0.02	0.16 ± 0.01	0.17 ± 0.00	0.16 ± 0.01
Brain	0.47 ± 0.01	0.47 ± 0.01	0.43 ± 0.01	0.45 ± 0.02

& - weight does not represent the total tissue from the animal.

Then, I evaluated several parameters in plasma collected from mice. The analysis of hepatic enzymes ALT and AST revealed hepatocyte damage with AST and ALT presenting 282% and 763% higher activities in WD + vehicle group than in SD + vehicle group (**Figure 54C**). Moreover, higher cholesterol levels (176%) were also found augmented in plasma of WD + vehicle mice (**Figure 54C**). While I did not observe significant alterations in those parameters between SD-fed groups, AntiOxCIN$_4$ supplementation improved plasmatic-related parameters in WD + vehicle-fed mice. Indeed, I observed a reduction in AST (193%), ALT (628%), and cholesterol (157%) levels in WD + AntiOxCIN$_4$ versus WD + vehicle group (**Figure 54C**).

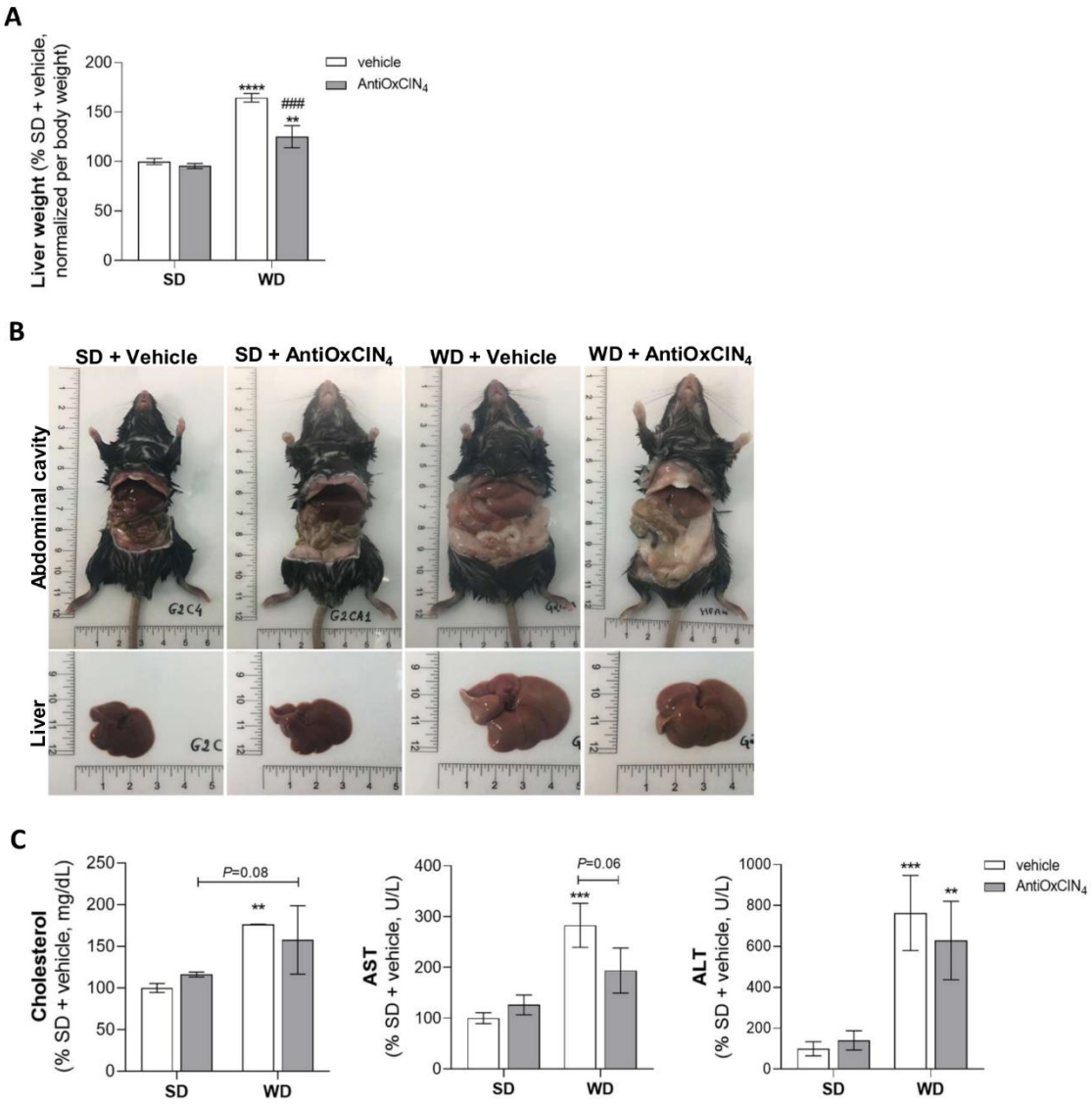

Figure 54. AntiOxCIN$_4$ decreases liver weight and hepatocyte damage of mice-induced NAFL phenotype. **(A)** Wet liver weight from euthanized animals after SD or WD feeding in the absence/presence of

AntiOxCIN$_4$. **(B)** Representative images of body (upper) and liver (lower) of euthanized mice. **(C)** Plasma cholesterol levels, and AST and ALT activity levels. All data are expressed as the mean ± SEM. *P* values were determined using two-way ANOVA followed by Fisher's LSD test for multiple comparisons. (**P < 0.01, ***P < 0.0005, ****P < 0.0001 vs. SD + vehicle); ($^{###}P$ < 0.0005 vs. WD + vehicle). ALT, alanine aminotransferase; AST, aspartate aminotransferase; SD, standard chow diet; WD, Western diet.

The H&E staining confirmed that WD-induced obesity and all the above alterations observed at hepatic level are correlated with steatosis development (**Figure 55A**). Moreover, analysis of Masson Trichrome staining and immunohistological staining of inflammatory markers confirmed the development of NAFL, generally named as simple steatosis (grade 3) with hepatocyte ballooning (grade 2) and absence of inflammation and fibrosis in WD + vehicle mice group (**Figure 55A, B** and **Table 8**).

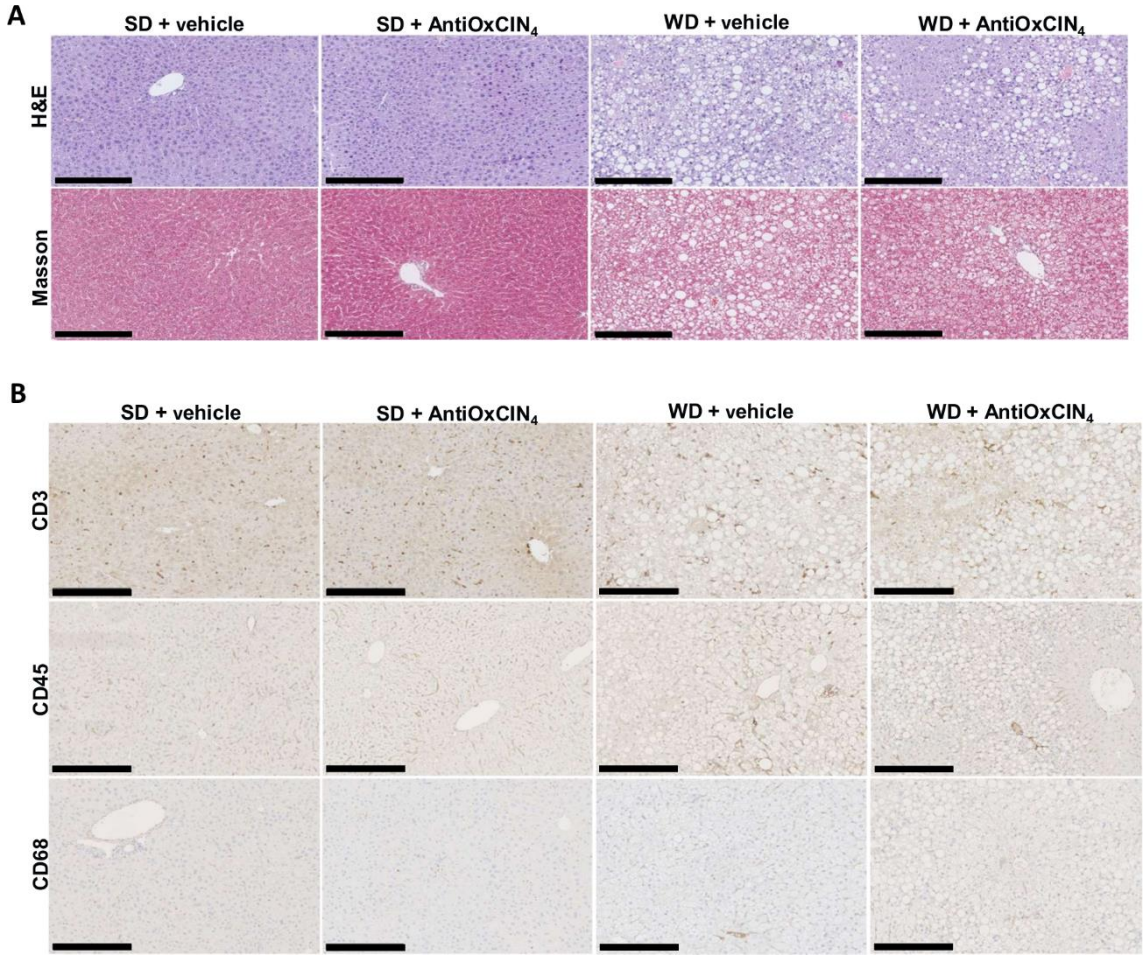

Figure 55. AntiOxCIN$_4$ decreases hepatic fat accumulation with no visible effects were detected in inflammatory associated markers. (A) Representative histological images of liver sections of SD- and WD-fed mice in the absence/presence of AntiOxCIN$_4$, stained with H&E and Masson's Trichrome stainings and

(B) Immunohistological stainings of CD3, CD45 and CD68 inflammatory markers. Scale bar: 250 µm with 10x magnification. H&E, Hematoxylin and eosin; SD, standard chow diet; WD, Western diet.

When this group of mice was supplemented with AntiOxCIN$_4$, I noticed a reduction of steatosis grade from 3 to 2, with no other alterations in WD + AntiOxCIN$_4$ group (**Table 8**). These results showed a beneficial effect of AntiOxCIN$_4$ at the body systemic level and at the hepatic level with a reduction of hepatic fat accumulation.

Table 8. AntiOxCIN$_4$ improves NAFLD activity score of WD-fed mice. NAFLD activity score (NAS) was calculated based of Hematoxylin & Eosin (H&E), Masson Trichrome and immunohistochemistry of CD3, CD45 and CD68 markers. Steatosis grade: 0 ≤ 5%; grade 1 = 5-33%; grade 2 = 34-66%; grade 3 ≥ 66%. Ballooning grade: 0 = absent; 1 = a few ballooned hepatocytes; 2 = many ballooned hepatocytes. Inflammation grade (magnification 200x): 0 = absent; 1 = up to two foci per field of view; 2 = two to four foci per field of view; 3 = more than four foci per field of view (lipogranulomas are counted in this category). Fibrosis grade: S0 = absent; S1a = zone 3, perisinusoidal fibrosis; S1b = zone 3, perisinusoidal fibrosis; S1c = only periportal/ portal fibrosis; S2 = zone 3, plus portal/ periportal fibrosis; S3 = zone 3, plus portal/ periportal fibrosis with bridging fibrosis; S4 = cirrhosis. [&]-NAS value is considered as the sum of the grades obtained from steatosis, ballooning, inflammation and fibrosis parameters. SD, standard chow diet; WD, Western diet.

NAFLD Activity Score (NAS)					NAS value[&]
Groups	**Steatosis**	**Ballooning**	**Inflammation**	**Fibrosis**	
SD + vehicle	Grade 0	Grade 0	Grade 0	Grade 0	0
SD + AntiOxCIN$_4$	Grade 0	Grade 0	Grade 1	Grade 0	1
WD + vehicle	Grade 3 mixed	Grade 2	Grade 0	Grade 0	5
WD + AntiOxCIN$_4$	Grade 2 mixed	Grade 2	Grade 0	Grade 0	4

6.1.2 AntiOxCIN$_4$ reduces hepatic lipid accumulation, with a remodelling in lipid droplets composition.

In line with the onset of a NAFL stage characterized by simple steatosis, the quantification of H&E staining revealed an accumulation of 2147% of hepatic fat accumulation in WD + vehicle group versus SD + vehicle group (**Figure 56A**). Next, a detailed analysis showed an increase in TGs (214%), DAGs (395%), CEs (411%) and

cholesterol (119%) levels inside lipid droplets of hepatocytes from WD-fed mice (**Figure 56B**).

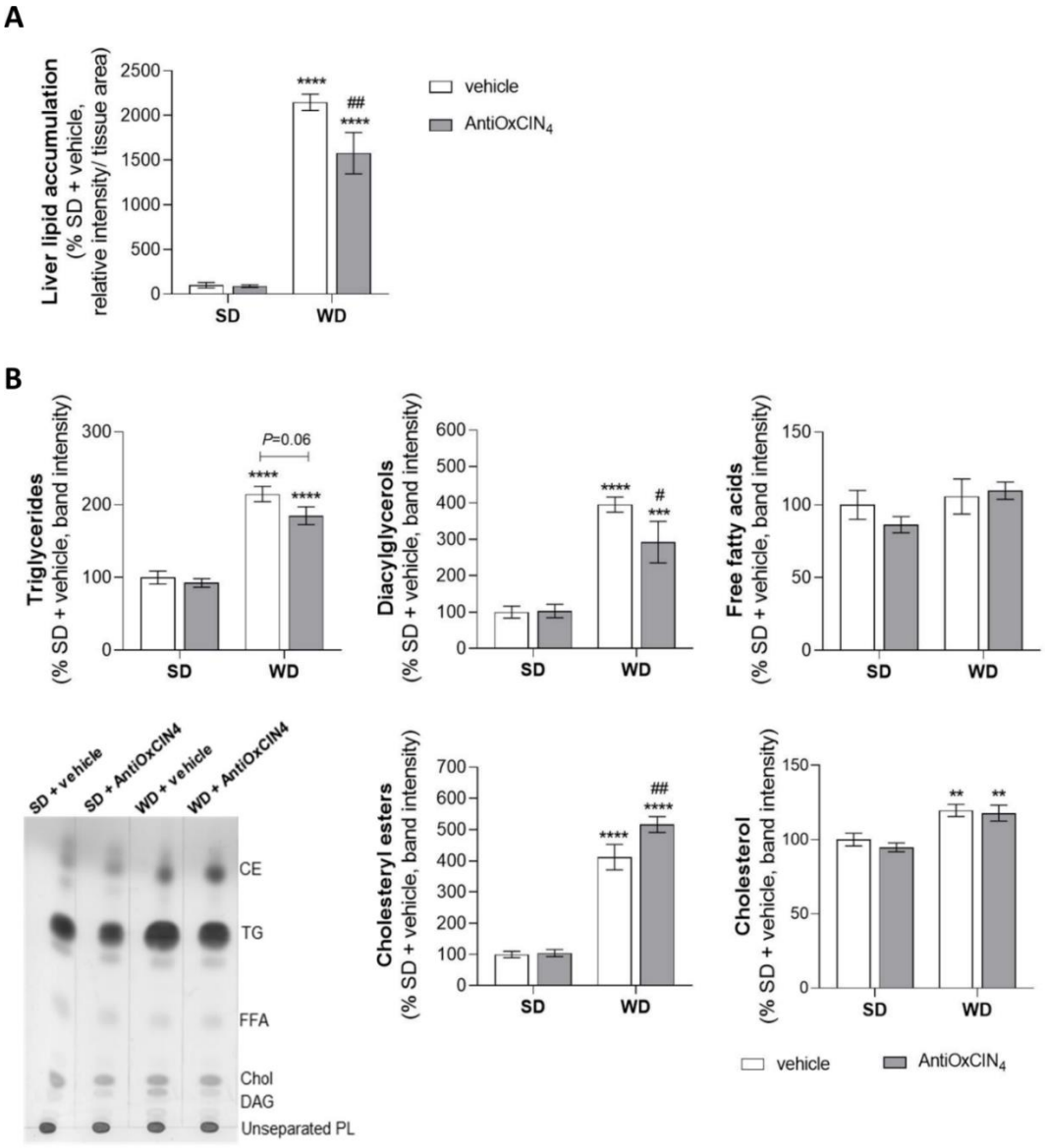

Figure 56. AntiOxCIN$_4$ decreases hepatic lipid accumulation, by decreasing TGs and DAGs levels. (A) Hepatic lipid accumulation in SD- and in WD-fed mice in the absence/presence of AntiOxCIN$_4$, obtained from three independent images/per animal of each experimental group of Hematoxylin and Eosin staining. **(B)** Triglycerides, diacylglycerols, free fatty acids, cholesteryl esters, and free cholesterol levels in livers, and a representative image of hepatic neutral lipid profile using thin-layer chromatography. All data are expressed as the mean ± SEM. *P* values were determined using two-way ANOVA followed by Fisher's LSD test for multiple comparisons. (***P* < 0.01, ****P* < 0.0005, *****P* < 0.0001 vs. SD + vehicle); ($^{\#}$*P* < 0.05, $^{\#\#}$*P* < 0.01 vs. WD + vehicle). CE, cholesteryl esters; Chol, free chloesterol; DAGs, diacylglycerols; FFA, free fatty acids; SD, standard chow diet; TGs, triglycerides; WD, Western diet.

Considering that TGs contitute the main fraction among neutral lipids species, I also analyzed its composition in terms of saturation/unsaturatin of FAs acyl chains. I observed that WD feeding induced a decrease of SFAs (23%) when compared with SD + vehicle group (50%) (**Figure 57A**).

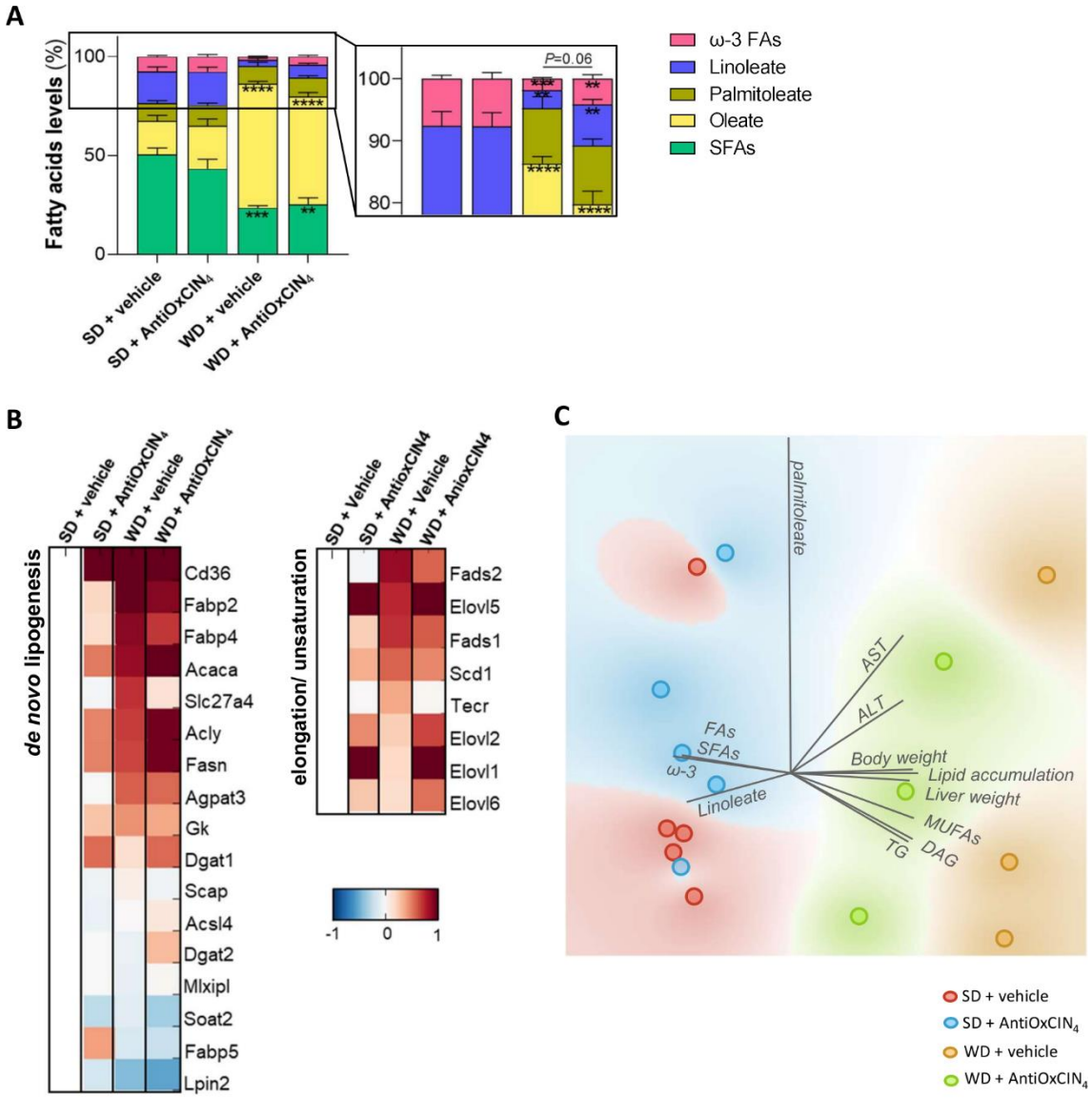

Figure 57. AntiOxCIN$_4$ improves fatty acyl chain composition of hepatic TGs and induces DNL/ elongation and unsaturation-related pathways. (A) Fatty acyl chain composition of hepatic TGs: saturated fatty acids, palmitoleate, oleate, linoleate and **ω**-3 fatty acids in total liver homogenates from SD- and WD-fed mice in the absence/presence of AntiOxCIN$_4$. **(B)** MS-proteomic analysis of hepatic DNL and fatty acids elongation/unsaturation-related proteins. The blue color represents a decrease, while the red color represents an increase of protein levels. **(C)** PCA of the following mice physiological parameters: body and liver weight, AST ALT, lipid quantification, TGs, DAGs, SFAs, oleate, palmitoleate, linoleate and **ω**-3 fatty acids. All data are expressed as the mean ± SEM. *P* values were determined using two-way

ANOVA followed by Fisher's LSD test for multiple comparisons. (**$P < 0.01$, ***$P < 0.0005$, ****$P < 0.0001$ vs. SD + vehicle). FAs, fatty acids; SD, standard chow diet; SFAs, saturated fatty acids; TGs, triglycerides; WD, Western diet.

Furthermore, this hypercaloric diet induced an accumulation of oleate (63%) while it was observed a reduction in the levels of linoleate (3%) and ω-3 FAs (2%) in comparison with respective counterparts oleate (17%), linoleate (15%) and ω-3 FAs (7%) in SD + vehicle group (**Figure 57A**). This hepatic fat accumulation profile is in accordance with an upregulation of protein expression levels involved in the DNL pathway and in elongation/unsaturation of FAs in WD-fed mice (**Figure 57B**).

I have previously reported that AntiOxCIN$_4$ supplementation decreased steatosis grade of NAS score in mice fed with WD for 16 weeks of feeding period (**Table 8**). Accordingly, I confirmed that AntiOxCIN$_4$ prevented hepatic lipid accumulation as observed in H&E relative intensity (1577%) compared with the WD + vehicle group (**Figure 56A**). Such decrease is correlated with a decrease in TGs (184%) and DAGs (292%) levels (**Figure 56B**). Somehow surprisingly, I have found higher CEs levels (516%) whereas no differences were observed in cholesterol levels in WD + AntiOxCIN$_4$ group versus WD + vehicle group (**Figure 56B**). Additionally, AntiOxCIN$_4$ remodelled the composition of FAs acyl chains in WD-fed mice to a more similar profile to the SD control group. While the levels of SFAs and palmitoleate were not significantly changed, there was a downward trend in oleate levels (54%) and an upward trend in linoleate (7%) and ω-3 FAs (4%) levels in WD + AntiOxCIN$_4$ group (**Figure 57A**). In parallel, such remodelling is correlated with an upregulation of protein expression levels of DNL pathway (e.g. CD36, ACACA, ACLY, FASN, DGAT1, FABP2, FABP4 and AGPAT3) and elongation/unsaturation-related pathways (e.g. ELOVL1, ELOVL5) (**Figure 57B**). Curiously, most of these proteins were also found increased in SD + AntiOxCIN$_4$ mice, but nevertheless, no alterations in hepatic lipid accumulation were reported in this mice group compared with SD-fed mice (**Figure 56A,B** and **57A,B**).

Then, I investigated whether the above-measured parameters allow to discriminate between the distinct experimental groups. PCA revealed that samples belonging to both SD-fed groups cluster together, which shows a lack of AntiOxCIN$_4$ effect in this diet regimen (**Figure 57C**). Notably, WD + vehicle group samples sit distant from SD-fed

groups, while samples belonging to WD + AntiOxCIN$_4$ sit between WD + vehicle group and SD-fed groups (**Figure 57C**). Altogether, these findings demonstrate that AntiOxCIN$_4$ supplementation prevents at a certain extent, the development of NAFL in mice.

6.1.3 AntiOxCIN$_4$ induces hepatic oxidative metabolism, with emphasis on mitochondrial and peroxisomal-FAO related pathways.

FAO is a main pathway involved in adapting hepatocytes to FAs overload during NAFL (Begriche, Massart et al. 2013). Therefore, I decided to check a possible involvement of this pathway in AntiOxCIN$_4$ effects in the experimental model, focusing on two main cellular pathways responsible for FAO: mitochondrial and peroxisomal-FAO. I observed that WD feeding induced an augment of mitochondrial- (ACOT12) and peroxisomal- (ACOT3, ABCD2, ABCD1, ACOT4, SLC27A4, and ACOX1I2) related protein expression levels (**Figure 58A**).

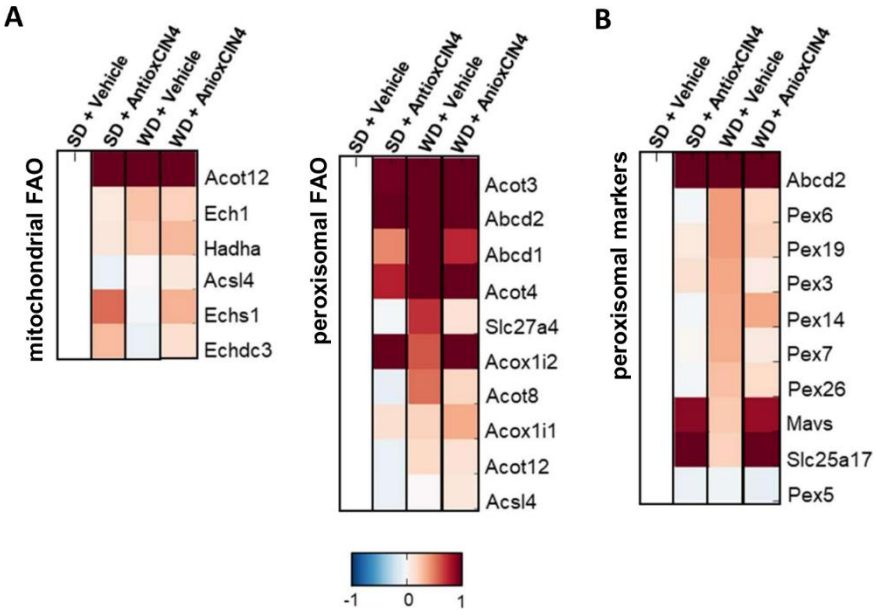

Figure 58. AntiOxCIN$_4$ induces hepatic oxidative metabolism – mitochondrial and peroxisomal FAO in SD- and in WD-fed mice. (A) MS-proteomic analysis of hepatic mitochondrial and peroxisomal FAO-related proteins in SD- and WD-fed mice in the absence/presence of AntiOxCIN$_4$. **(B)** MS-proteomic analysis of hepatic peroxisomal markers. The blue color represents a decrease, while the red color represents an increase of protein levels. FAO, fatty acid oxidation; SD, standard chow diet; WD, Western diet.

Interestingly, AntiOxCIN$_4$ supplementation *per se* already induced most of the above-described FAO-related proteins in SD-fed mice, with protein expression profile shown to be maintained or slightly exacerbated in WD-fed mice supplemented with AntiOxCIN$_4$ (**Figure 58A**). Moreover, I demonstrated that AntiOxCIN$_4$ supplementation favored peroxisomal-FAO and induced a higher protein expression level of peroxisomal proteins such as ABCD2, MAVS and SLC25A17 in SD- and in WD-fed mice (**Figure 58B**). These findings suggest a role of AntiOxCIN$_4$ in the induction of peroxisomal abundance and in the stimulation of peroxisomal-FAO that, together with mitochondrial-FAO may reduce hepatic lipid accumulation.

6.1.4 AntiOxCIN$_4$ ameliorates hepatic mitochondrial respiration and prevents mPTP opening of NAFL-induced mice.

In line with increased mitochondrial FAO in mice fed with AntiOxCIN$_4$, I next examined whether AntiOxCIN$_4$ can also impact other mitochondrial functional-related parameters. Therefore, I assessed oxygen consumption in isolated mitochondrial fractions. In the presence of pyruvate/malate, I observed an increase of OCR in ADP-stimulated respiration (State 3) and in FCCP-induced uncoupled respiration (State 3u) in WD-fed mice (**Figure 59A**). This latter increase in State 3u was prevented when WD-fed mice were supplemented with AntiOxCIN$_4$ (**Figure 59A**). AntiOxCIN$_4$ *per se* also induced a decrease in State 3u of SD-fed mice (**Figure 59A**). Then, I measured RCR, an indicative of OXPHOS-coupling efficiency. Interestingly, I found a decrease of RCR in WD + vehicle group while such decrease was prevented in the presence of AntiOxCIN$_4$ supplementation (**Figure 59B**). In addition, I also examined Complex II-driven respiration. Hence, in the presence of succinate, I observed an increase of OCR in State 3, in non-ADP stimulated respiration (State 4o) and in State 3u in WD + vehicle group (**Figure 59A**). With this substrate, AntiOxCIN$_4$ *per se* induced an increase in State 3u in SD + vehicle group while its supplementation induced a decrease in State 3 and State 3u in WD + vehicle group (**Figure 59A**). Despite of that, RCR was not affected either with WD feeding regimen or in the presence of AntiOxCIN$_4$ (**Figure 59A**).

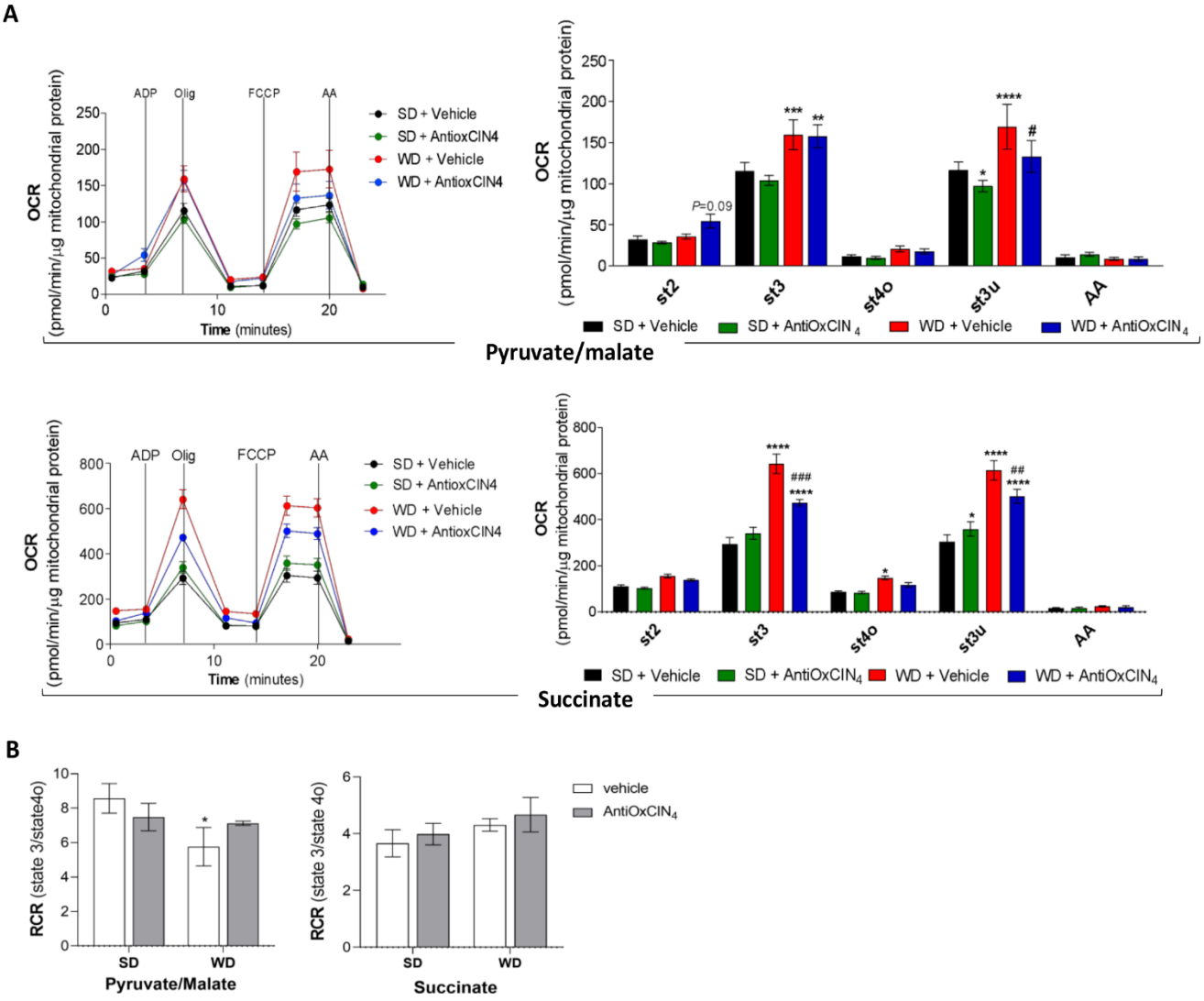

Figure 59. AntiOxCIN$_4$ improved hepatic mitochondrial respiration, being effects also observed in RCR of WD-fed mice. (A) OCR of Complex I-linked respiration (pyruvate/malate, 10 mM/5 mM) in isolated liver mitochondria of SD- and WD-fed mice in the absence/presence of AntiOxCIN$_4$ (upper). OCR of Complex II-linked respiration (succinate, 10 mM) in isolated liver mitochondria of SD- and WD-fed mice in the absence/presence of AntiOxCIN$_4$ (lower). **(B)** Respiratory control ratio (RCR) (state 3/state 4o) of pyruvate/malate (left) and succinate (right)-energized isolated liver mitochondria. All data are expressed as the mean ± SEM. *P* values were determined using two-way ANOVA followed by Fisher's LSD test for multiple comparisons. (*$P < 0.05$, **$P < 0.01$, ***$P < 0.0005$, ****$P < 0.0001$ vs. SD + vehicle); ($^{\#}P < 0.05$, $^{\#\#}P < 0.01$, $^{\#\#\#}P < 0.0005$ vs. WD + vehicle). AA, antimycin A; OCR, oxygen consumption rate; RCR, respiratory control ratio; SD, standard chow diet; WD, Western diet.

By evaluating electron flow assay, I observed an increase of OCR with the use of Complex I, Complex II and Complex III-linked substrates in both WD + vehicle and WD + AntiOxCIN$_4$ groups compared with SD-fed groups (**Figure 60A**). Notwithstanding, no

differences were found between WD-fed groups in the presence of AntiOxCIN$_4$ (**Figure 60A**). Next, we examined the susceptibility of mPTP opening in the presence of mPTP inducers such as Ca^{2+} and tBHP. In the previous parts of my thesis, I have already demonstrated that WD feeding induced an augmented susceptibility of mPTP opening. Here, I again confirmed those observations in WD + vehicle group at 16 weeks of feeding regimen, with an increase by 150% versus SD + vehicle group (**Figure 60B**). Importantly, AntiOxCIN$_4$ supplementation induce a downward trend (132%) of mPTP opening in WD-fed mice (**Figure 60B**).

Altogether, I have shown that AntiOxCIN$_4$ supplementation could ameliorate mitochondrial function on NAFL-induced mice.

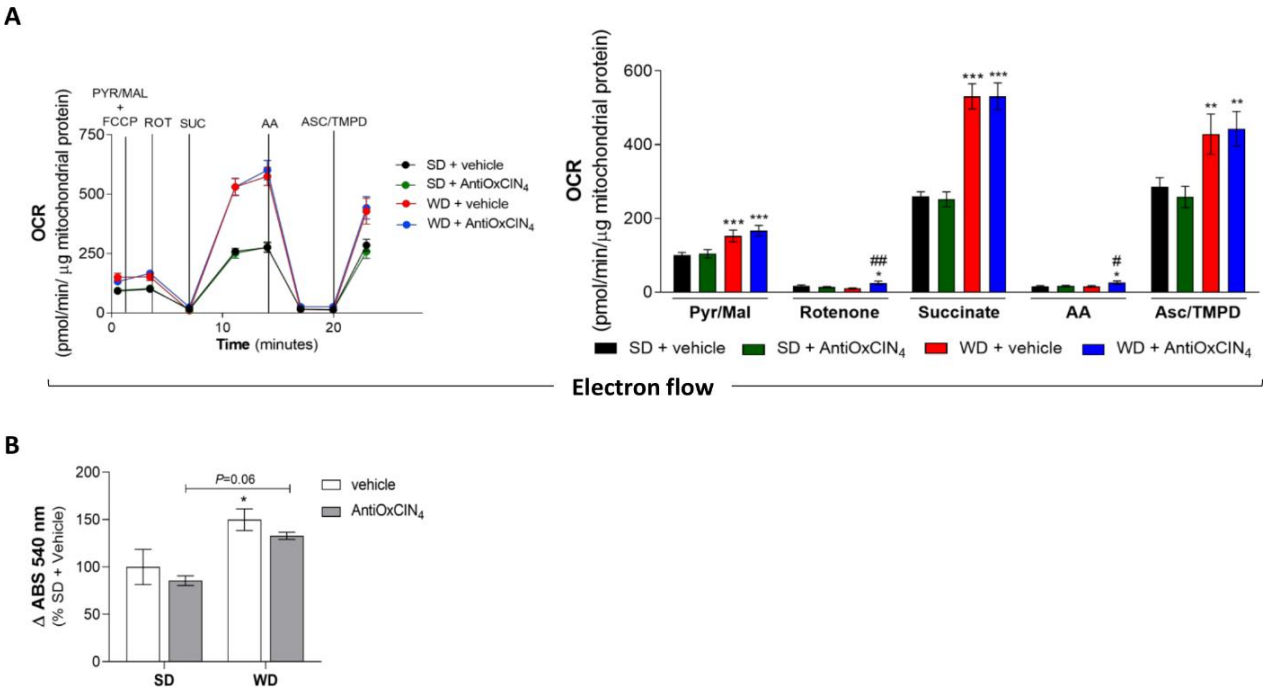

Figure 60. AntiOxCIN$_4$ decreases the susceptibility of mitochondrial permeability transition pore opening in WD-fed mice. (A) Mitochondrial electron flow-associated oxygen consumption rate measurement in isolated liver mitochondria, in the presence of pyruvate/malate (10 mM/5 mM) and supplemented with FCCP (2 µM), of WD-fed mice in the absence/presence of AntiOxCIN$_4$ with the following additions: rotenone (2 µM), succinate (10 mM), antimycin A (2 µM) and Asc/TMPD (10 mM/100 µM). **(B)** Mitochondrial permeability transition pore opening in succinate-energized isolated liver mitochondria of WD-fed mice in the absence/presence of AntiOxCIN$_4$. All data are expressed as the mean ± SEM. *P* values were determined using two-way ANOVA followed by Fisher's LSD test for multiple comparisons. (*$P < 0.05$, **$P < 0.01$, ***$P < 0.0005$ vs. SD + vehicle); ($^{\#}P < 0.05$, $^{\#\#}P < 0.01$ vs. WD + vehicle). AA, antimycin A; Asc, ascorbate; Mal, malate; OCR, oxygen consumption rate; Pyr, pyruvate; RCR,

respiratory control ratio; SD, standard chow diet; TMPD, N,N,N',N'-tetramethyl-p-phenylenediamine; WD, Western diet.

6.1.5 AntiOxCIN$_4$ induces mitochondrial phospholipid remodelling, with increased protein levels of mitochondrial biogenesis modulators PGC-1α and SIRT3, and OXPHOS complexes subunits.

Considering that mitochondrial membrane composition directly modulates the structure and function of mitochondria (van der Veen, Kennelly et al. 2017), I next investigated the phospholipid composition of isolated liver mitochondria in NAFL-induced mice without or with AntiOxCIN$_4$ supplementation. WD feeding induced diminished levels of sphingomyelin (62%) and PE (77%) while PC/PE ratio was found augmented (126%) in comparison with SD + vehicle group (**Figure 61A**). Then, when these WD-fed mice were supplemented with AntiOxCIN$_4$, I have shown a decrease in cardiolipin (85%) in comparison with WD + vehicle group, and a downward trend in PC levels (84%) in comparison with SD + AntiOxCIN$_4$ (**Figure 61A**). Of note, WD + AntiOxCIN$_4$-treated mice maintained of PC/PE ratio at similar levels of SD-fed groups (**Figure 61A**). AntiOxCIN$_4$ supplementation *per se* did not induce any alterations in SD + vehicle group (**Figure 61A**). These findings suggest that AntiOxCIN$_4$ supplementation may prevent mitochondrial membrane phospholipid composition alterations induced by WD feeding, which can be involved in the distinct mitochondrial bioenergetic response described in the above section.

In order to better understand the effect of AntiOxCIN$_4$ in isolated liver mitochondria, I measured protein levels of two main regulators of mitochondrial biogenesis and respiration: PGC-1α and SIRT3 (Kong, Wang et al. 2010). Both protein levels were found to increase slightly by 173% and 500%, respectively in the WD + vehicle group (**Figure 61B**). Then, AntiOxCIN$_4$ supplementation increases PGC-1α protein levels by 53%, and SIRT3 protein levels by 603% in this mice group (**Figure 61B**). Additionally, I have also found that AntiOxCIN$_4$ *per se* induced an upward trend of PGC-1α (122%) (**Figure 61B**).

There is an evidence that AntiOxCIN$_4$ supplementation by inducing PGC-1α and SIRT3 protein expression, favors higher protein expression levels of OXPHOS complexes

subunits. I have observed augmented levels most of the Complex I-related subunits, namely MTND5, NDUFA3, NDUFV2, NDUFB4, NDUFS8, NDUFS3 in both AntiOxCIN$_4$ supplemented SD- and WD-fed groups (**Figure 61C**). Despite that, MS-proteomic analysis also revealed that AntiOxCIN$_4$ reduced ATP synthase subunits - ATP5L and MTATP8 protein levels (**Figure 61C**) again in both mice groups. No other major alterations were observed in the remaining OXPHOS complexes subunits analyzed. Nevertheless, MS-proteomic levels of all OXPHOS complexes subunits are provided in **Figure 62A-E.**

Overall, our observations demonstrate that AntiOxCIN$_4$ supplementation modulates mitochondrial transcriptional regulators, contributing to mitochondrial membrane and OXPHOS complexes remodelling in SD- and WD-fed mice.

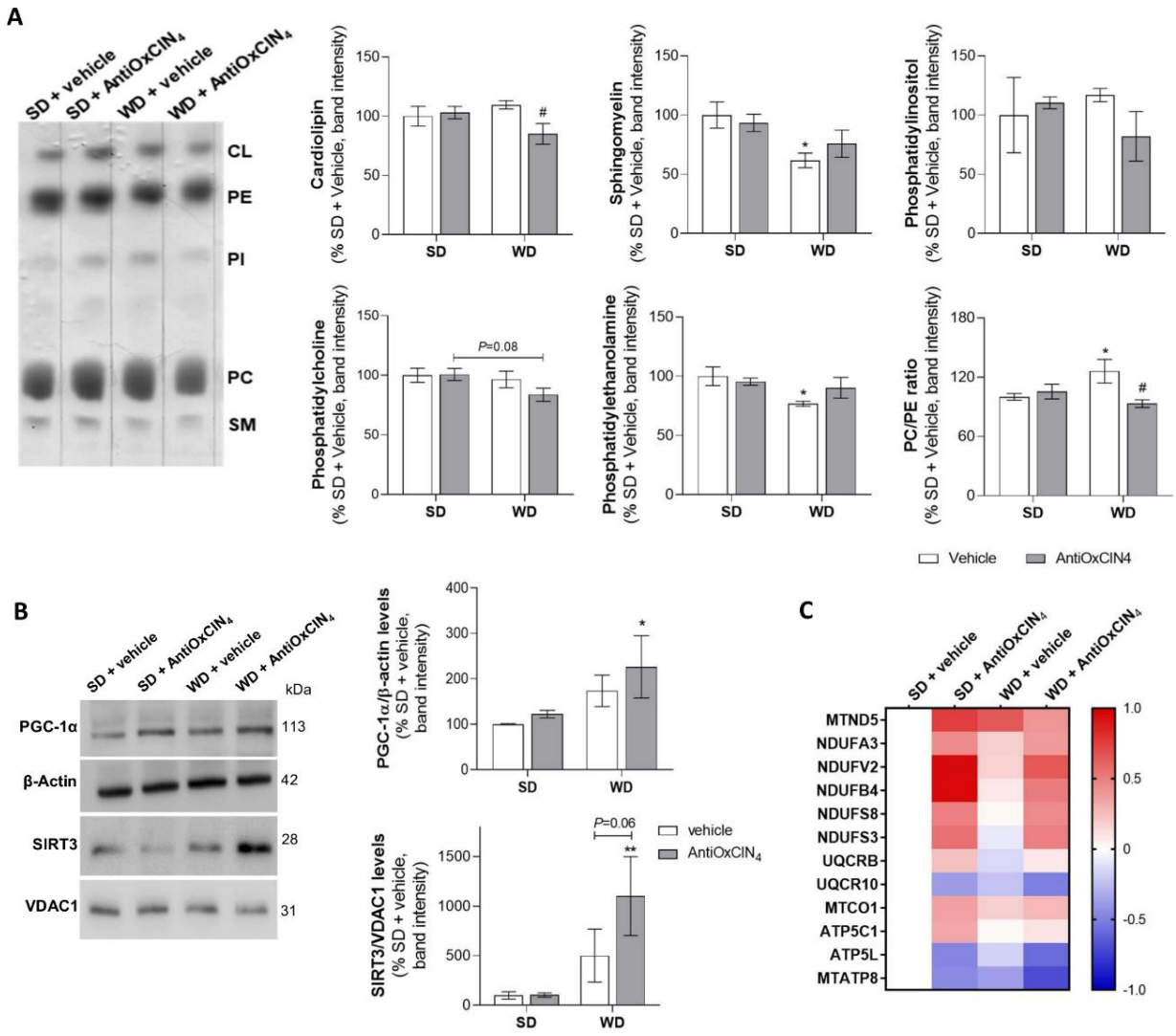

Figure 61. AntiOxCIN$_4$ decreases the susceptibility of mitochondrial permeability transition pore opening in WD-fed mice. (A) Representative thin-layer chromatography image of hepatic mitochondrial phospholipids in SD- and WD-fed mice in the absence/presence of AntiOxCIN$_4$, and mitochondrial membrane phospholipids levels: cardiolipin (CL), sphingomyelin (SM), phosphatidylinositol (PI), phosphatidylcholine (PC), phosphatidylethanolamine (PE) and PC/PE ratio. **(B)** Representative Western blot image of whole-liver homogenate showing PGC-1α and SIRT3 protein levels in the cytosol (normalized to β-actin) and isolated mitochondria (normalized to VDAC1), respectively; and protein quantification levels. **(C)** MS-proteomic analysis of the most altered mitochondrial OXPHOS complexes subunits protein levels in total liver homogenates (total subunits are shown in Figure 62). The blue color represents a decrease, while the red color represents an increase of protein levels. All data are expressed as the mean ± SEM. *P* values were determined using two-way ANOVA followed by Fisher's LSD test for multiple comparisons. (*P < 0.05, **P < 0.01 vs. SD + vehicle); ($^{\#}P$ < 0.05 vs. WD + vehicle). PGC1-α, peroxisome proliferator-activated receptor-γ coactivator-1α; SD, standard chow diet; SIRT3, sirtuin 3; VDAC1, voltage-dependent anion channel 1; WD, Western diet.

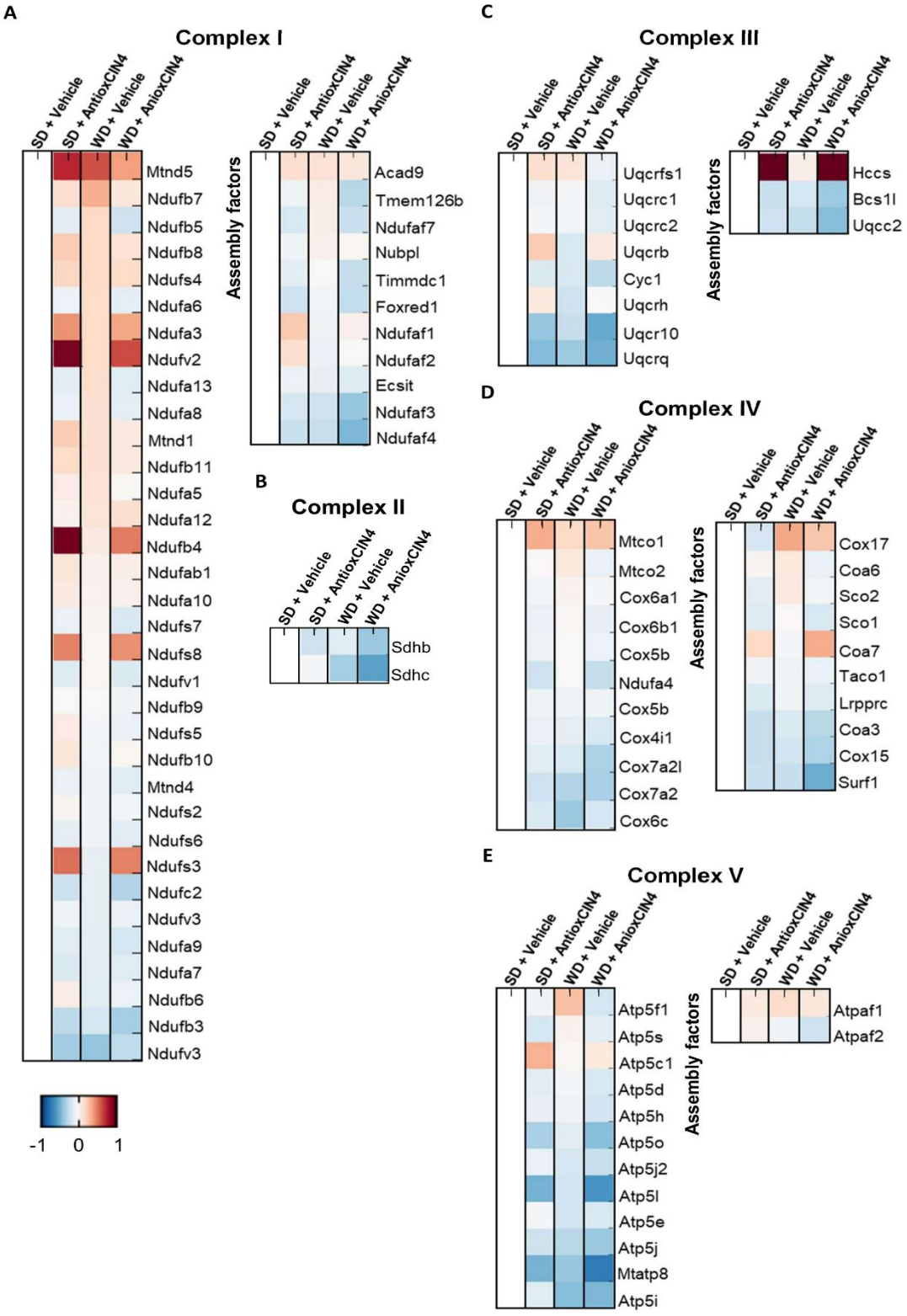

Figure 62. AntiOxCIN$_4$ induces mitochondrial OXPHOS complexes subunits remodelling in SD- and WD-fed mice. Complete MS-proteomic analysis of mitochondrial OXPHOS complexes subunits protein levels in total liver homogenates of SD- and WD-fed mice in the absence/presence of AntiOxCIN$_4$. The blue color represents a decrease, while the red color represents an increase of protein levels. SD, standard chow diet; WD, Western diet.

6.1.6 AntiOxCIN$_4$ stimulates antioxidant defense system in both SD- and WD-fed mice groups.

Because oxidative stress is a crucial player in the pathophysiology of NAFLD, I investigated the effects of AntiOxCIN$_4$ on this parameter in WD-fed mice. Initially, I measured the effects of this antioxidant on H_2O_2 generation using isolated liver mitochondria. As shown in the previous parts of my thesis, any alterations in H_2O_2 generation were observed in SD- and in WD-fed mice, and similar findings were also observed when both dietary regimens were supplemented with AntiOxCIN$_4$ (**Figure 63A**). The purity of mitochondrial fractions was confirmed by assessing mitochondrial and cytosolic specific protein markers as VDAC1 and GAPDH or β-actin, respectively (**Figure 63B**). Although no alterations were observed in ROS formation, AntiOxCIN$_4$ has been described as cellular redox modulator (Benfeito, Oliveira et al. 2019, Deus, Pereira et al. 2021). Therefore, I further investigated mitochondrial and cytosolic antioxidant defense system. First, I assessed aconitase activity, a mitochondrial enzyme, known to be compromised in an oxidative stress condition.

Interestingly, I have found that AntiOxCIN$_4$ protects aconitase activity, by inducing the lowest percentage (28%) of its inhibition in SD + AntiOxCIN$_4$ mice group (**Figure 63C**). Nevertheless, no significant alterations in aconitase activity were found in WD + AntiOxCIN$_4$ mice group (**Figure 63C**). Interestingly, these findings are in agreement with the obtained mitochondrial antioxidant defense enzymes data. An increase in mitochondrial SOD (299%) and catalase (159%) activities were observed in SD + AntiOxCIN$_4$ group (**Figure 63D**). While no alterations were observed in WD-fed mice, an upward trend of mitochondrial SOD activity was also visible in WD + AntiOxCIN$_4$ group (**Figure 63D**).

Next, I evaluated antioxidant defense system in total liver homogenate. I did not find alterations in antioxidant defense enzymes activities in mice fed a WD regimen for 16 weeks (**Figure 64A**). Importantly, I showed an augmented TAA (124%), GR activity (142%) as well as GSH levels (121%) when this group of mice was supplemented with AntiOxCIN$_4$ (**Figure 64A**). In contrast to “mitochondrial observations”, AntiOxCIN$_4$ *per se* did not induce changes in cellular antioxidant defense enzymes (**Figure 64A**).

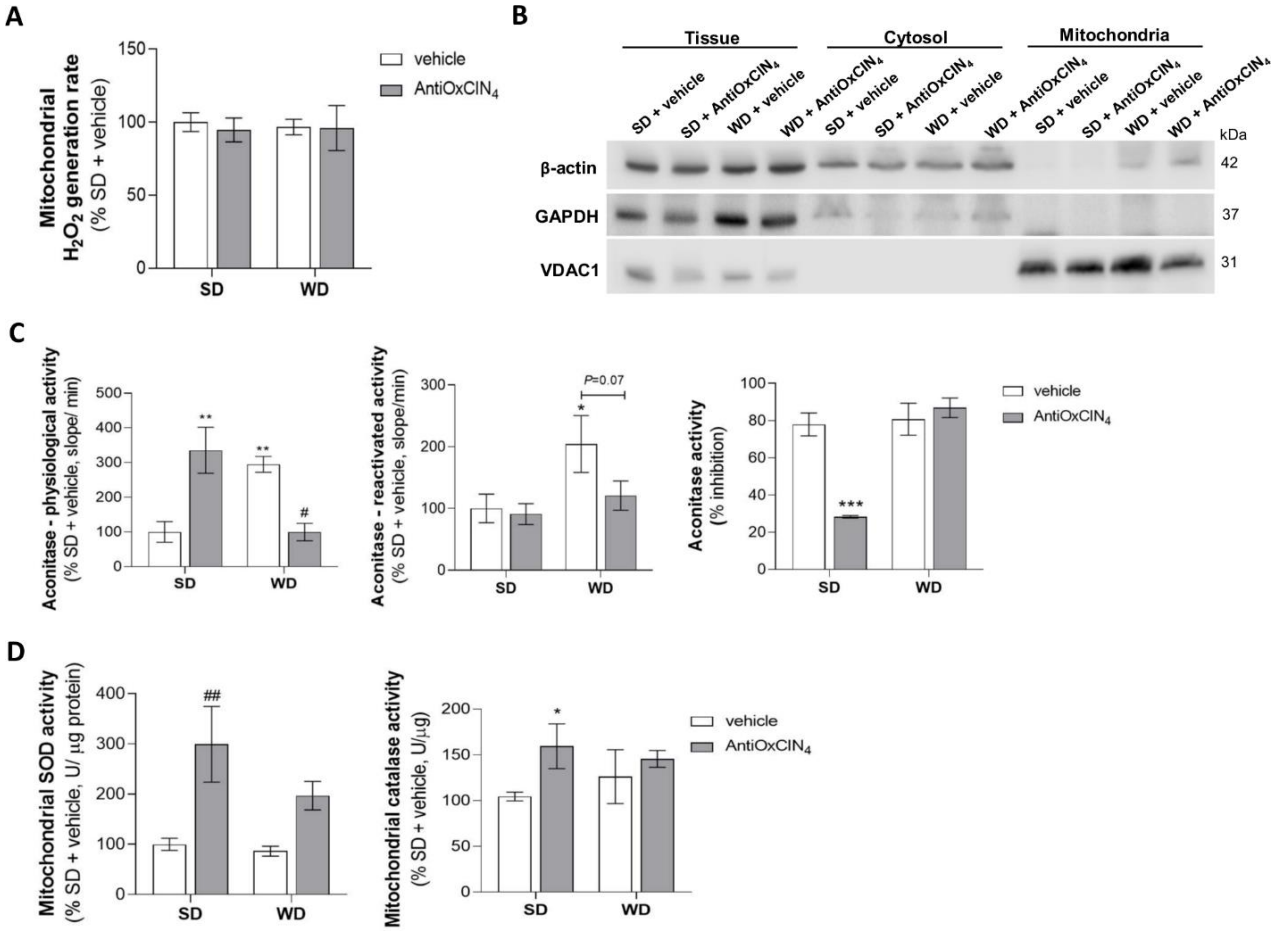

Figure 63. AntiOxCIN$_4$ protects aconitase activity and increases antioxidant defense enzymes activities in isolated liver mitochondria of SD-fed mice. (A) Hepatic mitochondrial H_2O_2 production rate in SD- and WD-fed mice in the absence/presence of AntiOxCIN$_4$. **(B)** Representative Western blot image showing the purity of total liver homogenate, cytosolic and mitochondrial fractions using β-actin, GAPDH and VDAC1 levels. **(C)** Aconitase physiological activity and reactivated activity and the respective aconitase activity expressed as % of inhibition in isolated liver mitochondria. **(D)** Superoxide dismutase (SOD) and catalase activities measured in isolated liver mitochondria. All data are expressed as the mean ± SEM. *P* values were determined using two-way ANOVA followed by Fisher's LSD test for multiple comparisons. (*P < 0.05, **P < 0.01, ***P < 0.0005 vs. SD + vehicle); ($^{\#}P$ < 0.05, $^{\#\#}P$ < 0.01 vs. WD + vehicle). H_2O_2, hydrogen peroxide; GAPDH, glyceraldehyde-3-phosphate dehydrogenase; SD, standard chow diet; VDAC1, voltage-dependent anion channel 1; WD, Western diet.

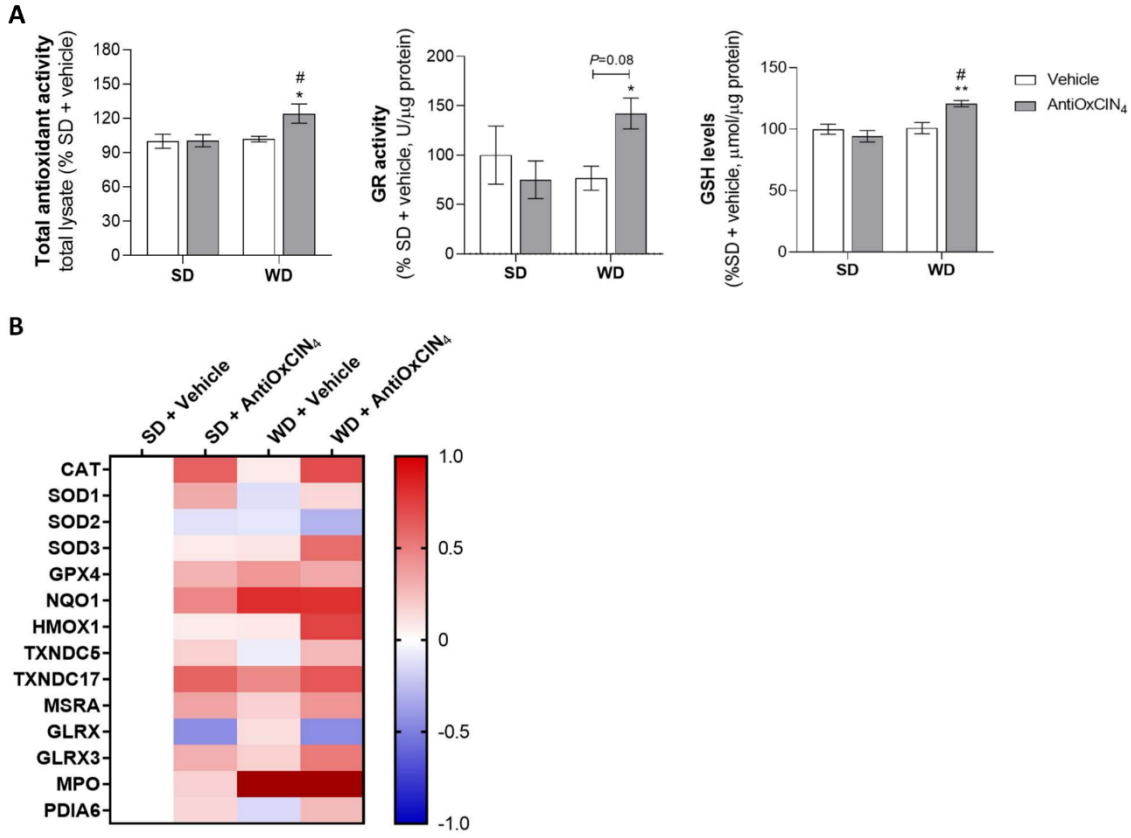

Figure 64. AntiOxCIN$_4$ increases hepatic antioxidant defense response in SD- and WD-fed mice. (A) Total antioxidant activity, glutathione reductase (GR) activity, and glutathione (GSH) levels in whole liver homogenate from SD- and WD-fed mice in the absence/presence of AntiOxCIN$_4$. **(B)** MS-proteomic analysis of total hepatic antioxidant defense enzymes levels of SD- and WD-fed mice in the absence/presence of AntiOxCIN4. The blue color represents a decrease, while the red color represents an increase of protein levels. All data are expressed as the mean ± SEM. *P* values were determined using two-way ANOVA followed by Fisher's LSD test for multiple comparisons. (*$P < 0.05$, **$P < 0.01$ vs. SD + vehicle); ($^{\#}P < 0.05$ vs. WD + vehicle). SD, standard chow diet; WD, Western diet.

In order to support my findings, MS-proteomic analysis has been performed. I presented diminished SOD1 and SOD2 and augmented GPX4, NQO1, TXNDC17 and MPO protein levels in WD + vehicle group (**Figure 64B**). Then, AntiOxCIN$_4$ supplementation caused higher CAT, SOD3, GPX4, NQO1, HMOX1, TXNDC17, MSRA, GLRX3 and MPO protein expression levels in this latter group (**Figure 64B**). Moreover, AntiOxCIN$_4$ *per se* showed to increase CAT, SOD1, GPX4, NQO1, HMOX1, TXNDC17, MSRA, GLRX3 and to decrease SOD2 and GLRX protein levels in SD-fed mice (**Figure 64B**). Overall, I demonstrated that AntiOxCIN$_4$ supplementation upregulates hepatic antioxidant defense system in both SD- and WD-fed mice.

6.1.7 AntiOxCIN$_4$ do not affect AKT/mTOR pathway but prevent autophagic flux impairment in WD-fed mice group.

In the next step of my study, I assessed the major cellular energy sensors – AMPK and mTOR which are involved in cellular adaptation to stress and responsible for the regulation of autophagy (Hardie 2011, Mihaylova and Shaw 2011). WD feeding induced higher ^{Ser473}p-AKT (248%) and an upward trend in the ^{Ser2448}p-mTOR (143%) (**Figure 65A, B**). Moreover, a reduction in the ^{Thr172}p-AMPKα (51%) supported the activation of PI3K-AKT-mTOR signaling pathway (**Figure 65A, B**). Subsequently, this activation induced the downstream pathway responsible for the regulation of protein synthesis as shown by higher protein expression levels of ^{Thr389}p-p70 ribosomal protein S6 kinase β1 (S6K1) (262%) and ^{Thr45}p- eukaryotic translation initiation factor 4E-binding protein 1 (4E-BP1) (392%) (**Figure 65A, B**). Likewise, the supplementation of AntiOxCIN$_4$ in WD-fed mice resulted in higher ^{Ser473}p-AKT (320%) and ^{Ser2448}p-mTOR (192%), lower ^{Thr172}p-AMPKα (33%) and higher ^{Thr389}p-p70 S6K1 (300%) and ^{Thr45}p-4E-BP1 (601%) (**Figure 65A, B**). AntiOxCIN$_4$ *per se* demonstrated to do not cause significant alterations in PI3K-AKT-mTOR pathway as well as in the downstream pathway (**Figure 65A, B**). Based on these findings, I demonstrated that in a FAs overload context, there is a decrease of AMPKα activation and an increase of mTOR activation. In addition to protein synthesis, autophagy is another pathway under the regulation of AKT/mTOR axis. In fact, a decreased autophagic flux has been previously reported in my NAFL mice model and in later disease stages (Razmara, Sunday et al. 2008). Next, I decided to explore a possible AntiOxCIN$_4$ effect in the modulation of autophagic flux. I found that WD feeding for 16 weeks favors an increase of LC3-II/LC3-I ratio (225%) while significantly increase SQSTM1 (267%) and decrease beclin-1 (54%) protein levels (**Figure 66A, B**). These findings indicate an impairment of the autophagic flux with autophagosome accumulation. Notably, AntiOxCIN$_4$ supplementation in WD-fed mice showed to prevent such impairment as revealed by an increase of LC3-II/LC3-I ratio (280%) and specially by the maintenance of SQSTM1 (112%) and beclin-1 (92%) at similar levels that respective SD-fed groups (**Figure 66A, B**).

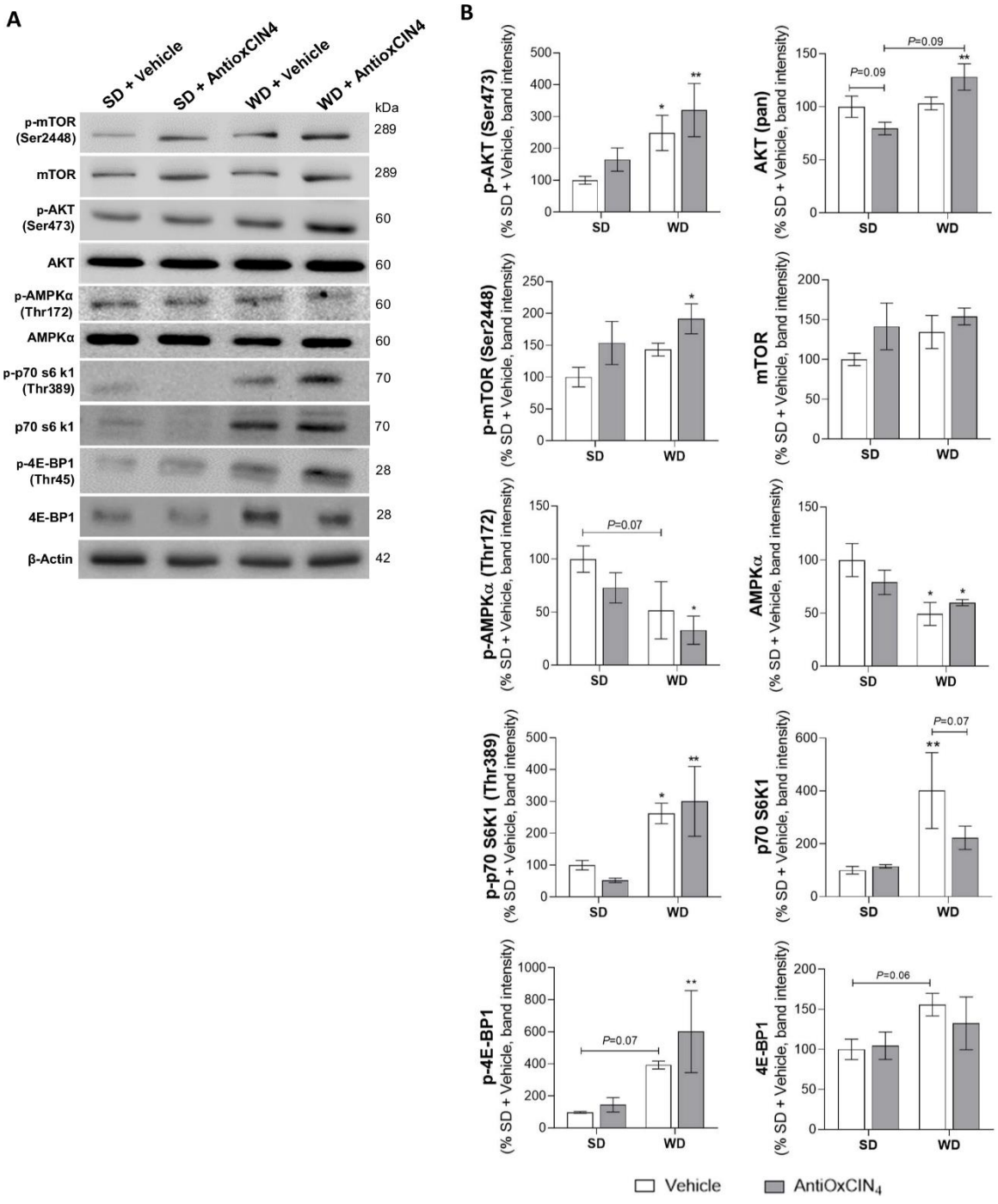

Figure 65. AntiOxCIN$_4$ activates AKT/mTOR axis pathway in SD- and WD-fed mice. (A) Representative Western blot images showing p-AKT (Ser473), AKT, p-mTOR C(Ser2448), mTOR, p-AMPKα (Thr172), AMPKα, p-p70 S6K1 (Thr389), p70 S6K1, p-4E-BP1 (Thr46), 4E-BP1 normalized to β-actin (cytosolic marker) on livers of SD- and WD-fed mice in the absence/presence of AntiOxCIN$_4$. **(B)** Hepatic protein quantification levels of p-AKT (Ser473), AKT, p-mTOR (Ser2448), mTOR, p-AMPKα (Thr172), AMPKα, p-p70 S6K1 (Thr389), p70 S6K1, p-4E-BP1 (Thr46) and 4E-BP1. All data are expressed as the mean ± SEM. *P* values were determined using two-way ANOVA followed by Fisher's LSD test for multiple comparisons. (**P* < 0.05, ***P* < 0.01 vs. SD + vehicle). 4E-BP1, eukaryotic translation initiation factor 4E-binding protein 1;

AKT, protein kinase B; AMPK, adenosine monophosphate-activated protein kinase; mTOR, mammalian target of rapamycin; S6K1, ribosomal protein S6 kinase β1; SD, standard chow diet; WD, Western diet.

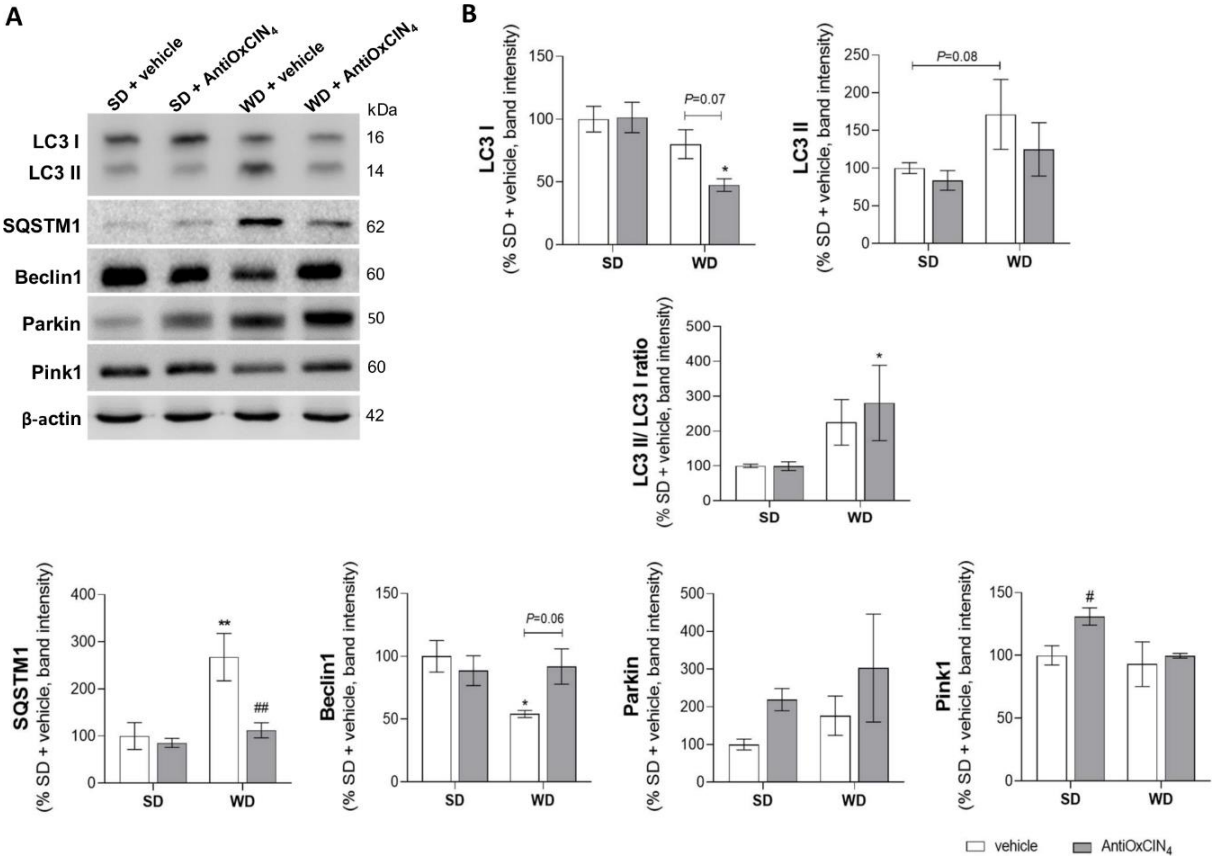

Figure 66. AntiOxCIN$_4$ ameliorates autophagic flux-related markers in WD-fed mice while increases mitophagy-related markers in SD-fed mice. (A) Representative Western blot images showing hepatic LC3-I, LC3-II, SQSTM1, Beclin1, Parkin, Pink1 normalized to β-actin (cytosolic marker) of SD- and WD-fed mice in the absence/presence of AntiOxCIN$_4$. **(B)** Hepatic protein quantification levels of LC3-I, LC3-II, LC3-I/ LC3-II ratio, SQSTM1, Beclin1, Parkin and Pink1. All data are expressed as the mean ± SEM. *P* values were determined using two-way ANOVA followed by Fisher's LSD test for multiple comparisons. (**P* < 0.05, ***P* < 0.01 vs. SD + vehicle); ($^{\#}$*P* < 0.05, $^{\#\#}$*P* < 0.01 vs. WD + vehicle). LC3, microtubule-associated protein 1A/1B-light chain 3; SD, standard chow diet; WD, Western diet.

Additionally, I have also investigated protein levels involved in mitophagy - a selective type of autophagy responsible for the elimination of damaged/dysfunctional mitochondria (Amorim, Simoes et al. 2021). The data obtained in mice fed with WD showed an upward trend of Parkin (176%) protein levels and no major alterations in Pink1 protein levels (**Figure 66A, B**). AntiOxCIN$_4$ supplementation induced an upward trend in Parkin (302%) protein levels (**Figure 66A, B**). Despite of that, AntiOxCIN$_4$

supplementation induced an upward trend in Parkin (219%) and a significant augment in Pink1 (130%) protein levels in SD-fed mice (**Figure 66A, B**).

WD feeding was shown to be associated with a blockage of the autophagic flux and a decrease of lysosome-associated membrane glycoprotein 2 (LAMP2), a specific lysosomal protein marker, and a reduced activity of cathepsin B (78%), a lysosomal enzyme (**Figure 67A, B**).

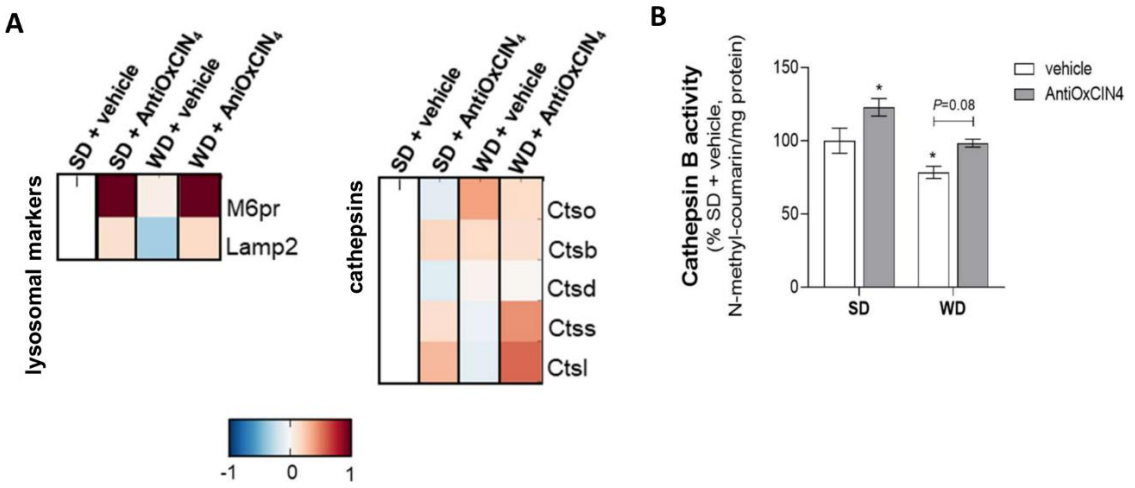

Figure 67. AntiOxCIN$_4$ increases lysosomal-related markers and lysosomal proteolytic activity in SD- and WD-fed mice. (A) MS-proteomic analysis of lysosomal-related markers and cathepsins levels on livers of SD- and WD-fed mice in the absence/presence of AntiOxCIN$_4$. The blue color represents a decrease, while the red color represents an increase of protein levels. **(B)** Cathepsin B activity in the whole liver homogenate. All data are expressed as the mean ± SEM. *P* values were determined using two-way ANOVA followed by Fisher's LSD test for multiple comparisons. (*P < 0.05 vs. SD + vehicle). SD, standard chow diet; WD, Western diet.

Interestingly, AntiOxCIN$_4$ supplementation prevented decreased LAMP2 protein levels and in addition, it also exacerbated cation-dependent mannose-6-phosphate receptor (M6PR) protein levels in both SD- and WD-fed mice (**Figure 67A**). According to literature, M6PR is a protein responsible for the binding and transport of hydrolases essential to lysosomal acidic activity from Golgi into lysosomes (Gary-Bobo, Nirde et al. 2007). Therefore, my results shows that AntiOxCIN$_4$ could induce higher lysosomal abundance and activity. Accordingly, this is supported by higher cathepsin CTSS and CTSL protein levels and an upward trend in cathepsin B activity (98%) in WD + AntiOxCIN$_4$ group (**Figure 67B**). AntiOxCIN$_4$ *per se* could also favor increased cathepsin B activity levels

(122%) in SD-fed mice (**Figure 67B**). These findings demonstrated that AntiOxCIN$_4$ can prevent the autophagic impairment with an increase of lysosomal activity.

6.2 Discussion of the data presented in Chapter 3

In the last section of my thesis, I reported for the first time an *in vivo* therapeutic effect of AntiOxCIN$_4$ compound in the prevention of NAFL development. Using a WD-induced mice model, I showed that 18 weeks AntiOxCIN$_4$ supplementation was able to reduce body weight gain while ameliorating several hepatic-related parameters, namely liver weight, hepatic lipid accumulation and hepatic damage. Importantly, these notable effects were explained by the stimulation of hepatic oxidative metabolism, specially focused on mitochondrial- and peroxisomal-FAO. Moreover, AntiOxCIN$_4$ augmented antioxidant defense system and prevented autophagic flux blockage, probably by increasing lysosomal proteolytic activity in WD-fed mice.

NAFLD is a multifactorial disease, being the mechanisms underlying its development and progression into more severe stages quite complex and still, not completely clarified. In this context, patient heterogeneity makes the diagnosis difficult, while pharmacological therapies are still needed considering that current therapies are based on lifestyle changes. This scenario urged the search for new potential treatments based on drug development. Mitochondria, considered as key organelles in hepatocyte metabolism, have been described to be particularly affected in animal-induced NAFLD models (Patterson, Kalavalapalli et al. 2016) as well as in NAFLD clinical cohorts (Koliaki, Szendroedi et al. 2015). Thus, structural and molecular mitochondrial alterations contribute to the mitochondrial impairment described in NAFLD (Rector, Thyfault et al. 2010). Importantly, oxidative stress has been pointed as the major contributor in the progression of the disease. Therefore, in this part of my thesis, I hypothesized that the supplementation with this mitochondrially-targeted antioxidant based on dietary caffeic acid – AntiOxCIN$_4$ would ameliorate NAFL-induced mice.

Previously, mitochondrially-targeted antioxidant compounds showed to improve mitochondrial function, induce antioxidant defense system and quality control mechanisms, namely, autophagy and mitophagy. Indeed, AntiOxCIN$_4$, by activating NRF2/KEAP1 pathway, up-regulated cellular antioxidant-defense pathways (Teixeira,

Basit et al. 2021)(Amorim et al. – paper under review), thereby protecting against oxidative stress-associated damage in different cellular disease models (Teixeira, Cagide et al. 2017, Benfeito, Oliveira et al. 2019)(Amorim et al. – paper under review). AntiOxCIN$_4$ also improved numerous mitochondrial-functional parameters in primary human sporadic fibroblasts from Parkinson disease patients (Deus, Pereira et al. 2021, Teixeira, Basit et al. 2021).

In my study, a WD composed by 30% of fat and 30% of sucrose was used to mimic the eating habits of Western society (Simoes, Karkucinska-Wieckowska et al. 2020, Simoes, Amorim et al. 2021). According to my previous studies, WD feeding provoked obesity-induced C57BL/6J mice characterized by augmented body weight gain, visceral adiposity and hepatic steatosis accompanied by increased ALT and AST circulating levels. Despite the evidence of hepatocyte damage, no significant histological alterations were visible regarding hepatic inflammatory markers and hepatic fibrosis. These findings confirmed the onset of a NAFL stage. Then, I demonstrated that 18 weeks of AntiOxCIN$_4$ supplementation on NAFL mice caused a decrease of body weight. Previously, the administration of another mitochondrially-targeted antioxidant known as MitoQ showed to improve several hepatic-related parameters, namely a decrease in hepatic fat content and hepatic damage in a metabolic syndrome mice model (Mercer, Yu et al. 2012). Similarly, AntiOxCIN$_4$ supplementation induced a reduction of liver weight and subsequent hepatic lipid accumulation, with hepatic damage found also reduced in WD-fed mice. These findings were correlated with lower TGs and DAGs levels. Interestingly, such AntiOxCIN$_4$ effect appears to be not associated with hepatic FFAs influx or DNL, it was observed higher protein expression of elongases ELOVL1 and ELOVL5. In line with my findings, higher ELOVL5 activity was previously shown to decrease TGs levels by stimulating TGs catabolism and protecting against ER stress in an obese mice model, being TGs catabolism stimulated in an independent-FAO related manner (Tripathy, Lytle et al. 2014). Nevertheless, increased amounts of MUFAs/PUFAs also play a hepatoprotective role against FFAs overload in WD-induced NAFL (Pardo, Gonzalez-Rodriguez et al. 2015).

It has been clearly showed that NAFLD development is correlated with a dysregulation between FAs synthesis and its respective storage and FAs oxidation. Of note, Naguib and co-workers have demonstrated that a reduced mitochondrial-FAO is

associated with a worse prognosis of NAFLD phenotype (Naguib, Morris et al. 2020). Notwithstanding, my study showed that WD-fed mice had increased protein expression of mitochondrial- and peroxisomal-FAO markers. Despite this hepatic adaptative response to WD feeding, I reported that accumulated TGs are enriched with oleate levels but have lower linoleate and ω-3 FAs content. In the presence of AntiOxCIN$_4$, the above WD-induced alterations were partially prevented as demonstrated by higher levels of linoleate and ω-3 FAs. Interestingly, it has been shown that ω-3 PUFA supplementation could decrease blood TGs levels (Parker, Johnson et al. 2012), activate PPARs which have a pivotal role in the upregulation of FAO (Lu, Li et al. 2016), and stimulate autophagic flux (Chen, Xu et al. 2015). Accordingly, my data demonstrated that AntiOxCIN$_4$ greatly increase FAO as indicated by higher levels of proteins involved in mitochondrial- and peroxisomal-FAO in SD-fed mice supplemented with the antioxidant. This event is clearly determinant for the reduction of hepatic fat accumulation, thereby preventing lipotoxicity-associated events.

In addition to a de-regulation of lipid homeostasis, other events such as oxidative stress and impairment of autophagic flux have been pointed to be critical in the development and progression of NAFLD. Regarding oxidative stress, it was shown that while mitochondrial- and peroxisomal-related pathways may contribute to ROS production, there is also a de-regulation of antioxidant defense system, which may contribute to an altered cellular redox state (Begriche, Massart et al. 2013). In this regard, it has been suggested that mitochondria are not the primary source of ROS in hepatocytes under FFAs overload (Einer, Hohenester et al. 2018, Simoes, Karkucinska-Wieckowska et al. 2020, Simoes, Amorim et al. 2021). Accordingly, I demonstrated the absence of ROS production and signs of oxidative stress in isolated liver mitochondria of WD-fed mice along 16 weeks. Thus, evidence of higher peroxisomal-linked activity strength the hypothesis that at this NAFL stage, other organelles such as peroxisomes may contribute to ROS production and subsequently to oxidative stress. Remarkably, I observed mitochondrial remodelling with higher OCR values but with a decrease of RCR, an increase of PC/PE ratio in mitochondrial membrane composition and a higher susceptibility to mPTP opening in WD-fed mice. Importantly, AntiOxCIN$_4$ supplementation was able to prevent the above-described alterations in PC/PE ratio, RCR and it also slightly protected mPTP opening in the presence of mPTP inducers.

AntiOxCIN$_4$ also induced higher protein expression of OXPHOS complexes subunits, particularly at Complex I level. These processes seem to be regulated by PGC-1α-SIRT3-pathway. Sirtuins are energetic cellular sensors specially activated in pathological situations. In the case of SIRT3, it is known that it controls mitochondrial protein acetylation, thereby acting as a guard of mitochondrial biogenesis, redox state and lipid metabolism in a NAFLD context (Kong, Wang et al. 2010, Li, Xin et al. 2018). Li and colleagues have reported that SIRT3 overexpression could protect liver from deleterious effects of chronic high-fat diet (HFD), by blocking cell programmed death and inducing BNIP3-mediated mitophagy (Li, Xin et al. 2018). Opposingly, SIRT3 deficiency was shown to increase acetylation of gluconeogenic- and mitochondrial-proteins with subsequent aggravation of steatosis in HFD-fed mice (Kendrick, Choudhury et al. 2011, Barroso, Rodriguez-Rodriguez et al. 2020). Hence, PGC-1α may stimulate SIRT3 with subsequent mitochondrial ROS generation, mitochondrial biogenesis and an increased redox power (Barroso, Rodriguez-Rodriguez et al. 2020). My results align with this evidence by showing that AntiOxCIN$_4$ stimulated antioxidant defense system, particularly total antioxidant activity, GR activity and GSH levels and at mitochondrial level – mitochondrial SOD activity. Altogether, it is suggested that AntiOxCIN$_4$ supplementation improves mitochondrial function in NAFL, even when there is an absence of oxidative stress-associated injury. By stimulating mitochondrial biogenesis, mitochondrial respiration and mitochondrial antioxidant defense enzymes, AntiOxCIN$_4$ demonstrates its capacity to empower hepatic mitochondria, making them more resistant to WD-induced damage in a NAFLD context.

As shown in the previous parts of my thesis, WD feeding and subsequent onset of NAFLD are associated with the de-regulation of autophagic-associated markers. AKT/mTOR axis is the pathway responsible for the regulation of this cellular quality control mechanism. In this regard, AKT and further mTORC1 activation leads to S6K1 phosphorylation which is responsible for protein translation and cell growth mediated by 4E-BP1 (Dowling, Topisirovic et al. 2010). Here, I have shown the activation of AKT/mTOR/S6K1/4E-BP1 pathway in a NAFL stage. Moreover, this pathway is also involved in the regulation of autophagy. By removing dysfunctional/damaged proteins and/-or organelles and degrading lipid droplets through lipophagy, autophagy can be determinant to the hepatic adaptation in NAFL. However, several authors have reported

impaired autophagic response in NAFLD, as well as in conditions that favors disease development (Fukuo, Yamashina et al. 2014, Gonzalez-Rodriguez, Mayoral et al. 2014). Previously, I have reported a de-regulation of the autophagic flux in WD-fed mice for 16 weeks feeding period (Simoes, Karkucinska-Wieckowska et al. 2020). Here, again I confirmed a blockage of the autophagic flux in NAFL as shown by higher protein levels of SQSTM1 and LC3-II/LC3-I ratio and lower protein levels of Beclin-1. Notably, AntiOxCIN$_4$ supplementation prevent autophagic impairment in NAFL mice as shown by SQSTM1, LC3-II/LC3-I ratio and Beclin-1 protein levels similar to SD-fed mice. Taking into consideration that higher SQSTM1 levels are linked to higher NAFLD severity (Wang, Zhang et al. 2018), I suggested that AntiOxCIN$_4$ supplementation by maintaining/increasing autophagic response can protect hepatocytes from FFA-induced deleterious effects. Moreover, I have also shown that this mitochondrially-targeted compound is able to increase lysosomal number and proteolytic activity in livers of WD-fed mice. This is according to higher protein expression of lysosomal markers, including cathepsins and the receptor responsible for the transport of hydrolases into the lysosome. Since defective lysosomal acidification has been pointed as a possible cause of autophagic blockage (Inami, Yamashina et al. 2011), it is proposed that AntiOxCIN$_4$ can prevent autophagic impairment by improving not only lysosomal abundance but also its proteolytic activity. My results align with the previous works in which the use of AntiOxCIN$_4$ proved to increase lysosomal number in PHSF from Parkinson disease patients (Deus, Pereira et al. 2021) and in HepG2 cells (Amorim et al- - unpublished data).

Another selective form of autophagy implicated in NAFLD pathophysiology is mitophagy (Li, Toan et al. 2020). As in autophagy, I have not clearly analyzed mitophagic flux. Although, the analysis of protein expression showed an augment of PINK1-PARKIN levels in SD-fed mice supplemented with AntiOxCIN$_4$ compound. These findings are in agreement with the co-localization of mitochondria with lysosomes when HepG2 cells were treated with AntiOxCIN$_4$ (Amorim et al. – unpublished data). Overall, these observations give support to a role of AntiOxCIN$_4$ in the regulation of cellular quality control processes, thereby allowing the removal of damaged organelles and fat-enriched lipid droplets during the development of NAFL.

In conclusion, my study demonstrated for the first time an *in vivo* beneficial effect of AntiOxCIN$_4$ in the prevention of NAFL development. These effects are summarized in the **Figure 68**. Importantly, I have shown the mechanisms underlying AntiOxCIN$_4$ supplementation in WD-fed mice for 16 week feeding period. Using this model, I presented a decrease of body weight and an improvement of plasmatic parameters, namely hepatic damage markers. Then, I observed a reduction of hepatic fat accumulation (TGs and DAGs levels) with a remodelling of fatty acyl chain composition. This was correlated with an augment of cellular FAO-related pathways. In addition, AntiOxCIN$_4$ appears to improve mitochondrial function, including higher OXPHOS complexes subunits and a remodelling of mitochondrial phospholipids with the prevention of mPTP opening. Moreover, the amelioration of hepatic phenotype included the stimulation of endogenous antioxidant defense enzymes and the re-storage of autophagic flux by the stimulation of lysosomal proteolytic activity.

The findings presented in my thesis by showing the improvement of whole-body and hepatic-parameters, demonstrate an unequivocal potential use of AntiOxCIN$_4$ not only in the prevention but also in the possible treatment of NAFLD.

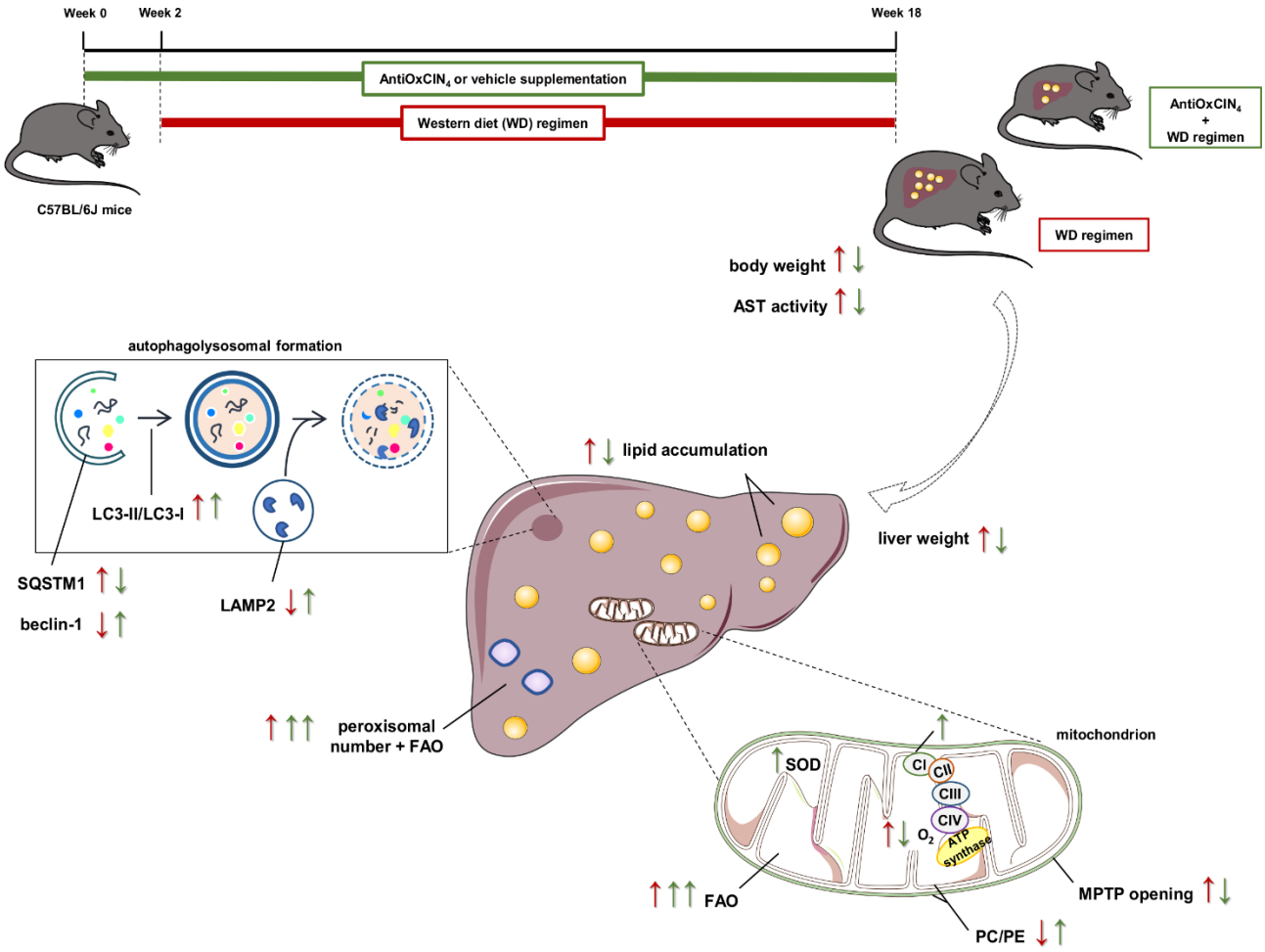

Figure 68. Schematic diagram summarizing the effect of AntiOxCIN4 supplementation in WD-fed mice in NAFL stage. AST, aspartate aminotransferase; CI, complex I ; CII, complex II; CIII, complex III; CIV, complex IV; FAO, fatty acid oxidation; LAMP2, lysosome-associated membrane glycoprotein 2; LC3, microtubule-associated protein 1A/1B-light chain 3; mPTP, mitochondrial permeability transition pore; PC, phosphatidylcholine; PE, phosphatidylethanolamine; SOD, superoxide dismutase; SQSM1, sequestosome-1; WD, Western diet.

Part V: Summary and Final conclusions

NAFLD is a major leading cause of chronic liver disease, being NASH currently considered as an indicator for liver transplantation only behind alcohol-related diseases in USA (Cholankeril and Ahmed 2018). Due to its rising prevalence in parallel with metabolic syndrome-associated diseases, there is an urge for a better understanding of pathophysiological mechanisms underlying the development and the progression of NAFLD. Notwithstanding, NAFLD is a relatively complex and multifactorial disease. Because of that, there is a lack of approved and effective therapeutic strategies with current strategies based mostly in lifestyle changes.

With this in mind, in my thesis, I aimed to study NAFLD pathogenesis, particularly focusing on the early mechanisms which I believe may lead to hepatic alterations that represent a point of no return and subsequently cause disease progression into NASH. Moreover, I also aimed to find a promising therapeutic strategy based on a mitochondrially-targeted compound derived from the dietary caffeic acid.

Firstly, I validated a NAFL C57BL/6J mice model. This part of the work described in the chapter 1 is the first comprehensive analysis showing the effects of fat, sucrose and its combination representing Western diet habits (WD) in hepatocytes, with a particular focus on mitochondrial function during the development of fatty liver. I provided evidence that no excess of mitochondrial ROS is generated in NAFL. Indeed, I have suggested that other cytosolic organelles e.g. peroxisomes rather mitochondria contribute to hepatic oxidative stress largely described in a NAFLD context. Moreover, I established that WD components differentially impair autophagic flux. These events may be determinant to instigate further and more severe NAFLD stages.

Secondly, using the same NAFL mice model fed with WD, I have studied the progression of the disease from an early stage into a more progressive stage (up to 24 weeks of feeding). In chapter 2, I demonstrated for the first time the sequential events of mitochondrial alterations during NAFL development and progression. Thus, I showed that a mitochondrial adaptation in a NAFL stage was followed by a progressive decrease of mitochondrial respiration concomitant with a higher susceptibility to mPTP opening in a more progressive NAFLD stage. Importantly, it was proven that mitochondrial ROS are not the first hit causing disease progression. Instead, my findings continue to support

the role of peroxisomes as possible contributors to the hepatic oxidative damage in the origin of hepatic injury and progression.

Thirdly, I tested the potential therapeutic effect of AntiOxCIN$_4$ supplementation in my pre-established NAFL C57BL/6J mice model. Previously, AntiOxCIN$_4$ has shown to prevent against lipotoxicity events and contributing to cellular redox status and quality control mechanisms. Chapter 3 showed that AntiOxCIN$_4$ supplementation improved the development of a NAFL phenotype, thereby inducing a healthier phenotype of hepatocytes. These effects are explained by the stimulation of hepatic oxidative metabolism, the stimulation of the endogenous antioxidant defense system and the prevention of autophagic flux blockage. These findings support the supplementation of AntiOxCIN$_4$ as a new promising NAFLD therapeutics.

Overall, these findings reported along my thesis provide new knowledge about hepatic cellular pathways taken place in NAFL stage. Importantly, I have clarified the role of mitochondria and mitochondrial ROS generation in this early NAFLD stage. Moreover, I opened new lines of research based on the evidence that peroxisomes are possible key players in NAFLD pathogenesis. This knowledge might be critical to a better understanding of the disease, allowing the design of new potential treatments based on drug development. Additionally, I have also validated for the first time a new promising mitochondria-targeted compound with antioxidant properties – AntiOxCIN$_4$ in the prevention of NAFL development.

Part VI: Bibliography

1. Abdelmegeed, M. A., A. Banerjee, S. H. Yoo, S. Jang, F. J. Gonzalez and B. J. Song (2012). "Critical role of cytochrome P450 2E1 (CYP2E1) in the development of high fat-induced non-alcoholic steatohepatitis." J Hepatol **57**(4): 860-866.
2. Acin-Perez, R. and J. A. Enriquez (2014). "The function of the respiratory supercomplexes: the plasticity model." Biochim Biophys Acta **1837**(4): 444-450.
3. Adams, L. A., Q. M. Anstee, H. Tilg and G. Targher (2017). "Non-alcoholic fatty liver disease and its relationship with cardiovascular disease and other extrahepatic diseases." Gut **66**(6): 1138-1153.
4. Adiels, M., M. R. Taskinen, C. Packard, M. J. Caslake, A. Soro-Paavonen, J. Westerbacka, S. Vehkavaara, A. Hakkinen, S. O. Olofsson, H. Yki-Jarvinen and J. Boren (2006). "Overproduction of large VLDL particles is driven by increased liver fat content in man." Diabetologia **49**(4): 755-765.
5. Adler, P., J. Reimand, J. Janes, R. Kolde, H. Peterson and J. Vilo (2008). "KEGGanim: pathway animations for high-throughput data." Bioinformatics **24**(4): 588-590.
6. Aharoni-Simon, M., M. Hann-Obercyger, S. Pen, Z. Madar and O. Tirosh (2011). "Fatty liver is associated with impaired activity of PPARgamma-coactivator 1alpha (PGC1alpha) and mitochondrial biogenesis in mice." Lab Invest **91**(7): 1018-1028.
7. Ahsan, H. (2013). "3-Nitrotyrosine: A biomarker of nitrogen free radical species modified proteins in systemic autoimmunogenic conditions." Hum Immunol **74**(10): 1392-1399.
8. Ahuja, M. and S. Muallem (2014). "The gatekeepers of mitochondrial calcium influx: MICU1 and MICU2." EMBO Rep **15**(3): 205-206.
9. Alavian, K. N., G. Beutner, E. Lazrove, S. Sacchetti, H. A. Park, P. Licznerski, H. Li, P. Nabili, K. Hockensmith, M. Graham, G. A. Porter, Jr. and E. A. Jonas (2014). "An uncoupling channel within the c-subunit ring of the F1FO ATP synthase is the mitochondrial permeability transition pore." Proc Natl Acad Sci U S A **111**(29): 10580-10585.
10. Amorim, R., I. C. M. Simoes, C. Veloso, A. Carvalho, R. F. Simoes, F. B. Pereira, T. Thiel, A. Normann, C. Morais, A. S. Jurado, M. R. Wieckowski, J. Teixeira and P. J. Oliveira (2021). "Exploratory Data Analysis of Cell and Mitochondrial High-Fat, High-Sugar Toxicity on Human HepG2 Cells." Nutrients **13**(5).
11. Antonenkov, V. D., S. Grunau, S. Ohlmeier and J. K. Hiltunen (2010). "Peroxisomes are oxidative organelles." Antioxid Redox Signal **13**(4): 525-537.
12. Aoun, M., G. Fouret, F. Michel, B. Bonafos, J. Ramos, J. P. Cristol, M. A. Carbonneau, C. Coudray and C. Feillet-Coudray (2012). "Dietary fatty acids modulate liver mitochondrial cardiolipin content and its fatty acid composition in rats with non alcoholic fatty liver disease." J Bioenerg Biomembr **44**(4): 439-452.
13. Arendt, B. M., D. W. Ma, B. Simons, S. A. Noureldin, G. Therapondos, M. Guindi, M. Sherman and J. P. Allard (2013). "Nonalcoholic fatty liver disease is associated with lower hepatic and erythrocyte ratios of phosphatidylcholine to phosphatidylethanolamine." Appl Physiol Nutr Metab **38**(3): 334-340.
14. Arnao, M. B., A. Cano and M. Acosta (2001). "The hydrophilic and lipophilic contribution to total antioxidant activity." Food Chemistry **73**(2): 239-244.
15. Arnold, D. R. and P. O. Kwiterovich (2003). CHOLESTEROL | Absorption, Function, and Metabolism. Encyclopedia of Food Sciences and Nutrition (Second Edition). B. Caballero. Oxford, Academic Press**:** 1226-1237.
16. Asin-Cayuela, J., A. R. Manas, A. M. James, R. A. Smith and M. P. Murphy (2004). "Fine-tuning the hydrophobicity of a mitochondria-targeted antioxidant." FEBS Lett **571**(1-3): 9-16.
17. Asrih, M. and F. R. Jornayvaz (2014). "Diets and nonalcoholic fatty liver disease: the good and the bad." Clin Nutr **33**(2): 186-190.

18. Athari, A., K. Hanecke and K. Jungermann (1994). "Prostaglandin F2 alpha and D2 release from primary Ito cell cultures after stimulation with noradrenaline and ATP but not adenosine." Hepatology **20**(1 Pt 1): 142-148.
19. Aubert, J., K. Begriche, M. Delannoy, I. Morel, J. Pajaud, C. Ribault, S. Lepage, M. R. McGill, C. Lucas-Clerc, B. Turlin, M. A. Robin, H. Jaeschke and B. Fromenty (2012). "Differences in early acetaminophen hepatotoxicity between obese ob/ob and db/db mice." J Pharmacol Exp Ther **342**(3): 676-687.
20. Ayala, A., M. F. Munoz and S. Arguelles (2014). "Lipid peroxidation: production, metabolism, and signaling mechanisms of malondialdehyde and 4-hydroxy-2-nonenal." Oxid Med Cell Longev **2014**: 360438.
21. Aydin, S., Y. Ozturk, V. M. Altan, N. Yildizoglu-Ari and A. T. Ozcelikay (1996). "Effect of insulin treatment on smooth muscle calmodulin levels in rats with long-term streptozotocin-diabetes." Mol Cell Endocrinol **116**(1): 67-71.
22. Bachem, M. G., D. Meyer, R. Melchior, K. M. Sell and A. M. Gressner (1992). "Activation of rat liver perisinusoidal lipocytes by transforming growth factors derived from myofibroblastlike cells. A potential mechanism of self perpetuation in liver fibrogenesis." J Clin Invest **89**(1): 19-27.
23. Baeck, C., X. Wei, M. Bartneck, V. Fech, F. Heymann, N. Gassler, K. Hittatiya, D. Eulberg, T. Luedde, C. Trautwein and F. Tacke (2014). "Pharmacological inhibition of the chemokine C-C motif chemokine ligand 2 (monocyte chemoattractant protein 1) accelerates liver fibrosis regression by suppressing Ly-6C(+) macrophage infiltration in mice." Hepatology **59**(3): 1060-1072.
24. Bancroft, J. D. and C. Layton (2019). 12 - Connective and other mesenchymal tissues with their stains. Bancroft's Theory and Practice of Histological Techniques (Eighth Edition). S. K. Suvarna, C. Layton and J. D. Bancroft, Content Repository Only!**:** 153-175.
25. Barroso, E., R. Rodriguez-Rodriguez, M. Zarei, J. Pizarro-Degado, A. Planavila, X. Palomer, F. Villarroya and M. Vazquez-Carrera (2020). "SIRT3 deficiency exacerbates fatty liver by attenuating the HIF1alpha-LIPIN 1 pathway and increasing CD36 through Nrf2." Cell Commun Signal **18**(1): 147.
26. Bedossa, P., C. Poitou, N. Veyrie, J. L. Bouillot, A. Basdevant, V. Paradis, J. Tordjman and K. Clement (2012). "Histopathological algorithm and scoring system for evaluation of liver lesions in morbidly obese patients." Hepatology **56**(5): 1751-1759.
27. Begriche, K., J. Massart, M. A. Robin, F. Bonnet and B. Fromenty (2013). "Mitochondrial adaptations and dysfunctions in nonalcoholic fatty liver disease." Hepatology **58**(4): 1497-1507.
28. Bell, L. N., C. J. Temm, R. Saxena, R. Vuppalanchi, P. Schauer, M. Rabinovitz, A. Krasinskas, N. Chalasani and S. G. Mattar (2010). "Bariatric surgery-induced weight loss reduces hepatic lipid peroxidation levels and affects hepatic cytochrome P-450 protein content." Ann Surg **251**(6): 1041-1048.
29. Benfeito, S., C. Oliveira, C. Fernandes, F. Cagide, J. Teixeira, R. Amorim, J. Garrido, C. Martins, B. Sarmento, R. Silva, F. Remiao, E. Uriarte, P. J. Oliveira and F. Borges (2019). "Fine-tuning the neuroprotective and blood-brain barrier permeability profile of multi-target agents designed to prevent progressive mitochondrial dysfunction." Eur J Med Chem **167**: 525-545.
30. Bernardi, P. and F. Di Lisa (2015). "The mitochondrial permeability transition pore: molecular nature and role as a target in cardioprotection." J Mol Cell Cardiol **78**: 100-106.
31. Besse-Patin, A., M. Leveille, D. Oropeza, B. N. Nguyen, A. Prat and J. L. Estall (2017). "Estrogen Signals Through Peroxisome Proliferator-Activated Receptor-gamma Coactivator 1alpha to Reduce Oxidative Damage Associated With Diet-Induced Fatty Liver Disease." Gastroenterology **152**(1): 243-256.

32. Bhattacharyya, S., K. Sinha and P. C. Sil (2014). "Cytochrome P450s: mechanisms and biological implications in drug metabolism and its interaction with oxidative stress." Curr Drug Metab **15**(7): 719-742.
33. Bleier, L. and S. Drose (2013). "Superoxide generation by complex III: from mechanistic rationales to functional consequences." Biochim Biophys Acta **1827**(11-12): 1320-1331.
34. Bligh, E. G. and W. J. Dyer (1959). "A rapid method of total lipid extraction and purification." Can J Biochem Physiol **37**(8): 911-917.
35. Blouin, A., R. P. Bolender and E. R. Weibel (1977). "Distribution of organelles and membranes between hepatocytes and nonhepatocytes in the rat liver parenchyma. A stereological study." J Cell Biol **72**(2): 441-455.
36. Bonekamp, N. A., A. Volkl, H. D. Fahimi and M. Schrader (2009). "Reactive oxygen species and peroxisomes: struggling for balance." Biofactors **35**(4): 346-355.
37. Boveris, A., N. Oshino and B. Chance (1972). "The cellular production of hydrogen peroxide." Biochem J **128**(3): 617-630.
38. Bradford, M. M. (1976). "A rapid and sensitive method for the quantitation of microgram quantities of protein utilizing the principle of protein-dye binding." Anal Biochem **72**: 248-254.
39. Brand, M. D. (2016). "Mitochondrial generation of superoxide and hydrogen peroxide as the source of mitochondrial redox signaling." Free Radic Biol Med **100**: 14-31.
40. Braud, L., S. Battault, G. Meyer, A. Nascimento, S. Gaillard, G. de Sousa, R. Rahmani, C. Riva, M. Armand, J. M. Maixent and C. Reboul (2017). "Antioxidant properties of tea blunt ROS-dependent lipogenesis: beneficial effect on hepatic steatosis in a high fat-high sucrose diet NAFLD obese rat model." J Nutr Biochem **40**: 95-104.
41. Bugianesi, E., S. Moscatiello, M. F. Ciaravella and G. Marchesini (2010). "Insulin resistance in nonalcoholic fatty liver disease." Curr Pharm Des **16**(17): 1941-1951.
42. Button, R. W., S. L. Roberts, T. L. Willis, C. O. Hanemann and S. Luo (2017). "Accumulation of autophagosomes confers cytotoxicity." J Biol Chem **292**(33): 13599-13614.
43. Bzowej, N. H. (2018). "Nonalcoholic steatohepatitis: the new frontier for liver transplantation." Curr Opin Organ Transplant **23**(2): 169-174.
44. Chalasani, N., Z. Younossi, J. E. Lavine, A. M. Diehl, E. M. Brunt, K. Cusi, M. Charlton and A. J. Sanyal (2012). "The diagnosis and management of non-alcoholic fatty liver disease: practice Guideline by the American Association for the Study of Liver Diseases, American College of Gastroenterology, and the American Gastroenterological Association." Hepatology **55**(6): 2005-2023.
45. Chance, B., H. Sies and A. Boveris (1979). "Hydroperoxide metabolism in mammalian organs." Physiol Rev **59**(3): 527-605.
46. Chance, B. and G. R. Williams (1955). "A method for the localization of sites for oxidative phosphorylation." Nature **176**(4475): 250-254.
47. Chaurasia, B., T. S. Tippetts, R. Mayoral Monibas, J. Liu, Y. Li, L. Wang, J. L. Wilkerson, C. R. Sweeney, R. F. Pereira, D. H. Sumida, J. A. Maschek, J. E. Cox, V. Kaddai, G. I. Lancaster, M. M. Siddique, A. Poss, M. Pearson, S. Satapati, H. Zhou, D. G. McLaren, S. F. Previs, Y. Chen, Y. Qian, A. Petrov, M. Wu, X. Shen, J. Yao, C. N. Nunes, A. D. Howard, L. Wang, M. D. Erion, J. Rutter, W. L. Holland, D. E. Kelley and S. A. Summers (2019). "Targeting a ceramide double bond improves insulin resistance and hepatic steatosis." Science **365**(6451): 386-392.
48. Chavez, J. A., M. M. Siddique, S. T. Wang, J. Ching, J. A. Shayman and S. A. Summers (2014). "Ceramides and glucosylceramides are independent antagonists of insulin signaling." J Biol Chem **289**(2): 723-734.

49. Chen, Y., C. Xu, T. Yan, C. Yu and Y. Li (2015). "omega-3 Fatty acids reverse lipotoxity through induction of autophagy in nonalcoholic fatty liver disease." Nutrition **31**(11-12): 1423-1429 e1422.
50. Chen, Z., R. Tian, Z. She, J. Cai and H. Li (2020). "Role of oxidative stress in the pathogenesis of nonalcoholic fatty liver disease." Free Radic Biol Med **152**: 116-141.
51. Chitturi, S. and G. C. Farrell (2001). "Etiopathogenesis of nonalcoholic steatohepatitis." Semin Liver Dis **21**(1): 27-41.
52. Cholankeril, G. and A. Ahmed (2018). "Alcoholic Liver Disease Replaces Hepatitis C Virus Infection as the Leading Indication for Liver Transplantation in the United States." Clin Gastroenterol Hepatol **16**(8): 1356-1358.
53. Clark, I. and M. S. Torbenson (2017). "Immunohistochemistry and Special Stains in Medical Liver Pathology." Adv Anat Pathol **24**(2): 99-109.
54. Cole, L. and P. R. Kramer (2016). Chapter 1.3 - Sugars, Fatty Acids, and Energy Biochemistry. Human Physiology, Biochemistry and Basic Medicine. L. Cole and P. R. Kramer. Boston, Academic Press**:** 17-30.
55. Colell, A., C. Garcia-Ruiz, J. M. Lluis, O. Coll, M. Mari and J. C. Fernandez-Checa (2003). "Cholesterol impairs the adenine nucleotide translocator-mediated mitochondrial permeability transition through altered membrane fluidity." J Biol Chem **278**(36): 33928-33935.
56. Collins, J. C., I. H. Scheinberg, D. R. Giblin and I. Sternlieb (1989). "Hepatic peroxisomal abnormalities in abetalipoproteinemia." Gastroenterology **97**(3): 766-770.
57. Colombini, M. (2004). "VDAC: the channel at the interface between mitochondria and the cytosol." Mol Cell Biochem **256-257**(1-2): 107-115.
58. Croci, I., N. M. Byrne, S. Choquette, A. P. Hills, V. S. Chachay, A. D. Clouston, T. M. O'Moore-Sullivan, G. A. Macdonald, J. B. Prins and I. J. Hickman (2013). "Whole-body substrate metabolism is associated with disease severity in patients with non-alcoholic fatty liver disease." Gut **62**(11): 1625-1633.
59. Crompton, M. (1999). "The mitochondrial permeability transition pore and its role in cell death." Biochem J **341 (Pt 2)**: 233-249.
60. Crompton, M., E. Barksby, N. Johnson and M. Capano (2002). "Mitochondrial intermembrane junctional complexes and their involvement in cell death." Biochimie **84**(2-3): 143-152.
61. Crompton, M., A. Costi and L. Hayat (1987). "Evidence for the presence of a reversible Ca2+-dependent pore activated by oxidative stress in heart mitochondria." Biochem J **245**(3): 915-918.
62. D'Autreaux, B. and M. B. Toledano (2007). "ROS as signalling molecules: mechanisms that generate specificity in ROS homeostasis." Nat Rev Mol Cell Biol **8**(10): 813-824.
63. D'Erchia, A. M., A. Atlante, G. Gadaleta, G. Pavesi, M. Chiara, C. De Virgilio, C. Manzari, F. Mastropasqua, G. M. Prazzoli, E. Picardi, C. Gissi, D. Horner, A. Reyes, E. Sbisa, A. Tullo and G. Pesole (2015). "Tissue-specific mtDNA abundance from exome data and its correlation with mitochondrial transcription, mass and respiratory activity." Mitochondrion **20**: 13-21.
64. Dasarathy, S., T. Kasumov, J. M. Edmison, L. L. Gruca, C. Bennett, C. Duenas, S. Marczewski, A. J. McCullough, R. W. Hanson and S. C. Kalhan (2009). "Glycine and urea kinetics in nonalcoholic steatohepatitis in human: effect of intralipid infusion." Am J Physiol Gastrointest Liver Physiol **297**(3): G567-575.
65. Dawaliby, R., C. Trubbia, C. Delporte, C. Noyon, J. M. Ruysschaert, P. Van Antwerpen and C. Govaerts (2016). "Phosphatidylethanolamine Is a Key Regulator of Membrane Fluidity in Eukaryotic Cells." J Biol Chem **291**(7): 3658-3667.

66. De Craemer, D., M. Pauwels and C. Van den Branden (1995). "Alterations of peroxisomes in steatosis of the human liver: a quantitative study." Hepatology **22**(3): 744-752.
67. de Gonzalo-Calvo, D., K. Neitzert, M. Fernández, I. Vega-Naredo, B. Caballero, M. García-Macía, F. M. Suárez, M. J. Rodríguez-Colunga, J. J. Solano and A. Coto-Montes (2010). "Differential inflammatory responses in aging and disease: TNF-α and IL-6 as possible biomarkers." Free Radical Biology and Medicine **49**(5): 733-737.
68. Debosch, B. J., Z. Chen, J. L. Saben, B. N. Finck and K. H. Moley (2014). "Glucose transporter 8 (GLUT8) mediates fructose-induced de novo lipogenesis and macrosteatosis." J Biol Chem **289**(16): 10989-10998.
69. Delierneux, C., S. Kouba, S. Shanmughapriya, M. Potier-Cartereau, M. Trebak and N. Hempel (2020). "Mitochondrial Calcium Regulation of Redox Signaling in Cancer." Cells **9**(2).
70. Dentin, R., J. Girard and C. Postic (2005). "Carbohydrate responsive element binding protein (ChREBP) and sterol regulatory element binding protein-1c (SREBP-1c): two key regulators of glucose metabolism and lipid synthesis in liver." Biochimie **87**(1): 81-86.
71. Deus, C. M., S. P. Pereira, T. Cunha-Oliveira, J. Teixeira, R. F. Simoes, F. Cagide, S. Benfeito, F. Borges, N. Raimundo and P. J. Oliveira (2021). "A mitochondria-targeted caffeic acid derivative reverts cellular and mitochondrial defects in human skin fibroblasts from male sporadic Parkinson's disease patients." Redox Biol **45**: 102037.
72. Doguer, C., J. H. Ha and J. F. Collins (2018). "Intersection of Iron and Copper Metabolism in the Mammalian Intestine and Liver." Compr Physiol **8**(4): 1433-1461.
73. Donati, A., G. Cavallini, C. Paradiso, S. Vittorini, M. Pollera, Z. Gori and E. Bergamini (2001). "Age-related changes in the regulation of autophagic proteolysis in rat isolated hepatocytes." J Gerontol A Biol Sci Med Sci **56**(7): B288-293.
74. Donnelly, K. L., C. I. Smith, S. J. Schwarzenberg, J. Jessurun, M. D. Boldt and E. J. Parks (2005). "Sources of fatty acids stored in liver and secreted via lipoproteins in patients with nonalcoholic fatty liver disease." J Clin Invest **115**(5): 1343-1351.
75. Doughan, A. K. and S. I. Dikalov (2007). "Mitochondrial redox cycling of mitoquinone leads to superoxide production and cellular apoptosis." Antioxid Redox Signal **9**(11): 1825-1836.
76. Dowling, R. J., I. Topisirovic, B. D. Fonseca and N. Sonenberg (2010). "Dissecting the role of mTOR: lessons from mTOR inhibitors." Biochim Biophys Acta **1804**(3): 433-439.
77. Duarte, J. A., F. Carvalho, M. Pearson, J. D. Horton, J. D. Browning, J. G. Jones and S. C. Burgess (2014). "A high-fat diet suppresses de novo lipogenesis and desaturation but not elongation and triglyceride synthesis in mice." J Lipid Res **55**(12): 2541-2553.
78. Dufour, D. R., J. A. Lott, F. S. Nolte, D. R. Gretch, R. S. Koff and L. B. Seeff (2000). "Diagnosis and monitoring of hepatic injury. II. Recommendations for use of laboratory tests in screening, diagnosis, and monitoring." Clin Chem **46**(12): 2050-2068.
79. Dyson, J., B. Jaques, D. Chattopadyhay, R. Lochan, J. Graham, D. Das, T. Aslam, I. Patanwala, S. Gaggar, M. Cole, K. Sumpter, S. Stewart, J. Rose, M. Hudson, D. Manas and H. L. Reeves (2014). "Hepatocellular cancer: the impact of obesity, type 2 diabetes and a multidisciplinary team." J Hepatol **60**(1): 110-117.
80. Eccleston, H. B., K. K. Andringa, A. M. Betancourt, A. L. King, S. K. Mantena, T. M. Swain, H. N. Tinsley, R. N. Nolte, T. R. Nagy, G. A. Abrams and S. M. Bailey (2011). "Chronic exposure to a high-fat diet induces hepatic steatosis, impairs nitric oxide bioavailability, and modifies the mitochondrial proteome in mice." Antioxid Redox Signal **15**(2): 447-459.
81. Ehling, J., M. Bartneck, X. Wei, F. Gremse, V. Fech, D. Mockel, C. Baeck, K. Hittatiya, D. Eulberg, T. Luedde, F. Kiessling, C. Trautwein, T. Lammers and F. Tacke (2014). "CCL2-dependent infiltrating macrophages promote angiogenesis in progressive liver fibrosis." Gut **63**(12): 1960-1971.

82. Einer, C., S. Hohenester, R. Wimmer, L. Wottke, R. Artmann, S. Schulz, C. Gosmann, A. Simmons, C. Leitzinger, C. Eberhagen, S. Borchard, S. Schmitt, S. M. Hauck, C. von Toerne, M. Jastroch, E. Walheim, C. Rust, A. L. Gerbes, B. Popper, D. Mayr, M. Schnurr, A. M. Vollmar, G. Denk and H. Zischka (2018). "Mitochondrial adaptation in steatotic mice." Mitochondrion **40**: 1-12.
83. Ekstedt, M., H. Hagstrom, P. Nasr, M. Fredrikson, P. Stal, S. Kechagias and R. Hultcrantz (2015). "Fibrosis stage is the strongest predictor for disease-specific mortality in NAFLD after up to 33 years of follow-up." Hepatology **61**(5): 1547-1554.
84. Elsner, M., W. Gehrmann and S. Lenzen (2011). "Peroxisome-generated hydrogen peroxide as important mediator of lipotoxicity in insulin-producing cells." Diabetes **60**(1): 200-208.
85. Emery, M. G., J. M. Fisher, J. Y. Chien, E. D. Kharasch, E. P. Dellinger, K. V. Kowdley and K. E. Thummel (2003). "CYP2E1 activity before and after weight loss in morbidly obese subjects with nonalcoholic fatty liver disease." Hepatology **38**(2): 428-435.
86. Estabrook, R. W. (1967). [7] Mitochondrial respiratory control and the polarographic measurement of ADP : O ratios. Methods in Enzymology, Academic Press. **10:** 41-47.
87. Fabbrini, E., F. Magkos, B. S. Mohammed, T. Pietka, N. A. Abumrad, B. W. Patterson, A. Okunade and S. Klein (2009). "Intrahepatic fat, not visceral fat, is linked with metabolic complications of obesity." Proc Natl Acad Sci U S A **106**(36): 15430-15435.
88. Fabbrini, E., B. S. Mohammed, F. Magkos, K. M. Korenblat, B. W. Patterson and S. Klein (2008). "Alterations in adipose tissue and hepatic lipid kinetics in obese men and women with nonalcoholic fatty liver disease." Gastroenterology **134**(2): 424-431.
89. Faeh, D., K. Minehira, J. M. Schwarz, R. Periasamy, S. Park and L. Tappy (2005). "Effect of fructose overfeeding and fish oil administration on hepatic de novo lipogenesis and insulin sensitivity in healthy men." Diabetes **54**(7): 1907-1913.
90. Fan, J. G., S. U. Kim and V. W. Wong (2017). "New trends on obesity and NAFLD in Asia." J Hepatol **67**(4): 862-873.
91. Fan, R., J. Wang and J. Du (2018). "Association between body mass index and fatty liver risk: A dose-response analysis." Sci Rep **8**(1): 15273.
92. Fan, T. W. M. (1996). "Metabolite profiling by one- and two-dimensional NMR analysis of complex mixtures." Progress in Nuclear Magnetic Resonance Spectroscopy **28**(2): 161-219.
93. Feillet-Coudray, C., G. Fouret, R. Ebabe Elle, J. Rieusset, B. Bonafos, B. Chabi, D. Crouzier, K. Zarkovic, N. Zarkovic, J. Ramos, E. Badia, M. P. Murphy, J. P. Cristol and C. Coudray (2014). "The mitochondrial-targeted antioxidant MitoQ ameliorates metabolic syndrome features in obesogenic diet-fed rats better than Apocynin or Allopurinol." Free Radic Res **48**(10): 1232-1246.
94. Fernandez-Checa, J. C. and N. Kaplowitz (2005). "Hepatic mitochondrial glutathione: transport and role in disease and toxicity." Toxicol Appl Pharmacol **204**(3): 263-273.
95. Ferramosca, A. and V. Zara (2014). "Modulation of hepatic steatosis by dietary fatty acids." World J Gastroenterol **20**(7): 1746-1755.
96. Figueira, T. R., D. R. Melo, A. E. Vercesi and R. F. Castilho (2012). "Safranine as a fluorescent probe for the evaluation of mitochondrial membrane potential in isolated organelles and permeabilized cells." Methods Mol Biol **810**: 103-117.
97. Folch, J., M. Lees and G. H. Sloane Stanley (1957). "A simple method for the isolation and purification of total lipides from animal tissues." J Biol Chem **226**(1): 497-509.
98. Fouret, G., S. Gaillet, J. Lecomte, B. Bonafos, F. Djohan, B. Barea, E. Badia, C. Coudray and C. Feillet-Coudray (2018). "20-Week follow-up of hepatic steatosis installation and liver mitochondrial structure and activity and their interrelation in rats fed a high-fat-high-fructose diet." Br J Nutr **119**(4): 368-380.

99. Fouret, G., E. Tolika, J. Lecomte, B. Bonafos, M. Aoun, M. P. Murphy, C. Ferreri, C. Chatgilialoglu, E. Dubreucq, C. Coudray and C. Feillet-Coudray (2015). "The mitochondrial-targeted antioxidant, MitoQ, increases liver mitochondrial cardiolipin content in obesogenic diet-fed rats." Biochim Biophys Acta **1847**(10): 1025-1035.
100. Francque, S., A. Verrijken, S. Caron, J. Prawitt, R. Paumelle, B. Derudas, P. Lefebvre, M. R. Taskinen, W. Van Hul, I. Mertens, G. Hubens, E. Van Marck, P. Michielsen, L. Van Gaal and B. Staels (2015). "PPARalpha gene expression correlates with severity and histological treatment response in patients with non-alcoholic steatohepatitis." J Hepatol **63**(1): 164-173.
101. Fransen, M., C. Lismont and P. Walton (2017). "The Peroxisome-Mitochondria Connection: How and Why?" Int J Mol Sci **18**(6).
102. Frey, T. G. and C. A. Mannella (2000). "The internal structure of mitochondria." Trends Biochem Sci **25**(7): 319-324.
103. Friedman, G., L. M. Liu, S. L. Friedman and J. K. Boyles (1991). "Apolipoprotein E is secreted by cultured lipocytes of the rat liver." J Lipid Res **32**(1): 107-114.
104. Friedman, S. L., B. A. Neuschwander-Tetri, M. Rinella and A. J. Sanyal (2018). "Mechanisms of NAFLD development and therapeutic strategies." Nat Med **24**(7): 908-922.
105. Fukuo, Y., S. Yamashina, H. Sonoue, A. Arakawa, E. Nakadera, T. Aoyama, A. Uchiyama, K. Kon, K. Ikejima and S. Watanabe (2014). "Abnormality of autophagic function and cathepsin expression in the liver from patients with non-alcoholic fatty liver disease." Hepatol Res **44**(9): 1026-1036.
106. Gan, L. T., D. M. Van Rooyen, M. E. Koina, R. S. McCuskey, N. C. Teoh and G. C. Farrell (2014). "Hepatocyte free cholesterol lipotoxicity results from JNK1-mediated mitochondrial injury and is HMGB1 and TLR4-dependent." J Hepatol **61**(6): 1376-1384.
107. Gane, E. J., F. Weilert, D. W. Orr, G. F. Keogh, M. Gibson, M. M. Lockhart, C. M. Frampton, K. M. Taylor, R. A. Smith and M. P. Murphy (2010). "The mitochondria-targeted anti-oxidant mitoquinone decreases liver damage in a phase II study of hepatitis C patients." Liver Int **30**(7): 1019-1026.
108. Garcia-Martinez, I., N. Santoro, Y. Chen, R. Hoque, X. Ouyang, S. Caprio, M. J. Shlomchik, R. L. Coffman, A. Candia and W. Z. Mehal (2016). "Hepatocyte mitochondrial DNA drives nonalcoholic steatohepatitis by activation of TLR9." J Clin Invest **126**(3): 859-864.
109. Gary-Bobo, M., P. Nirde, A. Jeanjean, A. Morere and M. Garcia (2007). "Mannose 6-phosphate receptor targeting and its applications in human diseases." Curr Med Chem **14**(28): 2945-2953.
110. Geng, C., H. Xu, Y. Zhang, Y. Gao, M. Li, X. Liu, M. Gao, X. Wang, X. Liu, F. Fang and Y. Chang (2017). "Retinoic acid ameliorates high-fat diet-induced liver steatosis through sirt1." Sci China Life Sci **60**(11): 1234-1241.
111. Gerard-Monnier, D., I. Erdelmeier, K. Regnard, N. Moze-Henry, J. C. Yadan and J. Chaudiere (1998). "Reactions of 1-methyl-2-phenylindole with malondialdehyde and 4-hydroxyalkenals. Analytical applications to a colorimetric assay of lipid peroxidation." Chem Res Toxicol **11**(10): 1176-1183.
112. Giorgi, C., S. Marchi, I. C. M. Simoes, Z. Ren, G. Morciano, M. Perrone, P. Patalas-Krawczyk, S. Borchard, P. Jedrak, K. Pierzynowska, J. Szymanski, D. Q. Wang, P. Portincasa, G. Wegrzyn, H. Zischka, P. Dobrzyn, M. Bonora, J. Duszynski, A. Rimessi, A. Karkucinska-Wieckowska, A. Dobrzyn, G. Szabadkai, B. Zavan, P. J. Oliveira, V. A. Sardao, P. Pinton and M. R. Wieckowski (2018). "Mitochondria and Reactive Oxygen Species in Aging and Age-Related Diseases." Int Rev Cell Mol Biol **340**: 209-344.
113. Giorgio, V., S. von Stockum, M. Antoniel, A. Fabbro, F. Fogolari, M. Forte, G. D. Glick, V. Petronilli, M. Zoratti, I. Szabo, G. Lippe and P. Bernardi (2013). "Dimers of mitochondrial ATP synthase form the permeability transition pore." Proc Natl Acad Sci U S A **110**(15): 5887-5892.

114. Gomez, B., Jr. and N. C. Robinson (1999). "Phospholipase digestion of bound cardiolipin reversibly inactivates bovine cytochrome bc1." Biochemistry **38**(28): 9031-9038.
115. Goncalves, I. O., E. Maciel, E. Passos, J. R. Torrella, D. Rizo, G. Viscor, S. Rocha-Rodrigues, E. Santos-Alves, M. R. Domingues, P. J. Oliveira, A. Ascensao and J. Magalhaes (2014). "Exercise alters liver mitochondria phospholipidomic profile and mitochondrial activity in non-alcoholic steatohepatitis." Int J Biochem Cell Biol **54**: 163-173.
116. Gong, J., X. Z. Wang, T. Wang, J. J. Chen, X. Y. Xie, H. Hu, F. Yu, H. L. Liu, X. Y. Jiang and H. D. Fan (2017). "Molecular signal networks and regulating mechanisms of the unfolded protein response." J Zhejiang Univ Sci B **18**(1): 1-14.
117. Gonzalez-Rodriguez, A., R. Mayoral, N. Agra, M. P. Valdecantos, V. Pardo, M. E. Miquilena-Colina, J. Vargas-Castrillon, O. Lo Iacono, M. Corazzari, G. M. Fimia, M. Piacentini, J. Muntane, L. Bosca, C. Garcia-Monzon, P. Martin-Sanz and A. M. Valverde (2014). "Impaired autophagic flux is associated with increased endoplasmic reticulum stress during the development of NAFLD." Cell Death Dis **5**: e1179.
118. Graier, W. F., M. Trenker and R. Malli (2008). "Mitochondrial Ca2+, the secret behind the function of uncoupling proteins 2 and 3?" Cell Calcium **44**(1): 36-50.
119. Grant, D. M. (1991). "Detoxification pathways in the liver." J Inherit Metab Dis **14**(4): 421-430.
120. Grattagliano, I., O. de Bari, T. C. Bernardo, P. J. Oliveira, D. Q. Wang and P. Portincasa (2012). "Role of mitochondria in nonalcoholic fatty liver disease--from origin to propagation." Clin Biochem **45**(9): 610-618.
121. Green, D. E. and A. Tzagoloff (1966). "The mitochondrial electron transfer chain." Arch Biochem Biophys **116**(1): 293-304.
122. Green, D. R. and G. Kroemer (2004). "The pathophysiology of mitochondrial cell death." Science **305**(5684): 626-629.
123. Grilo, L. F., J. D. Martins, C. H. Cavallaro, P. W. Nathanielsz, P. J. Oliveira and S. P. Pereira (2020). "Development of a 96-well based assay for kinetic determination of catalase enzymatic-activity in biological samples." Toxicol In Vitro **69**: 104996.
124. Guilherme, A., J. V. Virbasius, V. Puri and M. P. Czech (2008). "Adipocyte dysfunctions linking obesity to insulin resistance and type 2 diabetes." Nat Rev Mol Cell Biol **9**(5): 367-377.
125. Gunter, T. E. and D. R. Pfeiffer (1990). "Mechanisms by which mitochondria transport calcium." Am J Physiol **258**(5 Pt 1): C755-786.
126. Haldar, D., B. Kern, J. Hodson, M. J. Armstrong, R. Adam, G. Berlakovich, J. Fritz, B. Feurstein, W. Popp, V. Karam, P. Muiesan, J. O'Grady, N. Jamieson, S. J. Wigmore, J. Pirenne, S. A. Malek-Hosseini, E. Hidalgo, Y. Tokat, A. Paul, J. Pratschke, M. Bartels, P. Trunecka, U. Settmacher, M. Pinzani, C. Duvoux, P. N. Newsome, S. Schneeberger, L. European and A. Intestine Transplant (2019). "Outcomes of liver transplantation for non-alcoholic steatohepatitis: A European Liver Transplant Registry study." J Hepatol **71**(2): 313-322.
127. Halestrap, A. P. and C. Brenner (2003). "The adenine nucleotide translocase: a central component of the mitochondrial permeability transition pore and key player in cell death." Curr Med Chem **10**(16): 1507-1525.
128. Halestrap, A. P. and A. M. Davidson (1990). "Inhibition of Ca2(+)-induced large-amplitude swelling of liver and heart mitochondria by cyclosporin is probably caused by the inhibitor binding to mitochondrial-matrix peptidyl-prolyl cis-trans isomerase and preventing it interacting with the adenine nucleotide translocase." Biochem J **268**(1): 153-160.
129. Halestrap, A. P. and A. P. Richardson (2015). "The mitochondrial permeability transition: a current perspective on its identity and role in ischaemia/reperfusion injury." J Mol Cell Cardiol **78**: 129-141.

130. Hall, D., C. Poussin, V. R. Velagapudi, C. Empsen, M. Joffraud, J. S. Beckmann, A. E. Geerts, Y. Ravussin, M. Ibberson, M. Oresic and B. Thorens (2020). "Correction: Peroxisomal and microsomal lipid pathways associated with resistance to hepatic steatosis and reduced pro-inflammatory state." J Biol Chem **295**(22): 7813.
131. Hamilton, J. G. and K. Comai (1988). "Rapid separation of neutral lipids, free fatty acids and polar lipids using prepacked silica Sep-Pak columns." Lipids **23**(12): 1146-1149.
132. Harada, M., S. Hanada, D. M. Toivola, N. Ghori and M. B. Omary (2008). "Autophagy activation by rapamycin eliminates mouse Mallory-Denk bodies and blocks their proteasome inhibitor-mediated formation." Hepatology **47**(6): 2026-2035.
133. Hardie, D. G. (2011). "AMP-activated protein kinase: an energy sensor that regulates all aspects of cell function." Genes Dev **25**(18): 1895-1908.
134. Hawkins, R. A., A. M. Mans and D. W. Davis (1986). "Regional ketone body utilization by rat brain in starvation and diabetes." Am J Physiol **250**(2 Pt 1): E169-178.
135. Haworth, R. A. and D. R. Hunter (1979). "The Ca2+-induced membrane transition in mitochondria. II. Nature of the Ca2+ trigger site." Arch Biochem Biophys **195**(2): 460-467.
136. Hayes, J. D. and M. McMahon (2009). "NRF2 and KEAP1 mutations: permanent activation of an adaptive response in cancer." Trends Biochem Sci **34**(4): 176-188.
137. He, J., H. C. Ford, J. Carroll, S. Ding, I. M. Fearnley and J. E. Walker (2017). "Persistence of the mitochondrial permeability transition in the absence of subunit c of human ATP synthase." Proc Natl Acad Sci U S A **114**(13): 3409-3414.
138. Heinz, S. and J. Braspenning (2015). "Measurement of Blood Coagulation Factor Synthesis in Cultures of Human Hepatocytes." Methods Mol Biol **1250**: 309-316.
139. Henkel, A. and R. M. Green (2013). "The unfolded protein response in fatty liver disease." Semin Liver Dis **33**(4): 321-329.
140. Henkel, A. S. (2018). "Unfolded Protein Response Sensors in Hepatic Lipid Metabolism and Nonalcoholic Fatty Liver Disease." Semin Liver Dis **38**(4): 320-332.
141. Heymann, F., L. Hammerich, D. Storch, M. Bartneck, S. Huss, V. Russeler, N. Gassler, S. A. Lira, T. Luedde, C. Trautwein and F. Tacke (2012). "Hepatic macrophage migration and differentiation critical for liver fibrosis is mediated by the chemokine receptor C-C motif chemokine receptor 8 in mice." Hepatology **55**(3): 898-909.
142. Higuchi, N., M. Kato, Y. Shundo, H. Tajiri, M. Tanaka, N. Yamashita, M. Kohjima, K. Kotoh, M. Nakamuta, R. Takayanagi and M. Enjoji (2008). "Liver X receptor in cooperation with SREBP-1c is a major lipid synthesis regulator in nonalcoholic fatty liver disease." Hepatol Res **38**(11): 1122-1129.
143. Holt, M. P., L. Cheng and C. Ju (2008). "Identification and characterization of infiltrating macrophages in acetaminophen-induced liver injury." J Leukoc Biol **84**(6): 1410-1421.
144. Horvath, S. E. and G. Daum (2013). "Lipids of mitochondria." Prog Lipid Res **52**(4): 590-614.
145. Houten, S. M., S. Violante, F. V. Ventura and R. J. Wanders (2016). "The Biochemistry and Physiology of Mitochondrial Fatty Acid beta-Oxidation and Its Genetic Disorders." Annu Rev Physiol **78**: 23-44.
146. Huebener, P., J. P. Pradere, C. Hernandez, G. Y. Gwak, J. M. Caviglia, X. Mu, J. D. Loike and R. F. Schwabe (2015). "The HMGB1/RAGE axis triggers neutrophil-mediated injury amplification following necrosis." J Clin Invest **125**(2): 539-550.
147. Hunter, D. R., R. A. Haworth and J. H. Southard (1976). "Relationship between configuration, function, and permeability in calcium-treated mitochondria." J Biol Chem **251**(16): 5069-5077.
148. Huynh, K. K., E. L. Eskelinen, C. C. Scott, A. Malevanets, P. Saftig and S. Grinstein (2007). "LAMP proteins are required for fusion of lysosomes with phagosomes." EMBO J **26**(2): 313-324.

149. Iizuka, K. (2017). "The Role of Carbohydrate Response Element Binding Protein in Intestinal and Hepatic Fructose Metabolism." Nutrients **9**(2).
150. Inami, Y., S. Yamashina, K. Izumi, T. Ueno, I. Tanida, K. Ikejima and S. Watanabe (2011). "Hepatic steatosis inhibits autophagic proteolysis via impairment of autophagosomal acidification and cathepsin expression." Biochem Biophys Res Commun **412**(4): 618-625.
151. Iredale, J. P. (2001). "Hepatic stellate cell behavior during resolution of liver injury." Semin Liver Dis **21**(3): 427-436.
152. Jiang, C., C. Xie, F. Li, L. Zhang, R. G. Nichols, K. W. Krausz, J. Cai, Y. Qi, Z. Z. Fang, S. Takahashi, N. Tanaka, D. Desai, S. G. Amin, I. Albert, A. D. Patterson and F. J. Gonzalez (2015). "Intestinal farnesoid X receptor signaling promotes nonalcoholic fatty liver disease." J Clin Invest **125**(1): 386-402.
153. Jouaville, L. S., P. Pinton, C. Bastianutto, G. A. Rutter and R. Rizzuto (1999). "Regulation of mitochondrial ATP synthesis by calcium: evidence for a long-term metabolic priming." Proc Natl Acad Sci U S A **96**(24): 13807-13812.
154. Ju, C. and F. Tacke (2016). "Hepatic macrophages in homeostasis and liver diseases: from pathogenesis to novel therapeutic strategies." Cell Mol Immunol **13**(3): 316-327.
155. Kagan, V. E., V. A. Tyurin, J. Jiang, Y. Y. Tyurina, V. B. Ritov, A. A. Amoscato, A. N. Osipov, N. A. Belikova, A. A. Kapralov, V. Kini, Vlasova, II, Q. Zhao, M. Zou, P. Di, D. A. Svistunenko, I. V. Kurnikov and G. G. Borisenko (2005). "Cytochrome c acts as a cardiolipin oxygenase required for release of proapoptotic factors." Nat Chem Biol **1**(4): 223-232.
156. Karkucinska-Wieckowska, A., I. C. M. Simoes, P. Kalinowski, M. Lebiedzinska-Arciszewska, K. Zieniewicz, P. Milkiewicz, M. Gorska-Ponikowska, P. Pinton, A. N. Malik, M. Krawczyk, P. J. Oliveira and M. R. Wieckowski (2021). "Mitochondria, oxidative stress and nonalcoholic fatty liver disease: A complex relationship." Eur J Clin Invest: e13622.
157. Karlmark, K. R., R. Weiskirchen, H. W. Zimmermann, N. Gassler, F. Ginhoux, C. Weber, M. Merad, T. Luedde, C. Trautwein and F. Tacke (2009). "Hepatic recruitment of the inflammatory Gr1+ monocyte subset upon liver injury promotes hepatic fibrosis." Hepatology **50**(1): 261-274.
158. Kashima, J., K. Shintani-Ishida, M. Nakajima, H. Maeda, K. Unuma, Y. Uchiyama and K. Yoshida (2014). "Immunohistochemical study of the autophagy marker microtubule-associated protein 1 light chain 3 in normal and steatotic human livers." Hepatol Res **44**(7): 779-787.
159. Kendrick, A. A., M. Choudhury, S. M. Rahman, C. E. McCurdy, M. Friederich, J. L. Van Hove, P. A. Watson, N. Birdsey, J. Bao, D. Gius, M. N. Sack, E. Jing, C. R. Kahn, J. E. Friedman and K. R. Jonscher (2011). "Fatty liver is associated with reduced SIRT3 activity and mitochondrial protein hyperacetylation." Biochem J **433**(3): 505-514.
160. Kerner, J. and C. Hoppel (2000). "Fatty acid import into mitochondria." Biochim Biophys Acta **1486**(1): 1-17.
161. Kim, Y. C. and K. L. Guan (2015). "mTOR: a pharmacologic target for autophagy regulation." J Clin Invest **125**(1): 25-32.
162. Kleiner, D. E., E. M. Brunt, M. Van Natta, C. Behling, M. J. Contos, O. W. Cummings, L. D. Ferrell, Y. C. Liu, M. S. Torbenson, A. Unalp-Arida, M. Yeh, A. J. McCullough, A. J. Sanyal and N. Nonalcoholic Steatohepatitis Clinical Research (2005). "Design and validation of a histological scoring system for nonalcoholic fatty liver disease." Hepatology **41**(6): 1313-1321.
163. Kleiner, D. E., E. M. Brunt, L. A. Wilson, C. Behling, C. Guy, M. Contos, O. Cummings, M. Yeh, R. Gill, N. Chalasani, B. A. Neuschwander-Tetri, A. M. Diehl, S. Dasarathy, N. Terrault, K. Kowdley, R. Loomba, P. Belt, J. Tonascia, J. E. Lavine, A. J. Sanyal and N. Nonalcoholic Steatohepatitis Clinical Research (2019). "Association of Histologic Disease Activity With Progression of Nonalcoholic Fatty Liver Disease." JAMA Netw Open **2**(10): e1912565.

164. Knebel, B., S. Goddeke, S. Hartwig, T. Horbelt, P. Fahlbusch, H. Al-Hasani, S. Jacob, C. Koellmer, U. Nitzgen, M. Schiller, S. Lehr and J. Kotzka (2018). "Alteration of Liver Peroxisomal and Mitochondrial Functionality in the NZO Mouse Model of Metabolic Syndrome." Proteomics Clin Appl **12**(1).
165. Knebel, B., S. Hartwig, J. Haas, S. Lehr, S. Goeddeke, F. Susanto, L. Bohne, S. Jacob, C. Koellmer, U. Nitzgen, D. Muller-Wieland and J. Kotzka (2015). "Peroxisomes compensate hepatic lipid overflow in mice with fatty liver." Biochim Biophys Acta **1851**(7): 965-976.
166. Knolle, P. A., T. Germann, U. Treichel, A. Uhrig, E. Schmitt, S. Hegenbarth, A. W. Lohse and G. Gerken (1999). "Endotoxin down-regulates T cell activation by antigen-presenting liver sinusoidal endothelial cells." J Immunol **162**(3): 1401-1407.
167. Koga, H., S. Kaushik and A. M. Cuervo (2010). "Altered lipid content inhibits autophagic vesicular fusion." FASEB J **24**(8): 3052-3065.
168. Koh, J. H., L. Wang, C. Beaudoin-Chabot and G. Thibault (2018). "Lipid bilayer stress-activated IRE-1 modulates autophagy during endoplasmic reticulum stress." J Cell Sci **131**(22).
169. Kohjima, M., M. Enjoji, N. Higuchi, M. Kato, K. Kotoh, T. Yoshimoto, T. Fujino, M. Yada, R. Yada, N. Harada, R. Takayanagi and M. Nakamuta (2007). "Re-evaluation of fatty acid metabolism-related gene expression in nonalcoholic fatty liver disease." Int J Mol Med **20**(3): 351-358.
170. Koliaki, C., J. Szendroedi, K. Kaul, T. Jelenik, P. Nowotny, F. Jankowiak, C. Herder, M. Carstensen, M. Krausch, W. T. Knoefel, M. Schlensak and M. Roden (2015). "Adaptation of hepatic mitochondrial function in humans with non-alcoholic fatty liver is lost in steatohepatitis." Cell Metab **21**(5): 739-746.
171. Komatsu, M., H. Kurokawa, S. Waguri, K. Taguchi, A. Kobayashi, Y. Ichimura, Y.-S. Sou, I. Ueno, A. Sakamoto, K. I. Tong, M. Kim, Y. Nishito, S.-i. Iemura, T. Natsume, T. Ueno, E. Kominami, H. Motohashi, K. Tanaka and M. Yamamoto (2010). "The selective autophagy substrate p62 activates the stress responsive transcription factor Nrf2 through inactivation of Keap1." Nature Cell Biology **12**(3): 213-223.
172. Kong, X., R. Wang, Y. Xue, X. Liu, H. Zhang, Y. Chen, F. Fang and Y. Chang (2010). "Sirtuin 3, a new target of PGC-1alpha, plays an important role in the suppression of ROS and mitochondrial biogenesis." PLoS One **5**(7): e11707.
173. Koruk, M., S. Taysi, M. C. Savas, O. Yilmaz, F. Akcay and M. Karakok (2004). "Oxidative stress and enzymatic antioxidant status in patients with nonalcoholic steatohepatitis." Ann Clin Lab Sci **34**(1): 57-62.
174. Krawczyk, M., M. Rau, J. M. Schattenberg, H. Bantel, A. Pathil, M. Demir, J. Kluwe, T. Boettler, F. Lammert, A. Geier and N. C. S. Group (2017). "Combined effects of the PNPLA3 rs738409, TM6SF2 rs58542926, and MBOAT7 rs641738 variants on NAFLD severity: a multicenter biopsy-based study." J Lipid Res **58**(1): 247-255.
175. Kumar, A., A. Sharma, A. Duseja, A. Das, R. K. Dhiman, Y. K. Chawla, K. K. Kohli and A. Bhansali (2013). "Patients with Nonalcoholic Fatty Liver Disease (NAFLD) have Higher Oxidative Stress in Comparison to Chronic Viral Hepatitis." J Clin Exp Hepatol **3**(1): 12-18.
176. Kussmaul, L. and J. Hirst (2006). "The mechanism of superoxide production by NADH:ubiquinone oxidoreductase (complex I) from bovine heart mitochondria." Proc Natl Acad Sci U S A **103**(20): 7607-7612.
177. Lagouge, M., C. Argmann, Z. Gerhart-Hines, H. Meziane, C. Lerin, F. Daussin, N. Messadeq, J. Milne, P. Lambert, P. Elliott, B. Geny, M. Laakso, P. Puigserver and J. Auwerx (2006). "Resveratrol improves mitochondrial function and protects against metabolic disease by activating SIRT1 and PGC-1alpha." Cell **127**(6): 1109-1122.
178. Lambert, J. E., M. A. Ramos-Roman, J. D. Browning and E. J. Parks (2014). "Increased de novo lipogenesis is a distinct characteristic of individuals with nonalcoholic fatty liver disease." Gastroenterology **146**(3): 726-735.

179. Lazarow, P. B. and C. De Duve (1976). "A fatty acyl-CoA oxidizing system in rat liver peroxisomes; enhancement by clofibrate, a hypolipidemic drug." Proc Natl Acad Sci U S A **73**(6): 2043-2046.
180. Lee, J., T. Homma and J. Fujii (2017). "Mice in the early stage of liver steatosis caused by a high fat diet are resistant to thioacetamide-induced hepatotoxicity and oxidative stress." Toxicol Lett **277**: 92-103.
181. Lee, K., A. Haddad, A. Osme, C. Kim, A. Borzou, S. Ilchenko, D. Allende, S. Dasarathy, A. McCullough, R. G. Sadygov and T. Kasumov (2018). "Hepatic Mitochondrial Defects in a Nonalcoholic Fatty Liver Disease Mouse Model Are Associated with Increased Degradation of Oxidative Phosphorylation Subunits." Mol Cell Proteomics **17**(12): 2371-2386.
182. Lee, S., S. Kim, S. Hwang, N. J. Cherrington and D. Y. Ryu (2017). "Dysregulated expression of proteins associated with ER stress, autophagy and apoptosis in tissues from nonalcoholic fatty liver disease." Oncotarget **8**(38): 63370-63381.
183. Lee, Y. M., H. C. Low, L. G. Lim, Y. Y. Dan, M. O. Aung, C. L. Cheng, A. Wee, S. G. Lim and K. Y. Ho (2012). "Intragastric balloon significantly improves nonalcoholic fatty liver disease activity score in obese patients with nonalcoholic steatohepatitis: a pilot study." Gastrointest Endosc **76**(4): 756-760.
184. Lehninger, A. L., C. S. Rossi and J. W. Greenawalt (1963). "Respiration-dependent accumulation of inorganic phosphate and Ca++ by rat liver mitochondria." Biochemical and Biophysical Research Communications **10**(6): 444-448.
185. Lemasters, J. J. (2005). "Selective mitochondrial autophagy, or mitophagy, as a targeted defense against oxidative stress, mitochondrial dysfunction, and aging." Rejuvenation Res **8**(1): 3-5.
186. Lenaz, G., A. Baracca, G. Barbero, C. Bergamini, M. E. Dalmonte, M. Del Sole, M. Faccioli, A. Falasca, R. Fato, M. L. Genova, G. Sgarbi and G. Solaini (2010). "Mitochondrial respiratory chain super-complex I-III in physiology and pathology." Biochim Biophys Acta **1797**(6-7): 633-640.
187. Leturque, A., E. Brot-Laroche, M. Le Gall, E. Stolarczyk and V. Tobin (2005). "The role of GLUT2 in dietary sugar handling." J Physiol Biochem **61**(4): 529-537.
188. Leung, A. W., P. Varanyuwatana and A. P. Halestrap (2008). "The mitochondrial phosphate carrier interacts with cyclophilin D and may play a key role in the permeability transition." J Biol Chem **283**(39): 26312-26323.
189. Li, J., C. Romestaing, X. Han, Y. Li, X. Hao, Y. Wu, C. Sun, X. Liu, L. S. Jefferson, J. Xiong, K. F. Lanoue, Z. Chang, C. J. Lynch, H. Wang and Y. Shi (2010). "Cardiolipin remodeling by ALCAT1 links oxidative stress and mitochondrial dysfunction to obesity." Cell Metab **12**(2): 154-165.
190. Li, R., S. Toan and H. Zhou (2020). "Role of mitochondrial quality control in the pathogenesis of nonalcoholic fatty liver disease." Aging (Albany NY) **12**(7): 6467-6485.
191. Li, R., T. Xin, D. Li, C. Wang, H. Zhu and H. Zhou (2018). "Therapeutic effect of Sirtuin 3 on ameliorating nonalcoholic fatty liver disease: The role of the ERK-CREB pathway and Bnip3-mediated mitophagy." Redox Biol **18**: 229-243.
192. Li, Z. Z., M. Berk, T. M. McIntyre and A. E. Feldstein (2009). "Hepatic lipid partitioning and liver damage in nonalcoholic fatty liver disease: role of stearoyl-CoA desaturase." J Biol Chem **284**(9): 5637-5644.
193. Lim, J. K., S. L. Flamm, S. Singh, Y. T. Falck-Ytter and A. Clinical Guidelines Committee of the American Gastroenterological (2017). "American Gastroenterological Association Institute Guideline on the Role of Elastography in the Evaluation of Liver Fibrosis." Gastroenterology **152**(6): 1536-1543.

194. Lin, C. W., H. Zhang, M. Li, X. Xiong, X. Chen, X. Chen, X. C. Dong and X. M. Yin (2013). "Pharmacological promotion of autophagy alleviates steatosis and injury in alcoholic and non-alcoholic fatty liver conditions in mice." J Hepatol **58**(5): 993-999.
195. Listenberger, L. L., X. Han, S. E. Lewis, S. Cases, R. V. Farese, Jr., D. S. Ory and J. E. Schaffer (2003). "Triglyceride accumulation protects against fatty acid-induced lipotoxicity." Proc Natl Acad Sci U S A **100**(6): 3077-3082.
196. Liu, H. Y., J. Han, S. Y. Cao, T. Hong, D. Zhuo, J. Shi, Z. Liu and W. Cao (2009). "Hepatic autophagy is suppressed in the presence of insulin resistance and hyperinsulinemia: inhibition of FoxO1-dependent expression of key autophagy genes by insulin." J Biol Chem **284**(45): 31484-31492.
197. Lockman, K. A., J. P. Baren, C. J. Pemberton, H. Baghdadi, K. E. Burgess, N. Plevris-Papaioannou, P. Lee, F. Howie, G. Beckett, A. Pryde, A. J. Jaap, P. C. Hayes, C. Filippi and J. N. Plevris (2012). "Oxidative stress rather than triglyceride accumulation is a determinant of mitochondrial dysfunction in in vitro models of hepatic cellular steatosis." Liver Int **32**(7): 1079-1092.
198. Lohr, K., F. Pachl, A. Moghaddas Gholami, K. E. Geillinger, H. Daniel, B. Kuster and M. Klingenspor (2016). "Reduced mitochondrial mass and function add to age-related susceptibility toward diet-induced fatty liver in C57BL/6J mice." Physiol Rep **4**(19).
199. Lu, W., S. Li, J. Li, J. Wang, R. Zhang, Y. Zhou, Q. Yin, Y. Zheng, F. Wang, Y. Xia, K. Chen, T. Liu, J. Lu, Y. Zhou and C. Guo (2016). "Effects of Omega-3 Fatty Acid in Nonalcoholic Fatty Liver Disease: A Meta-Analysis." Gastroenterol Res Pract **2016**: 1459790.
200. Lu, Y. W. and S. M. Claypool (2015). "Disorders of phospholipid metabolism: an emerging class of mitochondrial disease due to defects in nuclear genes." Front Genet **6**: 3.
201. MacPhee, P. J., E. E. Schmidt and A. C. Groom (1992). "Evidence for Kupffer cell migration along liver sinusoids, from high-resolution in vivo microscopy." Am J Physiol **263**(1 Pt 1): G17-23.
202. Mahmood, T. and P. C. Yang (2012). "Western blot: technique, theory, and trouble shooting." N Am J Med Sci **4**(9): 429-434.
203. Mallilankaraman, K., C. Cardenas, P. J. Doonan, H. C. Chandramoorthy, K. M. Irrinki, T. Golenar, G. Csordas, P. Madireddi, J. Yang, M. Muller, R. Miller, J. E. Kolesar, J. Molgo, B. Kaufman, G. Hajnoczky, J. K. Foskett and M. Madesh (2012). "MCUR1 is an essential component of mitochondrial Ca2+ uptake that regulates cellular metabolism." Nat Cell Biol **14**(12): 1336-1343.
204. Mancina, R. M., P. Dongiovanni, S. Petta, P. Pingitore, M. Meroni, R. Rametta, J. Boren, T. Montalcini, A. Pujia, O. Wiklund, G. Hindy, R. Spagnuolo, B. M. Motta, R. M. Pipitone, A. Craxi, S. Fargion, V. Nobili, P. Kakela, V. Karja, V. Mannisto, J. Pihlajamaki, D. F. Reilly, J. Castro-Perez, J. Kozlitina, L. Valenti and S. Romeo (2016). "The MBOAT7-TMC4 Variant rs641738 Increases Risk of Nonalcoholic Fatty Liver Disease in Individuals of European Descent." Gastroenterology **150**(5): 1219-1230 e1216.
205. Mansouri, A., C. H. Gattolliat and T. Asselah (2018). "Mitochondrial Dysfunction and Signaling in Chronic Liver Diseases." Gastroenterology **155**(3): 629-647.
206. Mantena, S. K., D. P. Vaughn, K. K. Andringa, H. B. Eccleston, A. L. King, G. A. Abrams, J. E. Doeller, D. W. Kraus, V. M. Darley-Usmar and S. M. Bailey (2009). "High fat diet induces dysregulation of hepatic oxygen gradients and mitochondrial function in vivo." Biochem J **417**(1): 183-193.
207. Mari, M., F. Caballero, A. Colell, A. Morales, J. Caballeria, A. Fernandez, C. Enrich, J. C. Fernandez-Checa and C. Garcia-Ruiz (2006). "Mitochondrial free cholesterol loading sensitizes to TNF- and Fas-mediated steatohepatitis." Cell Metab **4**(3): 185-198.
208. Martinou, J. C. and D. R. Green (2001). "Breaking the mitochondrial barrier." Nat Rev Mol Cell Biol **2**(1): 63-67.

209. Matsuzawa-Nagata, N., T. Takamura, H. Ando, S. Nakamura, S. Kurita, H. Misu, T. Ota, M. Yokoyama, M. Honda, K. Miyamoto and S. Kaneko (2008). "Increased oxidative stress precedes the onset of high-fat diet-induced insulin resistance and obesity." Metabolism **57**(8): 1071-1077.
210. Mayes, P. A. (1993). "Intermediary metabolism of fructose." Am J Clin Nutr **58**(5 Suppl): 754S-765S.
211. McAlister, G. C., D. P. Nusinow, M. P. Jedrychowski, M. Wuhr, E. L. Huttlin, B. K. Erickson, R. Rad, W. Haas and S. P. Gygi (2014). "MultiNotch MS3 enables accurate, sensitive, and multiplexed detection of differential expression across cancer cell line proteomes." Anal Chem **86**(14): 7150-7158.
212. McPherson, S., T. Hardy, E. Henderson, A. D. Burt, C. P. Day and Q. M. Anstee (2015). "Evidence of NAFLD progression from steatosis to fibrosing-steatohepatitis using paired biopsies: implications for prognosis and clinical management." J Hepatol **62**(5): 1148-1155.
213. Mei, S., H. M. Ni, S. Manley, A. Bockus, K. M. Kassel, J. P. Luyendyk, B. L. Copple and W. X. Ding (2011). "Differential roles of unsaturated and saturated fatty acids on autophagy and apoptosis in hepatocytes." J Pharmacol Exp Ther **339**(2): 487-498.
214. Mendez, L., M. Pazos, E. Molinar-Toribio, V. Sanchez-Martos, J. M. Gallardo, M. Rosa Nogues, J. L. Torres and I. Medina (2014). "Protein carbonylation associated to high-fat, high-sucrose diet and its metabolic effects." J Nutr Biochem **25**(12): 1243-1253.
215. Mercer, J. R., E. Yu, N. Figg, K. K. Cheng, T. A. Prime, J. L. Griffin, M. Masoodi, A. Vidal-Puig, M. P. Murphy and M. R. Bennett (2012). "The mitochondria-targeted antioxidant MitoQ decreases features of the metabolic syndrome in ATM+/-/ApoE-/- mice." Free Radic Biol Med **52**(5): 841-849.
216. Miele, L., A. Grieco, A. Armuzzi, M. Candelli, A. Forgione, A. Gasbarrini and G. Gasbarrini (2003). "Hepatic mitochondrial beta-oxidation in patients with nonalcoholic steatohepatitis assessed by 13C-octanoate breath test." Am J Gastroenterol **98**(10): 2335-2336.
217. Mihaylova, M. M. and R. J. Shaw (2011). "The AMPK signalling pathway coordinates cell growth, autophagy and metabolism." Nat Cell Biol **13**(9): 1016-1023.
218. Mitchell, P. (1961). "Coupling of Phosphorylation to Electron and Hydrogen Transfer by a Chemi-Osmotic type of Mechanism." Nature **191**(4784): 144-148.
219. Mizushima, N., T. Yoshimori and Y. Ohsumi (2011). "The role of Atg proteins in autophagosome formation." Annu Rev Cell Dev Biol **27**: 107-132.
220. Mortimore, G. E., A. R. Poso and B. R. Lardeux (1989). "Mechanism and regulation of protein degradation in liver." Diabetes Metab Rev **5**(1): 49-70.
221. Moslehi, A., M. Farahabadi, S. A. Chavoshzadeh, A. Barati, S. Ababzadeh and A. Mohammadbeigi (2018). "The Effect of Amygdalin on Endoplasmic Reticulum (ER) Stress Induced Hepatic Steatosis in Mice." Malays J Med Sci **25**(1): 16-23.
222. Mukherjee, T. K., A. K. Mishra, S. Mukhopadhyay and J. R. Hoidal (2007). "High concentration of antioxidants N-acetylcysteine and mitoquinone-Q induces intercellular adhesion molecule 1 and oxidative stress by increasing intracellular glutathione." J Immunol **178**(3): 1835-1844.
223. Muoio, D. M. (2014). "Metabolic inflexibility: when mitochondrial indecision leads to metabolic gridlock." Cell **159**(6): 1253-1262.
224. Naguib, G., N. Morris, S. Yang, N. Fryzek, V. Haynes-Williams, W. A. Huang, J. Norman-Wheeler and Y. Rotman (2020). "Dietary fatty acid oxidation is decreased in non-alcoholic fatty liver disease: A palmitate breath test study." Liver Int **40**(3): 590-597.
225. Naito, M., G. Hasegawa and K. Takahashi (1997). "Development, differentiation, and maturation of Kupffer cells." Microsc Res Tech **39**(4): 350-364.

226. Nakatogawa, H., K. Suzuki, Y. Kamada and Y. Ohsumi (2009). "Dynamics and diversity in autophagy mechanisms: lessons from yeast." Nat Rev Mol Cell Biol **10**(7): 458-467.
227. Nallagangula, K. S., S. K. Nagaraj, L. Venkataswamy and M. Chandrappa (2018). "Liver fibrosis: a compilation on the biomarkers status and their significance during disease progression." Future Sci OA **4**(1): FSO250.
228. Natarajan, S. K., C. E. Eapen, A. B. Pullimood and K. A. Balasubramanian (2006). "Oxidative stress in experimental liver microvesicular steatosis: role of mitochondria and peroxisomes." J Gastroenterol Hepatol **21**(8): 1240-1249.
229. Neupert, W. (1997). "Protein import into mitochondria." Annu Rev Biochem **66**: 863-917.
230. Nguyen, T., P. J. Sherratt and C. B. Pickett (2003). "Regulatory mechanisms controlling gene expression mediated by the antioxidant response element." Annu Rev Pharmacol Toxicol **43**: 233-260.
231. Nicholls, D. G. and S. Ferguson (2013). Bioenergetics.
232. Nieto, N. (2006). "Oxidative-stress and IL-6 mediate the fibrogenic effects of [corrected] Kupffer cells on stellate cells." Hepatology **44**(6): 1487-1501.
233. Noel, H. and S. V. Pande (1986). "An essential requirement of cardiolipin for mitochondrial carnitine acylcarnitine translocase activity. Lipid requirement of carnitine acylcarnitine translocase." Eur J Biochem **155**(1): 99-102.
234. Nury, H., C. Dahout-Gonzalez, V. Trezeguet, G. J. Lauquin, G. Brandolin and E. Pebay-Peyroula (2006). "Relations between structure and function of the mitochondrial ADP/ATP carrier." Annu Rev Biochem **75**: 713-741.
235. Oh, K. J., H. S. Han, M. J. Kim and S. H. Koo (2013). "CREB and FoxO1: two transcription factors for the regulation of hepatic gluconeogenesis." BMB Rep **46**(12): 567-574.
236. Olde Damink, S. W., R. Jalan and C. H. Dejong (2009). "Interorgan ammonia trafficking in liver disease." Metab Brain Dis **24**(1): 169-181.
237. Palmeira, C. M. and K. B. Wallace (1997). "Benzoquinone inhibits the voltage-dependent induction of the mitochondrial permeability transition caused by redox-cycling naphthoquinones." Toxicol Appl Pharmacol **143**(2): 338-347.
238. Palty, R., W. F. Silverman, M. Hershfinkel, T. Caporale, S. L. Sensi, J. Parnis, C. Nolte, D. Fishman, V. Shoshan-Barmatz, S. Herrmann, D. Khananshvili and I. Sekler (2010). "NCLX is an essential component of mitochondrial Na+/Ca2+ exchange." Proc Natl Acad Sci U S A **107**(1): 436-441.
239. Paradies, G., G. Petrosillo, M. Pistolese and F. M. Ruggiero (2000). "The effect of reactive oxygen species generated from the mitochondrial electron transport chain on the cytochrome c oxidase activity and on the cardiolipin content in bovine heart submitochondrial particles." FEBS Lett **466**(2-3): 323-326.
240. Pardo, V., A. Gonzalez-Rodriguez, J. Muntane, S. C. Kozma and A. M. Valverde (2015). "Role of hepatocyte S6K1 in palmitic acid-induced endoplasmic reticulum stress, lipotoxicity, insulin resistance and in oleic acid-induced protection." Food Chem Toxicol **80**: 298-309.
241. Parker, H. M., N. A. Johnson, C. A. Burdon, J. S. Cohn, H. T. O'Connor and J. George (2012). "Omega-3 supplementation and non-alcoholic fatty liver disease: a systematic review and meta-analysis." J Hepatol **56**(4): 944-951.
242. Passi, S., M. Picardo, M. Nazzaro-Porro, A. Breathnach, A. M. Confaloni and G. Serlupi-Crescenzi (1984). "Antimitochondrial effect of saturated medium chain length (C8-C13) dicarboxylic acids." Biochem Pharmacol **33**(1): 103-108.
243. Patterson, R. E., S. Kalavalapalli, C. M. Williams, M. Nautiyal, J. T. Mathew, J. Martinez, M. K. Reinhard, D. J. McDougall, J. R. Rocca, R. A. Yost, K. Cusi, T. J. Garrett and N. E. Sunny (2016). "Lipotoxicity in steatohepatitis occurs despite an increase in tricarboxylic acid cycle activity." Am J Physiol Endocrinol Metab **310**(7): E484-494.

244. Peng, K. Y., M. J. Watt, S. Rensen, J. W. Greve, K. Huynh, K. S. Jayawardana, P. J. Meikle and R. C. R. Meex (2018). "Mitochondrial dysfunction-related lipid changes occur in nonalcoholic fatty liver disease progression." J Lipid Res **59**(10): 1977-1986.
245. Perevoshchikova, I. V., C. L. Quinlan, A. L. Orr, A. A. Gerencser and M. D. Brand (2013). "Sites of superoxide and hydrogen peroxide production during fatty acid oxidation in rat skeletal muscle mitochondria." Free Radic Biol Med **61**: 298-309.
246. Perfield, J. W., 2nd, L. C. Ortinau, R. T. Pickering, M. L. Ruebel, G. M. Meers and R. S. Rector (2013). "Altered hepatic lipid metabolism contributes to nonalcoholic fatty liver disease in leptin-deficient Ob/Ob mice." J Obes **2013**: 296537.
247. Petersen, M. C., A. K. Madiraju, B. M. Gassaway, M. Marcel, A. R. Nasiri, G. Butrico, M. J. Marcucci, D. Zhang, A. Abulizi, X. M. Zhang, W. Philbrick, S. R. Hubbard, M. J. Jurczak, V. T. Samuel, J. Rinehart and G. I. Shulman (2016). "Insulin receptor Thr1160 phosphorylation mediates lipid-induced hepatic insulin resistance." J Clin Invest **126**(11): 4361-4371.
248. Pinzani, M., H. E. Abboud and D. C. Aron (1990). "Secretion of insulin-like growth factor-I and binding proteins by rat liver fat-storing cells: regulatory role of platelet-derived growth factor." Endocrinology **127**(5): 2343-2349.
249. Porteous, C. M., A. Logan, C. Evans, E. C. Ledgerwood, D. K. Menon, F. Aigbirhio, R. A. Smith and M. P. Murphy (2010). "Rapid uptake of lipophilic triphenylphosphonium cations by mitochondria in vivo following intravenous injection: implications for mitochondria-specific therapies and probes." Biochim Biophys Acta **1800**(9): 1009-1017.
250. Pradere, J. P., J. Kluwe, S. De Minicis, J. J. Jiao, G. Y. Gwak, D. H. Dapito, M. K. Jang, N. D. Guenther, I. Mederacke, R. Friedman, A. C. Dragomir, C. Aloman and R. F. Schwabe (2013). "Hepatic macrophages but not dendritic cells contribute to liver fibrosis by promoting the survival of activated hepatic stellate cells in mice." Hepatology **58**(4): 1461-1473.
251. Prola, A., J. Blondelle, A. Vandestienne, J. Piquereau, R. G. P. Denis, S. Guyot, H. Chauvin, A. Mourier, M. Maurer, C. Henry, N. Khadhraoui, C. Gallerne, T. Molinie, G. Courtin, L. Guillaud, M. Gressette, A. Solgadi, F. Dumont, J. Castel, J. Ternacle, J. Demarquoy, A. Malgoyre, N. Koulmann, G. Derumeaux, M. F. Giraud, F. Joubert, V. Veksler, S. Luquet, F. Relaix, L. Tiret and F. Pilot-Storck (2021). "Cardiolipin content controls mitochondrial coupling and energetic efficiency in muscle." Sci Adv **7**(1).
252. Quinlan, C. L., I. V. Perevoschikova, R. L. Goncalves, M. Hey-Mogensen and M. D. Brand (2013). "The determination and analysis of site-specific rates of mitochondrial reactive oxygen species production." Methods Enzymol **526**: 189-217.
253. Quiros, P. M. (2018). "Determination of Aconitase Activity: A Substrate of the Mitochondrial Lon Protease." Methods Mol Biol **1731**: 49-56.
254. Ramachandran, P., A. Pellicoro, M. A. Vernon, L. Boulter, R. L. Aucott, A. Ali, S. N. Hartland, V. K. Snowdon, A. Cappon, T. T. Gordon-Walker, M. J. Williams, D. R. Dunbar, J. R. Manning, N. van Rooijen, J. A. Fallowfield, S. J. Forbes and J. P. Iredale (2012). "Differential Ly-6C expression identifies the recruited macrophage phenotype, which orchestrates the regression of murine liver fibrosis." Proc Natl Acad Sci U S A **109**(46): E3186-3195.
255. Rasola, A. and P. Bernardi (2011). "Mitochondrial permeability transition in Ca(2+)-dependent apoptosis and necrosis." Cell Calcium **50**(3): 222-233.
256. Razmara, A., L. Sunday, C. Stirone, X. B. Wang, D. N. Krause, S. P. Duckles and V. Procaccio (2008). "Mitochondrial effects of estrogen are mediated by estrogen receptor alpha in brain endothelial cells." J Pharmacol Exp Ther **325**(3): 782-790.
257. Rector, R. S., J. P. Thyfault, G. M. Uptergrove, E. M. Morris, S. P. Naples, S. J. Borengasser, C. R. Mikus, M. J. Laye, M. H. Laughlin, F. W. Booth and J. A. Ibdah (2010). "Mitochondrial dysfunction precedes insulin resistance and hepatic steatosis and contributes to the natural history of non-alcoholic fatty liver disease in an obese rodent model." J Hepatol **52**(5): 727-736.

258. Reid, D. T., J. L. Reyes, B. A. McDonald, T. Vo, R. A. Reimer and B. Eksteen (2016). "Kupffer Cells Undergo Fundamental Changes during the Development of Experimental NASH and Are Critical in Initiating Liver Damage and Inflammation." PLoS One **11**(7): e0159524.
259. Rizki, G., L. Arnaboldi, B. Gabrielli, J. Yan, G. S. Lee, R. K. Ng, S. M. Turner, T. M. Badger, R. E. Pitas and J. J. Maher (2006). "Mice fed a lipogenic methionine-choline-deficient diet develop hypermetabolism coincident with hepatic suppression of SCD-1." J Lipid Res **47**(10): 2280-2290.
260. Rodrigo, R., A. Miranda and L. Vergara (2011). "Modulation of endogenous antioxidant system by wine polyphenols in human disease." Clin Chim Acta **412**(5-6): 410-424.
261. Rodriguez-Cuenca, S., H. M. Cocheme, A. Logan, I. Abakumova, T. A. Prime, C. Rose, A. Vidal-Puig, A. C. Smith, D. C. Rubinsztein, I. M. Fearnley, B. A. Jones, S. Pope, S. J. Heales, B. Y. Lam, S. G. Neogi, I. McFarlane, A. M. James, R. A. Smith and M. P. Murphy (2010). "Consequences of long-term oral administration of the mitochondria-targeted antioxidant MitoQ to wild-type mice." Free Radic Biol Med **48**(1): 161-172.
262. Roeb, E. and A. Geier (2019). "Nonalcoholic steatohepatitis (NASH) - current treatment recommendations and future developments." Z Gastroenterol **57**(4): 508-517.
263. Roeb, E., H. M. Steffen, H. Bantel, U. Baumann, A. Canbay, M. Demir, U. Drebber, A. Geier, J. Hampe, C. Hellerbrand, A. Pathil-Warth, J. M. Schattenberg, C. Schramm, H. K. Seitz, N. Stefan, F. Tacke, A. Tannapfel, P. Lynen Jansen and J. Bojunga (2015). "[S2k Guideline non-alcoholic fatty liver disease]." Z Gastroenterol **53**(7): 668-723.
264. Rokitskaya, T. I., S. S. Klishin, Severina, II, V. P. Skulachev and Y. N. Antonenko (2008). "Kinetic analysis of permeation of mitochondria-targeted antioxidants across bilayer lipid membranes." J Membr Biol **224**(1-3): 9-19.
265. Rolo, A. P., J. S. Teodoro and C. M. Palmeira (2012). "Role of oxidative stress in the pathogenesis of nonalcoholic steatohepatitis." Free Radic Biol Med **52**(1): 59-69.
266. Romeo, S., J. Kozlitina, C. Xing, A. Pertsemlidis, D. Cox, L. A. Pennacchio, E. Boerwinkle, J. C. Cohen and H. H. Hobbs (2008). "Genetic variation in PNPLA3 confers susceptibility to nonalcoholic fatty liver disease." Nat Genet **40**(12): 1461-1465.
267. Romero-Gomez, M., S. Zelber-Sagi and M. Trenell (2017). "Treatment of NAFLD with diet, physical activity and exercise." J Hepatol **67**(4): 829-846.
268. Rysted, J. E., Z. Lin, G. C. Walters, A. J. Rauckhorst, M. Noterman, G. Liu, E. B. Taylor, S. Strack and Y. M. Usachev (2021). "Distinct properties of Ca(2+) efflux from brain, heart and liver mitochondria: The effects of Na(+), Li(+) and the mitochondrial Na(+)/Ca(2+) exchange inhibitor CGP37157." Cell Calcium **96**: 102382.
269. Salvi, M., V. Battaglia, A. M. Brunati, N. La Rocca, E. Tibaldi, P. Pietrangeli, L. Marcocci, B. Mondovi, C. A. Rossi and A. Toninello (2007). "Catalase takes part in rat liver mitochondria oxidative stress defense." J Biol Chem **282**(33): 24407-24415.
270. Sanyal, A. J., E. M. Brunt, D. E. Kleiner, K. V. Kowdley, N. Chalasani, J. E. Lavine, V. Ratziu and A. McCullough (2011). "Endpoints and clinical trial design for nonalcoholic steatohepatitis." Hepatology **54**(1): 344-353.
271. Sanyal, A. J., C. Campbell-Sargent, F. Mirshahi, W. B. Rizzo, M. J. Contos, R. K. Sterling, V. A. Luketic, M. L. Shiffman and J. N. Clore (2001). "Nonalcoholic steatohepatitis: association of insulin resistance and mitochondrial abnormalities." Gastroenterology **120**(5): 1183-1192.
272. Saraste, M. (1999). "Oxidative phosphorylation at the fin de siecle." Science **283**(5407): 1488-1493.
273. Satapati, S., N. E. Sunny, B. Kucejova, X. Fu, T. T. He, A. Mendez-Lucas, J. M. Shelton, J. C. Perales, J. D. Browning and S. C. Burgess (2012). "Elevated TCA cycle function in the pathology of diet-induced hepatic insulin resistance and fatty liver." J Lipid Res **53**(6): 1080-1092.

274. Savage, D. B., C. S. Choi, V. T. Samuel, Z. X. Liu, D. Zhang, A. Wang, X. M. Zhang, G. W. Cline, X. X. Yu, J. G. Geisler, S. Bhanot, B. P. Monia and G. I. Shulman (2006). "Reversal of diet-induced hepatic steatosis and hepatic insulin resistance by antisense oligonucleotide inhibitors of acetyl-CoA carboxylases 1 and 2." J Clin Invest **116**(3): 817-824.
275. Schagger, H. and K. Pfeiffer (2001). "The ratio of oxidative phosphorylation complexes I-V in bovine heart mitochondria and the composition of respiratory chain supercomplexes." J Biol Chem **276**(41): 37861-37867.
276. Schagger, H. and G. von Jagow (1991). "Blue native electrophoresis for isolation of membrane protein complexes in enzymatically active form." Anal Biochem **199**(2): 223-231.
277. Scheffler, I. E. (2001). "Mitochondria make a come back." Adv Drug Deliv Rev **49**(1-2): 3-26.
278. Schlame, M. (2008). "Cardiolipin synthesis for the assembly of bacterial and mitochondrial membranes." J Lipid Res **49**(8): 1607-1620.
279. Schneider, J. L. and A. M. Cuervo (2014). "Liver autophagy: much more than just taking out the trash." Nat Rev Gastroenterol Hepatol **11**(3): 187-200.
280. Schroder, M. and R. J. Kaufman (2005). "ER stress and the unfolded protein response." Mutat Res **569**(1-2): 29-63.
281. Scorrano, L., V. Petronilli and P. Bernardi (1997). "On the voltage dependence of the mitochondrial permeability transition pore. A critical appraisal." J Biol Chem **272**(19): 12295-12299.
282. Sedlak, E. and N. C. Robinson (1999). "Phospholipase A(2) digestion of cardiolipin bound to bovine cytochrome c oxidase alters both activity and quaternary structure." Biochemistry **38**(45): 14966-14972.
283. Seki, E. and D. A. Brenner (2015). "Recent advancement of molecular mechanisms of liver fibrosis." J Hepatobiliary Pancreat Sci **22**(7): 512-518.
284. Seki, E., S. De Minicis, G. Y. Gwak, J. Kluwe, S. Inokuchi, C. A. Bursill, J. M. Llovet, D. A. Brenner and R. F. Schwabe (2009). "CCR1 and CCR5 promote hepatic fibrosis in mice." J Clin Invest **119**(7): 1858-1870.
285. Serviddio, G., F. Bellanti, R. Tamborra, T. Rollo, N. Capitanio, A. D. Romano, J. Sastre, G. Vendemiale and E. Altomare (2008). "Uncoupling protein-2 (UCP2) induces mitochondrial proton leak and increases susceptibility of non-alcoholic steatohepatitis (NASH) liver to ischaemia-reperfusion injury." Gut **57**(7): 957-965.
286. Shanmughapriya, S., S. Rajan, N. E. Hoffman, A. M. Higgins, D. Tomar, N. Nemani, K. J. Hines, D. J. Smith, A. Eguchi, S. Vallem, F. Shaikh, M. Cheung, N. J. Leonard, R. S. Stolakis, M. P. Wolfers, J. Ibetti, J. K. Chuprun, N. R. Jog, S. R. Houser, W. J. Koch, J. W. Elrod and M. Madesh (2015). "SPG7 Is an Essential and Conserved Component of the Mitochondrial Permeability Transition Pore." Mol Cell **60**(1): 47-62.
287. Shao, J., Z. Fu, Y. Ji, X. Guan, S. Guo, Z. Ding, X. Yang, Y. Cong and Y. Shen (2016). "Leucine zipper-EF-hand containing transmembrane protein 1 (LETM1) forms a Ca(2+)/H(+) antiporter." Sci Rep **6**: 34174.
288. Shen, C., W. Ma, L. Ding, S. Li, X. Dou and Z. Song (2018). "The TLR4-IRE1alpha pathway activation contributes to palmitate-elicited lipotoxicity in hepatocytes." J Cell Mol Med **22**(7): 3572-3581.
289. Simoes, I. C. M., R. Amorim, J. Teixeira, A. Karkucinska-Wieckowska, A. Carvalho, S. P. Pereira, R. F. Simoes, S. Szymanska, M. Dabrowski, J. Janikiewicz, A. Dobrzyn, P. J. Oliveira, Y. Potes and M. R. Wieckowski (2021). "The Alterations of Mitochondrial Function during NAFLD Progression-An Independent Effect of Mitochondrial ROS Production." Int J Mol Sci **22**(13).

290. Simoes, I. C. M., A. Fontes, P. Pinton, H. Zischka and M. R. Wieckowski (2018). "Mitochondria in non-alcoholic fatty liver disease." Int J Biochem Cell Biol **95**: 93-99.
291. Simoes, I. C. M., J. Janikiewicz, J. Bauer, A. Karkucinska-Wieckowska, P. Kalinowski, A. Dobrzyn, A. Wolski, M. Pronicki, K. Zieniewicz, P. Dobrzyn, M. Krawczyk, H. Zischka, M. R. Wieckowski and Y. Potes (2019). "Fat and Sugar-A Dangerous Duet. A Comparative Review on Metabolic Remodeling in Rodent Models of Nonalcoholic Fatty Liver Disease." Nutrients **11**(12).
292. Simoes, I. C. M., A. Karkucinska-Wieckowska, J. Janikiewicz, S. Szymanska, M. Pronicki, P. Dobrzyn, M. Dabrowski, A. Dobrzyn, P. J. Oliveira, H. Zischka, Y. Potes and M. R. Wieckowski (2020). "Western Diet Causes Obesity-Induced Nonalcoholic Fatty Liver Disease Development by Differentially Compromising the Autophagic Response." Antioxidants (Basel) **9**(10).
293. Singh, R., S. Kaushik, Y. Wang, Y. Xiang, I. Novak, M. Komatsu, K. Tanaka, A. M. Cuervo and M. J. Czaja (2009). "Autophagy regulates lipid metabolism." Nature **458**(7242): 1131-1135.
294. Sinn, D. H., D. Kang, Y. Chang, S. Ryu, S. J. Cho, S. W. Paik, Y. B. Song, R. Pastor-Barriuso, E. Guallar, J. Cho and G. Y. Gwak (2020). "Non-alcoholic fatty liver disease and the incidence of myocardial infarction: A cohort study." J Gastroenterol Hepatol **35**(5): 833-839.
295. Smith, R. A., C. M. Porteous, A. M. Gane and M. P. Murphy (2003). "Delivery of bioactive molecules to mitochondria in vivo." Proc Natl Acad Sci U S A **100**(9): 5407-5412.
296. Sookoian, S. and C. J. Pirola (2017). "Systematic review with meta-analysis: risk factors for non-alcoholic fatty liver disease suggest a shared altered metabolic and cardiovascular profile between lean and obese patients." Aliment Pharmacol Ther **46**(2): 85-95.
297. Stanhope, K. L., J. M. Schwarz, N. L. Keim, S. C. Griffen, A. A. Bremer, J. L. Graham, B. Hatcher, C. L. Cox, A. Dyachenko, W. Zhang, J. P. McGahan, A. Seibert, R. M. Krauss, S. Chiu, E. J. Schaefer, M. Ai, S. Otokozawa, K. Nakajima, T. Nakano, C. Beysen, M. K. Hellerstein, L. Berglund and P. J. Havel (2009). "Consuming fructose-sweetened, not glucose-sweetened, beverages increases visceral adiposity and lipids and decreases insulin sensitivity in overweight/obese humans." J Clin Invest **119**(5): 1322-1334.
298. Sun, S. Z. and M. W. Empie (2012). "Fructose metabolism in humans - what isotopic tracer studies tell us." Nutr Metab (Lond) **9**(1): 89.
299. Sunny, N. E., E. J. Parks, J. D. Browning and S. C. Burgess (2011). "Excessive hepatic mitochondrial TCA cycle and gluconeogenesis in humans with nonalcoholic fatty liver disease." Cell Metab **14**(6): 804-810.
300. Suzuki, Y. J., M. Carini and D. A. Butterfield (2010). "Protein carbonylation." Antioxid Redox Signal **12**(3): 323-325.
301. Szabo, I., P. Bernardi and M. Zoratti (1992). "Modulation of the mitochondrial megachannel by divalent cations and protons." J Biol Chem **267**(5): 2940-2946.
302. Szymanska-Debinska, T., A. Karkucinska-Wieckowska, D. Piekutowska-Abramczuk, E. Jurkiewicz, K. Iwanicka-Pronicka, D. Rokicki and M. Pronicki (2015). "Leigh disease due to SCO2 mutations revealed at extended autopsy." J Clin Pathol **68**(5): 397-399.
303. Tacke, F., T. Luedde and C. Trautwein (2009). "Inflammatory pathways in liver homeostasis and liver injury." Clin Rev Allergy Immunol **36**(1): 4-12.
304. Taguchi, K., N. Fujikawa, M. Komatsu, T. Ishii, M. Unno, T. Akaike, H. Motohashi and M. Yamamoto (2012). "Keap1 degradation by autophagy for the maintenance of redox homeostasis." Proc Natl Acad Sci U S A **109**(34): 13561-13566.
305. Taguchi, K., H. Motohashi and M. Yamamoto (2011). "Molecular mechanisms of the Keap1-Nrf2 pathway in stress response and cancer evolution." Genes Cells **16**(2): 123-140.
306. Tamai, S., H. Iida, S. Yokota, T. Sayano, S. Kiguchiya, N. Ishihara, J. Hayashi, K. Mihara and T. Oka (2008). "Characterization of the mitochondrial protein LETM1, which maintains the

mitochondrial tubular shapes and interacts with the AAA-ATPase BCS1L." J Cell Sci **121**(Pt 15): 2588-2600.

307. Teixeira, J., F. Basit, P. Willems, J. A. Wagenaars, E. van de Westerlo, R. Amorim, F. Cagide, S. Benfeito, C. Oliveira, F. Borges, P. J. Oliveira and W. J. H. Koopman (2021). "Mitochondria-targeted phenolic antioxidants induce ROS-protective pathways in primary human skin fibroblasts." Free Radic Biol Med **163**: 314-324.
308. Teixeira, J., F. Cagide, S. Benfeito, P. Soares, J. Garrido, I. Baldeiras, J. A. Ribeiro, C. M. Pereira, A. F. Silva, P. B. Andrade, P. J. Oliveira and F. Borges (2017). "Development of a Mitochondriotropic Antioxidant Based on Caffeic Acid: Proof of Concept on Cellular and Mitochondrial Oxidative Stress Models." J Med Chem **60**(16): 7084-7098.
309. Teixeira, J., A. Gaspar, E. M. Garrido, J. Garrido and F. Borges (2013). "Hydroxycinnamic acid antioxidants: an electrochemical overview." Biomed Res Int **2013**: 251754.
310. Teixeira, J., C. Oliveira, R. Amorim, F. Cagide, J. Garrido, J. A. Ribeiro, C. M. Pereira, A. F. Silva, P. B. Andrade, P. J. Oliveira and F. Borges (2017). "Development of hydroxybenzoic-based platforms as a solution to deliver dietary antioxidants to mitochondria." Sci Rep **7**(1): 6842.
311. Teixeira, J., P. Soares, S. Benfeito, A. Gaspar, J. Garrido, M. P. Murphy and F. Borges (2012). "Rational discovery and development of a mitochondria-targeted antioxidant based on cinnamic acid scaffold." Free Radic Res **46**(5): 600-611.
312. Teodoro, J. S., A. P. Rolo, F. V. Duarte, A. M. Simoes and C. M. Palmeira (2008). "Differential alterations in mitochondrial function induced by a choline-deficient diet: understanding fatty liver disease progression." Mitochondrion **8**(5-6): 367-376.
313. Toime, L. J. and M. D. Brand (2010). "Uncoupling protein-3 lowers reactive oxygen species production in isolated mitochondria." Free Radic Biol Med **49**(4): 606-611.
314. Tosello-Trampont, A. C., P. Krueger, S. Narayanan, S. G. Landes, N. Leitinger and Y. S. Hahn (2016). "NKp46(+) natural killer cells attenuate metabolism-induced hepatic fibrosis by regulating macrophage activation in mice." Hepatology **63**(3): 799-812.
315. Treberg, J. R., C. L. Quinlan and M. D. Brand (2011). "Evidence for two sites of superoxide production by mitochondrial NADH-ubiquinone oxidoreductase (complex I)." J Biol Chem **286**(31): 27103-27110.
316. Tripathy, S., K. A. Lytle, R. D. Stevens, J. R. Bain, C. B. Newgard, A. S. Greenberg, L. S. Huang and D. B. Jump (2014). "Fatty acid elongase-5 (Elovl5) regulates hepatic triglyceride catabolism in obese C57BL/6J mice." J Lipid Res **55**(7): 1448-1464.
317. Turner, N., C. R. Bruce, S. M. Beale, K. L. Hoehn, T. So, M. S. Rolph and G. J. Cooney (2007). "Excess lipid availability increases mitochondrial fatty acid oxidative capacity in muscle: evidence against a role for reduced fatty acid oxidation in lipid-induced insulin resistance in rodents." Diabetes **56**(8): 2085-2092.
318. Uddin, M. N., N. Nishio, S. Ito, H. Suzuki and K. Isobe (2012). "Autophagic activity in thymus and liver during aging." Age (Dordr) **34**(1): 75-85.
319. Ueno, T. and M. Komatsu (2017). "Autophagy in the liver: functions in health and disease." Nat Rev Gastroenterol Hepatol **14**(3): 170-184.
320. Valdecantos, M. P., P. Perez-Matute, P. Gonzalez-Muniesa, P. L. Prieto-Hontoria, M. J. Moreno-Aliaga and J. A. Martinez (2012). "Lipoic acid improves mitochondrial function in nonalcoholic steatosis through the stimulation of sirtuin 1 and sirtuin 3." Obesity (Silver Spring) **20**(10): 1974-1983.
321. Valko, M., D. Leibfritz, J. Moncol, M. T. Cronin, M. Mazur and J. Telser (2007). "Free radicals and antioxidants in normal physiological functions and human disease." Int J Biochem Cell Biol **39**(1): 44-84.
322. van der Veen, J. N., J. P. Kennelly, S. Wan, J. E. Vance, D. E. Vance and R. L. Jacobs (2017). "The critical role of phosphatidylcholine and phosphatidylethanolamine metabolism in health and disease." Biochim Biophys Acta Biomembr **1859**(9 Pt B): 1558-1572.

323. Vasko, R. and M. S. Goligorsky (2013). "Dysfunctional lysosomal autophagy leads to peroxisomal oxidative burnout and damage during endotoxin-induced stress." Autophagy **9**(3): 442-444.
324. Vial, G., H. Dubouchaud, K. Couturier, C. Cottet-Rousselle, N. Taleux, A. Athias, A. Galinier, L. Casteilla and X. M. Leverve (2011). "Effects of a high-fat diet on energy metabolism and ROS production in rat liver." J Hepatol **54**(2): 348-356.
325. Vogel, F., C. Bornhovd, W. Neupert and A. S. Reichert (2006). "Dynamic subcompartmentalization of the mitochondrial inner membrane." J Cell Biol **175**(2): 237-247.
326. von Loeffelholz, C., S. Docke, J. F. Lock, S. Lieske, P. Horn, J. Kriebel, S. Wahl, P. Singmann, T. de Las Heras Gala, H. Grallert, N. Raschzok, I. M. Sauer, R. Heller, G. Jahreis, R. A. Claus, M. Bauer, M. Stockmann, A. L. Birkenfeld and A. F. H. Pfeiffer (2017). "Increased lipogenesis in spite of upregulated hepatic 5'AMP-activated protein kinase in human non-alcoholic fatty liver." Hepatol Res **47**(9): 890-901.
327. von Schonfels, W., J. H. Beckmann, M. Ahrens, A. Hendricks, C. Rocken, S. Szymczak, J. Hampe and C. Schafmayer (2018). "Histologic improvement of NAFLD in patients with obesity after bariatric surgery based on standardized NAS (NAFLD activity score)." Surg Obes Relat Dis **14**(10): 1607-1616.
328. Vreken, P., F. Valianpour, L. G. Nijtmans, L. A. Grivell, B. Plecko, R. J. Wanders and P. G. Barth (2000). "Defective remodeling of cardiolipin and phosphatidylglycerol in Barth syndrome." Biochem Biophys Res Commun **279**(2): 378-382.
329. Wake, K. (1971). ""Sternzellen" in the liver: perisinusoidal cells with special reference to storage of vitamin A." Am J Anat **132**(4): 429-462.
330. Walter, P. and D. Ron (2011). "The unfolded protein response: from stress pathway to homeostatic regulation." Science **334**(6059): 1081-1086.
331. Wan, S., E. Zhao, I. Kryczek, L. Vatan, A. Sadovskaya, G. Ludema, D. M. Simeone, W. Zou and T. H. Welling (2014). "Tumor-associated macrophages produce interleukin 6 and signal via STAT3 to promote expansion of human hepatocellular carcinoma stem cells." Gastroenterology **147**(6): 1393-1404.
332. Wang, D., Y. Wei and M. J. Pagliassotti (2006). "Saturated fatty acids promote endoplasmic reticulum stress and liver injury in rats with hepatic steatosis." Endocrinology **147**(2): 943-951.
333. Wang, L., X. Liu, J. Nie, J. Zhang, S. R. Kimball, H. Zhang, W. J. Zhang, L. S. Jefferson, Z. Cheng, Q. Ji and Y. Shi (2015). "ALCAT1 controls mitochondrial etiology of fatty liver diseases, linking defective mitophagy to steatosis." Hepatology **61**(2): 486-496.
334. Wang, X., X. Zhang, E. S. H. Chu, X. Chen, W. Kang, F. Wu, K. F. To, V. W. S. Wong, H. L. Y. Chan, M. T. V. Chan, J. J. Y. Sung, W. K. K. Wu and J. Yu (2018). "Defective lysosomal clearance of autophagosomes and its clinical implications in nonalcoholic steatohepatitis." FASEB J **32**(1): 37-51.
335. Weekes, M. P., P. Tomasec, E. L. Huttlin, C. A. Fielding, D. Nusinow, R. J. Stanton, E. C. Y. Wang, R. Aicheler, I. Murrell, G. W. G. Wilkinson, P. J. Lehner and S. P. Gygi (2014). "Quantitative temporal viromics: an approach to investigate host-pathogen interaction." Cell **157**(6): 1460-1472.
336. Wehr, A., C. Baeck, F. Heymann, P. M. Niemietz, L. Hammerich, C. Martin, H. W. Zimmermann, O. Pack, N. Gassler, K. Hittatiya, A. Ludwig, T. Luedde, C. Trautwein and F. Tacke (2013). "Chemokine receptor CXCR6-dependent hepatic NK T Cell accumulation promotes inflammation and liver fibrosis." J Immunol **190**(10): 5226-5236.
337. Wei, Y., D. Wang, F. Topczewski and M. J. Pagliassotti (2006). "Saturated fatty acids induce endoplasmic reticulum stress and apoptosis independently of ceramide in liver cells." Am J Physiol Endocrinol Metab **291**(2): E275-281.

338. Williams, R., R. Aspinall, M. Bellis, G. Camps-Walsh, M. Cramp, A. Dhawan, J. Ferguson, D. Forton, G. Foster, I. Gilmore, M. Hickman, M. Hudson, D. Kelly, A. Langford, M. Lombard, L. Longworth, N. Martin, K. Moriarty, P. Newsome, J. O'Grady, R. Pryke, H. Rutter, S. Ryder, N. Sheron and T. Smith (2014). "Addressing liver disease in the UK: a blueprint for attaining excellence in health care and reducing premature mortality from lifestyle issues of excess consumption of alcohol, obesity, and viral hepatitis." Lancet **384**(9958): 1953-1997.
339. Willy, J. A., S. K. Young, A. L. Mosley, S. Gawrieh, J. L. Stevens, H. C. Masuoka and R. C. Wek (2017). "Function of inhibitor of Bruton's tyrosine kinase isoform alpha (IBTKalpha) in nonalcoholic steatohepatitis links autophagy and the unfolded protein response." J Biol Chem **292**(34): 14050-14065.
340. Willy, J. A., S. K. Young, J. L. Stevens, H. C. Masuoka and R. C. Wek (2015). "CHOP links endoplasmic reticulum stress to NF-kappaB activation in the pathogenesis of nonalcoholic steatohepatitis." Mol Biol Cell **26**(12): 2190-2204.
341. Wisse, E., F. Braet, D. Luo, R. De Zanger, D. Jans, E. Crabbe and A. Vermoesen (1996). "Structure and function of sinusoidal lining cells in the liver." Toxicol Pathol **24**(1): 100-111
342. Xiao, C., J. Hsieh, K. Adeli and G. F. Lewis (2011). "Gut-liver interaction in triglyceride-rich lipoprotein metabolism." Am J Physiol Endocrinol Metab **301**(3): E429-446.
343. Xie, C., C. Jiang, J. Shi, X. Gao, D. Sun, L. Sun, T. Wang, S. Takahashi, M. Anitha, K. W. Krausz, A. D. Patterson and F. J. Gonzalez (2017). "An Intestinal Farnesoid X Receptor-Ceramide Signaling Axis Modulates Hepatic Gluconeogenesis in Mice." Diabetes **66**(3): 613-626.
344. Xie, Z., H. Li, K. Wang, J. Lin, Q. Wang, G. Zhao, W. Jia and Q. Zhang (2010). "Analysis of transcriptome and metabolome profiles alterations in fatty liver induced by high-fat diet in rat." Metabolism **59**(4): 554-560.
345. Xu, C., C. Yu, H. Ma, L. Xu, M. Miao and Y. Li (2013). "Prevalence and risk factors for the development of nonalcoholic fatty liver disease in a nonobese Chinese population: the Zhejiang Zhenhai Study." Am J Gastroenterol **108**(8): 1299-1304
346. Yamaguchi, K., L. Yang, S. McCall, J. Huang, X. X. Yu, S. K. Pandey, S. Bhanot, B. P. Monia, Y. X. Li and A. M. Diehl (2007). "Inhibiting triglyceride synthesis improves hepatic steatosis but exacerbates liver damage and fibrosis in obese mice with nonalcoholic steatohepatitis." Hepatology **45**(6): 1366-1374.
347. Yamaoka, S., R. Urade and M. Kito (1990). "Cardiolipin molecular species in rat heart mitochondria are sensitive to essential fatty acid-deficient dietary lipids." J Nutr **120**(5): 415-421.
348. Yang, L., P. Li, S. Fu, E. S. Calay and G. S. Hotamisligil (2010). "Defective hepatic autophagy in obesity promotes ER stress and causes insulin resistance." Cell Metab **11**(6): 467-478.
349. Yin, X. M., W. X. Ding and W. Gao (2008). "Autophagy in the liver." Hepatology **47**(5): 1773-1785.
350. Younossi, Z., Q. M. Anstee, M. Marietti, T. Hardy, L. Henry, M. Eslam, J. George and E. Bugianesi (2018). "Global burden of NAFLD and NASH: trends, predictions, risk factors and prevention." Nat Rev Gastroenterol Hepatol **15**(1): 11-20.
351. Younossi, Z. M., A. B. Koenig, D. Abdelatif, Y. Fazel, L. Henry and M. Wymer (2016). "Global epidemiology of nonalcoholic fatty liver disease-Meta-analytic assessment of prevalence, incidence, and outcomes." Hepatology **64**(1): 73-84.
352. Zhang, X., J. Han, K. Man, X. Li, J. Du, E. S. Chu, M. Y. Go, J. J. Sung and J. Yu (2016). "CXC chemokine receptor 3 promotes steatohepatitis in mice through mediating inflammatory cytokines, macrophages and autophagy." J Hepatol **64**(1): 160-170
353. Zhang, X., W. K. Wu, W. Xu, K. Man, X. Wang, J. Han, W. Y. Leung, R. Wu, K. Liu and J. Yu (2017). "C-X-C Motif Chemokine 10 Impairs Autophagy and Autolysosome Formation in Non-alcoholic Steatohepatitis." Theranostics **7**(11): 2822-2836.

354. Zigmond, E., S. Samia-Grinberg, M. Pasmanik-Chor, E. Brazowski, O. Shibolet, Z. Halpern and C. Varol (2014). "Infiltrating monocyte-derived macrophages and resident kupffer cells display different ontogeny and functions in acute liver injury." J Immunol **193**(1): 344-353.